*Contrails*

# STUDY OF SUPERSONIC RADIAL COMPRESSORS FOR REFRIGERATION AND PRESSURIZATION SYSTEMS

JUL 5 1957

*J. E. COPPAGE*

*F. DALLENBACH*

*H. P. EICHENBERGER*

*G. E. HLAVAKA*

*E. M. KNOERNSCHILD*

*N. VAN LE*

*AIRESEARCH MANUFACTURING COMPANY*

*DECEMBER 1956*

I

## FOREWORD

This report was prepared by AiResearch Manufacturing Company, 9851-9951 Sepulveda Boulevard, Los Angeles 45, California, in fulfillment of Contract No. AF33(616)-2318. The project was administered under the direction of the Equipment Laboratory, Directorate of Laboratories, Wright Air Development Center, with Mr. H. Ziebarth as project engineer.

The authors of this report are J. E. Coppage, F. Dallenbach, H. P. Eichenberger, G. E. Hlavaka, E. M. Knoernschild, and N. Van Le. In addition to the above named, W. W. English assisted materially in the aerodynamic design of the experimental compressor and D. E. Lewis carried out the instrumentation and testing phase.

WADC TR 55-257

## ABSTRACT

A theoretical and experimental investigation was carried out with the purpose of determining the design criteria for high pressure ratio centrifugal compressors for air conditioning applications. The concept of designing compressors both for air and Freon had to be reconsidered in view of the considerable problems involved in developing a machine for pressure ratios as high as $8{:}1$ in a single stage. A general optimization study indicated the over-all design parameters which must be chosen in order to arrive at efficient high pressure ratio compressors. Then to achieve the correct flow passages, a three-dimensional design theory was developed, and a practical method for designing efficient impellers was derived. The problems of supersonic diffuser flow were studied, and the optimization of the diffusion process is discussed. The possibility of using various types of prewhirl in order to influence the compressor performance is considered. Based on the theoretical studies, an experimental radial compressor for a pressure ratio of $6{:}1$ was designed, manufactured, and tested.

## PUBLICATION REVIEW

The publication of this report does not constitute approval by the Air Force of the findings or conclusions contained herein. It is published only for the exchange and stimulation of ideas.
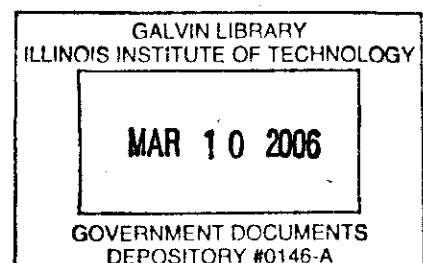
FOR THE COMMANDER:

F. R. EBERSBACH
Chief, Air Conditioning & Ice Prevention
Section

Mechanical Branch
Equipment Laboratory

CONTENTS

CONTENTS (Continued)

| | |
|---|---|
| a | velocity of sound |
| A | area |
| b | diffuser width, impeller tip width |
| B | dimensionless width |
| c | absolute velocity, chord |
| $c_p$ | specific heat at constant pressure, pressure coefficient |
| $c_v$ | specific heat at constant volume |
| $c_f$ | skin friction coefficient |
| C | constant of integration, dimensionless velocity |
| d | diameter |
| D | impeller tip diameter |
| f | friction factor (small) |
| F | force |
| g | conversion factor in Newton's second law – standard gravitational acceleration |
| h | enthalpy |
| H | head; also shape parameter |
| I | integral |
| J | mechanical equivalent of heat |
| k | ratio $c_p/c_v$ |
| K | constant |
| l | length along flow path |
| M | Mach number |
| m | coordinate along streamline in the meridional plane, momentum flux |
| n | coordinate normal to streamline in the meridional plane |
| N | rotational speed |
| O | higher order terms |
| p | polytropic exponent, pressure in boundary layer |
| P | static pressure |
| $P_T$ | total pressure |
| q | head loss or work parameter $gH/u_2^2$ |
| r | radius |
| R | dimensionless radius, gas constant, radius of curvature, radius of conical diffuser |

| | |
|---|---|
| Re | Reynolds number |
| $R_\theta$ | Reynolds number based on momentum thickness |
| s | blade spacing $= \dfrac{2\pi r}{Z}$ |
| S | entropy |
| t | blade thickness in tangential direction |
| T | static temperature |
| $T_T$ | total temperature |
| u | tangential rotor velocity, fluid velocity within boundary layer in x direction |
| U | freestream velocity in x direction |
| V | freestream velocity in x direction |
| w | relative velocity |
| W | mass rate of flow |
| x | coordinate |
| y | coordinate |
| z | coordinate along the axis |
| Z | number of blades |

## Greek Letters

| | |
|---|---|
| $\alpha$ | angle between the absolute velocity vector and the meridional plane |
| $\beta$ | angle between the relative velocity vector and the meridional plane |
| $\beta_b$ | blade angle |
| $\gamma$ | local cone angle tangent to streamline, angle between relative velocity and radial direction |
| $\Gamma$ | circulation, function in auxiliary momentum equation |
| $\delta$ | 99 per cent thickness boundary layer, also rake angle of blades, also ratio $P/P_{std}$ |
| $\delta^*$ | displacement thickness |
| $\Delta$ | diffusion factor |
| $\Delta(\ )$ | change of ( ) |
| $\mu$ | viscosity |
| $\nu$ | inducer hub-tip diameter ratio |
| $\eta$ | efficiency |
| $\epsilon$ | clogging factor |
| $\rho$ | density |
| $\zeta$ | loss coefficient, vorticity |
| $\tau$ | shear stress |

WADC TR 55-257

$\lambda$     $C_{u_2}/u_2$, friction factor $= 4f$

$\varphi$     coordinate, flow factor $\dfrac{c_{m_1}}{u_2}$

$\theta$     momentum thickness, ratio $T/T_{std}$

$\quad$ dimensionless specific speed

$\quad$ slip $= \dfrac{C_{u_{th}} - C_{u_2}}{u_2}$

$\psi$     blade tilt angle

$\omega$     angular velocity

## Subscripts

Note:   Capitalized subscripts are used locally and are defined where found.

$(\ )_{ad}$     adiabatic

$(\ )_b$     blade

$(\ )_c$     absolute

$(\ )_f$     final

$(\ )_h$     inducer hub

$(\ )_i$     inducer tip, inlet

$(\ )_m$     meridional

$(\ )_p$     potential, pressure side

$(\ )_s$     suction side, separation

$(\ )_t$     impeller tip

$(\ )_T$     total

$(\ )_u$     tangential

$(\ )_w$     relative

$(\ )_o$     total ambient

$(\ )_1$     inducer inlet

$(\ )_2$     impeller outlet

## Superscript

$(\ )^*$     condition at which local velocity is sonic

WADC TR 55-257

# INTRODUCTION

This report deals with the theoretical and experimental investigation of the problems one must solve in designing a high pressure ratio centrifugal compressor for air conditioning applications. Problem statements contained in exhibits for current aircraft high-altitude air conditioning indicate that compressor pressure ratios of up to 6:1 would be desirable for air conditioning use. At the time of initiation of this study, AiResearch felt that this pressure ratio presented a challenge in spite of considerable experience in the field of centrifugal compressors, since similar machinery developed here were well below this pressure ratio limit. A thorough search of the literature indicated that there was no machine available at the time even approaching the 6:1 pressure ratio. It appeared, therefore, to be necessary to reconsider the concept of designing compressors as it was used at AiResearch in view of the considerable problems which arise from developing a machine for such high pressure ratios.

It was realized that the impeller would be the most difficult part of the compressor. Therefore, more emphasis was given to problems involved in designing impellers for such high pressure ratios, and design methods were evolved. The problems of diffuser flow were mainly investigated from the viewpoint of boundary layer theory. A considerable effort was devoted to evaluating the state of the art of decelerating flow and boundary layer separation. The flow conditions in the impeller inlet present three-dimensional transonic flow problems. In view of insufficient information on this kind of flow, only an approximate flow calculation could be made.

The report is broken down in six main subjects. After a general discussion (Section I), a study is made with the purpose of optimizing the design of a compressor suitable for pressure ratios as high as 8:1 (Section II). In Section III, the available theories on impeller design are reviewed and a design method is presented. In Section IV, a short discussion about the possibilities of influencing the compressor performance by various types of prewhirl is given. Following this, in Section V, an investigation of considerable length covering the present state of diffuser theory is presented. Its results are utilized for the design of diffusers of centrifugal compressors. Finally, in Section VI, one compressor with two different impellers is designed on the theories presented in the above sections and is manufactured. Test results with this compressor are shown and discussed.

## THE BASIC APPROACH

The problems of designing high pressure ratio compressors are basically similar to those for low pressure ratio compressors. However, because compressibility effects are more pronounced, the flow conditions have to be known more accurately, and optimization studies were considered desirable from which a design providing the least losses could be selected. The method chosen is a performance prediction method based on a one-dimensional flow theory. It was intended to show quite generally the changes in the basic geometric parameters; these appear as dimensionless quantities in the loss prediction. The effect of Reynolds number changes in the performance could also be investigated here as well as basic performance differences between air and Freon. The objective of this program was to indicate the more promising configurations for future machines, and, as pointed out in the next section, the concept of the specific speed proved to be very valuable, and it could be shown that highest specific speed machinery is required in order to make efficient high pressure ratio compressors.

Based on this one-dimensional approach, the external shape of the compressor that is, the inducer and tip diameters, tip width, degree of backward curvature of blades, is determined. In connection with the tip speed, the velocity triangles are established. Another phase of the program deals with the internal phase of the impeller design, or answers the problem of which passage shape produces the desired velocity triangles. The main problem was now to provide the desirable velocity distribution in the impeller as a key to a compressor with best efficiency. The knowledge of two-dimensional boundary layer is applied as far as possible. Qualitative knowledge of the secondary flow in the boundary layers and of the laws of separated flow is used to modify the knowledge of two-dimensional boundary layer calculations. A special problem connected with the impeller is the three-dimensional transonic flow in the inducer inlet. Theoretical design criteria for this flow condition could not be found in the literature. It was, therefore, decided to use NACA test information as a guide and to treat the three-dimensional transonic flow essentially according to the supersonic isentropic gas dynamic equations, disregarding any shock phenomena.

The study conducted in Section II indicates clearly the advantages of high specific speed design. A high specific speed compressor is characterized by having a high flow rate for its size, which means a large inducer eye diameter compared to the tip diameter of the impeller. With high pressure ratios and large inducer-to-tip ratios, the relative velocity at the eye approaches and exceeds the sonic value. A study was conducted to evaluate the advantages of introducing prewhirl to the design of the impeller. By application of prewhirl with rotation of the wheel, the relative inlet Mach

number at the inducer can be reduced considerably, thus eliminating conditions which may arise from near sonic flow velocities. However, as became known during the period of this study, moderate supersonic velocities near the inducer tip are not detrimental to the performance, if a reasonable subsonic region at the leading edge is provided. This being mostly the case, the decision could be reached that high pressure ratio compressors should not incorporate prewhirl except in cases where a variation of prewhirl is desirable.

Considerable effort went into the study of viscous flow in vaneless and guide-vaned diffusers of centrifugal compressors. Data from experimental conical diffusers setups cannot be used without modification for vaned diffusers of a compressor, since the vaned diffusers generally have a much thicker boundary layer than commonly found in conical diffusers.

The calculation of the growth of the boundary layer of the conical diffuser was achieved by use of a semi-empirical procedure. From this, a method was evolved for the prediction of the maximum deceleration that can be achieved for a given initial flow condition. The results of this study were applied to determine loss coefficients of diffusers for centrifugal compressors and a simple method is presented for the design of subsonic vaned diffusers.

PERFORMANCE PREDICTION FOR CENTRIFUGAL COMPRESSORS

## 2.1  Introduction

Performance prediction is an endeavor which is necessary in the design of almost every type of turbomachinery.  It is based on establishing the individual losses within a machine and relating them to the work input which is found by applying the Euler equation.  By subdividing the losses into individual fractions, a better approximation to the actual over-all loss can be made.  Errors in the assumption of an individual loss influence the result only to a small degree.  Though an absolutely accurate performance prediction covering the entire range of performance of the compressor has not been achieved as yet, a reasonably accurate prediction of that performance within the limits required for practical turbomachinery is possible, and has been proven.  This performance prediction is especially suited to investigate changes in the basic geometric parameters.  Thus, they appear as dimensionless quantities in the loss prediction.  Also, considerable changes in the Reynolds number as they are occurring in machinery operating at various altitudes can be predicted very satisfactorily.  The effect of Reynolds number changes on performance are especially pronounced for the small size machinery which is considered here.  The performance differences between air and Freon can also be brought out reasonably well, in the performance prediction, as shown later.

Generally, the performance prediction may be divided into two classes: (a) predicting the performance of a given piece of machinery under a wide range of operating conditions; (b) predicting the performance of a number of possible design configurations, each of which is as near to its design point as can be fixed in advance.  The latter is the "design study" which is intended to point the way to the optimum design for a given job.  The former is the study of the specific machine, selected from the design study, to determine its off-design performance; this may also be of a higher accuracy than the general study.

It is the "design study" which will be presented below, since it is an objective of this program to indicate the most promising configurations for future machines.  Consideration of performance prediction of a specific machine will be made in connection with the test results for the compressor being developed under this program.

## 2.2  Literature Survey

Making a satisfactory prediction of performance requires the best possible information concerning the losses associated with the operation of the machine. In turbomachinery these losses (or at least certain coefficients) must generally be found experimentally, since the flow behavior is usually far too complicated to permit theoretical treatment.  A thorough literature survey was undertaken to make sure that all available significant data related to compressor losses is incorporated in the prediction method.

Unfortunately, in the field of centrifugal turbomachinery there is but little data available which is both complete and accurate enough to permit deduction of individual losses. This is due to the great difficulties which arise in the study of the three-dimensional flow with which we have to deal here.

Where accurate work has been done, the range of variables covered has been rather small. The best single reference is Baljé's work (Reference 2.1.) This pioneer effort represents the first really comprehensive approach to performance predictions for compressors. (For water pumps there is a separate literature which will not be cited here. See, for example, Reference 2.2.) In addition, Baljé has digested the more important German data and applied it to the coefficients of his loss relations. Liberal use of this reference was made in the establishment of the method outlined herein. Also, unpublished work by Knoernschild, on more elaborate loss configurations including blade loading and diffusion losses, was used.

The second general source of information is the NACA literature. There are numerous NACA reports which help shed light on the behavior of centrifugal compressors. These mainly comprise References 2.3 to 2.11. Performance prediction as such is not the topic of these reports; rather, they treat more basic aspects of the flow mechanism which we have to understand, before a logical approach to a prediction can be made.

Information concerning diffuser performance is covered in a separate section of this report. However, two references (Reference 2.9 and 2.10) were found to be helpful for estimating one-dimensional vaneless diffuser performance. Certain simplifications and approximations can be obtained from these papers, and reference will be made to them below in the discussion of the prediction method.

Lieblein (Reference 2.11) introduced the concept of a diffusion factor in order to correlate losses in axial-flow machines. In the present study, a similar diffusion factor was developed for centrifugal machines.

## 2.3  Overall Considerations

The problems of performance prediction can best be attacked by examining the process path followed by the fluid flowing through the compressor on the enthalpy-entropy diagram. Sketch 2.1 on the following page shows a typical process path. The process 0-1 is in the inlet, from ambient conditions up to the impeller face. The process 1-2 is in the impeller, 2-3 in the vaneless diffuser, 3-4 in the vaned diffuser, 4-5 in the collector and discharge to plenum. (Note that throughout this study a vaneless space will always be assumed to exist before the vaned diffuser, so as to reduce the velocity to a subsonic value before entering the guide vanes.)

In passing through the compressor a certain amount of work is done on each unit mass of fluid; this is given the designation $H_{TOT}$, that is, total head or total work per unit mass of fluid. It is clear that an energy balance yields

$$H_{TOT} = h_a - h_o \qquad (2.1)$$

$P_{T5}$ = EXIT TOTAL AND STATIC PRESSURE

LINES OF CONSTANT PRESSURE

a    g    h    1    5

$\Delta H_{DF} + \Delta H_{RC}$

b

$\Delta H_{SF} + \Delta H_{DEL}$
$+ \Delta H_I + \Delta H_{SW}$

c

j    k

SCROLL AND DISCHARGE

$\Delta H_{rLD}$

d

4

VANED DIFFUSER

$\Delta H_{GV}$

e

$\Delta H_{EXIT}$

f

3

$H_{TOT}$

VANELESS DIFFUSER

$H_{TH}$

2

$H_{AD}$

IMPELLER

$P_o$ = INLET TOTAL PRESSURE

O

PROCESS PATH OF FLUID ELEMENT IN COMPRESSOR

1

ENTROPY
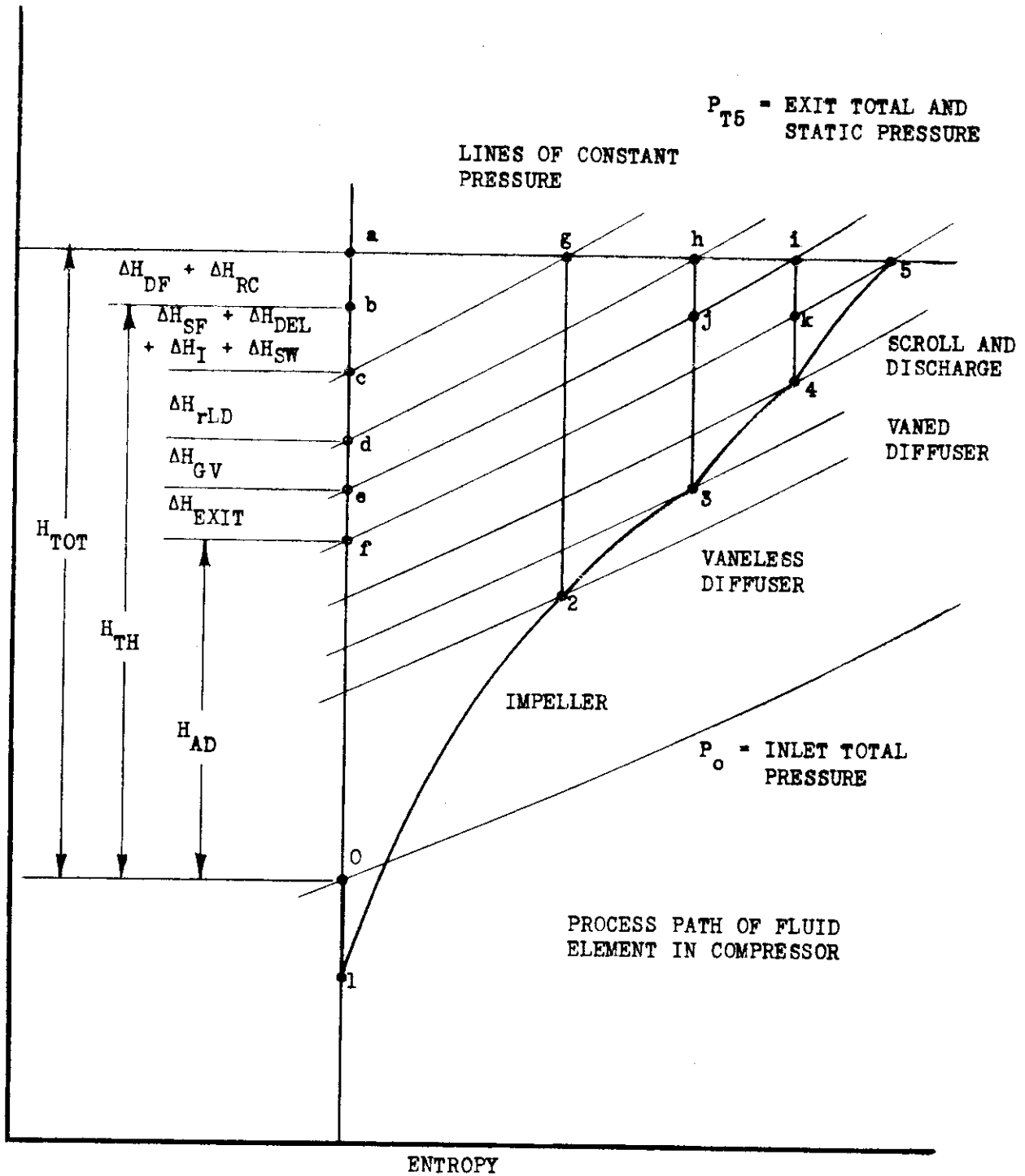
SKETCH 2.1

In the subsequent development, lower case  h  represents the enthalpy at a state, whereas capital  H  represents head or enthalpy differences.  If this entire work were added reversibly and adiabatically, the exit state of the fluid would be at a , and the whole amount of energy would be available for useful work in an expansion process between the pressures corresponding to states a and o.  However, because of irreversibilities (principally viscous effects) some of this energy is made unavailable for useful work in an expansion.  That is, the losses result in a decrease in discharge pressure of the compressor, and thereby reduce the pressure ratio available to a subsequent expansion process.  Sketch 2.1 shows that the total losses have reduced the pressure from that at $\underline{a}$ to that at $\underline{f}$.

The losses, then, reflect pressure reductions.  A convenient way of measuring these reductions is in terms of the enthalpy differences between constant pressure lines from various points in the compressor as they intercept the isentrope through the initial state.  In Figure 2.1, these intercepts are designated $\underline{a}$, $\underline{b}$, $\underline{c}$, $\underline{d}$, $\underline{e}$, $\underline{f}$. It is convenient principally because it leads directly to a calculation of the compressor efficiency.  That is, from the usual definition of adiabatic, or isentropic, efficiency the above loss measurements give

$$\eta_{AD} = \frac{H_{TOT} - \Sigma\ LOSSES}{H_{TOT}} = \frac{H_{AD}}{H_{TOT}} \qquad (2.2)$$

where  $H_{AD}$  is the work required to produce the actual discharge pressure by an isentropic process.  (See Sketch 2.1.)  Thus it is necessary only to sum directly the losses computed in this way to determine the efficiency.  It is these losses, then, which are the principal concern of any performance prediction method.  It is important to have a good qualitative idea of the origins of the losses before any quantitative evaluation is attempted.  Consequently, a brief outline of a general nature is given below.

### 2.3.1  Sources of Losses

In deriving the AiResearch approach to the performance prediction, a critical re-examination of the sources of centrifugal compressor losses was made.  After studies of the literature noted above and of AiResearch experience the following division of losses was constructed:

Impeller Internal Losses - losses associated with the flow inside the impeller passages.

Skin Friction - losses due to shear forces exerted on the fluid in the boundary layer; "pipe friction" type.

Diffusion and Blade Loading Losses - losses due to boundary layer growth and separation, and secondary flows.

Blade Incidence Losses - losses due to boundary layer separation at the leading edge of the inducer blades, at off-design angles of attack

**Shock Wave Losses** - losses resulting from shock waves formed in supersonic flow, including direct total pressure losses through the wave and boundary layer separation caused by shock interaction.

**Impeller External Losses** - losses chargeable to the impeller but occurring externally to the flow passages.

    **Disk Friction** - losses due to shearing of fluid in any spaces between the wheel and stationary boundaries.

    **Recirculation Loss** - loss involved in the backflow of fluid from the diffuser into the impeller, caused by the action of the diffuser static pressure gradient in forcing inward fluid which has lost most of its kinetic energy in the boundary layer at the diffuser walls.

**Diffuser Losses**

    **Vaneless Diffuser Losses** - losses due to skin friction

    **Vaned Diffuser Losses** - losses due to skin friction and boundary layer growth up to separation

**Exit Losses** - losses occurring in any collector ring or scroll, and in the discharge to a plenum chamber.

These divisions are not all mutually exclusive, nor do they always represent a single physical phenomena. It is believed that they go as far towards considering separate phenomena as is justifiable at the moment, in view of the amount and quality of the currently available information. Even this detailed a breakdown is stretching our knowledge to the limit. Further discussion will be made as the loss expressions are developed.

### 2.3.2 Loss Definitions

With these general considerations of losses in mind, definitions can now be made. Referring to Sketch 2.1:

$$\Sigma \text{ Impeller Losses } = \Delta H_{IMP. \; TOT.} = h_a - h_c \qquad (2.3)$$

$$\Sigma \text{ Impeller External Losses } = \Delta H_{IMP. \; EXT} = h_a - h_b \qquad (2.4)$$

$$\Sigma \text{ Impeller Internal Losses } = \Delta H_{IMP.} = h_b - h_c \qquad (2.5)$$

$$\text{Vaneless Diffuser Loss } = \Delta H_{VLD} = h_c - h_d \qquad (2.6)$$

$$\text{Vaned Diffuser Loss } = \Delta H_{GV} = h_d - h_e \qquad (2.7)$$

$$\text{Exit Loss } = \Delta H_{EXIT} = h_e - h_f \qquad (2.8)$$

The impeller losses are further broken down, as indicated previously, to give these additional definitions:

### Internal

Impeller Skin Friction Loss = $\Delta H_{SF}$ 　　　　(2.9)

Diffusion and Blade Loading Loss = $\Delta H_{DBL}$ 　　　　(2.10)

Blade Incidence Loss = $\Delta H_I$ 　　　　(2.11)

Shock Wave Losses = $\Delta H_{SW}$ 　　　　(2.12)

### External

Disk Friction Loss = $\Delta H_{DF}$ 　　　　(2.13)

Recirculation Loss = $\Delta H_{RC}$ 　　　　(2.14)

The impeller internal losses occur simultaneously and no further breakdown with respect to pressures between $h_b$ and $h_c$ is desirable; only the net reduction of pressure at the impeller exit is of any significance. The external losses are also not separable with respect to effects on pressure.

The discussion so far has been conducted on the assumption that $H_{TOT}$, the total work done, is known. Such is the case when experimental data for a given compressor is being considered; or, in a performance prediction study this could be an assumed quantity. However, it is somewhat more logical to work with the "Theoretical Head" = $H_{TH}$, which is also known as the Euler work, or Euler head. This quantity is given by the well-known Euler relation (along a streamline)

$$H_{TH} = \frac{u_2 c_{u_2} - u_1 c_{u_1}}{g} \qquad (2.15)$$

where the velocities are defined in Figure 2.1. This relation gives the work imparted to the fluid through the change in its angular momentum, and is the governing factor in determining the pressure ratio which the compressor can deliver. A given value of $H_{TH}$ will fix the pressure ratio within ±5 per cent, for reasonable efficiencies. The total head is related to $H_{TH}$ by

$$H_{TOT} = H_{TH} + \Sigma \text{ Impeller External Losses} \qquad (2.16)$$

(In reality this constitutes a definition of the <u>division</u> between internal and external impeller losses.) From Equation (2.16) <u>it might</u> appear that $H_{TOT}$ would determine the pressure ratio equally as well as $H_{TH}$, but, in general, the work done in overcoming the external impeller losses cannot be made available for useful work. A reduction in these losses does not imply an increase in discharge pressure.

Throughout the present study, then, $H_{TH}$ will be a fundamental parameter. Due to the near constancy of pressure ratio for a given $H_{TH}$, this quantity will be used in place of pressure ratio as a primary independent variable. This results in great simplifications in the computing procedure, since fixing the pressure ratio would have required an extensive iteration to obtain the desired value.

## 2.3.3 Dimensionless Loss and Head Definitions

It is natural in a generalized study such as this to employ dimensionless variables. A logical way to make the various heads or losses dimensionless is to divide by $u_2^2/g$, which represents the maximum theoretical head for a straight bladed impeller with no pre-whirl. The dimensionless heads will be given the symbol $q$ and the losses $\Delta q$, essentially following Balje's notation. Thus the previous expressions become, in dimensionless terms,

### 2.3.3.1 Losses

$$\text{Impeller External Losses} = \Delta q_{IMP\ EXT} = \Delta H_{IMP\ EXT}/(u_2^2/g) \qquad (2.4a)$$

$$\text{Impeller Internal Losses} = \Delta q_{IMP} = \Delta H_{IMP}/(u_2^2/g) \qquad (2.5a)$$

$$\text{Vaneless Diffuser Losses} = \Delta q_{VLD} = \Delta H_{VLD}/(u_2^2/g) \qquad (2.6a)$$

$$\text{Vaned Diffuser Losses} = \Delta q_{GV} = \Delta H_{GV}/(u_2^2/g) \qquad (2.7a)$$

$$\text{Exit Loss} = \Delta q_{EXIT} = \Delta H_{EXIT}/(u_2^2/g) \qquad (2.8a)$$

$$\text{Impeller Skin Friction Loss} = \Delta q_{SF} = \Delta H_{SF}/(u_2^2/g) \qquad (2.9a)$$

$$\text{Diffusion and Blade Loading Loss} = \Delta q_{DBL} = \Delta H_{DBL}/(u_2^2/g) \qquad (2.10a)$$

$$\text{Blade Incidence Loss} = \Delta q_I = \Delta H_I/(u_2^2/g) \qquad (2.11a)$$

$$\text{Shock Wave Losses} = \Delta q_{SW} = \Delta H_{SW}/(u_2^2/g) \qquad (2.12a)$$

$$\text{Disk Friction Losses} = \Delta q_{DF} = \Delta H_{DF}/(u_2{}^2/g) \qquad (2.13a)$$

$$\text{Recirculation Loss} = \Delta q_{RC} = \Delta H_{RC}/(u_2{}^2/g) \qquad (2.14a)$$

## 2.3.3.2  Heads

$$\text{Total Head or Total Work} = q = H_{TOT}/(u_2{}^2/g) \qquad (2.1a)$$

$$\text{Theoretical Head or Euler Work} = q_{TH} = H_{TH}/(u_2{}^2/g) \qquad (2.15a)$$

$$\text{Adiabatic Head} = q_{AD} = H_{AD}/(u_2{}^2/g) \qquad (2.17)$$

## 2.3.4  Impeller Efficiency

In addition to the overall adiabatic compressor efficiency, it is very useful to define an impeller efficiency. As in the overall efficiency, the impeller efficiency is based on the total pressure at the impeller exit. Thus (see SK 2.1)

$$\eta_{AD\ IMP} = \frac{h_c - h_o}{H_{TOT}} = \frac{q_{AD\ IMP}}{q}$$

where

$$(2.18)$$

$$q_{AD\ IMP} = q_{TH} - (\Delta q_{SF} + \Delta q_{DBL})$$

Before proceeding with the development of the equations for determining these losses, it should be noted that no blade incidence losses will be considered here. In line with the philosophy that this will be a design point study, it is clear the incidence angle may be assumed zero, and therefore, the incidence loss is zero. However, in case of supersonic regions, within the impeller passages, shock wave losses have to be introduced. It can be shown that the shock wave losses, which are equivalent to the entropy change through the shock waves, are small so that they can be neglected if the inlet portion of the impeller is reasonably designed. A more important part of the losses in supersonic flow is due to boundary layer separation as a result of interaction of shock waves and the boundary layer. These losses are to a certain extent being taken care of by the diffusion and blade loading loss since they result from attempting to produce a loading of the blades in subsonic as well as in supersonic flow. Summarizing, supersonic phenomena are assumed to follow the subsonic loss pattern and are taken care of as such. In case of strong supersonic flows, this method of loss calculation may be somewhat on the low side and efficiencies may therefore be regarded as upper limits.

## 2.4 Equations for Head and Loss Estimation

Because of the complex three-dimensional nature of the flow in centrifugal compressors, a theoretical prediction of the flow behavior and therefore of the losses is extremely difficult. At present only a one-dimensional approach is justifiable, and heavy reliance must be placed on experimental data to provide the proper coefficients to the one-dimensional equations. By careful examination of AiResearch experimental results, of data in the literature, and by application of the experience of AiResearch personnel, the equations and coefficients which will be found in the following development were evolved. It is believed that the magnitudes are reasonable, and that the trends predicted by the one-dimensional theory are essentially confirmed by tests. In the cases of the diffusion and blade loading loss, and the recirculation loss, experimental results were too meager to be of much assistance. The expressions for these losses can only be regarded as hypotheses.

Some of the proposed equations may be questioned, but it is hoped that interest will be stimulated, leading to an improved prediction. It should be noted in advance, however, that the overall performance still seems to hinge on the already well-established concepts of disk friction and internal skin friction in impeller and diffuser. Thus, the essential trends are given considerable credence, and only the lesser variations are considered as tentative.

It is convenient first to write down the relations between the dimensionless heads and losses. These follow from Sketch 2.1 and the definitions given above.

$$q_{AD} = q_{TH} - \underbrace{(\Delta q_{SF} + \Delta q_{DBL} + \Delta q_{ULD} + \Delta q_{GV} + \Delta q_{EXIT})}_{\text{Total Internal Losses}} \qquad (2.19)$$

$$q = q_{TH} + \underbrace{(\Delta q_{DF} + \Delta q_{RC})}_{\substack{\text{Impeller External} \\ \text{Losses}}} \qquad (2.20)$$

$$\eta_{AD} = \frac{q_{AD}}{q} \qquad (2.2a)$$

From these equations it is clear that all one needs to know is $q_{TH}$ and the Losses.

### 2.4.1 Theoretical Head - Slip Calculations

By expanding Equation 2.15a there follows

$$q_{TH} = \frac{c_{u2}}{u_2} - \frac{u_1}{u_2} \frac{c_{u1}}{u_2} \qquad (2.15b)$$

It is seen that $q_{TH}$ is dependent on the tangential component of the inlet absolute velocity. This component is referred to as "prewhirl" and generally occurs only when inlet guide vanes are employed to turn the flow from the axial direction. Prewhirl is of interest as a possible means of improving compressor performance, and such is studied as a separate topic in this report (Section IV).

The considerations presented in this section will be made entirely for the case of zero prewhirl, i.e., $c_{u1} = 0$. It is logical to make this separation since the normal compressor without inlet guide vanes will have zero prewhirl, and the possible benefits of adding prewhirl must then be separately balanced against the losses with these guide vanes. Thus, for the case of zero prewhirl

$$q_{TH} = \frac{c_{u2}}{u_2} \qquad (2.15c)$$

It will be noted in the prewhirl study that $c_{u2}/u_2$ is given the symbol $\lambda$. Here, however, the emphasis is generally on the quantity $q_{TH}$ as representing the theoretical head, so the symbol $q_{TH}$ will be retained.

From Figure 2.1 it is seen that $q_{TH}$ is determined by certain quantities in the exit velocity triangle.

$$q_{TH} = \frac{u_2}{u_2} - \frac{w_{uB2}}{u_2} - (\xi = \text{"slip"}) = 1 - \xi - \frac{c_{m2}}{u2} \tan\beta_{B2} \qquad (2.21)$$

The "slip", $\xi$, is the result of the fact that for a finite number of impeller blades the mean flow at the exit is not guided perfectly by the blades, but emerges at an angle somewhat different from the blade angle, $\beta_{B2}$. $\xi$ is defined by

$$\xi = \frac{c_{u2\infty} - c_{u2}}{u_2} = \frac{w_{u2} - w_{u2\infty}}{u_2} \qquad (2.22)$$

where $c_{u2\infty}$ is the tangential component of the absolute velocity for the case of infinitely many blades. This slip may be predicted by inviscid theory as has been done by Busemann, Reference 2.12, Stodola, Reference 2.13, Eckert, Reference 2.14, and others. For this study a modified form of Eckert's equation will be used. The expression is

$$1 - \xi = \frac{1}{1 + K_f \dfrac{\pi \cos\beta_{B2}}{2z \left(1 - \dfrac{d_{FL}}{D}\right)}} \qquad (2.23)$$

where $Z$ = number of impeller blades

$d_{FL}$ = diameter of mean flow stream surface at inlet

$D$ = impeller diameter

$K_f$ = factor modifying Eckert expression to allow for viscous effects

The factor $K_f$ is intended to represent the effect of boundary layer growth on the streamline pattern at the exit. The present estimate of this factor is

$$K_f = 1 + \frac{0.08}{(w_2/w_i)^2} \qquad (2.24)$$

Greater deceleration (smaller $w_2/w_i$) leads to larger boundary layers and to increased accumulation on the suction side near the tip. It is believed that this causes greater streamline deviation from the blades and therefore greater slip.

Having estimated the slip, then $q_{TH}$ is determined by the exit meridional velocity ($c_{m2}/u_2$). Now, as discussed before, the quantity $H_{TH}$ is the principal factor in fixing pressure ratio. Thus if, for convenience, $H_{TH}$ is assigned a value, and if $q_{TH}$ is known, then from Equation (2.15a) the required tip speed $u_2$ can be found. In order to keep everything in dimensionless terms it is desirable to express the tip speed as

$$M_T = \frac{u_2}{a_o} \qquad (2.25)$$

where $a_o$ = speed of sound at ambient total conditions

Therefore (2.15a) becomes

$$q_{TH} = \frac{(gH_{TH}/a_o{}^2)}{M_T{}^2} \qquad (2.26)$$

and it is clear that $(gH_{TH}/a_o{}^2)$ is the appropriate quantity to prescribe in place of $H_{TH}$. Then, given $(gH_{TH}/a_o{}^2)$ and knowing $q_{TH}$, the required tip Mach number $M_T$ is determined.

## 2.4.2 Impeller Skin Friction Loss, $\Delta q_{SF}$

A suitable approximation to the impeller skin friction loss is given by the pipe friction type of equation. This gives

$$\Delta q_{SF} = K_1 (4f) \frac{L}{d_{HYD}} \frac{w_{AVE}^2}{2g} \frac{1}{u_2^2/g} \tag{2.27}$$

where $K_1$ = an empirical constant

$f$ = the Fanning friction factor

$L$ = length along mean flow path

$d_{HYD}$ = mean hydraulic diameter of impeller flow passage

$w_{AVE}$ = mean relative velocity

The length, $L$ may be approximated by

$$\frac{L}{D} = \frac{(r_2 - r_{FL})}{D \cos \beta_{B2}} = \frac{1}{2} \frac{(1 - d_{FL})}{\cos \beta_{B2}} \tag{2.28}$$

The hydraulic diameter, $d_{HYD}$, is the mean between inlet and exit, and is given by

$$\frac{d_{HYD}}{D} = \frac{1}{\frac{Z}{\pi \cos \beta_{B2}} + \frac{D}{b}} + \frac{d_i/D}{\frac{2}{1-\nu} + \frac{2Z}{\pi(1+\nu)}\sqrt{1+\tan^2 \beta_i (\frac{1+\nu^2}{2})}} \tag{2.29}$$

where $b$ = width of flow passage at impeller tip

$\beta_i$ = blade angle at inducer tip

The average relative velocity, $w_{AVE}$, is the mean between inlet (at $d_{FL}$) and exit. Thus

$$\left(\frac{w}{u_2}\right)^2_{AVE} = \frac{1}{2}\left[\phi^2 + \left(\frac{d_{FL}}{D}\right)^2 + \left(\frac{w_2}{w_i}\right)^2 \left(\phi^2 + \frac{d_i^2}{D^2}\right)\right] \tag{2.30}$$

where $\phi$ = flow factor $\frac{c_{m1}}{u_2}$

The final expression for $\Delta q_{SF}$ is then, including the empirical constant,

$$\Delta q_{SF} = 1.40 \, (4f) \, \frac{(L/D)}{(d_{HYD}/D)} \, \left(\frac{w}{u_2}\right)^2_{AVE} \tag{2.27a}$$

in which $L/D$, $d_{HYD}/D$, and $(w/u_2)^2_{AVE}$ are given by Equations (2.28), (2.29), and (2.30), respectively.

The friction factor may be found from curves such as those of Moody, Reference 2.15. For the present study a single curve of $4f$ ("large" friction factor) vs Reynolds number was used; this was for a roughness ratio of 0.0002. The Reynolds number which characterizes the impeller flow passages is

$$Re_{IMP} = \frac{w_{AVE} \, d_{HYD}}{(\mu/\rho)_o} = \left(\frac{w_{AVE}}{u_2}\right) \left(\frac{d_{HYD}}{D}\right) \, Re_t \tag{2.31}$$

where the "tip" Reynolds number $Re_t$ is

$$Re_t = \frac{u_2 \, D}{(\mu/\rho)_o} \tag{2.32}$$

The quantity $(\mu/\rho)_o$ is the kinematic viscosity at the ambient total conditions.

## 2.4.3 Diffusion and Blade Loading Losses

The boundary layer growth in the impeller appears to be governed by a "diffusion factor" of the type derived by Lieblein, Reference 2.11, for axial compressor stages. A derivation similar to this was made for centrifugal compressors. This was done for two types of blade loading: (1) uniform loading, in which velocity differences between one side of the blade and the other are essentially constant along the blade length; and (2) linearly increasing loading, in which the velocity difference increases linearly along the blade length. Since uniform blade loading appears to be the most promising way of designing efficient, high-pressure ratio impellers, the final expression for the diffusion factor of a centrifugal compressor reflects this design philosophy. The diffusion factor, $\Delta$, is then given by

$$\Delta = 1 - \frac{w_2}{w_i} + \frac{0.75 q_{TH}}{w_i/\mu_2 \left[\frac{Z}{\pi}\left(1 - \frac{d_i}{D}\right) + 2\frac{d_i}{D}\right]}$$

The expression for $\Delta q_{DBL}$ which is proposed, based on AiResearch experience, is

$$\Delta q_{DBL} = 0.050 \ \Delta^2 \qquad (2.34)$$

### 2.4.4 Disk Friction

Disk friction may be computed satisfactorily by an equation of the type given by Baljé, Reference 2.1. Instead of assuming that the loss factor varies with $(Re_t)^{1/5}$, which is only valid for lower turbulent Reynolds numbers, this factor was converted to the corresponding Moody friction factor at $Re_t = 10^6$ and relative roughness of 0.0002. The equation used is as follows:

$$\Delta q_{DF} = \frac{0.120 \ (4f) \ (1 + \rho_2/\rho_1)}{\phi \ (d_i/D)^2} \qquad (2.35)$$

### 2.4.5 Recirculation Loss

As indicated previously, the recirculation loss represents the additional work done on fluid which has not sufficient momentum to withstand the pressure gradient of the mean flow in the diffuser and is forced back into the impeller at the tip. It is physically clear that if the fluid were to enter the diffuser in a purely radial direction, then the potential for recirculation would be exceedingly small. The diffuser boundary layer would have to develop and then separate before back-flow could take place, and this would generally occur sufficiently far from the impeller to preclude recirculation. Thus, the loss depends on $\alpha_2$ (the exit absolute flow angle) in some manner. Now, since this work will exist even for zero through-flow, then the loss per pound of flowing fluid is infinite, and it appears that a reasonable expression for the functional dependence on $\alpha_2$ is $\tan \alpha_2$.

Furthermore, as the impeller boundary layer profile becomes worse, the proportion of fluid which has a large $\alpha_2$ associated with it becomes greater.

This is indicated by Sketch 2.1. Thus the recirculation must depend on the diffusion factor, $\Delta$. As a tentative expression for this loss the following simple equation is proposed:

MAIN FLOW
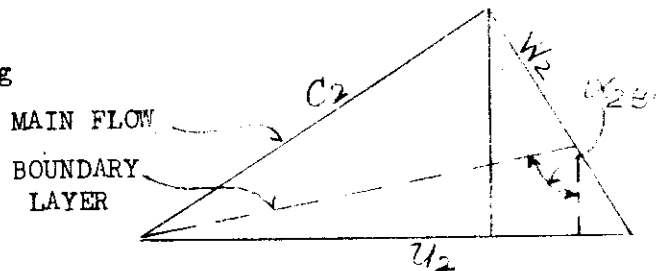
BOUNDARY LAYER

SKETCH 2.2

Velocity diagram for Boundary Layer Flow in Impeller

$$\Delta q_{RC} = 0.020 \tan \alpha_2 \, \Delta \tag{2.36}$$

For reasonable values of $\alpha_2$ this loss is small. But for the large $\alpha_2$ found, say in water pumps at low flows, the loss is quite appreciable (see Reference 2.2).

### 2.4.6  Vaneless Diffuser Losses

In Section V of this report, an extensive analysis of the performance of a vaneless diffuser is made. The methods and solutions presented there have a degree of accuracy which is not required for this general study and are somewhat too time consuming for the purpose intended. Consequently, they were simplified, the modification being a semiempirical alteration of the relation between velocity and radius to help account for compressibility effects. The incompressible equation gives all the major factors affecting vaneless diffuser performance, so that it is quite satisfactory as a comparative measure of losses. Furthermore, it is the radial component of velocity which governs the compressibility effects, and in the present study this component generally represents a Mach number of less than 0.7.

The incompressible problem has been considered by many investigators. Reference 2.9 covers the topic quite well, as does Reference 2.16. The differential equation for the loss is

$$dH_{VLD} = \left( \frac{4f}{8} \quad \frac{D}{b} \right) \frac{1}{\cos \alpha} \quad \frac{c^2}{g} \quad d\left( \frac{r}{r_2} \right) \tag{2.37}$$

where      $c$ = the velocity in the vaneless diffuser

              $r$ = radius to point on vaneless diffuser

Now from the calculations for some cases of compressible flow in Reference 2.10, it is found that the following relation between Mach number and radius is approximately true:

$$\frac{M_c^2}{M_{c2}^2} \approx \left( \frac{r_2}{r} \right)^{2.5} \tag{2.38}$$

To the same degree of approximation, it is also true then that

$$\frac{c^2}{c_2^2} \approx \left( \frac{r_2}{r} \right)^{2.5} \tag{2.39}$$

A further simplifying assumption is that $\alpha = \alpha_{AVE}$ = Const. This is actually a very good assumption in most cases.

Introducing Equation (2.39) into (2.37), integrating, and putting into the dimensionless form, there results

$$\Delta q_{VLD} = \frac{1}{1.5} \left(\frac{D}{d_3}\right)^{1.5} \left(\frac{4f}{8} \quad \frac{D}{b}\right) \frac{(c_2/u_2)^2}{\cos^2 \propto_{AVE}} \tag{2.40}$$

### 2.4.7 Vaned Diffuser Losses

Vaned diffusers are given extensive consideration in Section V of this report. Out of the theory and experimental data studied in that section a method was evolved for determining the optimum performance of a vaned diffuser, and the losses associated with this performance. For a compressor diffuser, optimum performance generally means maximum pressure recovery. Now the maximum pressure recovery depends principally on the flow conditions entering the guide vanes, that is, on the boundary layer momentum thickness and the shape parameter. Thus, a study was made which is represented in the appendix to determine approximately the relation between these two boundary layer parameters and the factors governing impeller and vaneless diffuser performance. After examining the available data on velocity profiles coming out of impellers and passing through vaneless diffusers, the following was concluded; (1) on the basis of rather limited information the boundary layer thickness and shape parameter at the impeller exit could be reasonably well correlated to the impeller deceleration ratio, $w_2/w_i$; and (2) the rather short lengths of vaneless diffusers required in the present study (to bring the Mach number to about 0.85) would have small effect on the boundary layer for reasonable initial conditions.

The relations between momentum thickness, shape parameter, and $w_2/w_i$ which were adopted for this study are shown in Figure 2.2. It shows that the greater the deceleration in the impeller (smaller $w_2/w_i$), the larger the boundary layer thickness and the "worse" its shape, equivalent to a larger shape factor, H.

Having the initial conditions expressed in terms of $w_2/w_i$ makes it possible to put the diffuser performance in terms of $w_2/w_i$. In addition, the friction factor of the guide vane flow passages must be known. The latter is determined by the Reynolds number of the entering flow based on the equivalent cone diameter of the entrance to the guide vanes. The resulting curves which determine guide vane performance are given in Figures 2.3, 2.4 and 2.5.

In Figure 2.3 is presented the loss coefficient defined as (refer to Sketch 2.1 for symbols)

$$\zeta_{GV} = \frac{h_h - h_j}{c_3^2/2g} \tag{2.41}$$

Given as a function of friction coefficient $\lambda$, which in turn is dependent on the Reynolds number, note that this loss is given in terms of entering conditions

into the diffuser, whereas all previous losses were immediately defined along the initial isentrope. Thus, the quantity $(h_n - h_j)$ must be related to $(h_d - h_e)$, Sketch 2.1, in order to obtain the correct $\Delta q_{GV}$. Since these two quantities lie between the same pair of constant pressure lines, the relation, assuming constant specific heats, is simply

$$\frac{h_d - h_e}{h_h - h_j} = \frac{T_d}{T_h} \tag{2.42}$$

This may be expressed in terms of previous losses by

$$\frac{h_d - h_e}{h_h - h_j} = \frac{T_j}{T_h} = \frac{1 + (k-1) M_T^2 (q_{TH} - \Delta q_{SF} - \Delta q_{DBL} - \Delta q_{VLD})}{1 + (k-1) M_T^2 q} \tag{2.43}$$

The final loss expression is then

$$\Delta q_{GV} = \zeta_{GV} \frac{1}{2} \left(\frac{c_3}{u_2}\right)^2 \frac{1 + (k-1) M_T^2 (q_{TH} - \Delta q_{SF} - \Delta_{DBL} - \Delta q_{VLD})}{1 + (k-1) M_T^2 q} \tag{2.44}$$

The velocity ratio of the diffuser which corresponds to the maximum pressure rise is shown in Figure 2.4. Finally, Figure 2.5 gives the length of flow passage required to perform this diffusion. From this length and the inlet flow angle the outer diameter of the diffuser may be estimated. The different outlet diameter (or rather its ratio to the impeller diameter) is thus a dependent variable in this generalized study. This was felt desirable in order to carry through the concept of a design point study, since maximum pressure recovery will generally be a design condition. It should be pointed out that the diameter so calculated in this study is a limiting value; it is probable that this diameter could be materially reduced in any real problem without a great sacrifice in performance.

## 2.4.8 Exit and Scroll Lines

In view of the large number of ways in which the flow from the diffuser may be handled (scrolls of many kinds, collector rings, discharge to a plenum or combustion chamber, etc), and in view of the generally small energy available for further recovery, it was decided to make an exit loss which was very simple yet indicative of the more typical cases. The loss was taken to be half of the kinetic energy leaving the diffuser. This is, of course, a very sweeping assumption, but it does not affect the value of this study as a comparative measure of performance. The only purpose of this loss is to make the final values of efficiency, etc , somewhat more realistic. This loss is given by

$$\Delta q_{EXIT} = 0.5 \frac{c_4^2}{2 u_2^2} = \frac{1}{4} \left(\frac{c_4}{u_2}\right)^2 \tag{2.45}$$

## 2.5 Some Additional Relations

In addition to the foregoing equations, continuity and energy relations must be used to make performance calculations. A dynamic equation for the impeller has already been used in Equation (2.20). The continuity equation for the impeller yields the following:

$$c_{m1} \ A_1 \ \rho_1 = c_{m2} \ A_2 \ \rho_2$$

$$\epsilon_1 \ \frac{c_{m1}}{u_2} \ \frac{\pi}{4} \ \frac{(d_i^2 - d_h^2)}{D^2} \ \rho_1 = \epsilon_2 \ \frac{c_{m2}}{u_2} \ \frac{\pi D b}{D^2} \ \rho_2 \tag{2.46}$$

$$\frac{D}{b} = \frac{4 \ (\epsilon_2/\epsilon_1) \ (c_{m2}/u_2) \ (\rho_2/\rho_1)}{\phi \ (d_i/D)^2 \ (1 - \nu^2)}$$

$\epsilon$ is the flow blockage factor; the ratio $\epsilon_2/\epsilon_1$ of the blockage factor at inlet and exit of the impeller was assigned the value of 0.95 in the present study. Energy equations are used in many places to express temperature in the terms of the heads and head losses. The most important relation of this type relates temperature $T_f$, associated with the intercept of the exit pressure line and the initial isentrope (Sketch 2.1), and the ambient total temperature.

$$\frac{T_f}{T_o} = 1 + (k-1) \ M_t^2 \ q_{AD} \tag{2.47}$$

This relation then yields the overall compressor pressure ratio $\frac{P_{T5}}{P_o}$ by introducing the isentropic relation between pressure and temperature at $f$ and $o$. Thus

$$\frac{P_{T5}}{P_o} = \left[1 + (k-1) \ M_t^2 \ q_{AD}\right]^{\frac{k}{k-1}} \tag{2.48}$$

It is of interest to further express $q_{AD}$ in terms of $\eta_{AD}$, $q_{TH}$, and external losses.

$$\frac{P_{T5}}{P_o} = \left[ 1 + (k-1)\, \eta_{AD}\, \frac{gH_{TH}}{a_o^2} \left( \frac{\Delta q_{DF}}{q_{TH}} + \frac{\Delta q_{RC}}{q_{TH}} \right) \right]^{\frac{k}{k-1}} \tag{2.49}$$

This equation shows why the quantity $gH_{TH}/a_o^2$ essentially determines pressure ratio, in particular for good designs.

Certain relations exist in and between the velocity triangles of the impeller. These are readily derivable and will only be stated here.

$$\frac{c_{m2}}{u_2} = \frac{(1-\xi_{i})}{\tan \alpha_2} \left( \frac{1}{1 + \dfrac{\tan \beta_{B2}}{\tan \alpha_2}} \right) \tag{2.50}$$

$$q_{TH} = (1 - \xi) \left( \frac{1}{1 + \dfrac{\tan \beta_{B2}}{\tan \alpha_2}} \right) \tag{2.51}$$

$$\frac{w_2}{w_i} = \frac{\sin \beta_i}{d_i/D} \sqrt{\left( \frac{c_{m2}}{u_2} \right)^2 + (1-q_{TH})^2} \tag{2.52}$$

$$\phi = \frac{d_i/D}{\tan \beta_i} \tag{2.53}$$

$$\frac{c_2}{u_2} = \frac{q_{TH}}{\sin \alpha_2} \tag{2.54}$$

## 2.6 Generalized Performance Calculations

### 2.6.1 Variables Involved

On examining all the foregoing equations it may be seen that centrifugal compressor performance may be expressed in terms of ten independent variables. The set of variables which appears to give the best presentation of performance is given in the following functional relations:

$$\eta_{AD} = f_1\left(\frac{d_i}{D}, \ \alpha_2, \ \beta_{B2}, \ \beta_i, \ \frac{gH_{TH}}{a_o^2}, \ Z, \ \nu, \ Z_{GV}, \ k\right)$$

$$\frac{P_{T5}}{P_o} = f_2 \ ( \qquad\qquad " \qquad\qquad ) \qquad (2.55)$$

$$\frac{d_H}{D} = f_3 \ ( \qquad\qquad " \qquad\qquad )$$

It is known from previous calculations of performance, from existing designs, and from basic flow considerations that some of these variables are only of secondary importance or that they must be fixed within certain limits for practical reasons. The number of guide vanes, $Z_{GV}$, in the vaned diffuser does not affect the performance significantly, as long as separation is avoided. Thus, $Z_{GV} = 23$ was assumed fixed for the calculations. The impeller blade number, Z, is more important; taking into account that stress limitations influence the blade thickness, 19 blades was considered a good choice.

The inlet hub-tip diameter ratio, $\nu$, is not of great importance; values between 0 and 0.5 yield little change in performance. $\nu = 0.4$ was assumed as a typical value, identical to about 15 per cent hub blocking, which allows for the shaft or other material near the axis. The quantity $\dfrac{a_o \rho_o D}{\mu_o}$ merely fixes the level of the Reynolds number, and was a given value which corresponds to the type of machinery covered by this study.

In addition to these four quantities, one other was held fixed in the generalized performance study. This was the inducer tip flow angle (equal to blade angle), $\beta_i$. It is known that for a given inlet relative Mach number, $M_{wi}$, there is an optimum angle $\beta_i$ for which the mass flow is a maximum. Expressing it differently this angle gives, for a given mass flow, the minimum $M_{wi}$. For a fairly wide range of subsonic Mach numbers, this angle is about $(\beta_i)_{OPT} \approx 60^o$. (See Section on

Prewhirl for a detailed study.) In case of incompressible flow (water pumps) this angle is about $55^\circ$. It is easily understood that the performance of a compressor will be good if the ratio of through-flow to inlet area is as large as possible, hence fixing the angle $\beta_i$ was felt to be a good preliminary optimization as well as an opportunity for reducing the large number of variables. In the present study, which will involve supersonic $M_{wi}$ in many cases, the value $\tan\beta_i = 2$ is used.

The diffuser arrangement assumed in this study consists of a vaneless, parallel wall diffuser extending from the impeller tip to a radius sufficient to $M_{c3} \leq 0.85$ at the entrance to a vaned diffuser, which in turn has a radius ratio sufficient to produce the maximum pressure recovery as discussed in Section 2.3.7.

In this general study, the ratio of specific heats k, was taken as 1.400 for air and k = 1.136 for Freon-11, which also was investigated.

It should be noted that after making the general study, each of the above fixed quantities ( $Z_{GV}$, $Z$, $\nu$, $a_0 D\rho_0/\mu_0$, $\beta_i$ ) was allowed to vary independently for a typical case. The results justified the assumptions, in general, and a discussion of those calculations will be made later on.

The remaining variables, $d_i/D$, $\alpha_2$, $\beta_{B2}$, and $gH_{TH}/a_0^2$, were judged to be the most important and were allowed to vary over fairly wide ranges so as to include all cases of interest. $gH_{th}/a_0^2$ was given four values to cover the range of pressure ratios from two to eight, which essentially covers the rotational Mach numbers required in the exhibit. $d_i/D$ varied from 0.2 to 0.8. $\alpha_2$ ranged from $55^\circ$ to $76^\circ$. $\beta_{B2}$ assumed values from $0^\circ$ to $65^\circ$.

For convenience in calculation, certain parameters were assumed in place of these particular variables, so the resulting values were usually fractional numbers. Since the study is intended mainly to show trends, no attempt was made to put all the basic variables into whole numbers and uniform intervals.

## 2.6.2  Results of Calculations

The principal results of the calculations for air employing the above assumptions are shown in Figures 2.6 through 2.14. Figures 2.6 through 2.9 show a more complete study for the case of $gH_{TH}/a_0^2 = 1.29$ $(P_{t5}/P_0 \approx 3.7)$. This case is typical of all pressure ratios studied. Figure 6 shows $\eta_{AD}$ vs $d_i/D$ with $\alpha_2$ as a parameter and for selected values of $\beta_{B2}$. The quantity $d_i/D$ is clearly the most important single variable. For highest efficiencies $d_i/D$ must be large, about 0.7 to 0.8. This is to be expected, since large $d_i/D$ implies a large through-flow relative to the surface area of the compressor, i.e., a high specific speed. For the high $d_i/D$, the flow should enter the diffuser rather steeply for best efficiency; i.e., $\alpha_2$ should be low, about $50^\circ$ to $55^\circ$. Also the blades should be straight-radial at at the exit, $\beta_{B2} = 0^\circ$.

A low $\alpha_2$ implies low recirculation losses, high $w_2/w_1$, and therefore a low diffusion factor and low diffusion and blade loading losses, and short diffuser flow path. Straight-radial blades mean highest $q_{th}$, which helps reduce the effect of losses on efficiency, and in addition, it means less impeller skin friction. At the same time, low $\alpha_2$ and zero blade angle means larger exit velocities and larger impeller relative velocities, so that it might be expected that some further study of these variables is required. For example, Figures 2.7, 2.8 and 2.9 show a detailed investigation of blade angle for the various $\alpha_2$, at $gH_{TH}/a_o^2 = 1.29$.

For the lowest $\alpha_2 = 55.3^o$, Figure 2.7 shows that a small exit blade angle is always best; angles between $0^o$ and $15^o$ are about equally good. Larger blade angles are decidedly poorer. For an intermediate $\alpha_2 = 68.2^o$, Figure 2.8 shows that backward curvature is beginning to give better efficiency for $d_i/D > 0.5$; the optimum $\beta_{B2}$ appears to increase with $d_i/D$ up to $\beta_{B2} = 40^o$ at $d_i/D = 0.7$, at which value further backward curvature does not pay. For a larger $\alpha_2 = 76^o$, Figure 2.9 shows that backward curvature is now very important, with optimum angles of about $40^o < \beta_{B2} < 60^o$ for $0.5 < d_i/D < 0.7$.

As regards $\alpha_2$ for a given blade angle, Figure 2.6 indicates that the optimum $\alpha_2$ increases as $d_i/D$ increases. For $0.2 < d_i/D < 0.4$, the optimum angle is about $76^o$; for $0.4 < d_i/D < 0.55$, the optimum is about $68^o$; and for $0.55 < d_i/D < 0.8$, the optimum is about $55^o$. One may well ask if an even lower $\alpha_2$ would be better at the higher $d_i/D$, say $d_i/D > 0.7$. An investigation was made in which $\alpha_2$ was varied, starting from a reference point for which $(\alpha_2)_{REF} = 55.3^o$, $(\beta_{B2})_{REF} = 0^o$, and $(d_i/D)_{REF} = 0.772$. The results are shown in Figure 2.10 for three different $gH_{TH}/a_o^2$. In all cases, there is an increase in efficiency when $\alpha_2$ was decreased. However, starting from values $\alpha_2 < 45^o$, the exit relative velocities are becoming supersonic, and it was felt that the losses involved in achieving such a flow would probably counterbalance any small gain of efficiency. Furthermore, the efficiency curve must come back down again, as has already happened for $gH_{TH}/a_o^2 = 0.776$ at $\alpha_2 = 42^o$, since impeller and vaneless diffuser skin friction losses are increasing rather rapidly. Thus, the subject was pursued no further.

It seems highly probable, though, for the type of diffuser arrangement assumed herein, that the angle $\alpha_2$ should be smaller than is generally employed in present practice. $\alpha_2 = 55^o$ would seem to be a good value to use, with $d_i/D \cong 0.75$ and $\beta_{B2} = 0$.

Figure 2.11 shows the results for the case of $gH_{TH}/a_o^2 = 0.776$, giving a pressure ratio of $P_{T5}/P_o \cong 2.3$. Only the more important regions were computed for this case, but the trends are very much the same as for $gH_{TH}/a_o^2 = 1.29$. Figure 2.12 is for $gH_{TH}/a_o^2 = 1.81$, and Figure 2.13 is for $gH_{TH}/a_o^2 = 2.33$, giving pressure ratios of about 5.6 and 8.0, respectively. It should be noted that a pressure ratio of 8.0 can apparently be achieved with $M_T = 1.70$ in air. This is definitely a possible value stresswise.

It is very interesting to note that the maximum computed efficiencies are virtually the same for all pressure ratios. The principal difficulty encountered at high pressure ratios is high inducer relative Mach numbers, implying some reduction of efficiency due to supersonic shock wave effects.

The effect of higher pressure ratio is seen by comparing Figure 2.13 with Figure 2.6. The trends are essentially the same, with efficiencies generally somewhat lower for the high pressure ratios.

Evidently, then, high pressure ratios can be achieved with good efficiency, providing that supersonic inducer problems can be solved. The study of supersonic flow in centrifugal impellers appears to be one of the more important research topics in this field.

Figure 2.14 shows the pressure ratios achieved by these various design conditions for the four values of $gH_{TH}/a_o^2$ which were investigated. The pressure ratios follow the efficiencies fairly closely, as would be expected from Equation (2.49). The figure shows, as stated previously, that in the region of higher efficiencies (larger $d_1/D$), the quantity $gH_{TH}/a_o^2$ determines pressure ratio within about 5 per cent. For lower efficiencies the deviation is much greater.

A word should be said about the overall diameter ratios, $d_4/D$ = outside diameter of guide vanes/impeller diameter, which are required for the above efficiencies and pressure ratios. Figures 2.15 and 2.16 show $d_4/D$ versus $d_1/D$, $\alpha_2$, and $\beta_{B2}$ for $gH_{TH}/a_o^2 = 1.29$ and 2.33, respectively. These plots correspond to the efficiencies given in Figures 2.6 and 2.13. For the two values of $gH_{TH}/a_o^2$ shown it is seen that $d_4/D$ is generally less than two; this is also true for the other $gH_{TH}/a_o^2$ investigated. The trend is for higher $d_4/D$ at the higher efficiencies, due mainly to the fact that the angles $\alpha_2$ are smaller and the velocities $c_2$ tend to be higher at the higher efficiencies. The diameters also tend to be larger for the higher pressure ratios, though the peak values are practically the same. The two $gH_{TH}/a_o^2$ shown are indicative of intermediate and lower values, and interpolation or extrapolation is quite satisfactory. As mentioned earlier, these diameter ratios are probably upper limits, though practical problems of collector rings, volutes, etc , might well require the ratios shown.

### 2.6.3 Freon Compressor Studies

Studies on Freon compressors were included in this study as required by the proposal. Quite generally, the theoretical approach to the design of freon compressors is the same as with air compressors. Certain pertinent differences, however, have to be pointed out.

An advantage of Freon turbomachinery compared to air is the fact that stress considerations influence the impeller design only to a very minor extent, since even a rotational Mach number of 2 requires no more than about 750 - 900 ft/sec tip speed. Hence the design of the impeller blades can be made on the basis of a three-dimensional theory which provides impeller shapes of completely arbitrary configuration. This especially means that the restrictions which are imposed on the design of air compressors by the necessity of having radial blades can be removed. This restriction is quite an obstacle to a good blade design, and the blade tilt can now be introduced in order to influence the meridional streamline. Tilt is specified as the angle between the intersection of the blade with a plane normal to the axis of rotation and a radial line.

The influence of the tilt can be used in order to eliminate the pressure drop along the shroud which occurs as a result of the turning of the flow from the axial towards the radial directions. A moving blade tilted in such a way that the high pressure side of the blade faces a passage wall reduces the meridional flow along this wall. Correspondingly, the meridional flow along the opposite passage wall is increased. By correctly applying tilt to the blade, the pressure and velocity distribution around the bend can, therefore, be improved considerably with a resulting reduction of losses in the remaining parts of the compressor. Quite generally, the restriction of having blades comprising only radial elements makes it difficult to select optimum deceleration rates for all streamlines from hub to shroud. With radial element blades the choice of the blade loading along one streamline, be it along the shroud or in the mean flow or at the hub, automatically fixes the loading distribution along the remaining streamlines, leaving no possibility to optimize these distributions. In Freon machinery, where the necessity of using radial element blades can be considerably relaxed, a better design can be accomplished.

With the exception of being able to use blades which do not consist of radial sections, the general considerations which lead to optimum design of air compressors apply to Freon too. They are, in short, considerations of the optimum geometry, which is equivalent to the concept of highest specific speed and consideration of the limits which are imposed on the aerodynamic design of diffusing machinery by the requirement that boundary layer separation has to be avoided in all parts of the turbomachine. The concepts, which lead to good aerodynamic performance of air compressors, however, are slightly modified in compressors for heavy gases (Freon), insofar that the specific heat ratio $c_p/c_v$ of these gases is considerably smaller than that of air, varying from 1.075 (Freon 113) to 1.14 (Freon 12). This drop of the $c_p/c_v$ value is equivalent to a much larger specific volume change for a given pressure change than with air, i.e., the process of compression approaches the isothermic process. In order to accommodate this trend, the outlet passages of the compressor (the tip width of the impeller and the diffusing parts) have to be made narrower than with air, if in both cases the deceleration is to be kept the same. This leads to a more unfavorable geometry of Freon compressors than exists

with air compressors. This disadvantage is partly offset by the lower friction loss of Freon machines which is due to the very low kinematic viscosity of the heavy gases. Hence, the Reynolds number of a Freon compressor is considerably larger than that of an air compressor of the same size.

With increased Reynolds number, however, the need for smoother surfaces is more critical, if the advantages of a high Reynolds number are to be utilized, as can be seen from any chart where friction coefficients vs Reynolds number with the surface roughness as a parameter are plotted. Smooth surfaces are, therefore, required for Freon compressors. This condition is sometimes difficult to maintain, since Freon corrodes most metals in the presence of some water.

Due to the different geometry of air and Freon compressors, an optimized Freon compressor cannot be used in tests with air and vice versa, since appreciable changes in performance result. If a Freon compressor with the usual backward-curved impeller blades is run with air, the meridional velocity at the impeller tip and in the diffuser is higher and the performance drops, due to a reduction of the work in the impeller and due to higher friction and incidence losses in the diffusing parts.

In view of the differences which exist between air and Freon compressors, as they are pointed out above, it appears to be absolutely necessary to use different designs for the study of air or Freon machinery. However, the basic design principles are more or less the same, and improvements in aerodynamic design can either be tested in air or Freon, depending on which facilities are most readily availabe.

With the above considerations in mind, performance calculations were made for one of the more conventional Freon compounds, F-11. The ratio of specific heats for the pressure and temperature range, which is customary for F-11, is $k = 1.36$.

The results of the calculation are presented on Figure 2.17, in the same manner as for the previous calculation for air. A head parameter $gH_{TH}/a_o^2 = 2.16$ was used, which is equivalent to a pressure ratio of about 6.8. The efficiencies are essentially the same as for air at the same pressure ratios. (Compare with Figures 2.12 and 2.13).

The pressure ratios are shown on Figure 14 along with those for air. It is seen that the parameter $gH_{TH}/a_o^2$ essentially gives the pressure ratio regardless of the value of k (within the limits given above, at least). Thus it appears that the present results of efficiency and pressure ratio are valid for any gas having $1.1 < k < 1.4$, and probably outside this range on the higher side of 1.4 as well. In the section on Prewhirl some more detailed studies are made with respect to Freon, and it is also concluded that the effect of k is negligible.

## 2.6.4 Impeller Performance

Part of the program of calculating overall performance was the computation of impeller efficiencies. These efficiencies, as defined in Equation (2.18) are presented in Figures 2.18, 2.19 and 2.20 for the heads $gH_{TH}/a_o^2 = 0.776$, 1.29 and 2.33, respectively. The trends are similar to those for overall efficiency, except that backward curvature has no beneficial effect on impeller efficiency for any of the cases computed. The optimum $\alpha_2$ values for various $d_i/D$ are still about the same as for overall performance, but straight radial blades at the exit are best for the impeller.

## 2.6.5 Study of Principal Dependent Variables

If one accepts the set of independent variables given in Equation (2.55), then all other parameters are, by definition only, dependent variables. For different types of studies, different sets of variables are given or known, and in each of these cases the prescribed values are logically considered as the independent variables. Rather than present efficiencies, etc , in terms of different sets of independent variables so as to cover these various cases, it is much simpler to show these other important parameters as dependent variables in terms of the one, consistent set of independent variables which has been used so far in this development. It is a relatively simple matter, then, to start from any of the various possible sets of given data and determine all the other performance parameters of interest.

In Figures 2.21 through 2.29 are presented the relations between the basic set of independent variables and $b/D$, $M_t$, $w_2/w_i$, $M_{wi}$ and dimensionless specific speed, $\eta$ (see Page 29), for both air and Freon. Figures 2.21 through 2.25 show $b/D$ vs $d_i/D$ with $\alpha_2$ and $\beta_{B2}$ as parameters for the four values of $gH_{TH}/a_o^2$ computed and for Freon. The tip width ratio, $b/D$, is seen to increase with increasing $d_i/D$, as would be expected from Equation (2.46). Referring back to the plots of efficiency, Figure 2.6 through 2.14, it may be seen that for a given $gH_{TH}/a_o^2$ the $b/D$ values corresponding to the best efficiency points at each $\alpha_2$ lie within a fairly narrow band. For $gH_{TH}/a_o^2 = 0.776$ the band is from 0.070 to 0.100; for $gH_{TH}/a_o^2 = 1.29$, it is from 0.050 to 0.070; for $gH_{TH}/a_o^2 = 1.81$, it is from 0.040 to 0.060; for $gH_{TH}/a_o^2 = 2.33$, it is from 0.040 to 0.050; for Freon with $gH_{TH}/a_o^2 = 2.16$, it is from 0.020 to 0.050. This trend as a function of pressure ratio is due mainly to the increasing density at the impeller exit, requiring a smaller passage width to produce the same exit velocity triangle.

Impeller tip Mach number $M_t$ is shown in Figure 2.26 for the various $gH_{TH}/a_o^2$ and Freon. For a given value of $gH_{TH}/a_o^2$, $M_t$ depends mainly on $\alpha_2$ and $\beta_{B2}$ . This is true because of the relation between $M_t$ and $q_{TH}$, Equation (2.26), and the fact that $q_{TH}$ depends principally on $\beta_{B2}$ and $\alpha_2$ in the present computations.

Furthermore, tip Mach numbers are lowest for the radial blade exit conditions. Thus, from the previous study of efficiency, it is seen that the best efficiencies are accompanied by low tip speeds, since $\beta_{B2} = 0$ (for the smaller $\alpha_2$) is indicated for the high efficiency points. This is a very gratifying state of affairs from the important standpoint of stresses in centrifugal machines. It is clearly seen that pressure ratios of eight (in air) can be expected with $M_t$ values of only 1.65, to 1.70; this is within present stress limits for air at reasonable temperatures.

Figure 2.27 shows the relation between $w_2/w_i$, $d/D$, $\alpha_2$, and $\beta_{B2}$ for any pressure ratio and any fluid, under the assumptions made for this study, of course. Equations (2.52), (2.51), (2.50), and (2.23) show that this unique relation exists. Referring back to the efficiency curves, it is seen that the best efficiency for a given $\alpha_2$ is found at a low value of $w_2/w_i$. But note that in moving from the best efficiency point at $\alpha_2 = 55.3°$ (increasing efficiency) the $w_2/w_i$ increases from 0.5 to 0.65. High efficiency is thus associated with $0.5 < w_2/w_i < 0.7$, with peak values to be found about $w_2/w_i = 0.65$.

Values of inlet relative Mach number at inducer tip, $M_{wi}$, are presented in Figure 2.28 for the various heads. As would be expected, $M_{wi}$ increases nearly linearly with $d_i/D$, since the inlet flow angle at the inducer tip, $\beta_2$ is held fixed in this study. Thus, since the higher efficiencies are found at larger $d_i/D$, it appears that the price of good performance is supersonic flow at the inducer tip. A "critical" Mach number at inducer tip $M_{wi} = 1.23$ is drawn on the figure. This Mach number corresponds to the case for which the mass-averaged relative Mach number is equal to one, or in other words, half the flow is supersonic and half is subsonic. This is not a limiting condition, but it should serve as a warning that designs at higher tip Mach numbers should be considered carefully.

Calculations were also made to show the relation between "specific speed" and performance in the generalized performance study. A dimensionless specific speed, $\nu$, was employed, wherein the volume flow was defined at the impeller inlet and the head was defined as the adiabatic head, $H_{AD}$. The defining equation is then

$$\nu = \left[\phi(d_i/D)^2 (1-\nu)\right]^{1/2} \left[q_{AD}\right]^{-3/4} \tag{2.56}$$

From the relation $\phi = (d_i/D)/\tan \beta_i$, and recalling that both $\beta_i$ and $\nu$ were held constant in these calculations it is evident that $\nu$ will be a strong function of $d_i/D$.

The results, shown in Figure 2.29, indicate this trend. Thus the concept of higher efficiencies at higher specific speeds is further verified by this study, since previous plots of $\eta_{AD}$ vs $d_i/D$ have shown clearly the general rise of efficiencies with increasing $d_i/D$.

## 2.7 Study of Variables Held Constant in Generalized Performance Calculations

At the beginning of the section on Generalized Performance Calculations, it was stated that certain of the variables of Equation (2.55) would be held constant, since they are either of secondary importance or the optimum was already known approximately. In order to verify the validity of these assumptions some calculations were made in which these fixed quantities were allowed to vary. A "typical point" was selected from the generalized calculations, and each of these quantities was allowed to vary, one at a time, from this initial point. Such a study is not totally conclusive, of course, since the effect of some variable may be much more when starting from one initial point, than from another. However, if the effects are not large, then the trends may be considered representative of a fairly wide variety of initial points. Such was generally the case here.

The "Typical Point" selected was

$$d_i/D = 0.606$$

$$\alpha_2 = 68.2^\circ$$

$$\beta_{B2} = 28^\circ$$

$$gH_{TH}/a_o^2 = 1.81$$

These conditions, for the previously stated values of $\beta_i$, $Z$, $Z_{GV}$, $Re_t/M_t$ and $\eta$ give

$$w_2/w_i = 0.60$$

$$D/b = 26.4$$

$$\phi = 0.303$$

$$M_t = 1.60$$

$$M_{wi} = 1.12$$

$$M_{c2} = 0.99$$

$$\eta_{AD} = 0.79$$

$$P_{T5}/P_o = 5.58$$

Now, holding all other variables in Equation (2.55) constant, the inducer tip flow angle $\beta_i$ was allowed to vary from $55^\circ$ to $68^\circ$. The effect of this change on $\eta_{AD}$ is shown in Figure 2.30. It is seen that the effect is rather small for these initial conditions; only a two per cent reduction from the initial efficiency is found. The peak values are found in the region of $55^\circ < \beta_i < 65^\circ$. Since the value used for the general study was $63.4^\circ$, then it is clear that this assumption was a reasonable one. For general design, however, a value around $60^\circ$ would seem more appropriate.

The effect of varying Reynolds number is shown in Figure 2.31. The "typical point" is for a 5-in. wheel at sea level conditions. It is implied that $M_t$ is fixed in this calculation and only $Re_t/M_t = a_o\rho_o/\mu_o$ is varying. The influence on $\eta_{AD}$ is similar to that found by many previous investigators. The present calculations have only considered $Re_t$ down to $10^5$. It is felt that considerable caution must be exercised for $Re_t < 10^5$, since it is believed possible that extensive laminar boundary layers may exist on the blades of some designs for lower Reynolds numbers. There is very little direct evidence of this for centrifugal machines; but axial cascade and compressor experiments indicate that large losses of performance may be encountered at low Reynolds numbers, due probably to laminar separation.

The effect of the inducer hub-tip diameter, $\eta = d_h/d_i$, is given in Figure 2.32. The effect is small between $0 < \eta < 0.6$, being less than a two per cent change of efficiency. Above $\eta > 0.6$, the reduction of through flow begins to have a strong effect. The assumption of $\eta = 0.4$ for the general study is observed to be quite satisfactory.

The effect of the number of guide vanes in the vaned diffuser, $Z_{GV}$, was computed and found to be wholly negligible. For this reason, no curve is shown for this variable.

The effect of the number of impeller blades, Z, was computed for the range $10 \leq Z \leq 30$. In this region the efficiency stays virtually constant, which is in essential agreement with the results of Reference 2.1; the differences lie only in the fact that different parameters were held fixed while varying Z. The reason for the small change in efficiency is that while some of the losses tend to increase with increasing numbers of blades, the value of $q_{TH}$ is also increasing, so that the efficiency changed very little. Similarly, pressure ratio stays very nearly constant. Since these changes are so slight, no curves will be presented to show the effect of Z. Reference 2.1 gives a reasonable picture of the influence of blade number and its optimization.

## 2.8  Clearance Effects

In a semishrouded impeller the blades are free at their outer radii, and a finite clearance must be maintained between the impeller blades and the stationary shroud. This situation gives rise to losses which result from vortex roll up and disintegration due to flow over the blade tips from pressure to suction side. For axial machinery, these losses appear to vary more or less linearly with clearance spacing, Reference 2.17. Data for centrifugal compressors is rather meager; Eckert (Reference 2.14) shows some results which indicate an increasing trend of loss with increasing clearance space, though Martinuzzi (Reference 2.18) shows some German DVL tests which incicate a reversal of this trend under certain conditions. A fully shrouded impeller (in which the shroud is fixed to the blades) eliminates this flow over the blade tips. It should be noted, though, that this tends to give rise to secondary flows from pressure to suction side on the inner side of the shroud, which when added to the skin friction of the relative flow on this new surface plus the disk friction between the outer side of the shroud and the surrounding fluid, may sometimes be worse than the vortices of semishhouded condition. In addition, for centrifugal machines there is the possibility of improving the boundary layer on the suction side somewhat, by the flow from the pressure side. Nonetheless, fully shrouded impellers do appear at the moment to be superior aerodynamically, though stress problems often prohibit their use.

Thus, it is not yet clear as to which configuration is best for various operating conditions. For the present study a semishrouded impeller was assumed, and a modified form of Baljé's loss equation was used. This question includes the clearance effect, and is intended to be representative of moderate clearances. Obviously, small impellers would suffer from increased clearance losses, since there is a lower practical limit on absolute clearance spacing. If it is assumed that this lower limit is, say, 0.020-in., and that the smallest impeller which would have this clearance and still maintain only the loss according to Equation (2.35) would have D = 5-in., then the clearance loss increase for impellers with $D < 5$-in. might be assumed proportional to $(5/D)$. If the clearance losses are about 1/3 of the total disk friction (including clearance effects), then the basic

disk friction would be modified to $(\Delta q_{DF})_{D < 5\text{-in.}} \approx \frac{1}{3}(2 + 5/D)_{\Delta q_{DF}}$. This is

a crude estimate intended only to indicate the trend.

## 2.9 Use of the Performance Curves

The use of the generalized performance curves is best illustrated by considering two classes of problems: (1) selection of a new design, and (2) analysis of a given design. Since pressure ratio is practically always used as a design parameter in place of $gH_{TH}/a_o^2$ , an auxiliary cross-plot of $P_{T5}/P_o$ vs $gH_{TH}/a_o^2$ is given in Figure 2.33 for the maximum pressure ratios at each $d_i/D$; this comes from the envelope of maximum pressure points for each $gH_{TH}/a_o^2$ as shown in Figure 2.14. This auxiliary curve makes it possible to interpolate for any pressure ratio with reasonable accuracy.

### Design Problem

Suppose that a new design is sought for a pressure ratio $P_{T5}/P_o$ = 4 and a corrected mass flow of $W\sqrt{\theta}/\delta$ = 5 lb/sec. What is the maximum efficiency that can be achieved, and what will be the general dimensions, operating speed, and inlet velocity triangles?

From Figure 2.33, $P_{T5}/P_o$ = 4 corresponds to $gH_{TH}/a_o^2$ = 1.37 at the maximum pressure ratio condition. Since this generally corresponds to maximum efficiency, it is the appropriate point. This value of $gH_{TH}/a_o^2$ = 1.37 is near to one of the computed values, i.e., 1.29, so this is a convenient guide. From Figure 2.6 the peak efficiency is seen to be $\eta_{AD}$ = 0.85. Knowing that peak efficiency does not depend much on pressure ratios, this value is valid for the present case. Thus, it is found that $d_i/D$ = 0.74, $\beta_2 = 0^\circ$, and $\alpha_2 = 55.3^\circ$ for the best efficiency.

The general study was made for certain fixed values of $\beta_1$ , $\gamma$, Z, $Z_{GV}$, and $Re_t/M_t$, so that these values are also implied in the results for this problem. However, the effect of these parameters is known to be rather small in general, as indicated by the brief study included herein, so that these quantities are not necessarily unalterable. Corrections may be made to efficiency based on the curves in Figures 2.30 to 2.32, if desired. Probably the most significant correction will be that for Reynolds number, when very low inlet densities are anticipated.

Assuming the fixed values of $\beta_1$, $\gamma$ , Z, etc , for the moment, then the remaining design variables can be established. Interpolating in Figures 2.21 through 2.29 yields the following:

$$b/D = 0.049$$
$$M_t = 1.28$$
$$w_2/w_1 = 0.69$$
$$M_{w1} = 1.10$$
$$\gamma = 0.530$$
$$d_4/D = 1.90 \text{ (Fig. 2.15)}$$

So far no mention of the mass flow has been made. Indeed, none is required in order to obtain the essential performance of a machine. The mass flow requirement merely fixes the absolute size of the machine, and thereby affects only the final actual Reynolds number. Absolute size, of course, has its influence through the practical problems of minimum clearances, surface finish, etc , but these effects are not large for reasonable sizes of machines ($D > 5$-in.). The absolute size can be obtained from the following relation for mass flow through the inlet:

$$W = \phi \, (d_1/D)^2 \, M_t(\rho_1/\rho_0)(1 - \nu^2)(\tfrac{\pi}{4} D^2 \, \epsilon_1 \, \rho_0 a_0) \tag{2.57}$$

or in terms of corrected mass flow

$$\frac{W\sqrt{\theta}}{\delta} = \phi \, (d_1/D)^2 \, M_t(\rho_1/\rho_0)(1 - \nu^2)(\tfrac{\pi}{4} D^2 \, \epsilon_1 \rho_{STD} \, a_{STD}) \tag{2.58}$$

wherein
$$\rho_1/\rho_0 = \left[ 1 - (k-1) \, M_t^2 \, \phi^2/2 \right]^{1/(k-1)}$$

For the present conditions and assuming the inlet flow clogging factor $\epsilon_1 = 0.95$, there results $D = 0.636$ ft $= 7.64$-in.

Thus the general configuration and the velocity triangles are established, and the detailed aerodynamic design can begin. Out of the detailed design will come exact lengths, diameters, velocities, etc , which can then be used for more accurate computation of performance, if desired.

Analysis of a Given Design

Suppose that a machine is given which has the following general configuration

$$D = 0.33 \text{ ft}$$
$$d_1/D = 0.65$$
$$\beta_{B2} = 0^\circ$$
$$b/D = 0.0625$$
$$\beta_{B1} = 60^\circ$$
$$\nu = 0.35$$
$$Z = 15$$
$$Z_{GV} = 31$$
$$d_4/D = 2.0$$

It is to be operated at $M_t = 1.0$ at sea level inlet conditions. What efficiency can be expected at the design conditions, and what pressure ratio and mass flow

will exist?  It is assumed that the diffuser is composed of a vaneless space to reduce the velocity to subsonic, followed by a good vaned diffuser.

From Figures 2.26 and 2.21, the conditions of $M_t = 1$ and $b/D = .0625$ lead to the conclusion that $gH_{TH}/a_o^2 = 0.80$ and $\alpha_2 = 68^o$.  Thus the efficiency to be expected is closely determined by Figure 10, from which $\eta_{AD} \cong 0.79$.  On checking the diffuser diameter ratio, $d_4/D = 2$, against Figures 2.15 and 2.16, it is seen that the diffuser is larger than optimum, so that some reduction in efficiency and pressure ratio might be expected.

The wheel Reynolds number, $Re_t$, is found to be $Re_t = 2.19 \times 10^6$.  This leads to a further reduction of efficiency, according to Figure 2.31, of about 1 per cent and another reduction in pressure ratio.  Figures 2.33 and 2.14 indicate an optimum pressure ratio of $P_{t5}/P_o = 2.30$.  Thus the expected values of $\eta_{AD}$ and $P_o$ would be

$$\eta_{AD} \cong 0.77$$

$$P_{T5}/P_o \cong 2.20$$

The mass flow at design conditions $\left( \beta_i / \beta_{Bi} \right)$ would be

$$\frac{\overline{w}\sqrt{\theta}}{\delta} = 0.92 \text{ lb/sec}$$

Note that the given values of $\beta_i$, $\nu$, $Z$ and $Z_{GV}$ do not coincide with the values used in the present generalized study.  The error involved in using the generalized performance curves is quite small in this case, since these quantities are the least sensitive to performance and the deviations from the standard values is small.

2.1 Balje, O. E. A Contribution to the Problem of Designing Radial Turbomachines. Translation ASME. Vol. 74, No. 4. May 1952.

2.2 Stepanoff, A. J. Centrifugal and Axial Flow Pumps. John Wiley and Sons. New York, 1948.

2.3 Prian, V. D., and Michel, D. J. An Analysis of the Flow in the Rotating Passage of Large Radial-inlet Centrifugal Compressor at a Tip Speed of 700 feet per Second. NACA TN 2548. December 1951.

2.4 Michel, D. J., Ginsburg, A., and Mizisin, J. Experimental Investigation of Flow in the Rotating Passages of a 48-inch Impeller at Low Tip Speeds. NACA RM E51D20. June 26, 1951.

2.5 Michel, D. J., Mizisin, J., and Prian, V. D. Effect of Changing Passage Configuration on Internal-Flow Characteristics of a 48-inch Centrifugal Compressor, I - Change in Blade Shape. NACA TN 2706. May 1952.

2.6 Mizisin, J., and Michel, D. J. Effect of Changing Passage Configuration on Internal-Flow Characteristics of a 48-inch Centrifugal Compressor, II - Change in Hub Shape. NACA TN 2835. November 1952.

2.7 Kovach, K., and Withee, J. R., Jr. Investigation of Effects of Reynolds Number on Large Double Entry Centrifugal Compressor. NACA RM E52H19. October 22, 1952.

2.8 Hamrick, J. T., and Mizisin, J. Investigation of Flow Fluctuations at the Exit of a Radial Flow Centrifugal Impeller. NACA RM E52H11. October 1952.

2.9 Polikovsky, V., and Nevelson, M. The Performance of a Vaneless Diffuser Fan. NACA TM 1038. December 1942.

2.10 Stanitz, J. D. One-Dimensional Compressible Flow in Vaneless Diffusers of Radial and Mixed-Flow Centrifugal Compressors, Including Effects of Friction, Heat Transfer and Area Change. NACA TN 2610. January 1952.

2.11 Lieblein, S., Schwenk, F. C., and Broderick, R. L. Diffusion Factor for Estimating Losses and Limiting Blade Loadings in Axial-Flow-Compressor Blade Elements. NACA RM E53D01. June 1953 (Confidential).

2.12 Busemann, A. Das Förderhöhenverhältnis Radialer Kreiselpumpen Mit Logarithmisch-Spiraligen Schaufeln. Z. Agnew Math Mech. Vol. 8. p 372. 1928.

2.13 Stodola, A. Steam and Gas Turbines. McGraw-Hill Book Co. New York. 1927.

2.14 Eckert, B. Axialkompressoren und Radialkompressoren. Springer Verlag. Berlin, 1953

2.15 Moody, L. F. Friction Factors for Pipe Flow. Trans. ASME. Nov. 1944

2.16 Faulders, C. R.  Experimental and Theoretical Study of Vaneless Diffuser
Flow with Supersonic Entry.  Gas Turbine Laboratory Report.  Mass. Inst.
of Technology.  June 1952.

2.17 Rains, D. A.  Tip Clearance Flows in Axial Flow Compressors and Pumps.
Report No. 5.  Navy Contract N6-ori-102, Task Order IV, and Nord 9612.
Calif. Inst. of Technology.  June 1954.
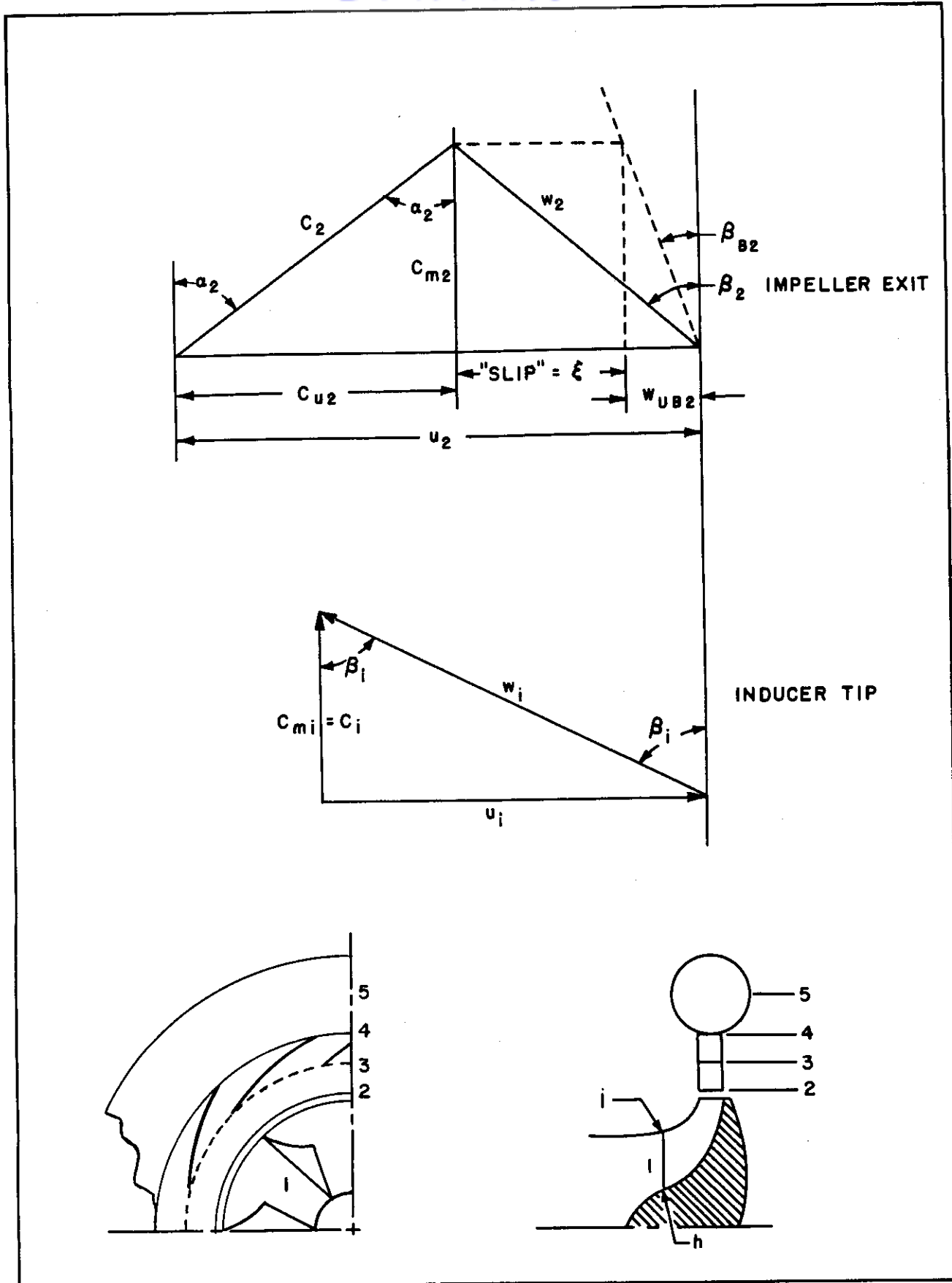
FIG. 2.1    VELOCITY, ANGLE, AND STATION DEFINITIONS

H, BOUNDARY LAYER SHAPE PARAMETER
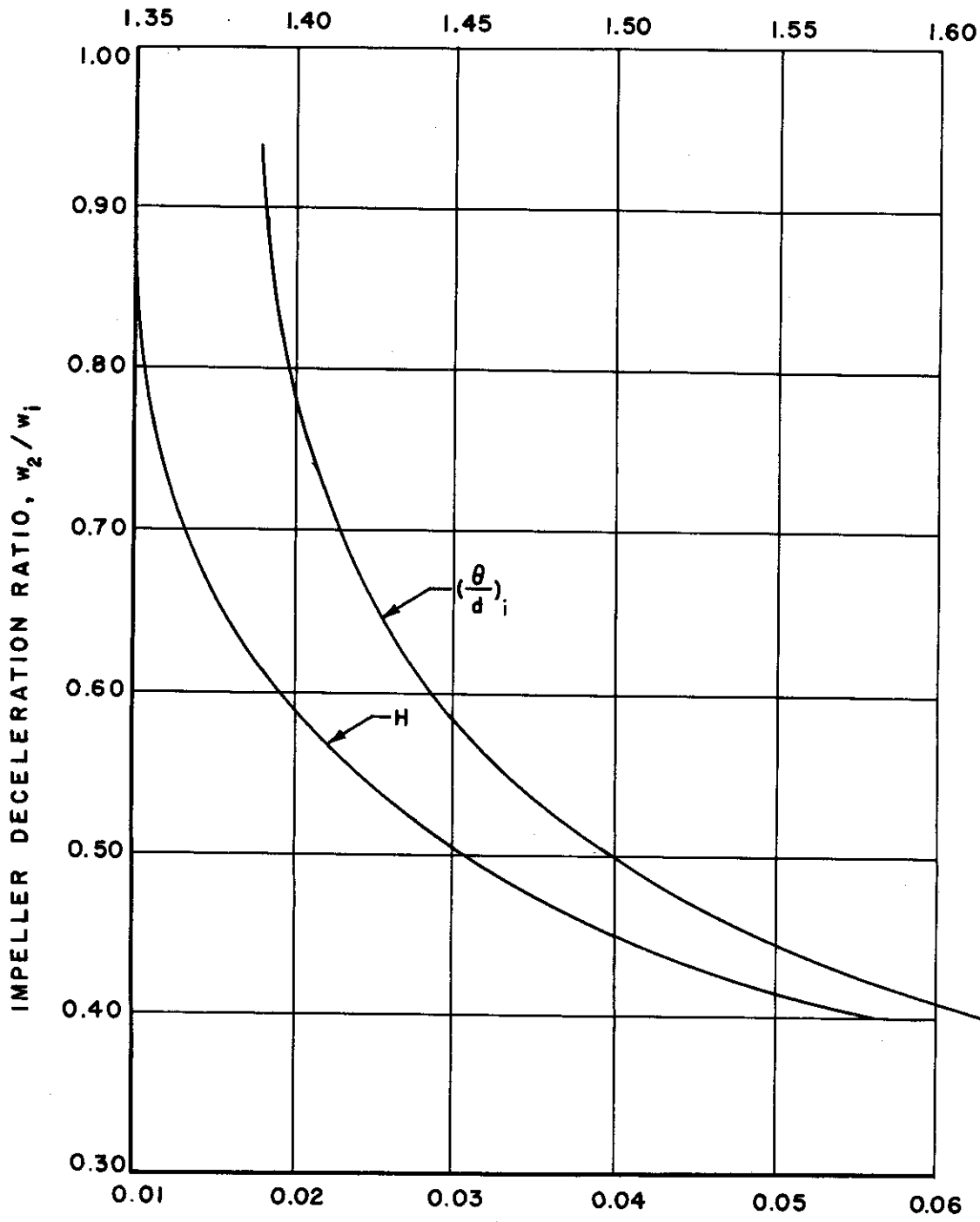


$(\frac{\theta}{d})_i$ BOUNDARY LAYER MOMENTUM THICKNESS
EQUIV. CONE DIAMETER AT DIFFUSER INLET

FIG. 2.2    INFLUENCE OF THE DIFFUSION IN THE IMPELLER ON
THE ENTRANCE CONDITIONS TO GUIDE VANES
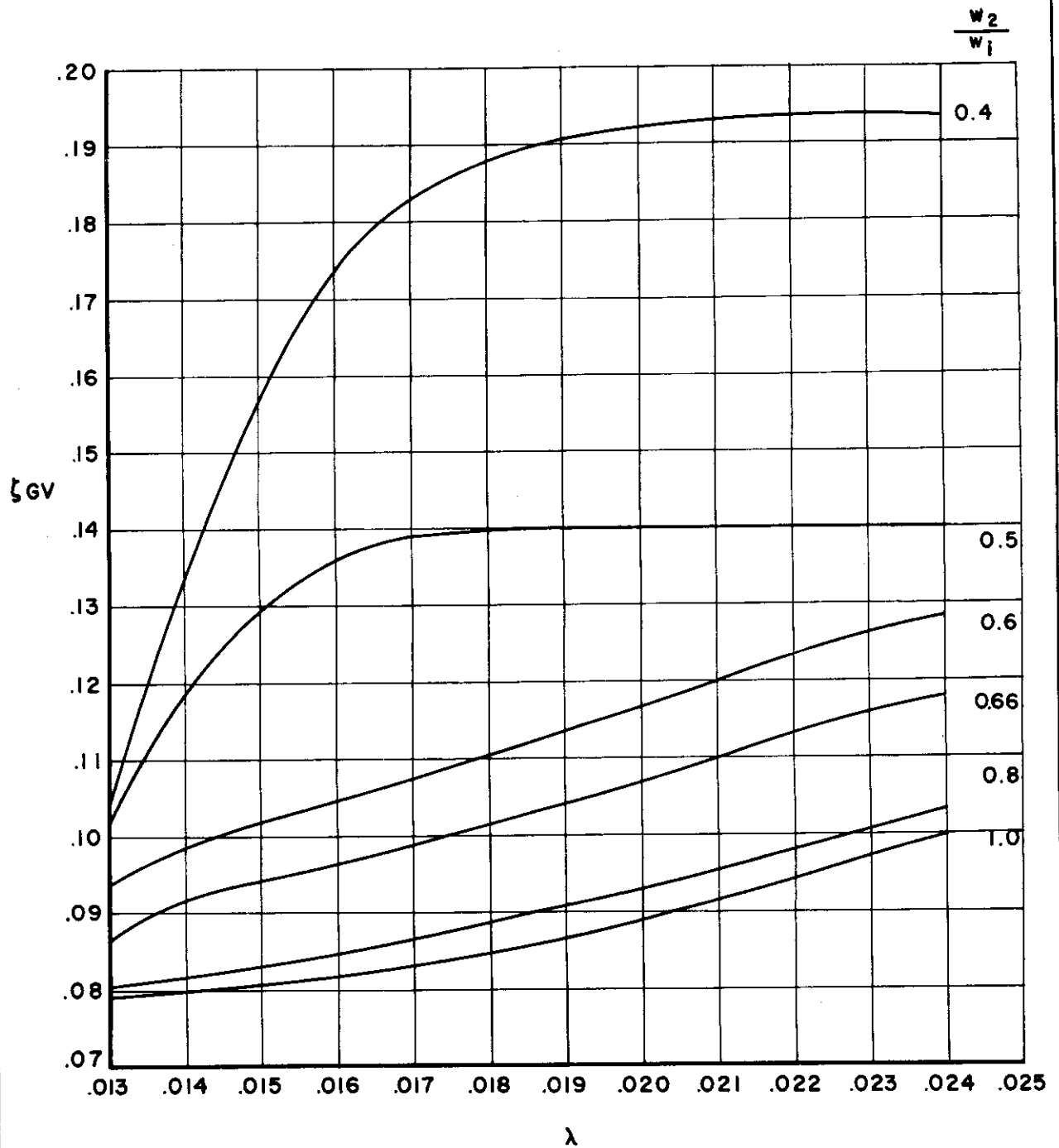
GUIDE VANE LOSS COEFFICIENT FOR
OPTIMUM DIFFUSER

FIG. 2.3
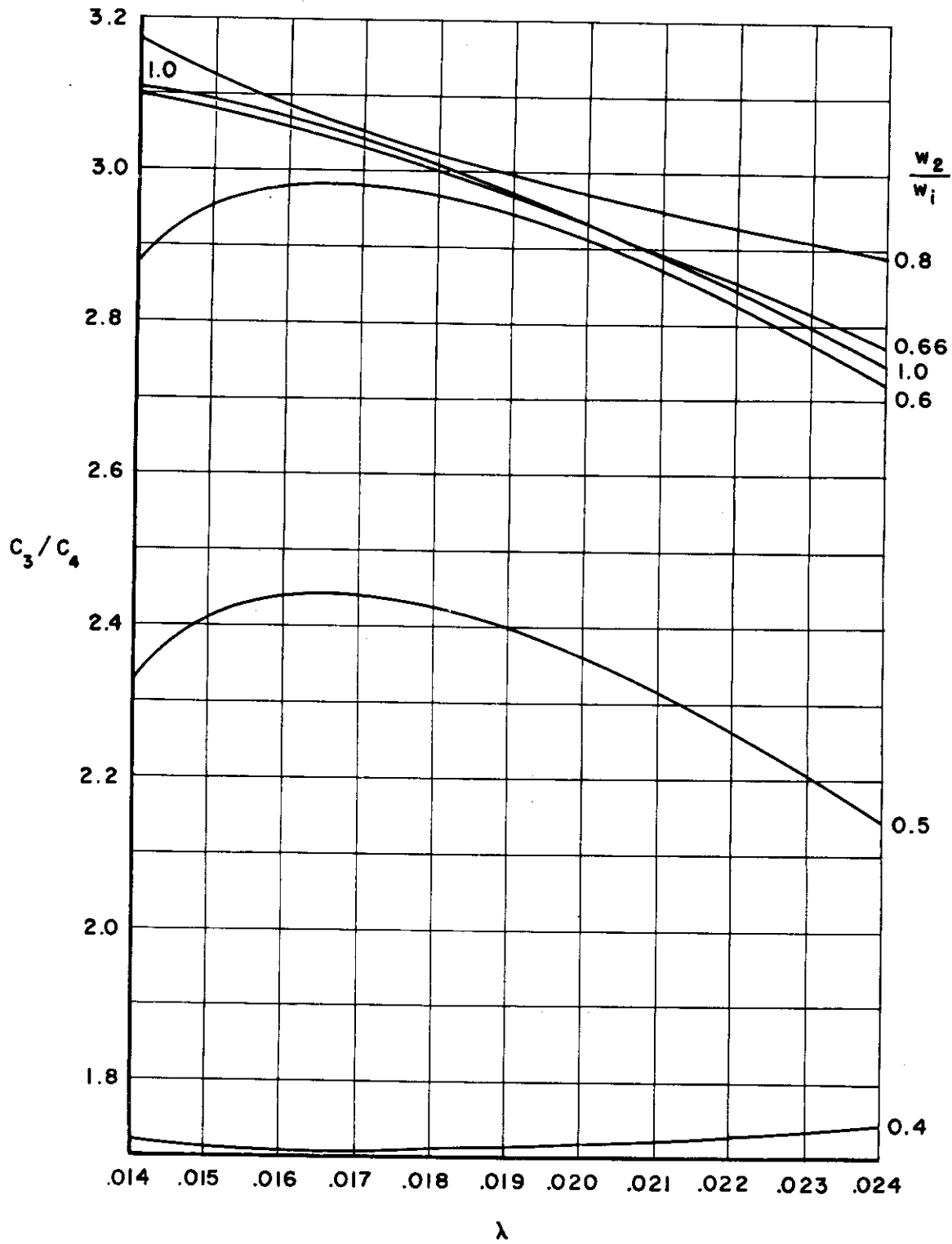
FIG. 2.4    GUIDE VANE DECELERATION RATIO
FOR OPTIMUM DIFFUSER
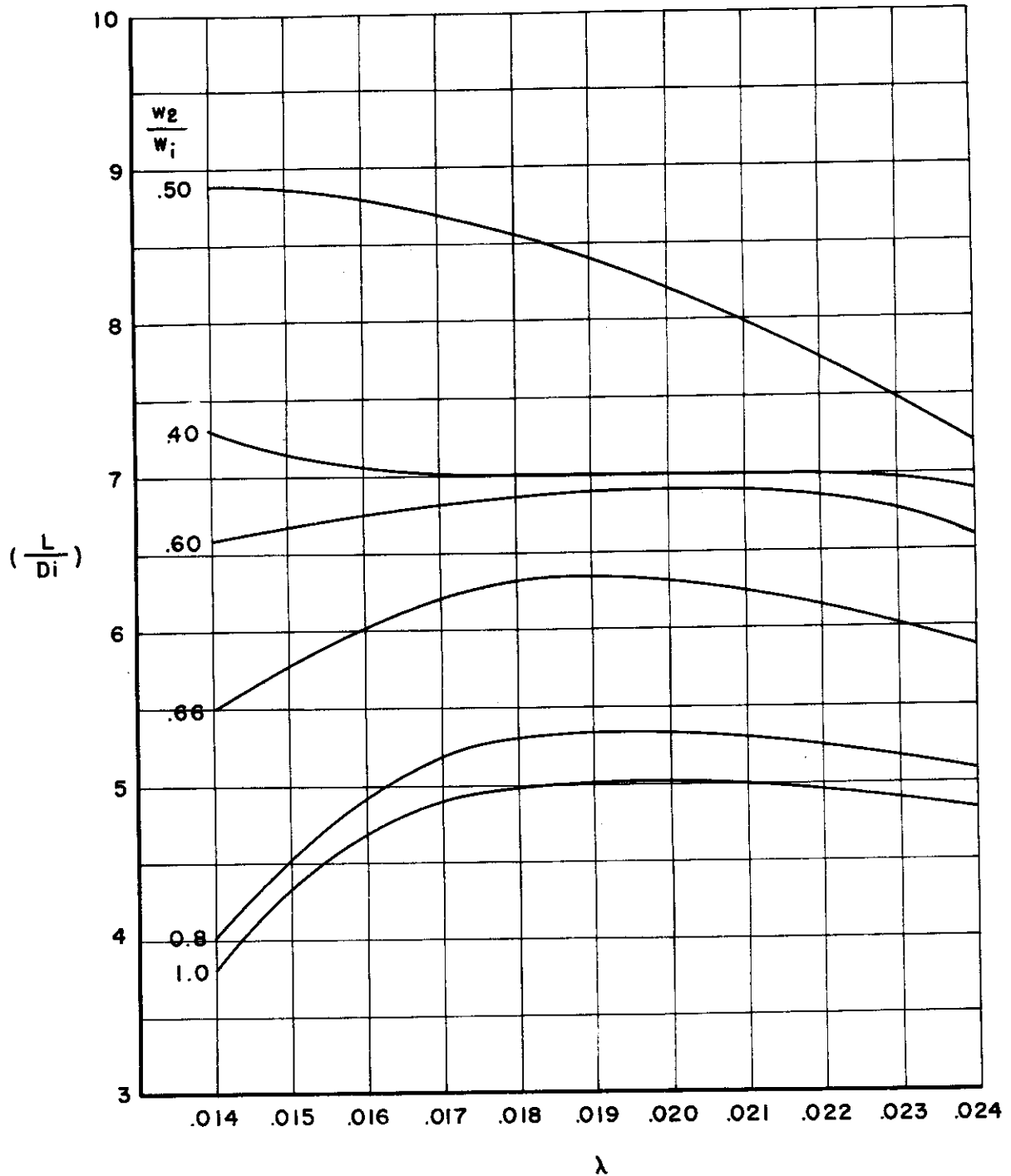
GUIDE' VANE FLOW PASSAGE LENGTH
FOR OPTIMUM DIFFUSER
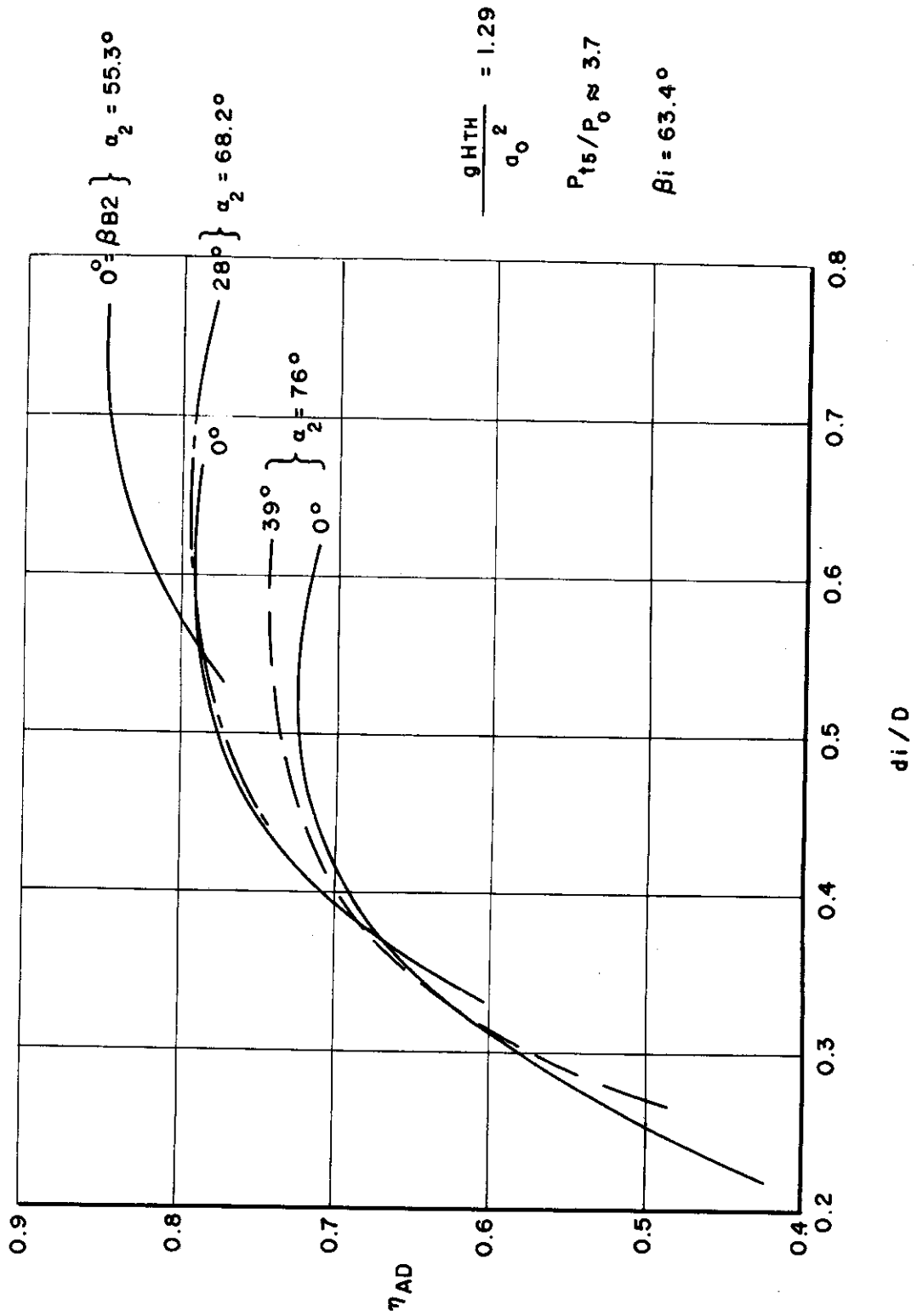
FIG. 2.5

FIG. 2.6    COMPRESSOR EFFICIENCIES FOR $gH_{TH}/a_0^2 = 1.29$

The figure plots $\eta_{AD}$ (vertical axis, 0.4 to 0.9) versus $d_i/D$ (horizontal axis, 0.2 to 0.8).

Curve labels:
- $0° = \beta_{B2}$ } $a_2 = 55.3°$
- $28°$ } $a_2 = 68.2°$
- $0°$
- $39°$ } $a_2 = 76°$
- $0°$

Conditions:
$$\frac{gH_{TH}}{a_0^2} = 1.29$$

$P_{t5}/P_0 \approx 3.7$

$\beta_i = 63.4°$

$$\frac{gH_{tH}}{a_0{}^2} = 1.29$$

$$a_2 = 55.3°$$

$$\beta_i = 63.4°$$
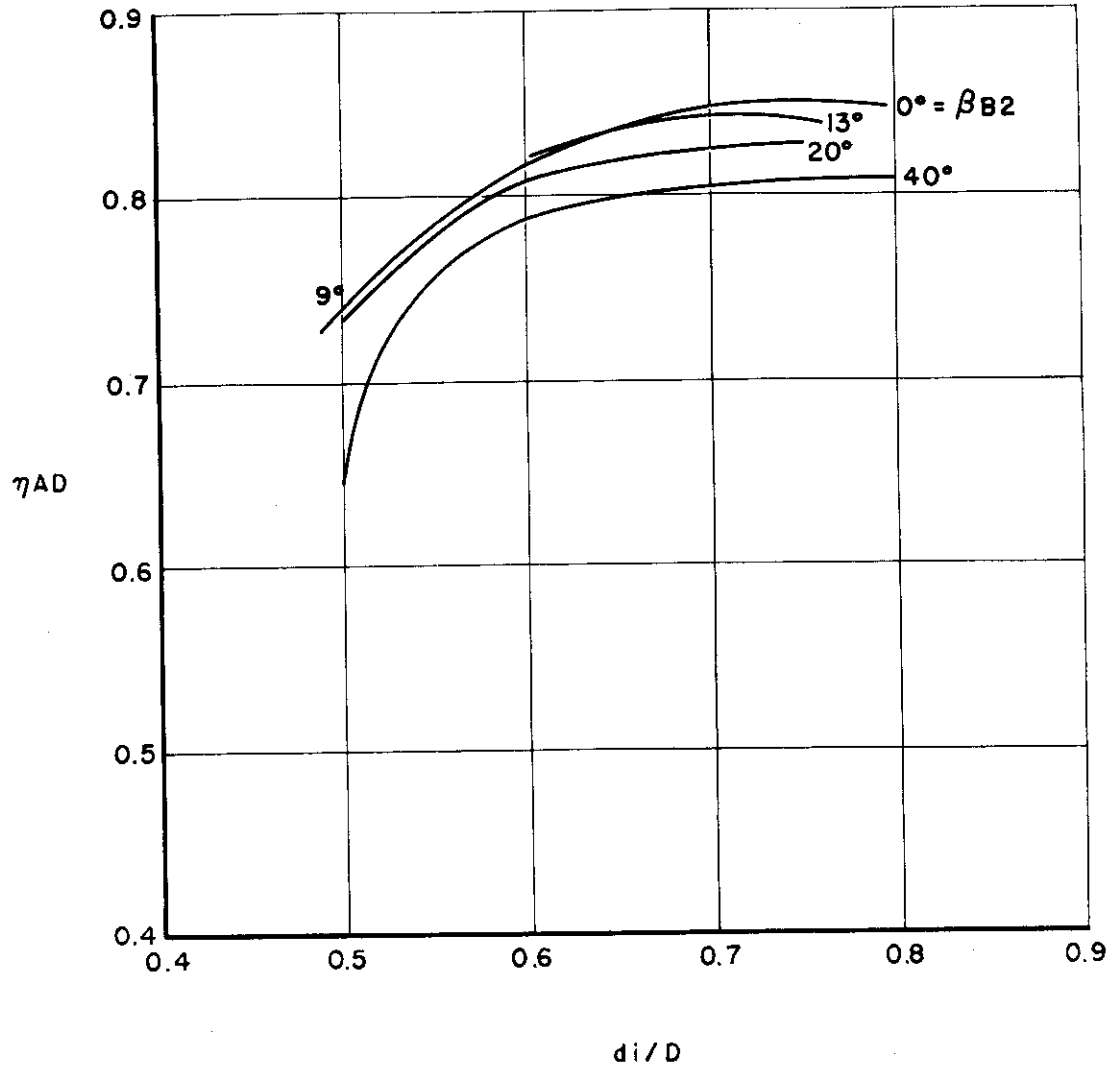


COMPRESSOR EFFICIENCIES FOR $gH_{TH}/a_0{}^2 = 1.29$
& $a_2 = 55.3°$; EXIT BLADE ANGLE INFLUENCE

FIG. 2.7

$$\frac{g H_{TH}}{a_0^2} = 1.29$$

$$\alpha_2 = 68.2°$$

$$\beta_i = 63.4$$
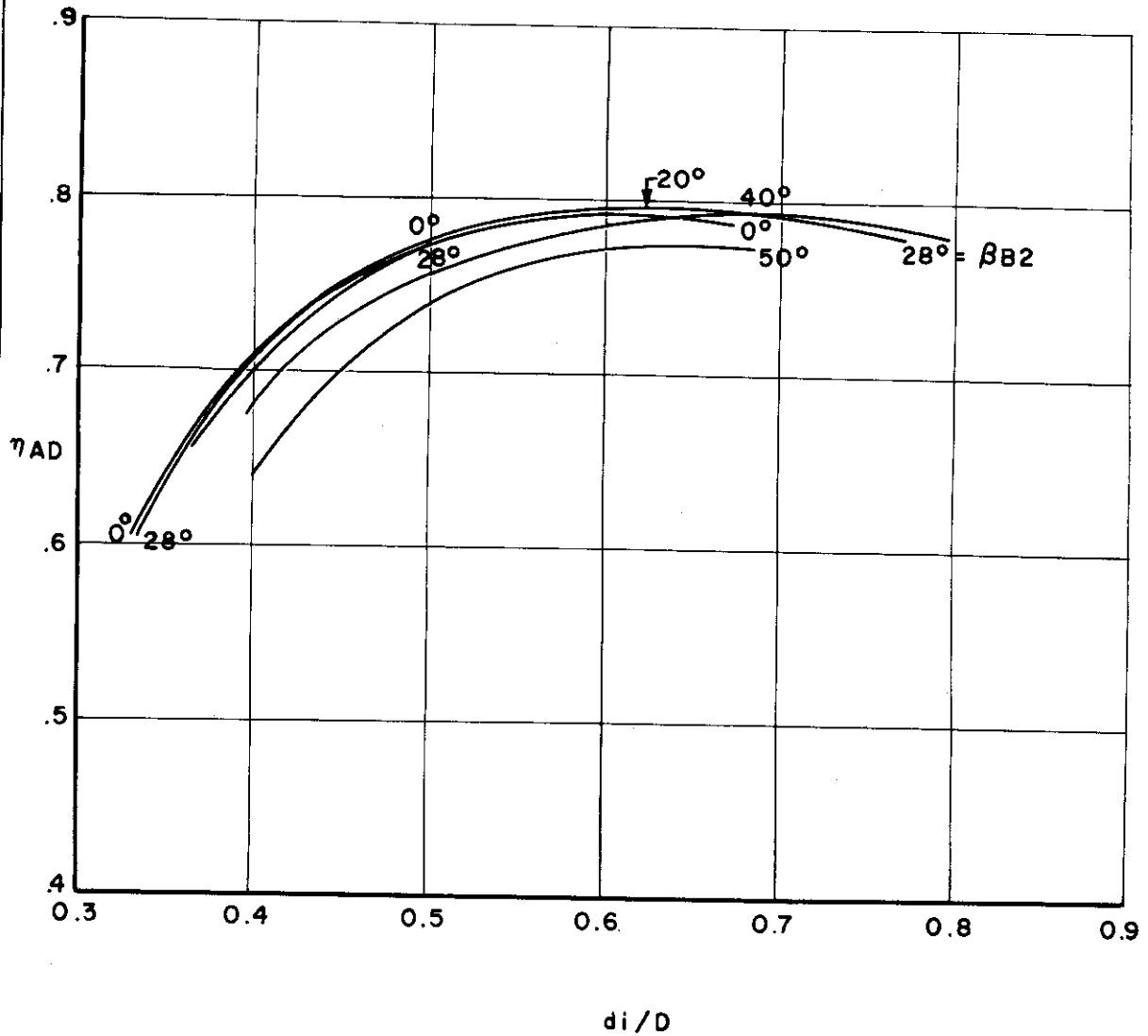
FIG. 2.8    COMPRESSOR EFFICIENCIES FOR $g H_{TH}/a_0^2 = 1.29$
& $\alpha_2 = 68.2°$; EXIT BLADE ANGLE INFLUENCE
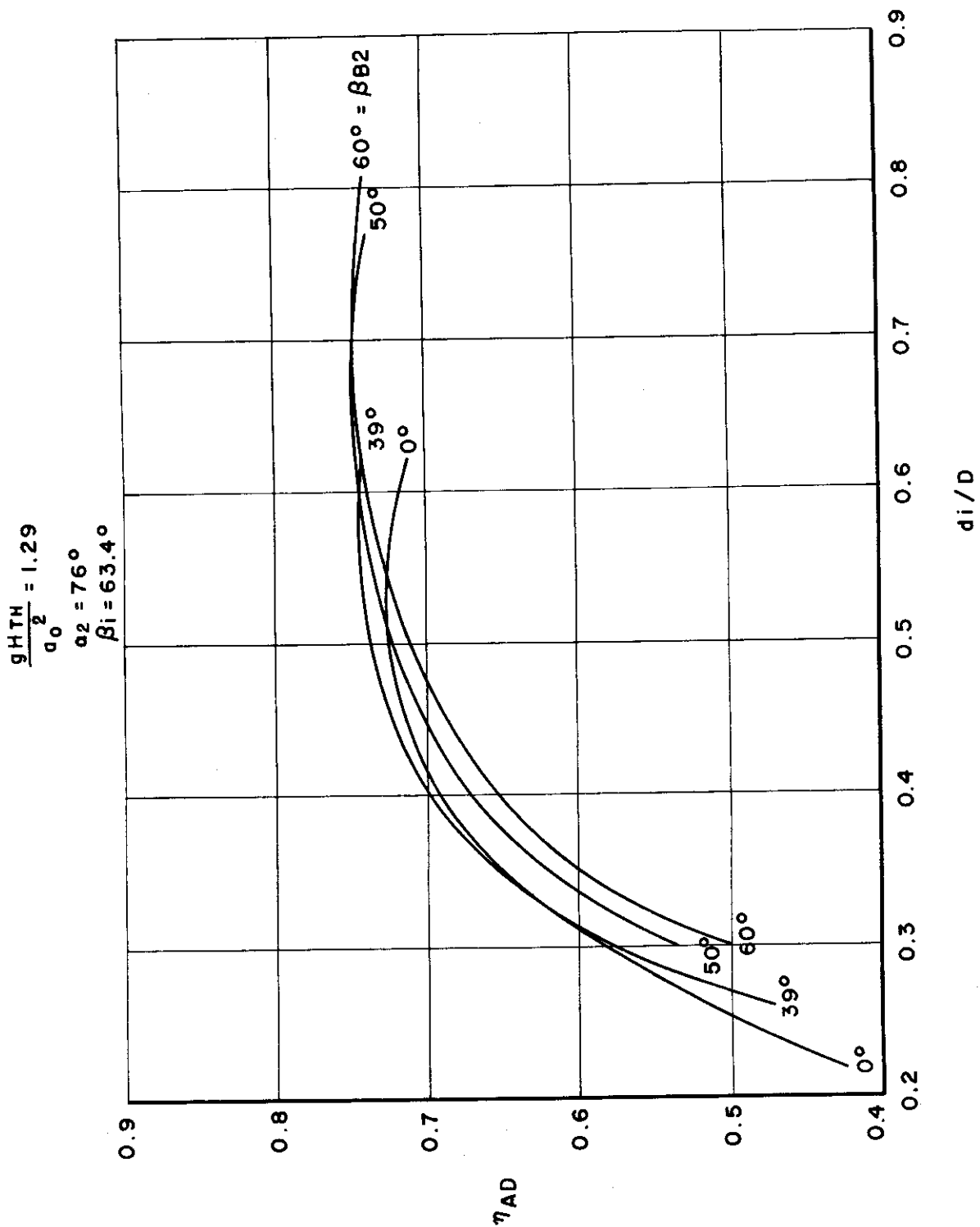
COMPRESSOR EFFICIENCIES FOR $gH_{TH}/a_0^2 = 1.29$ & $a_2 = 76°$; EXIT BLADE ANGLE INFLUENCE

FIG. 2.9

REF. POINT

$a_2 = 55.3°$

$\beta_{B2} = 0°$

$d_i / D = 0.772$
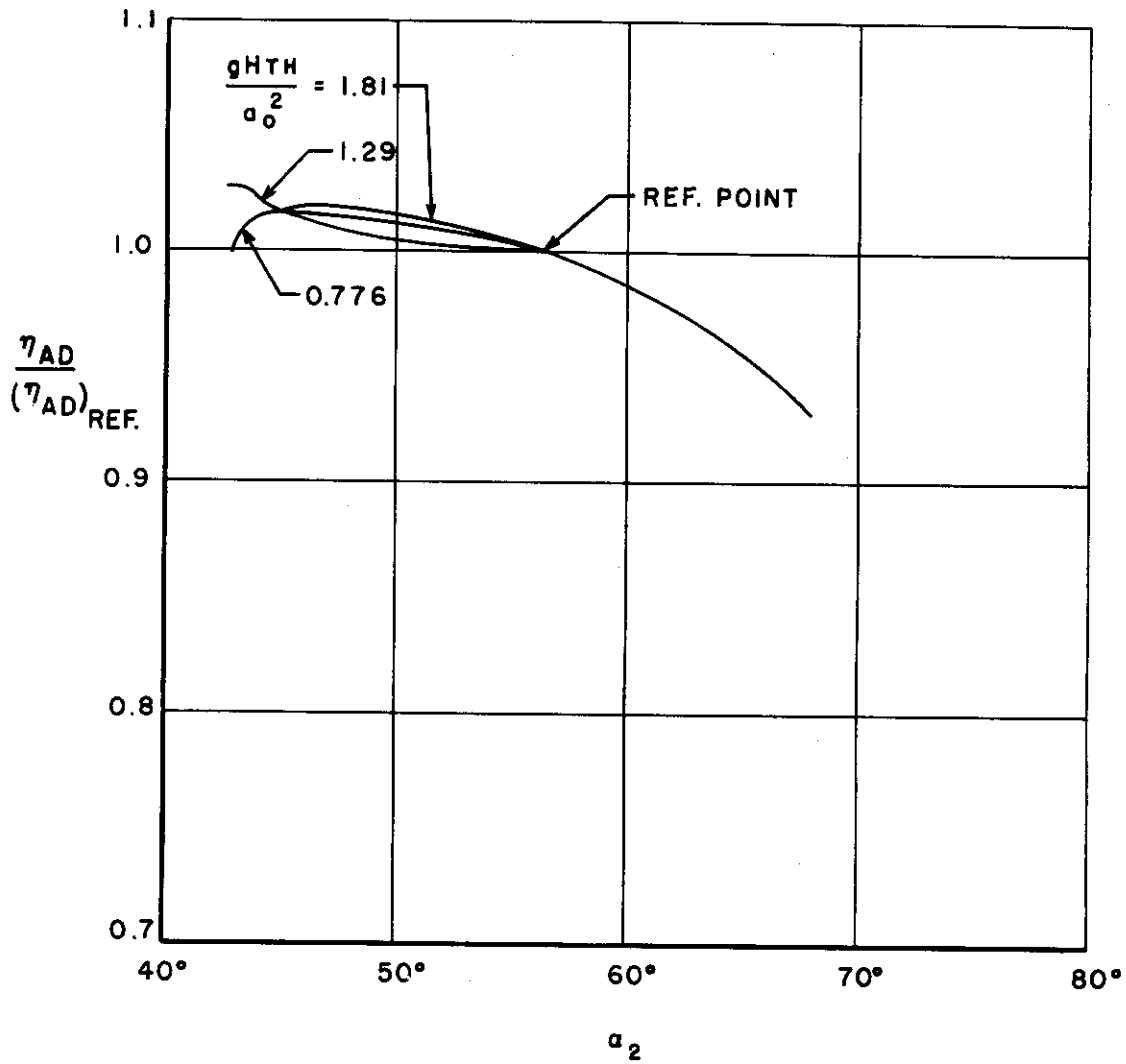
FIG. 2.10    COMPRESSOR EFFICIENCY VARIATION WITH $a_2$ ABOUT A PARTICULAR REFERENCE POINT
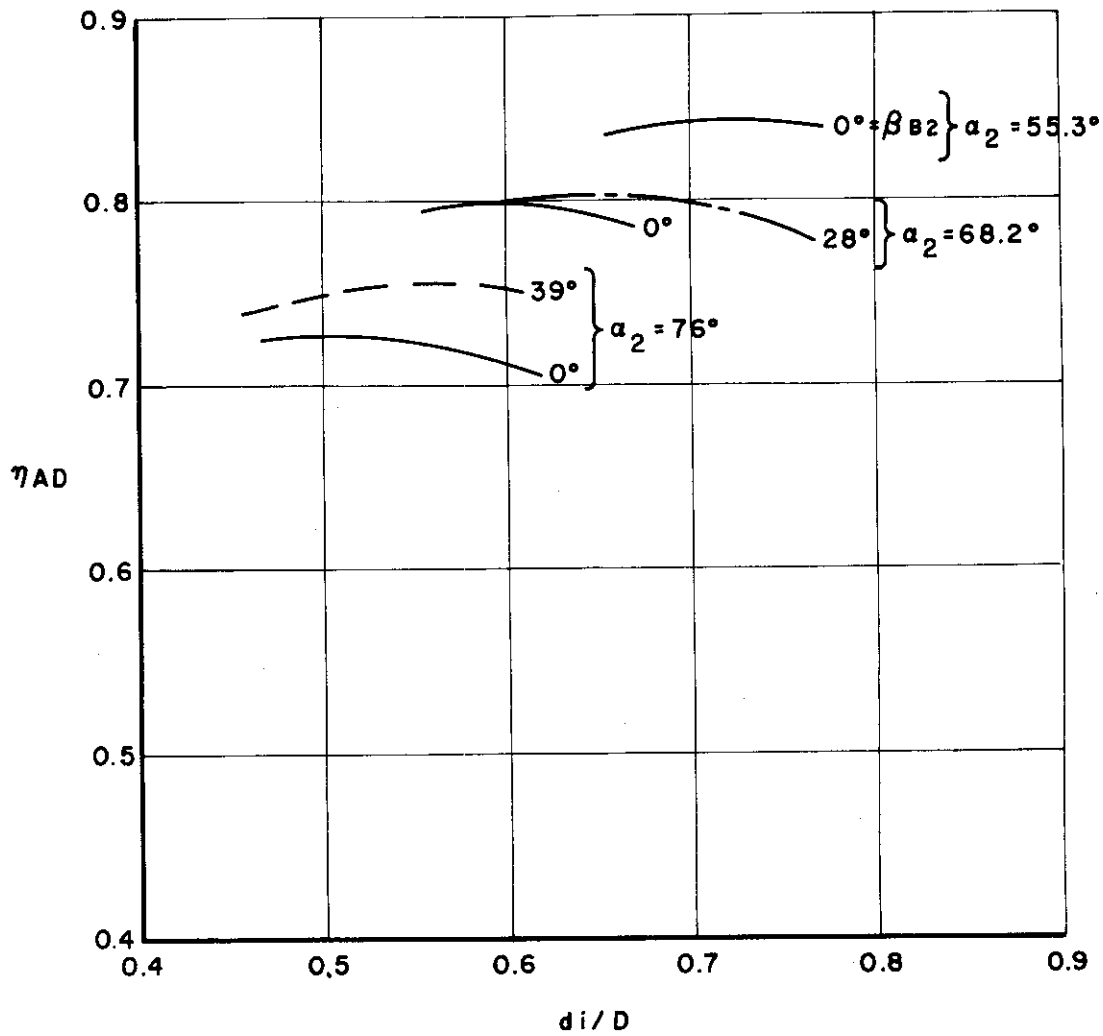
FIG. 2.11   COMPRESSOR EFFICIENCIES FOR $gH_{TH}/a_0^2 = 0.776$

$$\frac{gH_{TH}}{a_0^2} = 1.81$$

$$(P_{t5}/P_0 \approx 5.6)$$

$$\beta_i = 63.4°$$
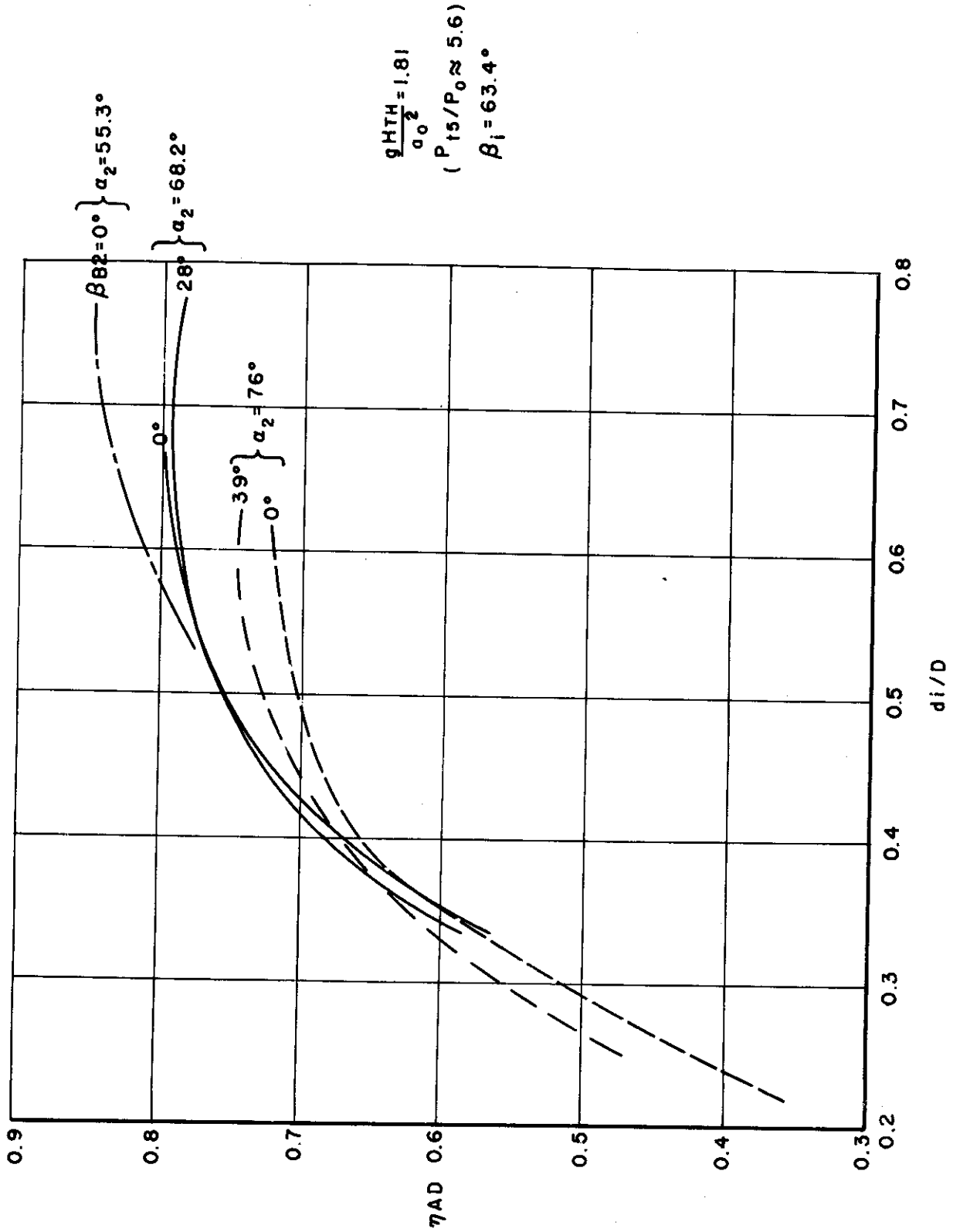
FIG. 2.12     COMPRESSOR EFFICIENCIES FOR $gH_{TH}/a_0^2 = 1.81$

$$\frac{gH_{TH}}{a_0^2} = 2.33$$
$$(P_{t5}/P_o \approx 8.0)$$
$$\beta_i = 63.4°$$
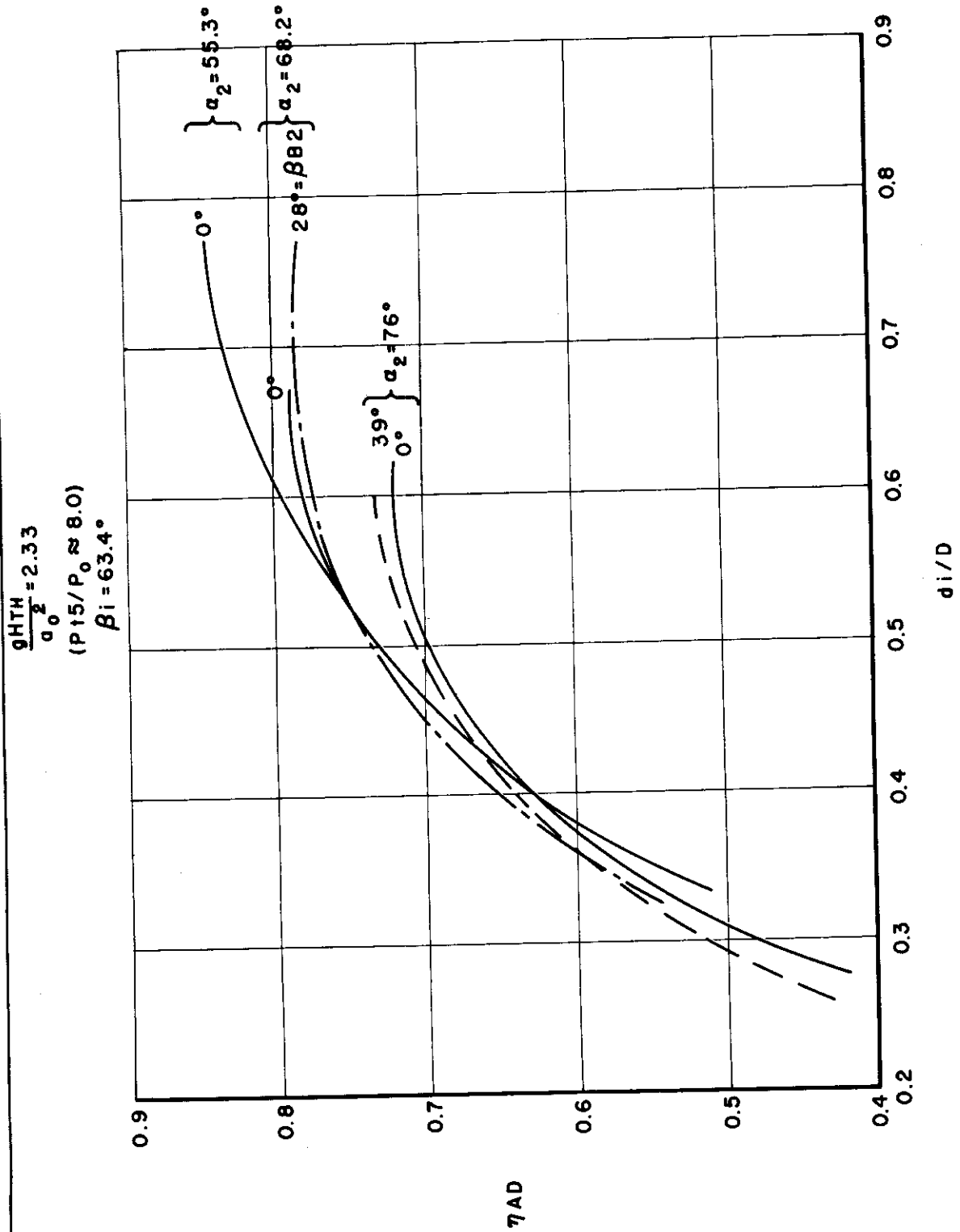
FIG. 2.13   COMPRESSOR EFFICIENCIES FOR $gH_{TH}/a_0^2 = 2.33$
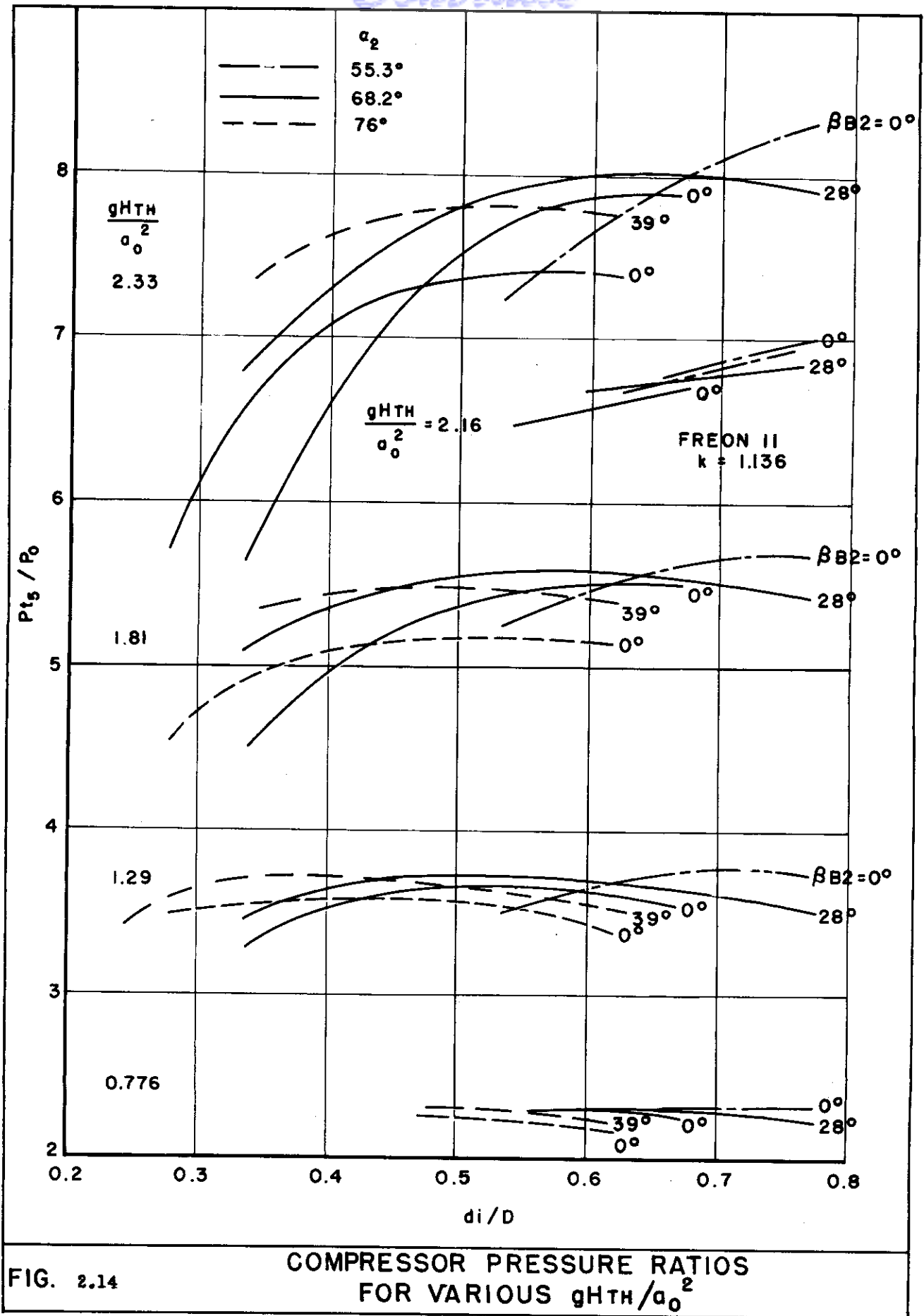
COMPRESSOR PRESSURE RATIOS
FOR VARIOUS $gH_{TH}/a_0^2$
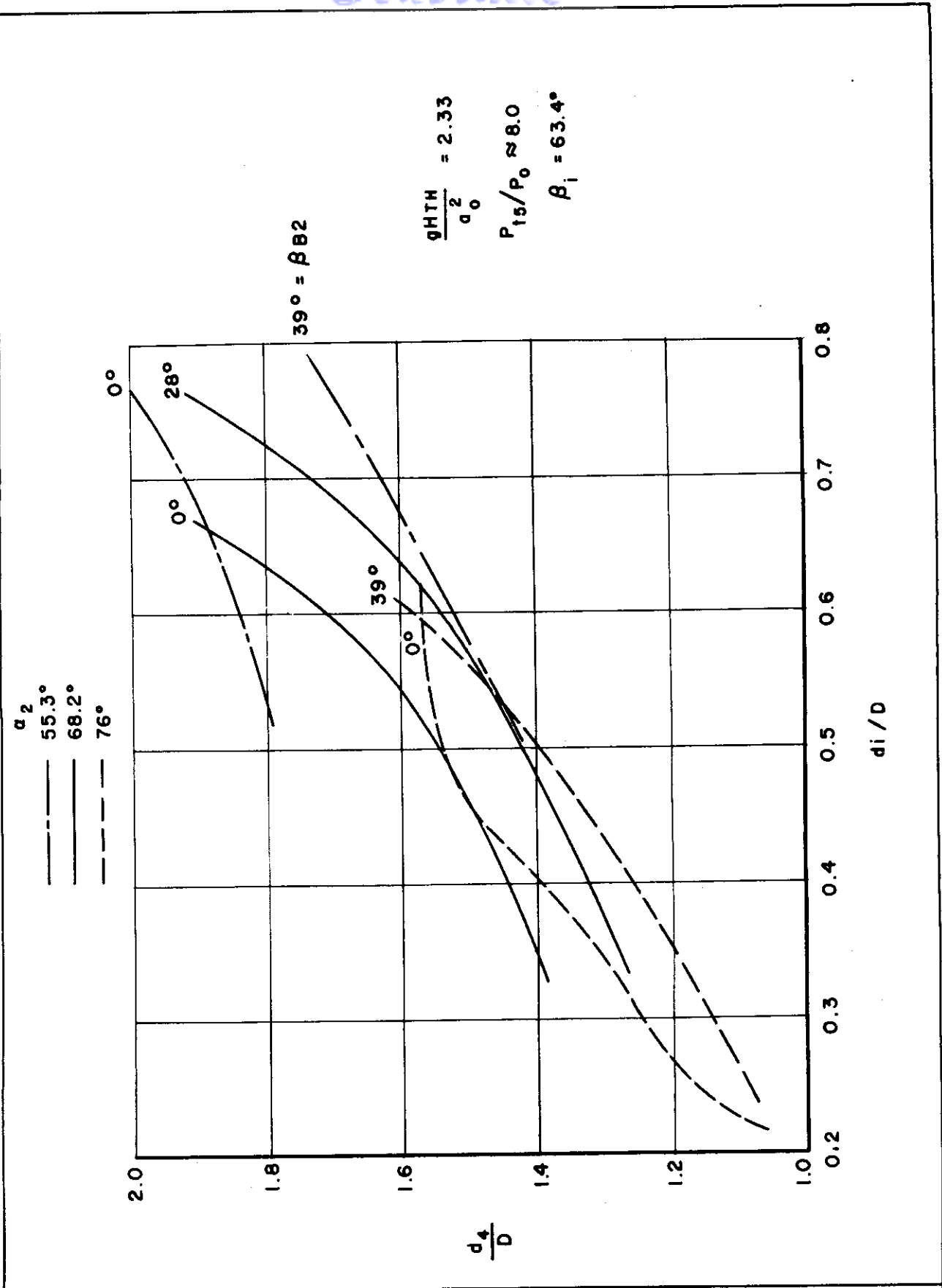
FIG. 2.14

FIG. 2.15   COMPRESSOR DIAMETER RATIOS FOR $gH_{TH}/a_0^2 = 2.33$
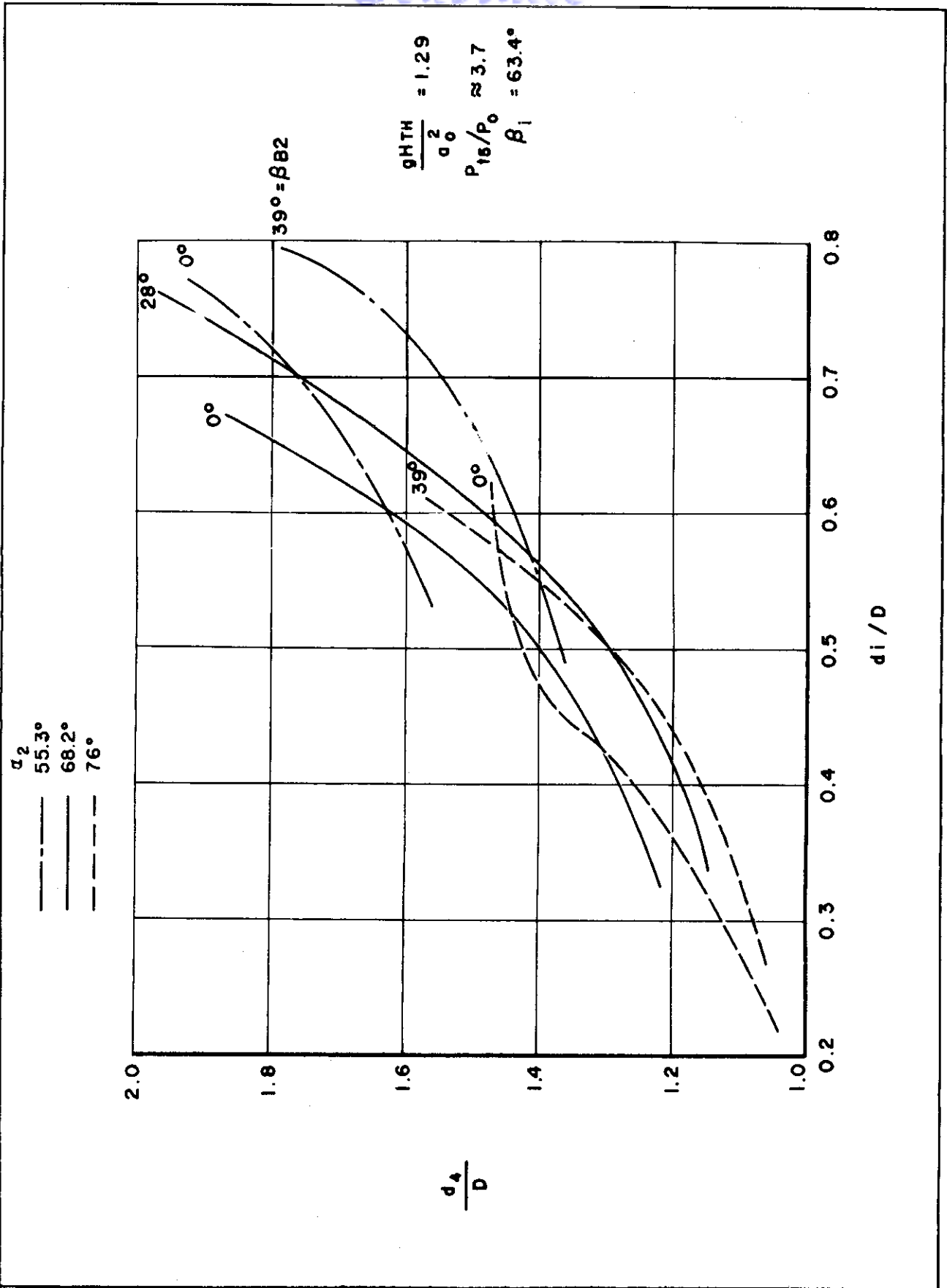
FIG. 2.16   COMPRESSOR DIAMETER RATIOS FOR $gH_{TH}/a_0^2 = 1.29$
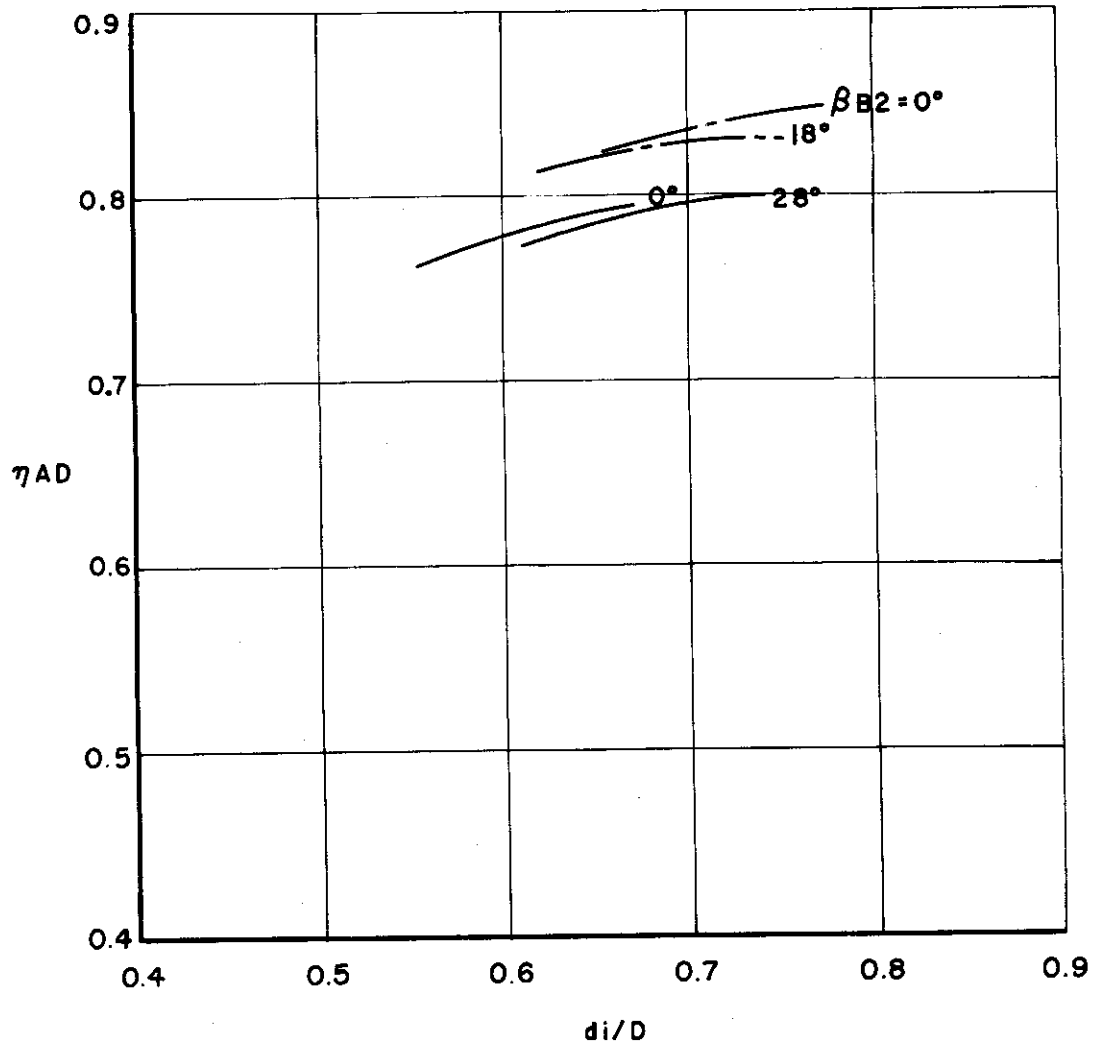
COMPRESSOR EFFICIENCIES FOR FREON II
AT $gH_{TH}/a_0^2$ = 2.16

FIG. 2.17

$$\frac{gH_{TH}}{a_0^2} = 0.776$$

$$\alpha_2$$

| | |
|---|---|
| — · — — | 55.3° |
| —————— | 68.2° |
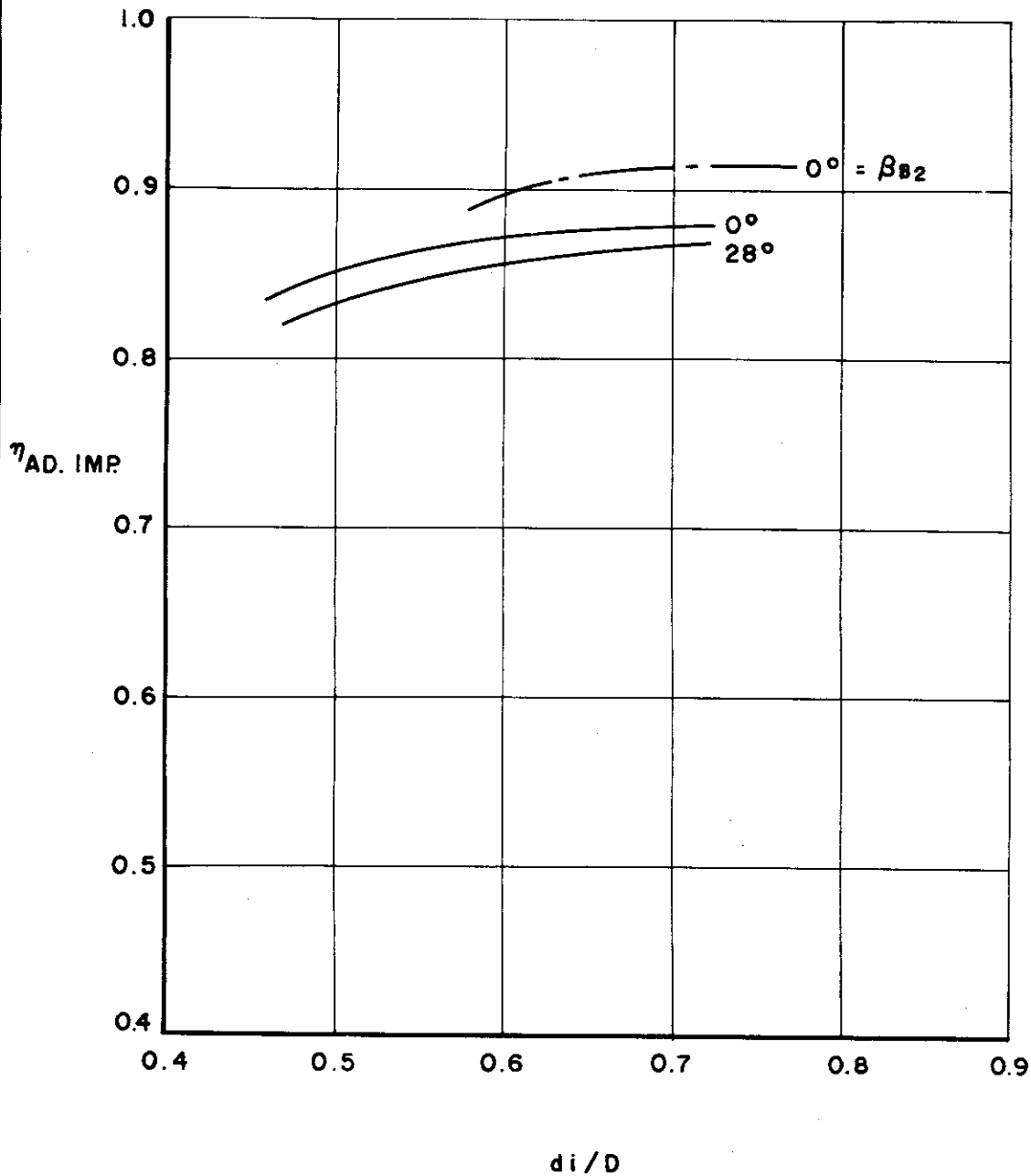


**FIG.** 2.18     IMPELLER EFFICIENCIES FOR $gH_{TH}/a_0^2 = 0.776$
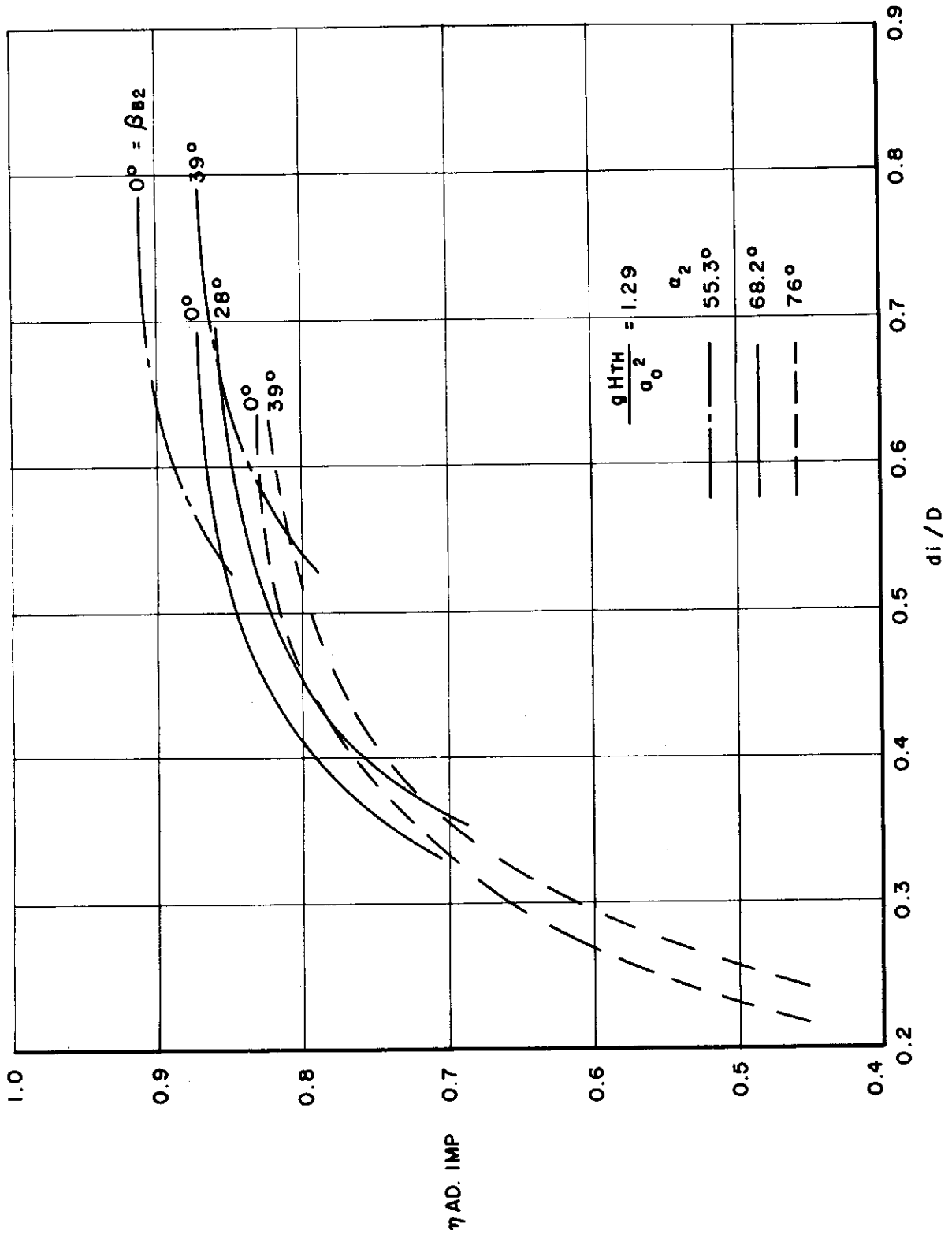
FIG. 2.19    IMPELLER EFFICIENCIES FOR $gH_{TH}/a_0^2 = 1.29$

$$\frac{gH_{TH}}{a_0^2} = 2.33$$

$\alpha_2$
—·— 55.3°
——— 68.2°
— — — 76°



0.9    0°

0° = $\beta_{B2}$
28°

0°
39°

$\eta_{AD.IMP}$

$d_i/D$
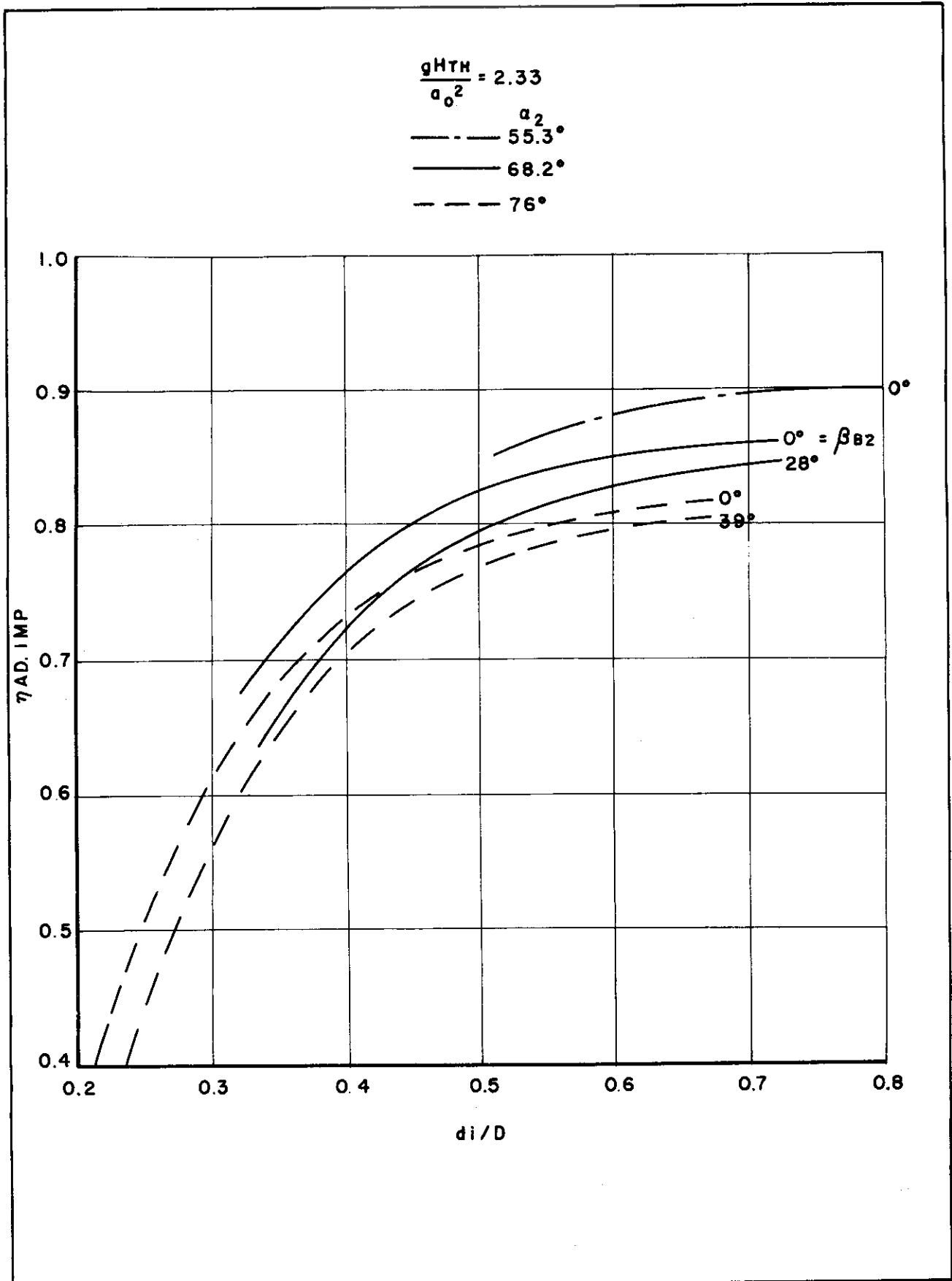
FIG. 2.20    IMPELLER EFFICIENCIES FOR $gH_{TH}/a_0^2 = 2.33$

WADC TR 55-257

$$\frac{gH_{TH}}{a_0^2} = 0.776$$

$\alpha_2$

——— · ——— 55.3°

——————— 68.2°

— — — 76°
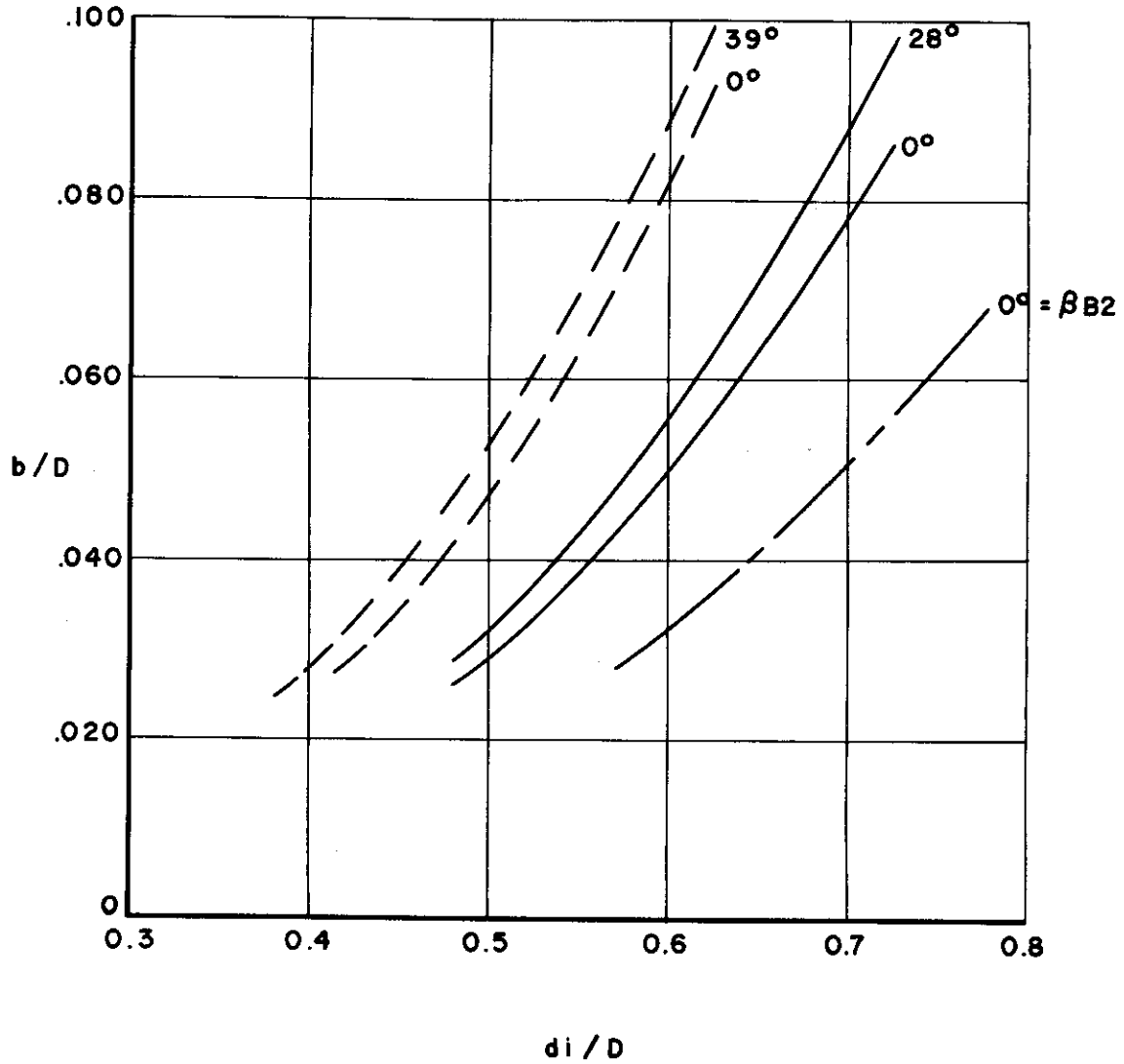


FIG. 2.21    IMPELLER TIP WIDTHS FOR $gH_{TH}/a_0^2 = 0.776$

$$\frac{gH_{TH}}{a_0^2} = 1.29$$

$$\alpha_2$$

| | |
|---|---|
| —  —  — | 55.3° |
| ———— | 68.2° |
| — — — | 76° |
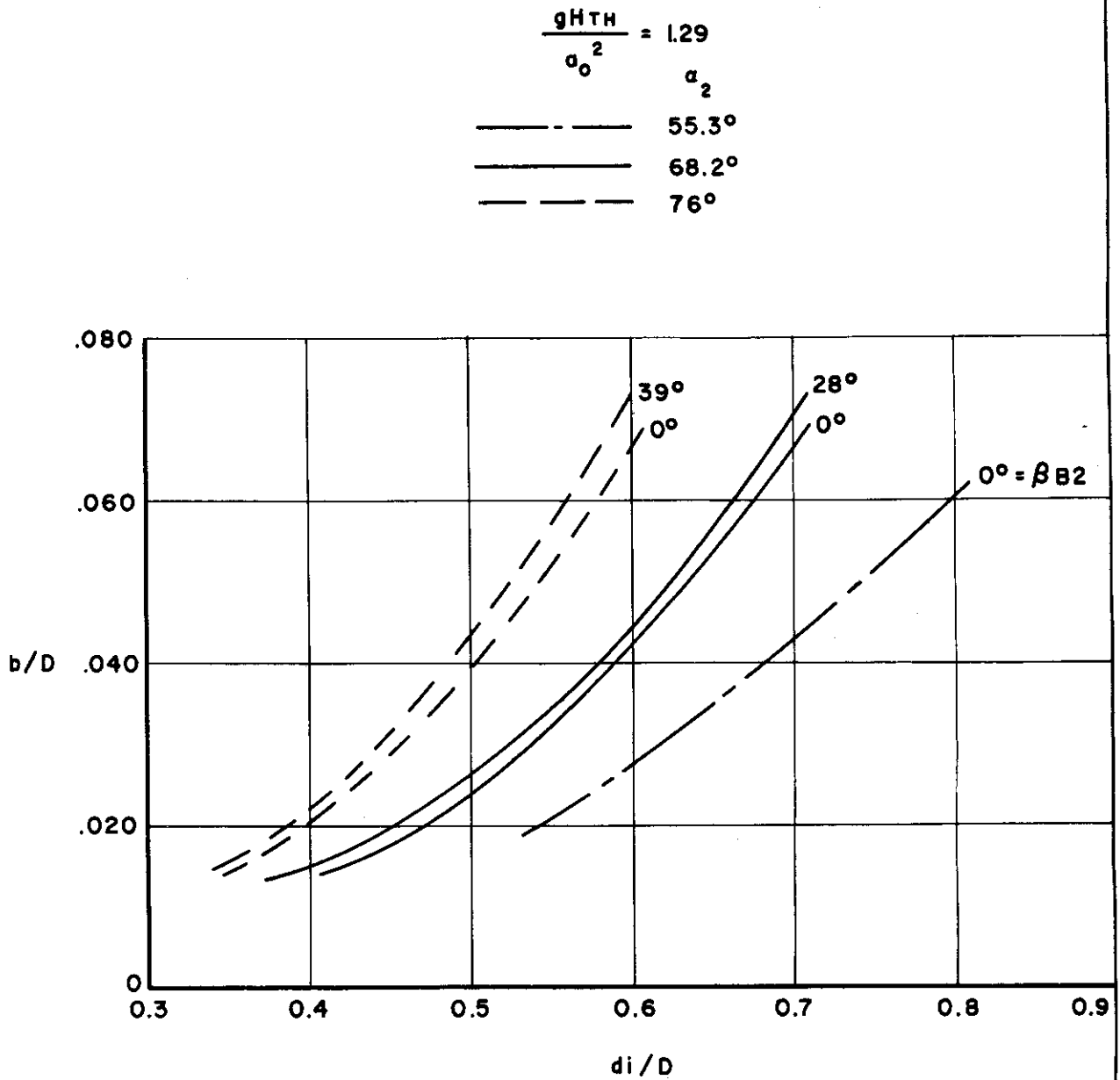


**FIG. 2.22     IMPELLER TIP WIDTHS FOR $gH_{TH}/a_0^2 = 1.29$**

$$\frac{gH_{TH}}{a_0^2} = 1.81$$

$$a_2$$

— · —    55.3°

———    68.2°

— — —    76°
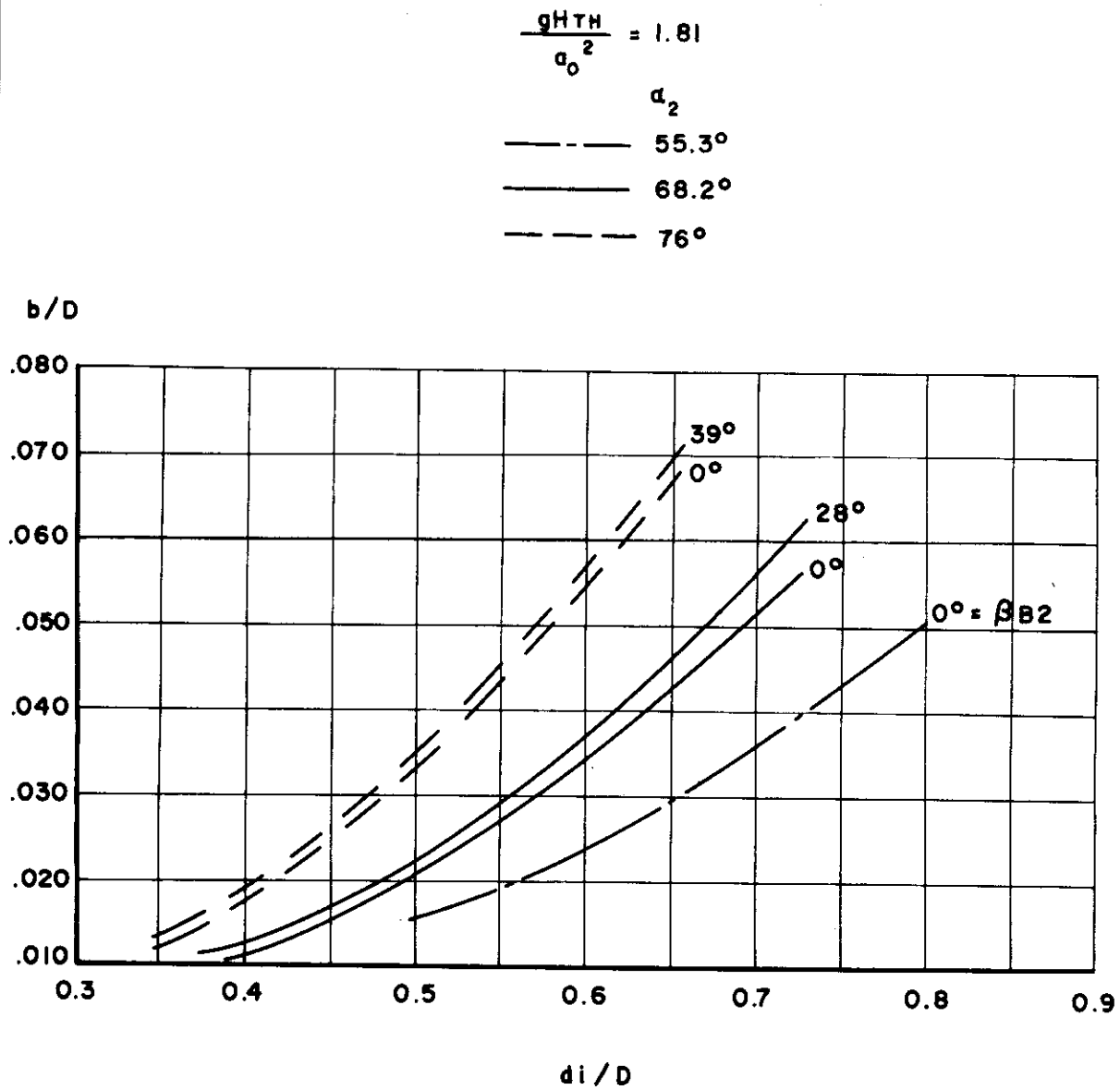


### FIG. 2.23    IMPELLER TIP WIDTHS FOR $gH_{TH}/a_0^2 = 1.81$

$$\frac{gH_{TH}}{a_0{}^2} = 2.33$$

| | $\alpha_2$ |
|---|---|
| —— · —— | 55.3° |
| —————— | 68.2° |
| —— —— —— | 76° |
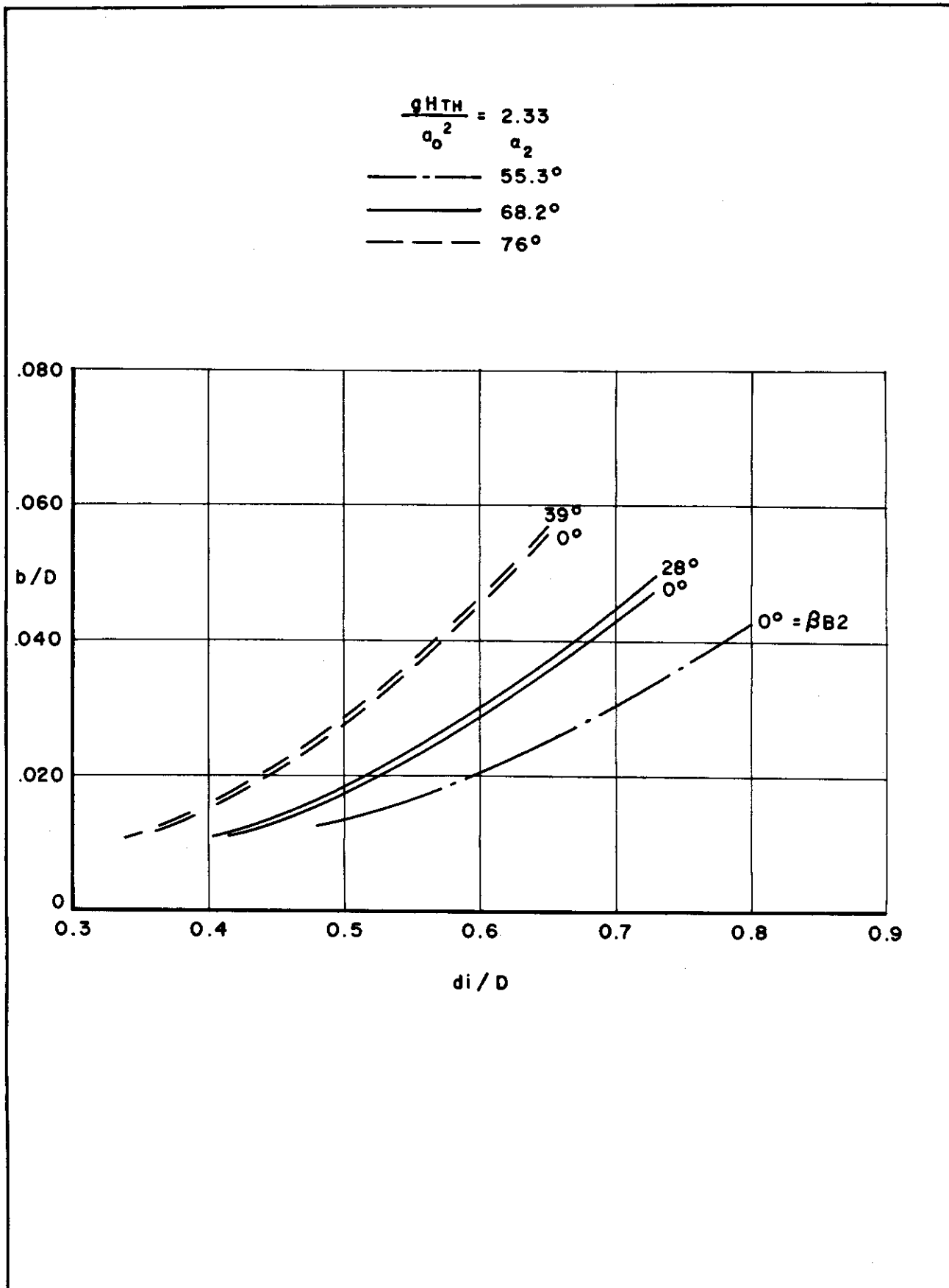
FIG. 2.24     IMPELLER TIP WIDTHS FOR $gH_{TH}/a_0{}^2 = 2.33$

FREON - II

$$\frac{gH_{TH}}{a_0^2} = 2.16$$

$\alpha_2$

— - — 55.3°

———— 68.2°
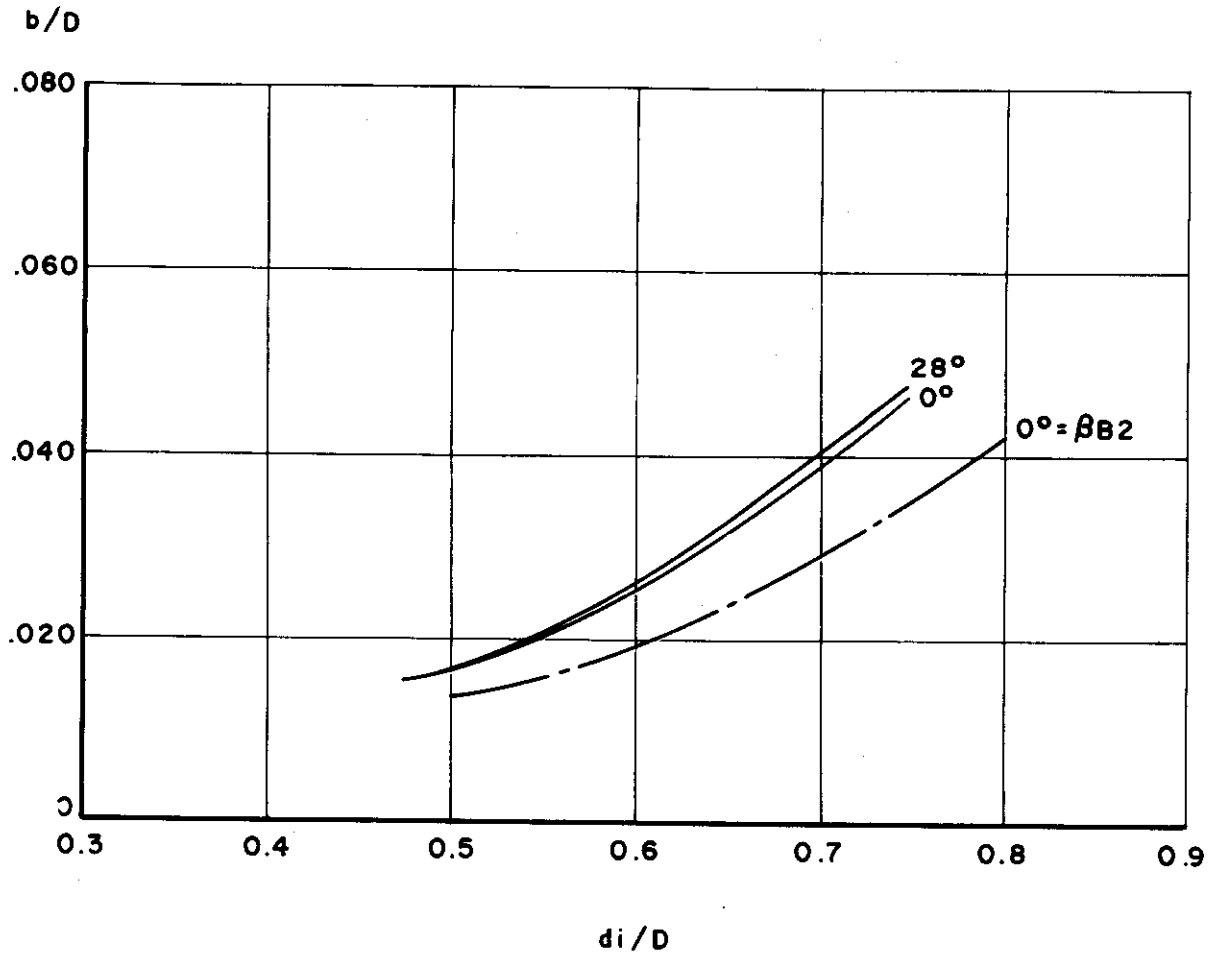


IMPELLER TIP WIDTHS FOR FREON II
AT $gH_{TH}/a_0^2 = 2.16$
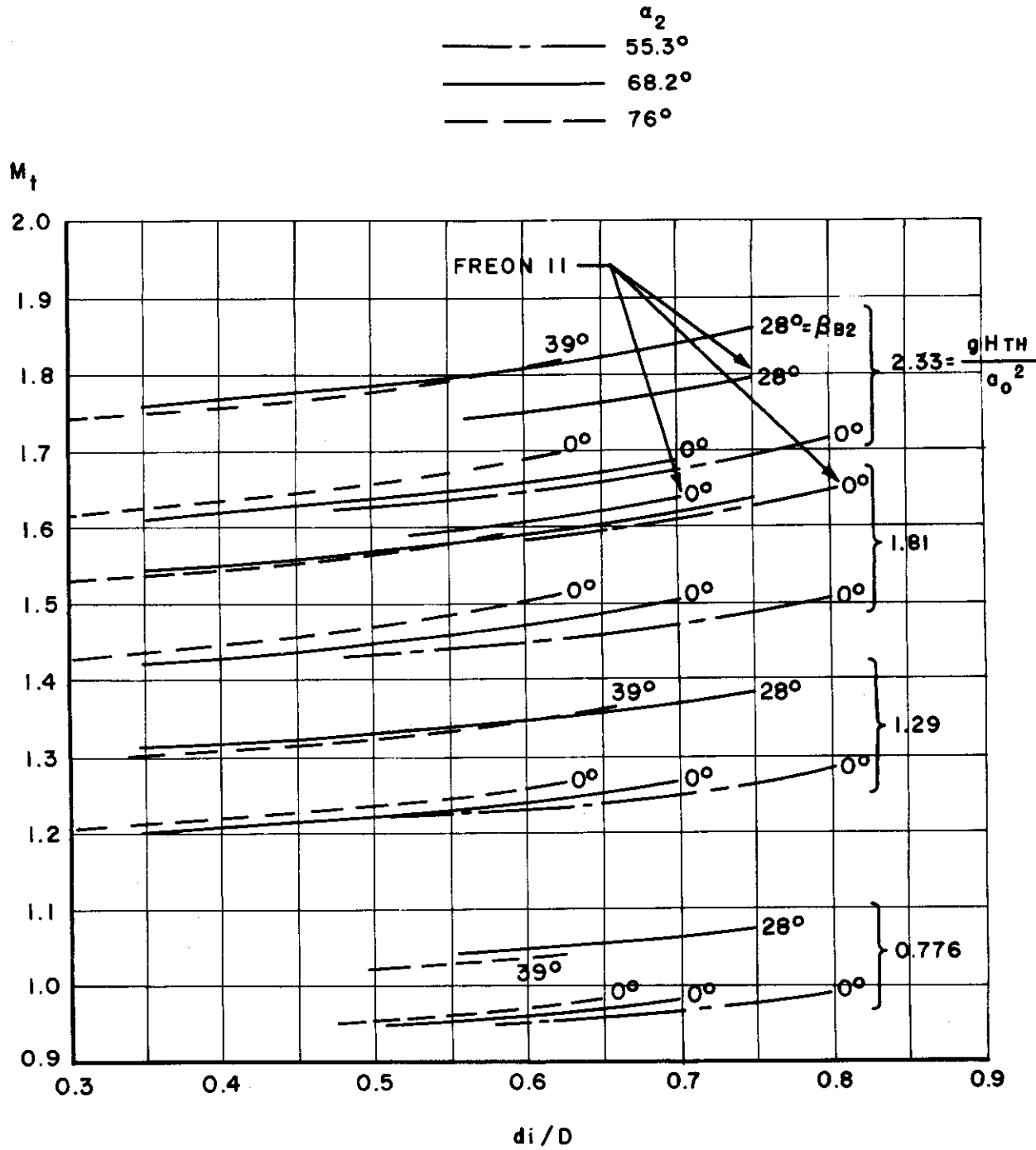
FIG. 2.25

FIG. 2.26   IMPELLER TIP MACH NUMBER FOR ALL $gH_{TH}/a_0^2$

ALL $\dfrac{gH_{TH}}{k^{a}o^{2}}$

ALL

$a_2$

———  · ———  55.3°

————————— 68.2°

— — — — 76°
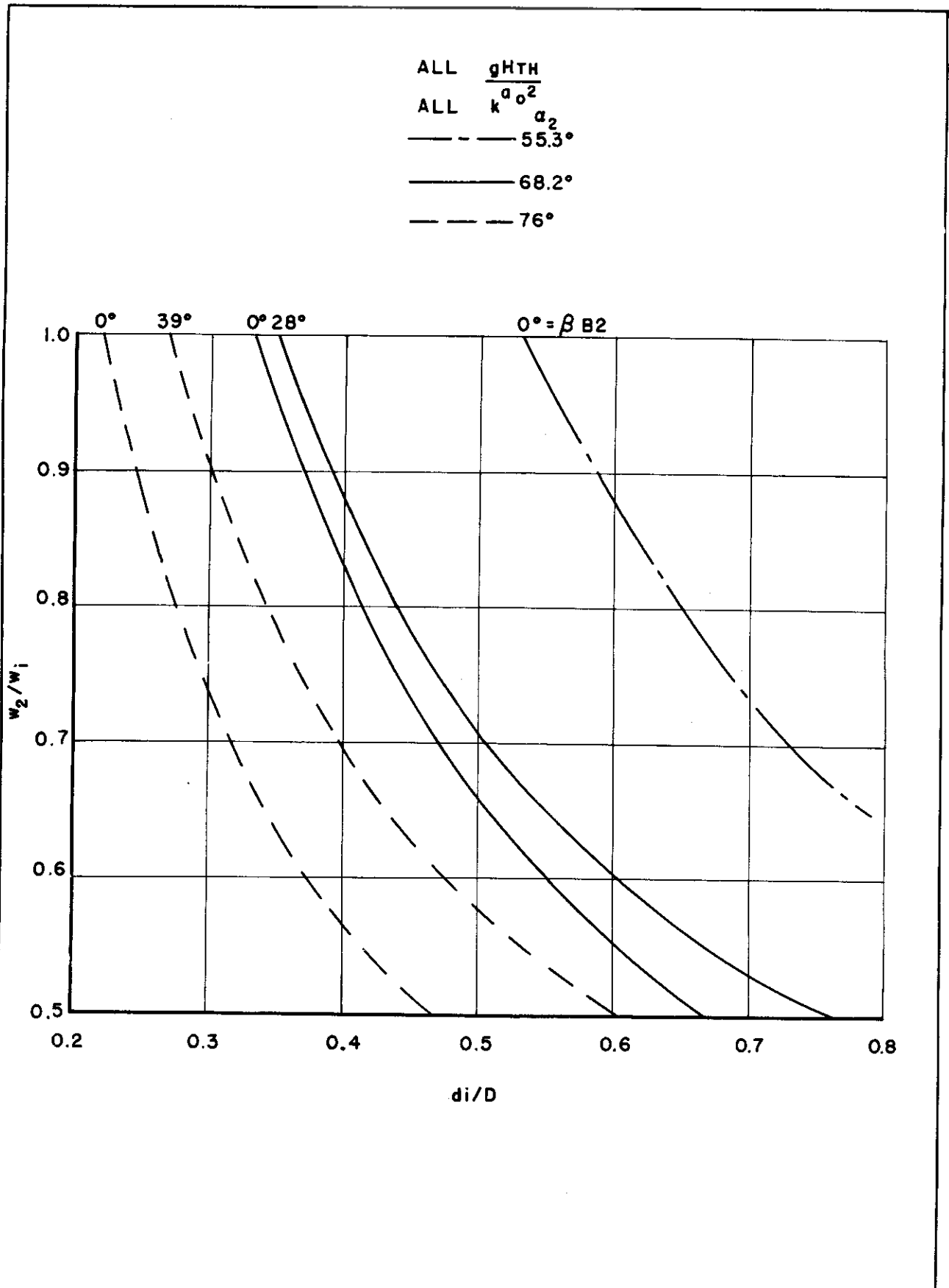
FIG. 2.27

IMPELLER DECELERATION RATIOS
FOR ALL $gH_{TH}/a_0^2$ AND ALL $K$
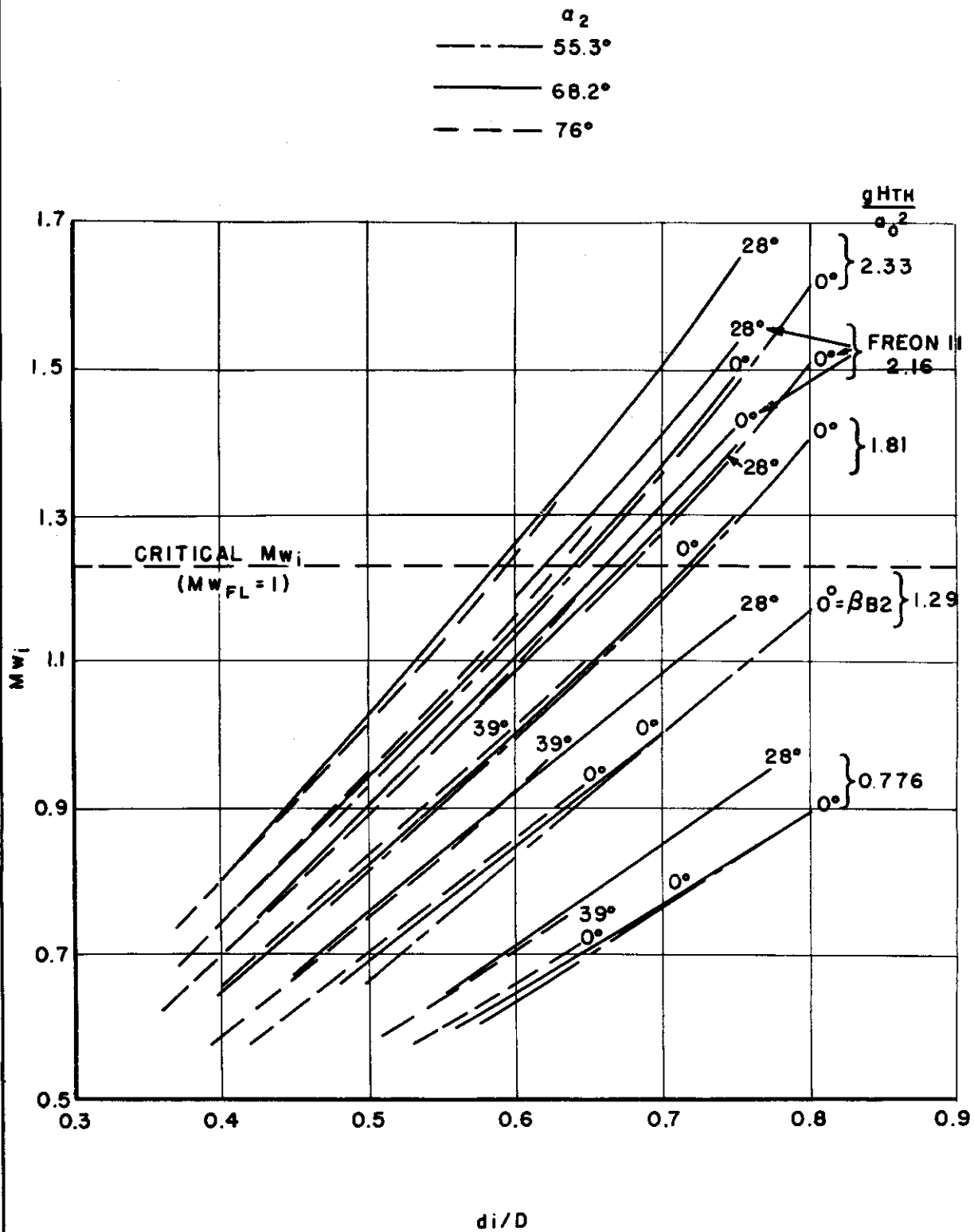
FIG. 2.28
INDUCER TIP RELATIVE MACH
NUMBERS FOR ALL $gH_{TH}/a_0^2$

ALL $\dfrac{gH_{TH}}{a_0{}^2}$ } ± 3% IN $\nu$

ALL k

| $a_2$ | |
|---|---|
| 55.3° | |
| 68.2° | |
| 76° | |

$0° = \beta_{B2}$

28°  0°

39°  0°

di/D

$\nu$ - DIMENSIONLESS SPECIFIC SPEED
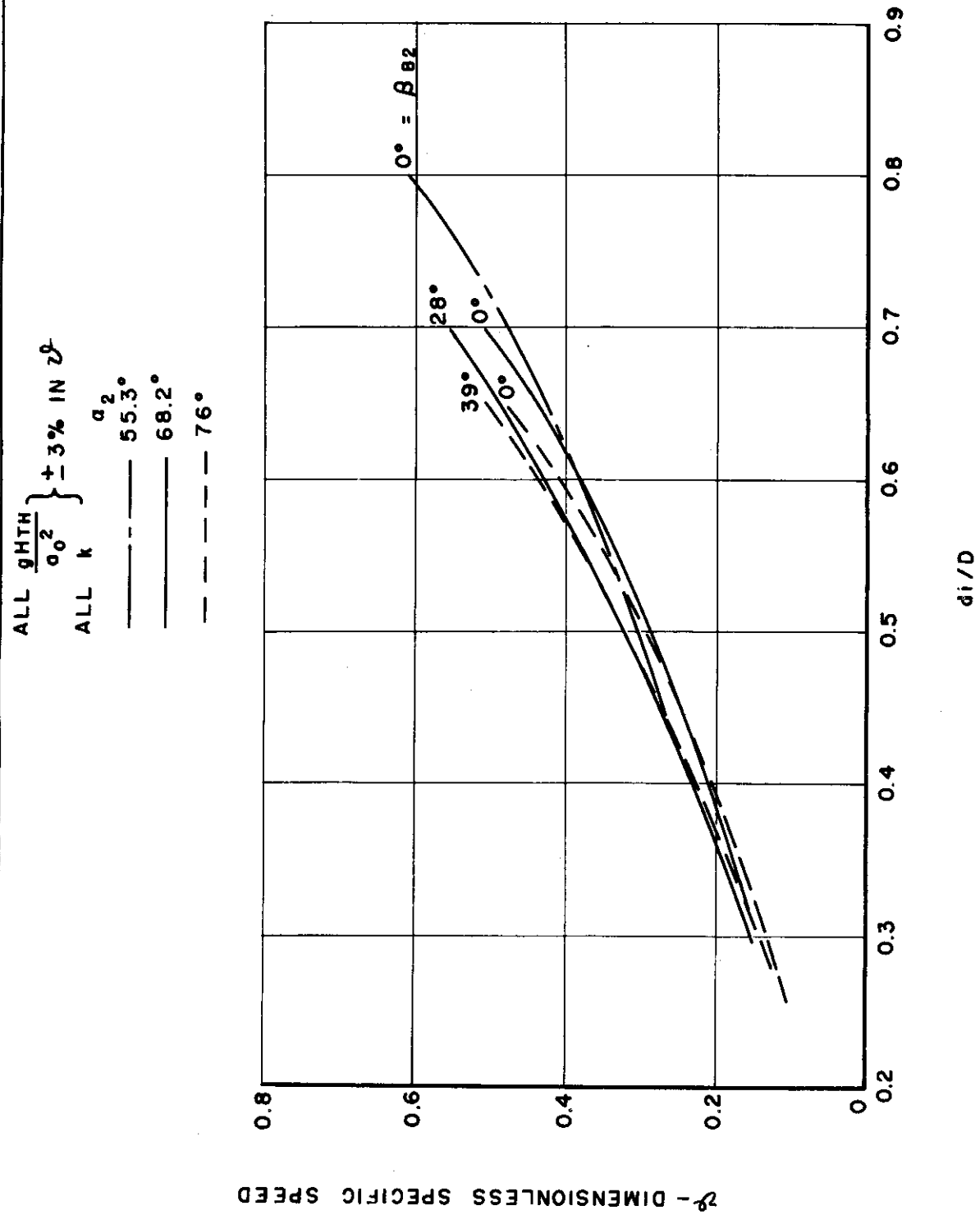
## DIMENSIONLESS SPECIFIC SPEED
## FOR ALL $gH_{TH}/a_0{}^2$ & ALL K

FIG. 2.29

$\dfrac{\eta_{AD}}{(\eta_{AD})_{T.P.}}$

TYPICAL POINT

$a_2 = 68.2°$

$\dfrac{d_i}{D} = 0.606$

$\beta_i$
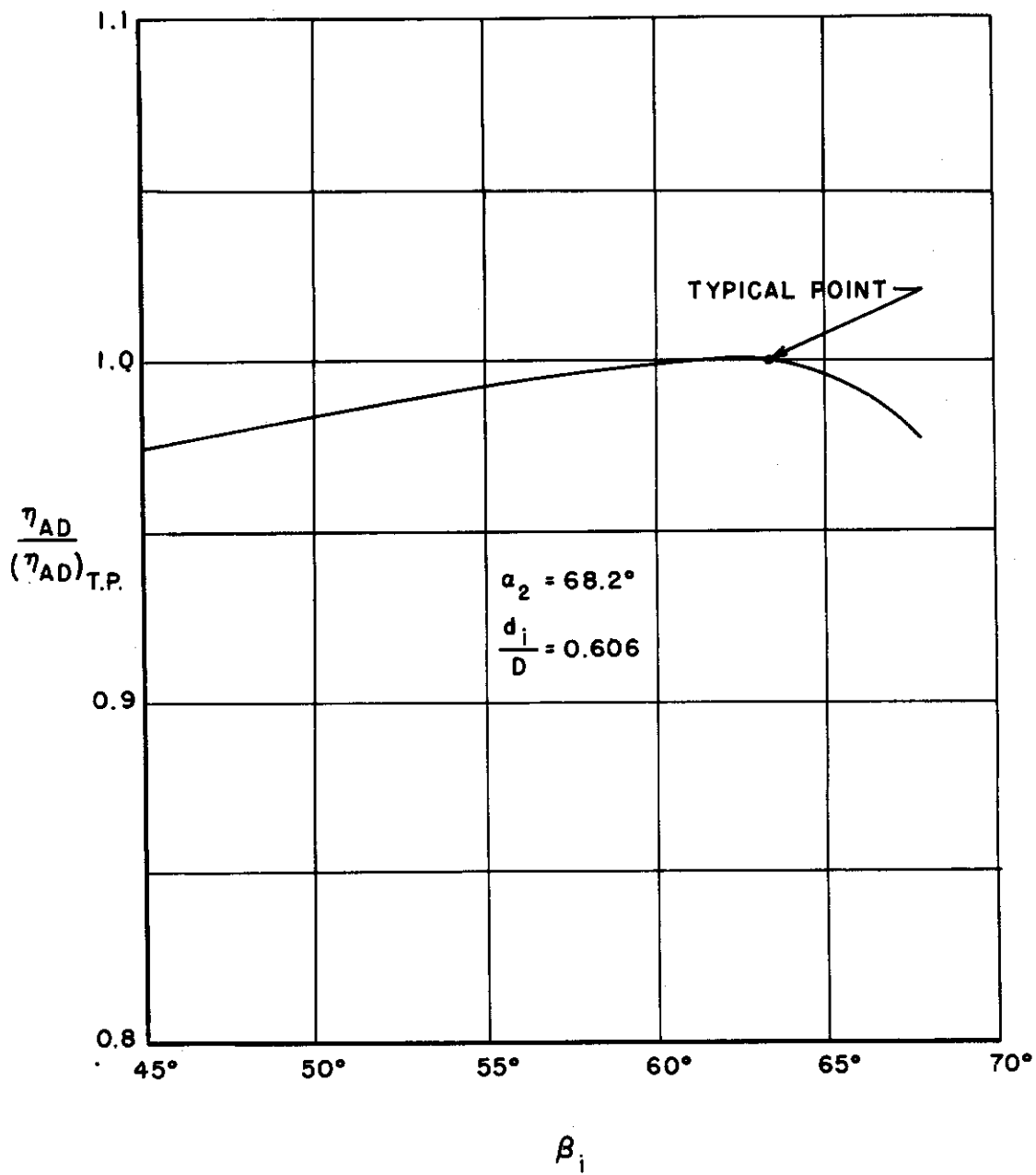
FIG. 2.30    EFFICIENCY VARIATION WITH INDUCER
TIP FLOW ANGLE (OR BLADE ANGLE)

NOTE : $M_t$ FIXED; VARIATION OF $Re_t$ IMPLIES ONLY VARIATION OF $\dfrac{a_0 D}{\left(\dfrac{\mu}{\rho}\right)_0}$



$\dfrac{\eta_{AD}}{(\eta_{AD})_{T.P.}}$

$\log_{10} Re_t$
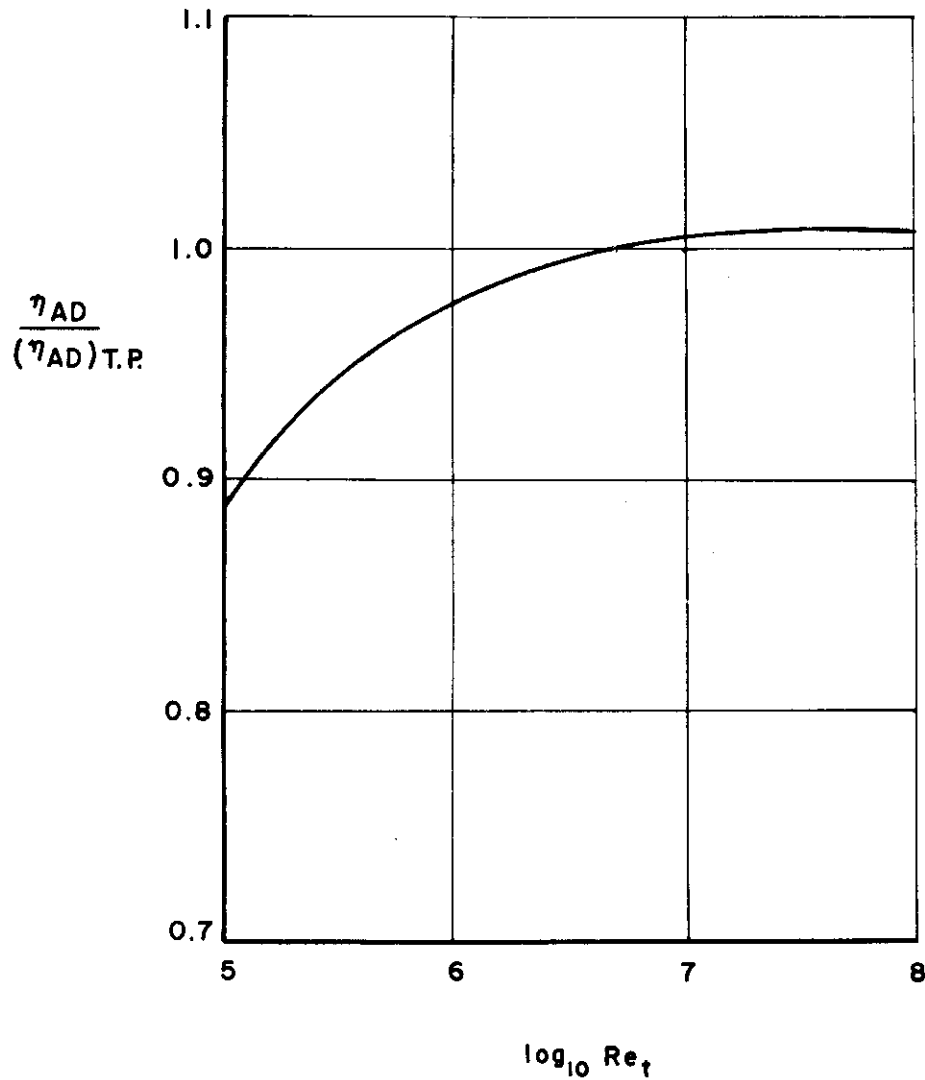
## FIG. 2.31    EFFICIENCY VARIATION WITH IMPELLER REYNOLDS NUMBER

WADC TR 55-257

$$\frac{\eta_{AD}}{(\eta_{AD})_{T.P.}}$$



$$\upsilon = d_h / d_i$$
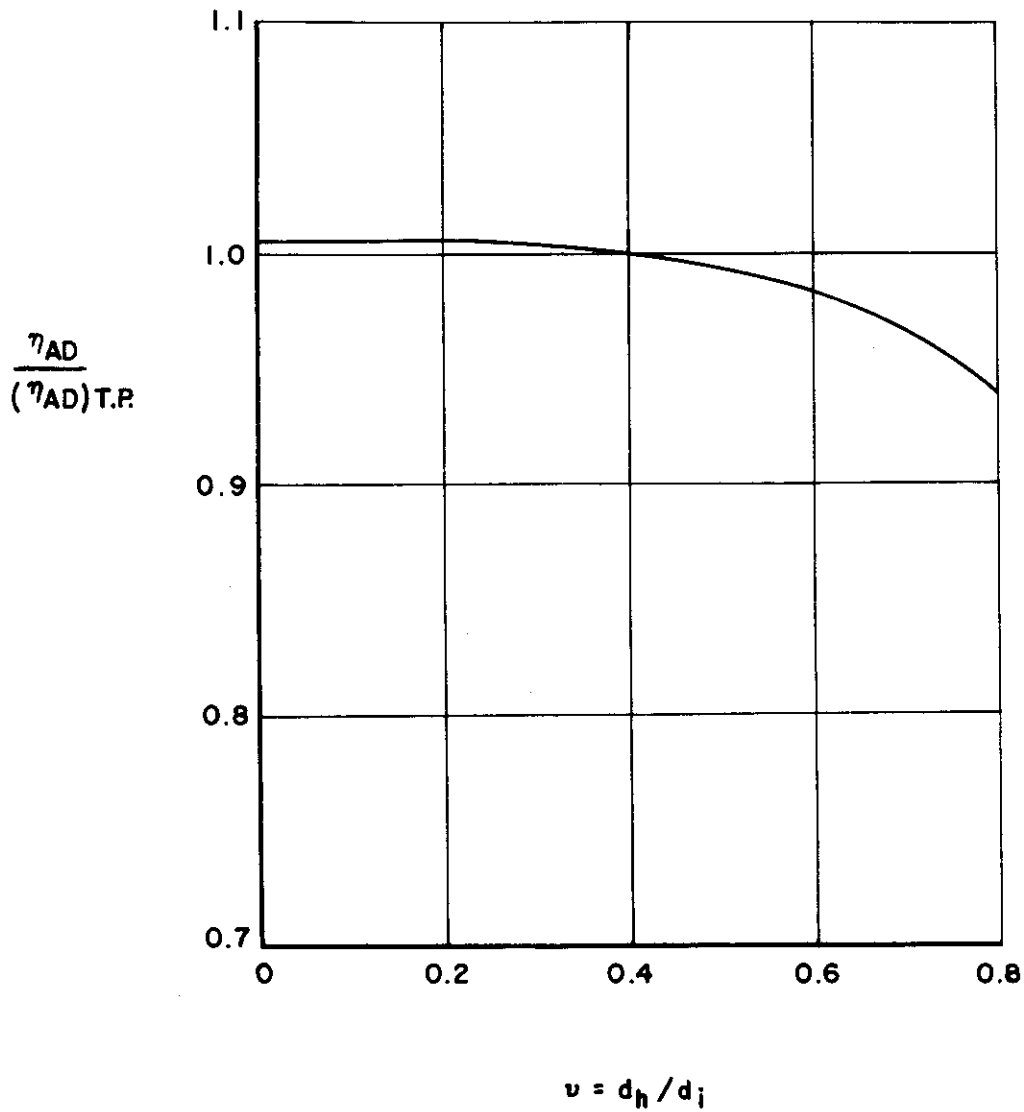
EFFICIENCY VARIATION WITH
INDUCER HUB-TIP RATIO
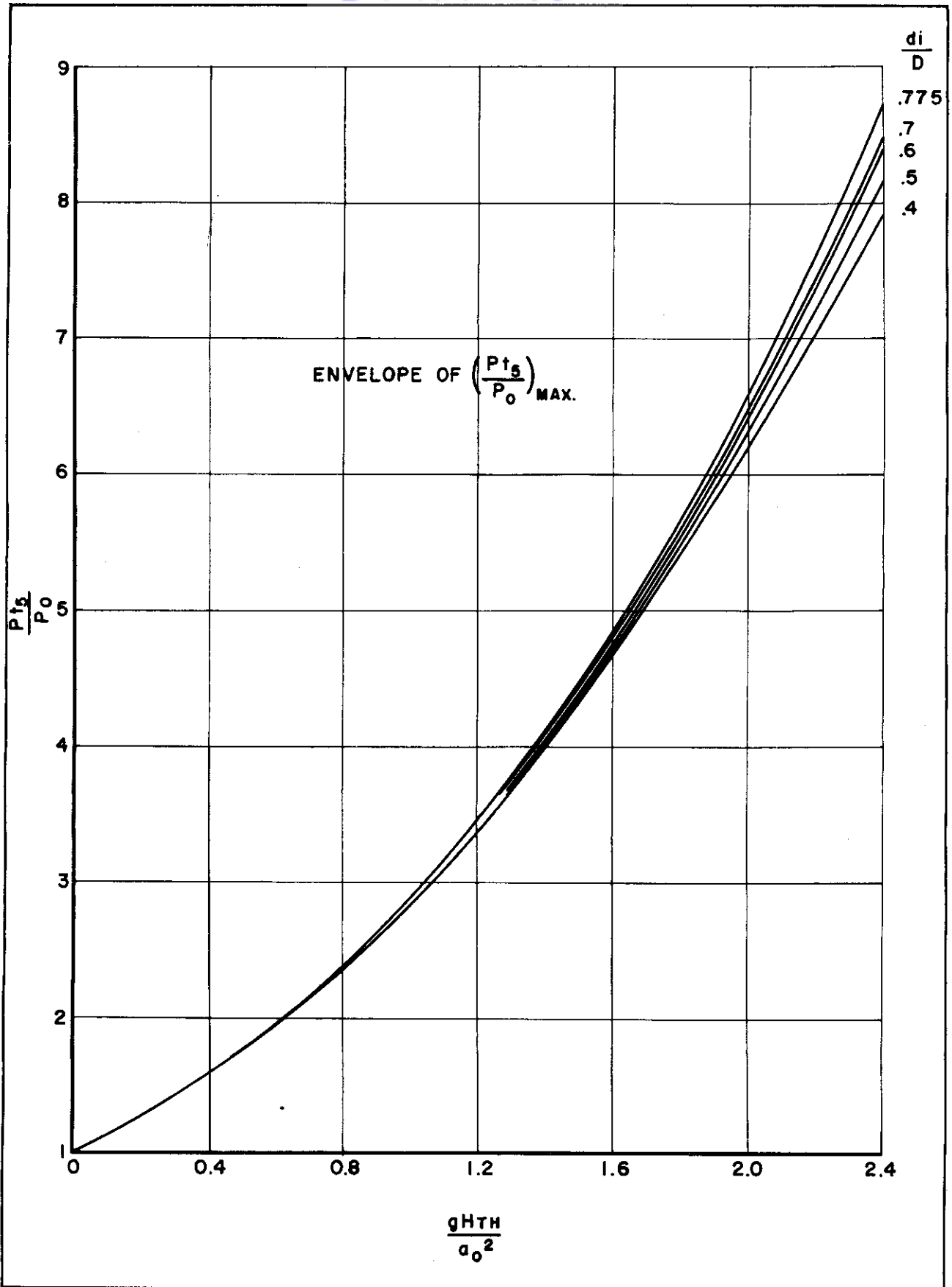
FIG. 2.32

ENVELOPES OF MAXIMUM PRESSURE RATIO CURVES, FOR PRESSURE RATIO INTERPOLATION

FIG. 2.33

IMPELLER DESIGN THEORY

## 3.1  Introduction

The impeller theory is intended to provide the designer with an analytical tool for an optimized impeller design.

A one-dimensional approach is generally used to arrive at the exterior shape of the compressor, thus determining the inducer and tip diameter, tip width, degree of backward curvature, and tip speed.  In short, the velocity triangles are established.  This phase of the work is treated in the preceding chapter.  A second phase  deals with the internal shape of the impeller passages, which lead to the desired velocity triangles.  The approaches to this second phase may be suitably divided into 4 chapters.

The first chapter (3.2.1) presents design criteria such as desirable velocity distributions on suction and pressure side of the blades at hub and shroud.

The second chapter (3.2.2) reviews the methods applicable to the design of impellers following the recommendations of chapter (3.2.1).

The third chapter (3.2.3) describes a method which is considered to be particularly suitable for the design problem at hand.

Finally, in the fourth chapter (3.2.4), some particular problems occurring with supersonic relative velocities at the inducer are treated.

Of these four chapters, the first is by far the most important:  it should provide the desirable velocity distribution as the key to the impeller with best efficiency.  Unfortunately, least is known about this topic.  The problem is approached first  by applying the knowledge of two-dimensional boundary layers as far as possible to the phenomena within the impeller.  Then qualitative knowledge of the secondary flow in boundary layers and of separated flow is used to modify conclusions drawn from two-dimensional boundary layer calculations.  In addition to this, some meager performance data of impellers with known velocity distributions are used to discuss a series of typical possible velocity distributions in radial or mixed-flow impellers.  This discussion leads to the choice of the most desirable velocity distribution.  There is certainly much speculation involved in this section; however, it is considered to represent the present state of the art.

The second section is essentially a review of the impeller design methods available in literature.  Most of those methods are not for design purposes, since they only allow to calculate the velocity in an already designed impeller.  However, each calculation method may also be used to design an impeller by assuming the shape of the impeller, calculating the velocities and comparing them to the velocities recommended from the design criteria of Chapter 3.2.1.  The procedure has to be repeated

71

and the impeller shape changed until sufficient agreement is obtained between calculated and desired velocity.

A calculation method well-adapted to this iteration process is presented step by step in Chapter 3.2.3. It consists of a combination of well-known and of some new procedures. This calculation method is especially well-adapted to the present design task because the accuracy of computation (and thus the time required) can be adjusted to the conditions. When the impeller shape is far from the final one, low accuracy is required, while after some iteration, the accuracy must be improved. This feature of adjustable accuracy results in a considerable saving of time.

Finally, in the fourth section, special problems occurring with supersonic relative velocities are discussed. A few remarks are made about computational procedure available in literature. Design criteria additional to those given in section one are mentioned (and the shape of an inducer which satisfies these criteria is shown).

The purpose of a compressor design is to conceive of a machine which compresses a fluid most efficiently under the given conditions of mass rate of flow, pressure ratio, rpm, tip speed, etc. Often two conditions only, mass rate of flow and pressure ratio, for example, are given. In all cases, however, the designer has a vast freedom in the design. Among all possible compressor shapes, there is one only which yields the best performance efficiency*. The purpose of this chapter is to limit the design freedom such that the final product is as near as possible to the optimum.

This goal is generally approached by first determining by means of one-dimensional calculations the exterior shape of the compressor such as inducer, tip diameter, tip width, and degree of backward curvature of blading. This is identical with establishing the velocity triangles. The internal shape of the impeller is then determined by three-dimensional flow calculations which will be treated in this chapter, while the first phase was already treated in Chapter 3.2.1. The two phases are naturally not independent of each other. In order to accomplish the first phase, losses had to be assumed which depend on the internal design, subject of the second phase. Thus the results of Phase 1 are based on the art used to build the machines whose test results influenced some assumptions used in the performance prediction. But it is probable that a slight shift only of the optimum will occur.

The design problem, essentially, is to find the impeller geometry which leads with least losses from given inlet to given outlet velocities. This problem has been treated quite thoroughly with axial-flow compressors. Extensive tests have been carried out on cascades with various solidities, stagger angles, camber lines and thickness distributions and aspect ratios. The best combinations of these variables are fairly well established today.

---

* It is understood that a restricting condition always maintained in this report is that we accomplish the compression in a one-stage machine.

The problem at hand, unfortunately, is more complicated, inasmuch as there are several additional degrees of freedom, factors which would have to be varied in an experimental investigation; such additional factors include the form of the camber line of the blades and the shape of hub and shroud.

The shape of the camber line of the blades in axial cascades cannot be varied very much since the camber angle and the fluid turning angle are relatively small. This is not so in our case. It is felt that the best radial or mixed-flow compressor cannot even nearly be obtained by prescribing a predetermined shape of the camber line such as a circular or parabolic arc to be varied, as in the case in axial compressors.

A similar situation arises with respect to the meridional shape of the impeller: an optimum shape cannot be obtained by varying a single parameter.

Because of this freedom of design, tests which vary the shape at random would be prohibitively expensive. Therefore, a more fundamental approach has to be chosen, or, in absence of a fundamental theory, more speculation has to be used.

Losses in the impeller are due to friction at the walls and due to boundary layer separation. This separation involves a loss for several reasons; such as, the kinetic energy in the vortices produced by the separation is lost by dissipation and the stagnating fluid clogging the passage increases the velocities at other places. The increased velocities raise the friction losses and, more important, the corresponding kinetic energy cannot be recovered efficiently since the stagnation pressure varies over the cross section from zero within the separated zone to the full value in the flow region. This means that mixing losses occur.

Whether and where the boundary layer will separate and how this can be avoided or postponed is then the more fundamental question.

It is well-known that the behavior of the boundary layer depends on the pressure and velocity distribution outside the boundary layer. Suppose now that within the limits of our problem we could find the velocity and pressure distribution which yield least separation, and thus least losses; then the problem would be reduced to that of finding the geometrical shape which gives this predetermined velocity and pressure distribution.

The task of finding the best velocity distribution, henceforth called the "design criteria", involves much speculation at the present state of the art.

On the other hand there exists a useful theory on how to design an impeller for a required velocity distribution. The opinions differ only as to the most practical combination of procedures. The answer to this question depends on circumstances such as accuracy required, or training of the men performing the calculations, etc. A method which is a combination of well-known and new procedures has evolved at AiResearch and is presented in the following chapters.

First,however, something must be said about the design criteria. Obviously,
these are the clue to a good design, since, if they are known, the actual design
follows uniquely. Unfortunately information which would allow us to establish such
design criteria is rare. The information available applies only indirectly to
the problem at hand: the radial-flow compressor. In the next chapter, it is
attempted to use the available knowledge and some speculation to arrive at the
best velocity distribution.

## 3.2    The Impeller Design Approach

### 3.2.1    The Design Criteria - The turbulent two-dimensional boundary layer can be
calculated when the velocity and,therefore,the pressure in the free stream,is
known. A necessary condition for the existence of a two-dimensional boundary
layer is the absence of a pressure gradient normal to the streamlines and parallel
to the solid surface. This not being the case in general, in a compressor, the
boundary layer is not two-dimensional and the calculations become very difficult.
In addition,centrifugal forces absent in conventional two-dimensional boundary
layer calculations  influence the situation  when the centrifugal forces on free
stream and boundary layer are unequal. In the inlet the tangential velocities
(and therefore the centrifugal forces) are certainly not equal, but in the radial
passages of a radial-flow machine these forces are not much different,since the
tangential velocities are about the same in main stream and boundary layer. Thus,
in most impellers it is useful to consider the relative velocities for the calcu-
lation of the boundary layers.

The pressure gradient perpendicular to the streamlines remains,of course,an
important factor. Its effect is to displace the boundary layer from high pressure
areas towards the low pressure areas; for instance,the boundary layer on the pres-
sure side of the blades gets thinner, because part of it accumulates on the suction
side of the blades. With this qualitative knowledge in mind,it makes sense to
make quantitative calculations of the boundary layer assuming it to be two-dimension-
al. Of course,into these calculations have to enter the local relative velocities
outside the boundary layer.

These relative velocities may not be assumed arbitrarily: Usually the
average exit velocity is considerably smaller than the average inlet velocity.
However,more deceleration is involved than is indicated by this velocity ratio,
since the turning of the flow in the impeller necessarily results in a velocity
on the blade suction side larger than the average used in the velocity triangles.

The question therefore arises: given an initial (maximum) velocity and a
final (minimum) velocity, what velocity distribution produces least losses?

Let us consider some typical possible relative velocity distribution with
given inlet and outlet relative velocities on Figure 3.1. On each figure,the
relative velocities on suction side, pressure side and in the middle of the
blades near shroud and hub is drawn. Because of stress consideration,we assume
that the blades consist of radial elements,and therefore,the blade form near the
hub follows from the blade form near the shroud,and so do the velocities. The
relative velocities can therefore not be chosen arbitrarily. One has to make a

compromise between the velocities along the shroud,along the middle streamline and along the hub. It is felt,however, that more attention has to be paid to the shroud velocity than to the hub velocity. Only where stress considerations do not enter, can both the velocity distribution at shroud and hub be chosen freely and improved aerodynamic design of the compressor is possible.

In Figure 3.1a the average velocity decreases linearly from inlet to outlet; calculations show that the average velocity at the hub decreases at a rapid rate at first and increases later on for the usual meridional shape of radial-flow impellers. In Figure 3.1b the average velocity at the shroud decelerates first at a rapid rate and at a slower rate later on. As a result,the velocity at the hub decreases such that the flow direction reverses. This may increase the relative velocities at the shroud from the full-drawn line to the dotted line (Figure 3.1b). Finally, in Figure 3.1c the velocity at the shroud stays constant at first and drops later. This results in uniform or slightly accelerated velocity at the hub.

Figure 3.1a' and Figure 3.1a" show typical variations of the loading keeping the average velocity the same as in Figure 3.1a: Figure 3.1a' shows an unloaded inducer, and Figure 3.1a" shows a loaded inducer while the other figures show evenly loaded blades. Both basic loading pattern a', a" may be combined with the basic average streamline velocities of Figure 3.1b and 3.1c. Hence nine basic velocity distributions may be considered.

Before being able to give preference to one of the discussed velocity distributions, some results of boundary layer calculations have to be considered.

Results of boundary layer calculations are presented in Figure 3.2 according to Reference 3.1. This method of calculation predicts quite reliably the behavior of the boundary layer under conditions as they exist on an airplane wing. This same method is used here to predict the boundary layer behavior when the free stream velocity decreases linearly with the distance along the boundary for various rates of diffusion. The conditions at the inlet, (i.e. boundary layer thickness $\delta$* and shape factor H), are kept constant. The result of the calculations is shown by means of lines of constant shape factor H and lines of constant-displacement thickness $\delta$*. The shape factor H is a measure of the boundary layer profile; the larger H is, the nearer is the point of separation, for instance, at H = 2,separation is imminent. Figure 3.2 shows that separation is imminent (i.e. H = 2) at the velocity ratio of .625 when decelerating slowly,and at a ratio of .675 when decelerating extremely fast (as in a shock). Apparently,the velocity ratio at which separation occurs is nearly the same independent of the deceleration rate. However, when decelerating at a slow rate,the boundary layer displacement thickness is considerably larger then in the case when the same final velocity is reached at a rapid rate of deceleration. Since a thick boundary layer is undesirable,an initial rapid rate of deceleration seems to be desirable.

An additional observation is worth mentioning. Design velocity ratios of two to one are not uncommon in impellers; but Figure 3.2 shows that such a velocity ratio cannot be reached without separation, even under the relatively favorable initial conditions assumed.

From boundary layer considerations the following conclusions can be made:

1. It is desirable to use a large deceleration rate prior to separation.

2. Separation will occur for velocity ratios commonly used in radial and mixed-flow machinery.

The last statement leads one to consider the region where the boundary layer assumes such a large proportion of the flow area that the boundary layer loses its meaning in the classical sense. The low stagnation pressure fluid in this region may not necessarily flow backward, but simply move in any direction. The whole region is unstable inasmuch as the main flow of high stagnation pressure has a tendency to adhere to one side of a duct while the stagnating fluid accumulates in the vicinity of the other side. Under these conditions only little pressure recovery may be expected. The main flow attached to one side of the channel behaves essentially like a free jet and maintains constant velocity, whose kinetic energy cannot be used easily in view of the presence of low stagnation pressure fluid. Secondary flow considerations show that the main stream adheres to the pressure side of the channel while the separated fluid accumulates, where, in potential flow, the pressure would be low. If the pressure difference between both sides of a channel is large, this flow pattern (no more pressure rise and jet behavior of the flow) is set quickly, while in a channel where no such pressure difference between the walls exists, the main stream may take considerable length until no more pressure rise occurs. Therefore, a very light loading in the region where this flow pattern is expected, i.e., near the outlet of the impeller, seems to be desirable.

In the light of this knowledge, we may now look again at the typical velocity distributions of Figure 3.1.

Considering the velocities near the shroud, our principle of rapid first deceleration will lead us to the preference of an average velocity as shown in Figure 3.1b, as long as no backflow occurs near the hub. Backflow at the hub would simply mean that the rapid deceleration would not occur in reality, because the flow area is restricted by stagnating fluid. The rapid deceleration at the hub has another drawback: If the boundary layer becomes thick, it flows along the blades towards the shroud and leads to flow separation there. Thus the rapid deceleration at the hub, if any, should be postponed so far towards the impeller outlet that the boundary layer developed there does not disturb the flow in the inducer section near the shroud.

Now, our desire to load the blades slightly near the outlet necessitates a high loading in the inducer region in order to impart to the flow a given moment of momentum. This leads to a loading distribution as shown in Figure 3.1a". The consequences of the highly loaded inducer are apparently these:

a. On the pressure side a very large deceleration occurs which might lead to separation since the velocity ratio of .65 tolerable in two-dimensional flow is exceeded. But this is not so: the boundary layer on the pressure side gets very rapidly thinner because of secondary flow and velocity ratios of .5 may therefore be obtained without backflow. Hence a rapid deceleration on the pressure side may not be too disadvantageous.

b.  On the suction side of the blades, the velocity increases high above
the average.  This is a serious drawback since this leads to earlier
boundary layer separation on the suction side with all its consequences.
Therefore, the maximum loading should be reached shortly after the
inlet, while maintaining the peak velocity at the minimum possible
value, consistent with the desired high blade loading.

We have as yet not mentioned the influence of transonic and supersonic con-
ditions.  A separate chapter will be devoted to this problem.  Here, it suffices
to say that the guiding "design criteria" are the same.

Summarizing the design principles, we may state:  An exact velocity distri-
bution leading to the optimum configuration cannot be given as yet.  The funda-
mental principles, that is, the boundary layer considerations, lead to different
results in different cases, and in addition, the fundamental principles themselves
are as yet not too well known.  However, it appears from theoretical considera-
tions that two requirements should be met.

a.  Rapid deceleration in the inducer region.

b.  High loading of the inducer as compared to the end part of the impeller.

Following these principles, the velocities in the impeller might look as
shown in Figure 3.3, a combination of Figure 3.1b and Figure 3.1a".

## 3.2.2  Review of Impeller Design Methods

This review does not intend to be complete nor to do justice to those who have
devised the methods.  The purpose is to inform the reader about the present state
of the methods in use.  References are therefore used only for the purpose of
avoiding lengthy explanation in the present report.

The problem is apparently to find the geometrical shape of an impeller which
provides a velocity distribution as shown in Chapter 3.2.1, "Design Criteria".
This problem is called "indirect" and is very difficult to solve, especially be-
cause not every velocity distribution leads to a solution; the design criteria
have to fulfill some conditions which cannot be easily formulated.  Usually it is
more convenient to use the "direct" approach by guessing at the shape first, then
calculating the velocities which correspond to it and changing the guessed shape
until the calculated velocities correspond closely enough to the velocities de-
sired.  The "direct" approach has the advantage that experience of the designer
can easily be embodied into the design.  Especially, experience relating to stresses
and manufacturing can be used in order to eliminate all designs which are impract-
ical from a mechanical standpoint, though favorable from an aerodynamic standpoint.
Combinations of direct and indirect methods may also be used, as will be shown in
the next chapter.

Basically, the problem to be solved is:  "Given an impeller with fixed
geometry and rpm, calculate the velocities at every place within the impeller."

Before the review of the publications treating this problem, a remark about the effect of the viscosity is in order. Be it said at the outset: All methods treat the flow in absence of viscosity. We know that in general the viscosity changes the flow picture fundamentally. Is, therefore, a method treating inviscid flow of any use? The answer is this: A good design should eliminate separation at least in the first part of the impeller. Hence the inviscid flow calculation may approach very closely the real flow, if the displacement effect of the boundary layer is taken into account. Whether a design is bad, i.e., whether it leads to early separation can be found from the calculated velocities as they would occur if no separation would take place and the design is changed correspondingly. Even in a good impeller, separation may occur towards the end of the passage and the calculated inviscid flow is then no more a good approximation to the real flow. Nevertheless, the calculated flow still is a good guide to the calculation of the secondary flow, which, when added to the inviscid flow, gives a fairly good picture of the reality. In any case, the inviscid flow has to be calculated first.

The problem can be formulated in the case of absolute irrotational, adiabatic flow by a single differential equation in terms of a velocity potential as given in Reference 3.3 (Eq 250), for instance. The solution of this equation with the corresponding boundary conditions is so cumbersome, however, that it is not a very useful tool for a design method where the calculations have to be repeated.

Wu (Ref. 3.3) reduced the partial differential equation of 3 variables to a pair of differential equations of 2 variables each, which makes the solution much less unwieldy if not too many iterations have to be used. Each equation describes the flow on a stream sheet ($S_1$) whose fluid particles lie upstream of the rotor on a circular arc (Fig. 3.4) or on a radial line (Surface $S_2$) (See Fig. 3.5). In order to solve the quasi- two-dimensional equation describing the flow on a stream sheet, the knowledge of the form and thickness distribution of the stream sheet is necessary. This knowledge is gained by a process of iteration: First, for instance, the shape and thickness distributions of two stream sheets ($S_1$) whose particles lie upstream on two circular arcs, one of large and the other one of small radius, are assumed. (See Fig. 3.4.) This calculation leads to the form and thickness distribution of a stream sheet whose particles upstream lie on radial lines such an angle apart that the stream sheets are between the same pair of blades as on Figure 3.5. The solutions of the partial differential equation for these stream sheets ($S_2$) lead to a better approximation of the assumed shape and thicknesses of stream sheets $S_1$; the partial differential equation for these surfaces $S_1$ have to be solved again, leading to a better value for the position of stream sheets $S_2$ etc.

This method of iteration is equivalent to the solution of the three-dimensional equation; but from a purely mathematical standpoint, it is just as complicated. The advantage lies in the possibility that the designer can use his experience in choosing the initial form and thickness distribution of the stream sheet so well that no iteration is necessary. This is possible in particular when the stream sheet does not twist much relatively to the blades, i.e., when the particles which lie on a circular arc upstream of the cascade remain nearly on a circular arc. For high specific speed machines this is so to a satisfactory degree of accuracy; for low specific speed machines, however, analysis shows that the stream sheets

distort considerably. This is shown in a striking manner in Figures of Reference 3.4 which present the solution of the exact three-dimensional equations of incompressible inviscid flow. One of these figures is reproduced here as Figure 3.6. A look at this figure shows that a guess of the form of these stream sheets is impossible, and an iteration which leads to it is impractical.

The question therefore arises whether the approximation is sufficient when not using any iteration at all and assuming the shape of the stream sheets a priori to be lying on a surface of revolution or on a plane midstream between the blades.

If this assumption is made, the solution of the axisymmetrical flow with an infinite number of blades is very near to the solution on the stream surface midway between two blades (Ref 3.5). This procedure, namely, calculating first an axisymmetrical solution and then a second solution on a surface of revolution obtained by rotating a streamline of the first solution around the axis bounded by two neighboring blades, has been used very extensively. This method (Ref 3.4 etc.) yields a quasi-three-dimensional solution, called henceforth q.3.d, three-dimensional, inasmuch as the solution allows one to calculate the velocity varying as a function of the three coordinates. The assumption that the streamlines lie on predetermined surfaces is, of course, mathematically wrong. The question as to the error of the calculated velocities has been answered by Reference 3.4 in the sense that such a method describes the flow with sufficient accuracy for engineering analysis. This result is arrived at by comparing an exact three-dimensional solution with the result of a quasi-three-dimensional calculation described above.

Considering the above-said, we find:

a. The accuracy of the q.3.d. procedure is within the accuracy of our knowledge of the design criteria.

b. The method is being used for design, i.e., the geometry is changed until the velocities are found satisfactory. The effect of design changes are just as well brought out by the q.3.d. procedure.

c. Since the calculations have to be repeated several times for different geometries, any saving in time is essential.

Hence we will use the q.3.d. approach, and we shall discuss only the two-dimensional procedures which lead to the axisymmetrical solution and the blade-to-blade solution which, when combined, constitute the q.3.d. solution.

Before we proceed to the detailed discussion of the two-dimensional solutions, a final remark about the differences between the three-dimensional solution and q.3.d. procedure is in order. In the chapter about design criteria, it was tacitly assumed that a particle which initially lies on a surface of revolution formed by the rotation of a streamline of the axisymmetrical flow remains on this surface of revolution, in particular, that a particle near the shroud remains near the shroud.

According to Reference 3.4 this is not so; for instance, a particle entering the inducer near the suction side of the blade at the shroud ends up, in potential flow, at the shroud near the pressure side of the blade. (See Fig. 3.6.) Thus, along this streamline the deceleration rate is larger than assumed in the discussion of the design criteria, although the local velocity may have been predicted correctly. Thus, the q.3.d. method predicts correctly the local velocities, but further knowledge is necessary to predict the correct deceleration rate, namely, the knowledge of the streamlines. This latter knowledge cannot follow from the q.3.d. However, this knowledge might not be too helpful since the flow in the boundary follows a still different path.

The different methods which lead to q.3.d. solutions will now be discussed briefly. Obviously, the q.3.d. solution will always have a combination of an axisymmetrical solution, which describes the flow on a stream surface between the blades, and a solution on a surface obtained by rotating a streamline of the former solution around the impeller axis, henceforth called the blade-to-blade solution.

For the purpose of designing radial and mixed flow impellers, it is adequate to begin with the axisymmetrical solution.

This solution can be obtained by solving the two-dimensional differential equation which governs this flow. The differential equation and the method of solution is given in Reference 3.4. Such a procedure is suitable when a staff of computers or computing machines are at disposition.

A procedure more adapted for usage by engineers is given in Reference 3.6. The basic equations of equilibrium and continuity are used separately such that the meaning of the different symbols does not get lost during computation. This procedure leaves considerable freedom as to the accuracy to be obtained, and thus the computational effort can be adapted to the circumstances.

In order to obtain the blade-to-blade solution, it is again possible to write the complete differential equation governing this flow. This has been done in Reference 3.3 and, more specifically applied to the problem of the radial compressor, in Reference 3.7. In this reference, several solutions for particular cases are given.

In view of the high solidity, the problem of finding the velocity variation from suction to pressure side of the blades can be simplified. Reference 3.8 uses such a procedure for the indirect or design problem. This reference gives two procedures of varying accuracy; the first is a procedure assuming essentially linear variation of the velocity from blade-to-blade and is very rapid. The second procedure uses parabolic variations of the velocities.

The decision, which of the above-mentioned procedures or combination thereof should be used, depends on the purpose of the calculations and also on the type of help (engineers, mechanical computers, etc ) available.

In the next chapter, a procedure will be outlined which proved best for the design of a compressor with the help of engineers and no high-speed computing device, a condition which might prevail in many medium-sized factories. In addition, more emphasis is given to the design instead of merely to the calculation of the velocities for a given design. This is important in view of the fact that the methods discussed so far are only intended to calculate velocities with various degrees of accuracy. The accuracy of the calculation, however, need not be large at the outset when large changes in the design geometry are being made. Later, however, when the geometry is near to the final one, a higher accuracy of calculation is required. Such a time-saving flexibility of accuracy is embodied in the method which is presented in the next chapter.

### 3.2.3  The Design Method

### 3.2.3.1  General Principles

It was mentioned previously that the most logical procedure would be to start from the "Design Criteria" with an indirect or design procedure. It must, however, be remembered that these aerodynamic design criteria are not exactly known, while other requirements dictated by stress considerations, for instance, are quite exactly known and lead immediately to a fixed geometrical form such as a certain blade taper. In other words, considerable experience would be needed to prescribe velocity distributions which are satisfactory in every respect, in particular in mechanical respects, while the assumption of the geometry leads with little experience not too far from the optimum, at least nearer than the assumption of velocities within the impeller. This is in particular true for the assumption of the meridional shape and the blade thickness distribution. Here are some examples. A cylindrical shroud shape in the inducer region may be considered a very good compromise between aerodynamic and manufacturing considerations. Such a shape could hardly be obtained when the velocities are prescribed a priori. Similarly, in high-speed machinery, stress considerations rather than aerodynamic considerations describe the blade thickness. Anyway, stress considerations lead immediately to a shape which is usually very near to the final one. In view of this situation, a direct procedure has been selected, where the shape will be assumed first, and then the velocities calculated.

The calculation of the velocities, however, depend also on the blade camber line which is difficult to assume at first. In order to determine the blade camber line, an indirect approach suggests itself, i.e., fixing the relative velocities and calculating the blade form. But such a procedure would determine the blade thickness too, which we wish to prescribe at the very start. A way out is to prescribe only the blade loading which is identical to the variation of the difference of the relative velocities, disregarding the magnitude of the velocity, which is done by establishing the moment of momentum distribution along the blades.

These remarks suggest a certain mixture of direct and indirect design procedures. The direct procedures necessitate repeated calculation of a slightly changed shape, as follows: First, the geometry is assumed and the corresponding velocities calculated. Should the calculated velocities be different from those

indicated in the chapter "Design Criteria", the geometrical shape must be changed
and the difference between calculated and desired velocities will become smaller
with each new geometry. This difference will be very large at the first trial,
especially when the designer has little or no experience with the particular
geometry. In view of this large difference, only very low accuracy is first re-
quired. This could be of advantage if reduced accuracy could also reduce the
calculation time. With subsequent calculations the accuracy should be improved,
corresponding to the smaller difference between calculated and desired velocities.
In short, the ideal method should incorporate a flexible accuracy allowing for
rough calculations as well as for later refinements. This is a feature of the
method evolved at AiResearch which will now be presented in detail.

### 3.2.3.2  Simplified Design Procedure

### 3.2.3.2.1  Meridional Flow Calculation (Step 1)

A meridional shape is selected on basis of considerations, as set forth in
the following paragraph. It is assumed that the rotational speed of the impeller
is given or selected.

The inducer tip diameter is chosen such that the relative velocity at the
inducer tip is a minimum for a given mass rate of flow. This condition leads
to a flow angle $\beta_i$ at the inducer tip of approximately 60 degrees.

The impeller tip diameter is selected as a function of the degree of
backward curvature of the blades.

The tip width is calculated from the state of the air at impeller discharge
and a flow factor $\epsilon$ which takes account of the clogging effect of the blades
and of the boundary layer. A reasonable assumption is $\epsilon = .80$.

The next step is to fix the axial length from inlet to outlet impeller.
Since short channels seem to have less aerodynamic losses than long ones, provided
the curvature is not excessive, radial discharge of the flow is favored for ratios
of inducer diameter to tip diameter up to 0.5. For higher inducer-to-impeller tip
diameter ratios, the requirement of gentle curvature (say radius of curvature of
shroud larger than distance shroud-hub) can best be met with the mixed-flow design.

A deviation from radial discharge may also be required if the blades are to
be backward curved and, in addition, should consist of radial elements in order to
withstand the stresses due to high tip speeds.

This is illustrated in Figure 3.7. A simple geometrical relation exists for
radial blade elements between the backward curvature $\beta_b$, the discharge angle $\gamma_t$ and
the rake angle of the trailing edges $\delta$ (See Fig. 3.7). The relation is

$$\tan \delta = \frac{\tan \beta_b}{\cos \gamma_t}$$

A rake angle $\delta$ of $50^{\circ}$ seems admissable.

With these preliminary considerations, the meridional outline may be drawn. It is important to realize that the flow passages leading to the impeller inlet are an integral part of this outline. Without the knowledge of the inlet conditions, the flow in the impeller region cannot accurately be determined.

The flow in front of the impeller eye may be axial or radial inward, or hampered by space limitations. Two extreme possibilities are shown on Figure 3.8 for radial inflow. Figure 3.8a shows a relatively long channel which will produce nearly constant axial velocity at the impeller eye. A check of the velocity along the wall will indicate a velocity peak at "a" with subsequent deceleration towards "b". This leads to a thick boundary layer at "b". By changing the contour in Figure 3.8b, the velocity is uniformly accelerated from "a" to "b". However, there will be a large velocity gradient from "b" to "c", increasing the relative velocity at the inducer tip. It is probable that this is less harmful than a thick or separated boundary layer, provided inducer blade angles setting takes care of the non-uniform axial velocity. The best design is apparently one where the velocity is slightly accelerated all along the wall. Such a shape is shown in Figure 3.9a.

Since we intend to arrive at a shape where the velocities on the boundaries are accelerated, we expect very thin boundary layers and may neglect viscous effect. However, the Mach number may be considerable and compressibility effects may have to be taken into account. Thus the problem is to find the axisymmetrical compressible flow for given boundaries. The very lengthy solution of the compressible flow equation is replaced by the following procedure.

## Calculation of the Axisymmetrical Flow

The shape such as in Figure 3.9a is cut out of a sheet of Teledeltos paper * and the ends are painted by conducting silverpaste along a guessed potential line. "Potential lines" are then drawn onto the conducting paper by means of the electric analog. The apparatus is explained in Reference 3.9. These "potential lines" are potential lines for two-dimensional incompressible flow and, in two-dimensional flow, the velocities along such a line are inversely proportional to their length $\Delta m$ (Fig. 3.9a). Appendix I shows that the velocity gradient in two-dimensional and in axisymmetrical flow of the same boundaries is very nearly the same. This fact is used for the determination of the velocities.

$$C_{m_i} = K_i \frac{1}{\Delta m}$$

(3.1)

where $K_i$ is determined from continuity; the index i denotes the particular potential line i. The weight flow is determined from:

$$W = \int_{hub}^{shroud} \rho \ c_m \ dA$$

(3.2)

*This paper, with the rectifier and potentiometer needed, and the silverpaste can be obtained from General Electric which sells the set under the trade name Analog Field Plotter. It is described in Reference 3.9. The paper can directly be obtained from Western Union, and the silverpaste is the same as used for printing electric circuits.

In general $\rho$ could be obtained from the local velocity. But usually it is sufficient to calculate an average $\rho$ for each potential line.

Defining:

$$A^* = \frac{W}{a^* \rho^*} \tag{3.3}$$

one obtains from compressible flow tables for every $A_i/A^*$, a value $\rho_i/\rho^*$, where $A_i$ is the area obtained by rotation of the considered potential lines i. Since $\rho_i$ is a known constant (3.1) and (3.2) yield the value for $K_i$

$$K_i = \frac{W}{\rho_i \displaystyle\int \frac{dA}{\Delta m}} \tag{3.4}$$

where the integral is evaluated graphically writing $dA = 2\pi r\, dn$, n being the length along the potential line.

The number of integrals to be evaluated are equal to the number of calculated points along the shroud. Five integrations are usually sufficient, although more potential lines should be drawn in order to make sure that no peak in velocity has been missed.

A skilled man needs 16 hours for the work described so far. The result is the velocity distribution in particular on hub and shroud. At the shroud it should not show any peak and the deceleration should be as small as possible. If the velocities are not satisfactory, the shape should be changed and the calculations repeated until a satisfactory final shape is obtained. The assumption is made that the presence of the impeller or its shape modifications do not influence the conditions upstream of the impeller.

After having fixed the conditions upstream of the impeller, we may proceed to calculate the axisymmetrical flow in the impeller region to a first approximation. The procedure is the same as the one used for the upstream calculations. In fact, the first step of the previous calculations which gives the gradient of the velocity along the potential lines is exactly the same and is done on the same piece of Teledeltos paper. Figure 3.10 shows the notation used.

Formula (3.2) determines $K_i$. However, the evaluation of $\rho$ and dA is slightly more complicated.

The density $\rho$ is calculated from the formula

$$\rho \Big/ \rho_o = \left[ 1 + \frac{k-1}{2a_o} (u^2 - w^2) \right]^{\frac{1}{p-1}} \tag{3.5}$$

where the index "o" indicates inlet stagnation condition; u and w are the wheel speed $\omega r$ and the relative velocity, respectively. Formula (3.5) follows from the

energy equation and the isentropic relationship where, however, the ratio of specific heat k has been replaced by p in order to take account of the irreversibilities. The polytropic exponent p is determined from the known state at the impeller tip using equation (3.5). As in the case of the inlet, an average p is used for each potential line. This average p is obtained in the following way: a meridional streamline which divides the mass rate of flow in half is approximately drawn. At the inducer inlet and impeller tip, the relative velocity is known and in between is assumed to vary linearly with the length of the meridional streamline. This is a sufficiently good approximation to the final result, if the design is well done. Thus the average $\rho_i$ on each

potential line is known.

The area dA in Eq (3.4) can be written as

$$dA = (2\pi r - Zt)\in dn \qquad\qquad (3.6)$$

where Z is the number of blades, t the local thickness of the blade in tangential direction and a factor which takes account of the displacement effect of the boundary layer. In the absence of sufficient knowledge about the boundary layer, a simple assumption of $\in$ may suffice for the whole design. Hence, we choose $\in = .95$ at inducer inlet varying linearly to .80 at impeller tip.

The number of blades is determined by the desired blade loading; longer channels require fewer blades. Thus, a mixed-flow impeller with its longer channels would need fewer blades than a radial-flow impeller both having the same inlet and outlet velocity triangles. In the impeller used as an example, the number of blades was chosen to be 19.

The blade thickness will not be prescribed by aerodynamic considerations except at the inlet where they have to be as thin as possible when the Mach number is large. Away from the inducer, the thickness variation of the blades has the same effect as a variation in meridional shape. Therefore, stress considerations alone shall specify the blade thickness while the aerodynamic considerations should emphasize the need of thin inducer vanes only. In this way, this design element (t) is fixed at the outset and t is known from stress calculations.

With all values in Eq (3.6) known as a function of the distance along a potential line, $K_i$ can now be evaluated by Eq (3.4) for each potential line. The result of these calculations, a work of about 24 hours, is the velocity distribution of say, 5 potential lines. The velocities at hub and shroud are now plotted, along the distance m (Fig. 3.11). If these curves show any undesirable features such as peaks, the meridional shape can be changed at this point. However, with insufficient experience, it is difficult to judge what is undesirable, and therefore, the next step is recommended.

### 3.2.3.2.2  The Blade-to-Blade Flow Analysis (Step 2)

The purpose of Step 2 is to find a blade shape which yields the desired loading, i.e., the desired velocities on suction and pressure side. This time, instead of assuming a priori the passage shape, we assume the variation of the moment of momentum $rc_u$ with the meridional length m.

From the assumed $rc_u$ the flow direction and magnitude is calculated. Then the blades are determined which give to the flow the turning calculated in Phase 1.

Let us consider a fluid slab between two blades of cross section as in Figure 3.12. The torque which acts on this fluid slab can be expressed by the surface pressures as well as by the change in momentum of the fluid.

$$\Delta P (\Delta m)(\Delta n) r = \rho \Delta n \, r \Delta \varphi \, w_{ave} \cos \beta \frac{\partial (rcu)}{\partial m} \Delta m$$

or

$$\frac{\Delta P}{\Delta \varphi} = \bar{\rho} \, w_{ave} \cos \beta \frac{\partial (r \, \bar{c}u)}{\partial m} \tag{3.7}$$

Where $\Delta P$ is the pressure difference between two blade surfaces, $\Delta \varphi$ the corresponding included angle, $\rho$ the density, $\beta$ the angle between the relative velocity and the meridional planes. $w_{av}$ is defined by Eq (3.7) as the velocity which yields the mass rate of low when multiplied by the flow area and the density. We assume now that this $w_{av}$ is the same velocity as the one obtained in the axially symmetric calculation, an assumption which is justified in Reference 3.5.

In order to calculate the velocities on pressure and suction side, the following two equations are used:

$$w_{ave} = \frac{w_s + w_p}{2} \tag{3.8}$$

$$\Delta P = \rho \frac{w_s^2 - w_p^2}{2} \tag{3.9}$$

Equation (3.9) is the energy equation for incompressible isentropic flow.

Equation (3.9) can be written

$$\Delta P = \bar{\rho} \, (w_s - w_p) \, w_{ave} \tag{3.9a}$$

Using this expression Equation (3.7) becomes

$$\frac{\Delta w}{\Delta \varphi} = \cos \beta \, \frac{\partial (rc_u)}{\partial m} \tag{3.10}$$

where $\Delta w = w_s - w_p$

From Eq (3.10) $\Delta w$ is obtained immediately since $\beta$ is known from

$$r \, c_u = r \, (u + c_m \tan \beta) \tag{3.11}$$

This procedure gives an approximate value of $\Delta w$, since only Eq (3.7) is exact while Eqs (3.8) and (3.9) are approximations. But we are not really interested in an exact value of $\Delta w$ since this value is mainly used to judge the smoothness of the blade loading or the smoothness of the velocities. Any sudden variation will show up as well in this simplified calculation as in an exact calculation. In other words, it is of no use to make more accurate calculations than the accuracy of the knowledge of the design criteria. On the other hand, slight differences between two impellers may be of importance and those differences are well brought out.

Finally, $w$ is calculated from

$$w = \frac{c_m}{\cos \beta} \qquad (3.12)$$

We may summarize Step 2:

a) $rc_u$ is assumed and plotted over the length $m$ of the meridional streamline as in Figure 3.13, noting that the tip value $rc_u$ is given by the velocity triangles, the shape determines the loading.

b) The angle $\beta$ is calculated from Eq (3.11) and plotted (Fig. 3.13).

c) By means of Eq (3.12), $w$ is calculated and plotted (Fig. 3.13).

d) The blade loading $\Delta w$ is obtained from Eq (3.10), and $w_s = w_{ave} + 1/2 \, \Delta w$ and $w_p = w_{ave} - 1/2 \, \Delta w$ are plotted.

Thus step 2 is concluded (about 2 hours of work), and the result must be compared with the desired velocities such as shown on Figure 3.3.

If the loading is very different from the desired one, the $rc_u$ versus $m$ curve should be changed until the $\Delta w$'s are not too far from the desired value. The repetition of step 2 does not take much time. However, a change of $\beta$, influences the relative velocity $w$. This velocity must now be examined carefully. A large $w$ indicates a large meridional component $c_m$. In order to reduce this component, the flow area should be made larger. This has to be accomplished by a change in the meridional shape only, if the blade thickness is established from stress considerations. If this is not so, the variation of the blade thickness is a means to arrive at the desired velocity $w$, requiring less computing work since the basic analogue field plot does not need to be changed. In general, however, the meridional shape must be changed.

Because a change of the meridional shape needs considerable time (about 24 hours), a careful estimate of the magnitude of the required change is advisable. Suppose the relative velocity is to be reduced 10 per cent. A 10 per cent area increase leads to approximately 10 per cent velocity if the angle $\beta$ remains the same. Since the change in $c_m$ changes the loading, $\beta$ has to be changed (using step 2) in order to re-establish the desired loading.

Such considerations should be used in arriving at a new meridional shape and at new meridional velocities. After the calculation of the blade loading is repeated, it is seen whether further iterations are necessary.

If $w_{ave}$ and the loading along the shroud are found satisfactory, we proceed to investigate the velocities at the hub. If stresses require radial blade elements, the blade shape at the hub is fixed and the velocities can be calculated. Otherwise, when the blade elements are not necessarily radial, the blade shape at the hub can be designed separately just as it was done at the shroud.

It is advisable to calculate the velocities also along a streamline in between the shroud and the hub.

In high-speed machinery, where the blade elements are radial, this step takes mostly the form of a check. Indeed, the velocity distribution near the shroud is considered the most important one and also the most sensitive to any change. Thus, a change which improves the velocities at the hub a little may considerably worsen the situation at the shroud. This is why, in the compromise between shroud and hub profile, the shroud profile is more influential. Generally negative velocities at the hub should be avoided because bad flow conditions at the hub will influence the flow at the shroud in an unfavorable sense, as indicated in Figure 3.1a and discussed previously.

It should be mentioned here that the density was initially assumed on the basis of a linear velocity distribution from inlet to outlet. If this design objective was achieved, then the initial assumption was correct in the final analysis, provided the streamline (on which w was measured) was chosen accurately. This can be checked now, the final $c_m$ and area distribution being known.

For many applications, the design may be completed with the addition of Chapter 3.2.3.4, which has the purpose of finding the blades which give to the fluid the directions as calculated in the two first steps.

It is understood that the calculation so far is an approximation. Subsequently, further steps will be indicated which refine the solution, inasmuch as some assumptions will be dropped and the corresponding corrections made. First, however, the assumptions which lead to this approximation will be discussed in the following paragraph.

### 3.2.3.3 Discussion of the Equations

The meridional components $c_m$ of the velocities as obtained from the analog field plot satisfy the equation for zero vorticity:

$$\frac{\partial c_m}{\partial n} + \frac{c_m}{R_p} = 0$$

(3.13)

where $R_p$ is the radius of curvature of the streamlines corresponding to the two-dimensional incompressible flow. The real velocities are different for several reasons.

a. The axisymmetrical flow is different from two-dimensional flow. However, the difference as shown in Appendix A as far as its effect upon $c_m$ is concerned seems to be small. It is true that the streamlines in axisymmetrical flow are quite different. But the local radii of curvature are nearly the same.

b. A larger difference in radius of curvature is due to the displacement effect of the blades as shown in Figure 3.14. Because the blades occupy a larger portion of the area near the hub than near the shroud, the flow is pushed away from the hub as indicated by the dotted lines in Figure 3.14. This, at least immediately before the blades, results in a considerable change of the radius of curvature.

c. The blades introduce vorticity into the meridional flow. If the number of blades approaches infinity, an assumption which is made in order to calculate the flow, the vorticity is distributed within the flow and has a component $\zeta_\mu$ perpendicular to the meridional plane.

The final meridional velicity $c_{mf}$ should satisfy the equation.

$$\frac{\partial c_{mf}}{\partial n} + \frac{c_{mf}}{R} = \zeta_\mu \qquad (3.14)$$

where R is the radius of curvature of the final streamlines.

In order that the physical insight not be lost, the transition from the calculated $c_m$ to $c_{mf}$ is made in two steps, writing

$$c_{mf} = c_m + \Delta c_{mR} + \Delta c_{m\zeta} \qquad (3.15)$$

where $\Delta c_{mR}$ is the correction due to the change in radius of curvature and $\Delta c_{m\zeta}$ the change which occurs because $\zeta_u$ is different from zero. If $\zeta_u$ would be zero, $\Delta c_{m\zeta}$ would be zero, and therefore

$$\frac{\partial(c_m + \Delta c_{mR})}{\partial n} + \frac{c_m + \Delta c_{mR}}{R} = 0 \qquad (3.16)$$

Making the assumption that n in equations (3.13),(3.14), and (3.15) are nearly equal, these equations together with continuity

$$\int \rho \Delta c_{mR} \, dA = 0 \qquad (3.17)$$

and

$$\int \rho \Delta c_{m\zeta} dA = 0 \qquad (3.18)$$

define $\Delta c_{mR}$ and $\Delta c_{m\zeta}$ uniquely. Subtracting (3.13) from (3.16) yields

$$\frac{\partial(\Delta c_{mR})}{\partial n} + \frac{\Delta c_{mR}}{R} = c_m \left(\frac{1}{R_p} - \frac{1}{R}\right) \qquad (3.19)$$

and subtracting (3.16) from (3.14)

$$\frac{\partial (\Delta \, c_m \zeta)}{\partial n} + \frac{\Delta \, c_m \zeta}{R} = \zeta_u \tag{3.20}$$

This equation has the solution

$$\Delta c_m \zeta = e^{-\int \frac{dn}{R}} \int e^{\int \frac{dn}{R}} \left[ \zeta_u \, dn \right] + K e^{-\int \frac{dn}{R}} \tag{3.21}$$

where the integration constant K is evaluated such that equation (3.18) is satisfied. R is the radius of curvature of the final streamlines which are not known as yet. But since $\Delta c_{mR}$ and $\Delta c_{m\zeta}$ are small corrections, a relatively large error in $\Delta c$ is not consequential. Thus in equation (3.21) R may be replaced by $R_p$, or better yet, by the radius of curvature R of the streamlines obtained by applying the equation of continuity to the initial $c_m$ and by dividing the area of equation (3.6) into such parts that through each area element flow the same quantity.

It is clear that the effect of the change in radius of curvature and the effect of vorticity can be lumped into a single equation, in which

$$\Delta \, c_m = \Delta \, c_{mR} + \Delta \, c_m \zeta \tag{3.22}$$

which has the solution

$$\Delta \, c_m = e^{-\int \frac{dn}{R}} \int e^{\int \frac{dn}{R}} \left[ \zeta_u + c_m \left( \frac{1}{R_p} - \frac{1}{R} \right) \right] dn + K e^{-\int \frac{dn}{R}} \tag{3.23}$$

where K is evaluated from

$$\int \rho \, \Delta \, c_m \, dA = 0 \tag{3.24}$$

Now the values in equation (3.23) can be evaluated. As mentioned above, the radii of curvature which are obtained from streamlines on basis of the original $c_m$ are known; later, the radii of curvatures based on iterated solutions should be used. However, in view of the small corrections, an iteration is seldom warranted. The vorticity is evaluated from

$$\zeta_u = \frac{\tan \beta}{r \cos \gamma} \frac{\partial (r \, c_u)}{\partial r} \tag{3.25}$$

This equation is derived in Appendix (B), which is correct for zero tilt angle In high-speed compressors, stress considerations lead to radial blade elements, that is, zero tilt angle $\nu$ . In the next chapter it is shown how these corrections are applied to the compressor design.

### 3.2.3.4 Refined Calculations

The streamlines corresponding to the meridional components $c_m$ of the velocities and the area A as given by Equation (3.6) are to be traced. Three streamlines in addition to the hub and shroud line divide the mass rate of flow in four equal parts. The intersection of these streamlines with the normal lines n is obtained in the following way:

As shown on Figure 3.15, the quantity $c_m \rho (2\pi r - Z t)$ and its integral over n are plotted. It is usually sufficiently accurate to assume $\rho$ constant along a normal n, although its value can easily be evaluated by Equation (3.5) since we know now the average velocities w between the blades. The total mass rate of flow $W = \int_{hub}^{shroud} \in c_m \rho (2\pi r - Z t) dn$ can be divided in, say, four equal parts and the corresponding positions n can be taken from Figure 3.15.

This procedure has to be repeated on several normals until enough points are found such that the streamlines can be traced as shown on Figure 3.14.

The radius of curvature R of these streamlines can be measured together with the streamline curvature $R_p$ of the initial streamlines (corresponding to two-dimensional potential flow). These measured values are plotted over n . This allows checking the measurement since the qualitative change in radius of curvature is easily obtained from the change in streamline form. Now the quantity $c_m (\frac{1}{R_p} - \frac{1}{R})$ needed in Equation (3.23) can be plotted along each normal (See Figure 3.16).

Finally, $\zeta_u$ has to be calculated on each normal from Equation (3.25). The flow angle $\beta$ and the angle $\gamma$ of the meridional streamlines with axial direction are quickly found. More lengthy is the evaluation of $\frac{\partial (r c_u)}{\partial r}$, which involved plotting $r c_u$ along several radial lines in the considered region and taking the derivative. If this is done, $\zeta_u$ can be plotted along each normal as shown in Figure 3.16.

At this point, one should make sure that the signs are chosen correctly. The easiest way is to interpret the result physically:

The effect of an increase in radius of curvature is obviously to decrease the velocity gradient.

The effect of the vorticity should be such that the meridional component of the velocity is increased where the work done by the blades is increased above the average value, that is, the value of the potential flow solution. Thus, if the leading edge of the inducer is radial, the work done over a given axial distance is larger near the shroud than near the hub. In accordance, the velocity near the

shroud is increased above the potential flow value and decreased near the hub.

Both $c_m \left(\frac{1}{R_p} - \frac{1}{R}\right)$ and $\zeta_u$ being known, $\Delta c_m$ can now be evaluated by Equations (3.23) and (3.24). Before performing this calculation, the following should, however, be realized:

If the length of calculation is warranted in view of the accuracy required, iteration is necessary. If this is decided, it is more practical to split Equations (3.23) and (3.24) using Equations (3.17) to (3.20) since Equation (3.19) needs little iteration while Equation (3.20) does need iteration. To know the reason for this may be of help in obtaining a better approximation for $\Delta c_m \zeta$ the first time. The correction $\Delta c_m \zeta$ is always so as to decrease $\frac{\partial (r c_u)}{\partial r}$ and thus $\zeta_u$, which means that the first correction $\Delta c_m \zeta$ is too large. This knowledge may help to choose a more accurate value when no iteration is to be performed or to reduce the number of iterations, choosing $\zeta_u$, only 3/4 the value given by Equation (3.25).

This concludes the calculations of the directions and velocities of the fluid, provided the meridional velocities and the blade loading are still satisfactory. In general, Steps 1 and 2 have to be repeated at this point in order to obtain the desired velocities exactly; thus Step 3 may lead to a change in the meridional shape and the blade form. An experienced designer tries to choose the velocities in Steps 1 and 2 in such a way that after Step 3 the velocities are the desired ones.

### 3.2.3.5  Design of Inlet and Outlet

So far, it was assumed that the direction of the flow is parallel to the blades. This is so, except near the inlet and outlet. In order to obtain an average flow direction near inlet and outlet consistent with the previous calculation, the blade shape near inlet and outlet has to be designed accordingly.

The inducer leading edge is laid out such that the camber line of the blades is parallel to the average streamlines. The blade thickness has been fixed previously. Then developments are made of several cylindrical cuts through the inducer.

The flow on these cylindrical section in the inducer region is treated as a two-dimensional or quasi-two-dimensional problem.

In case of subsonic flow, an analog field plot of the cascade as shown on the cylindrical section is made. This investigation should show the flow phenomena near the leading edge, so that high velocity peaks may be avoided. The local velocities on the blade surfaces resulting from the analog field plot have to be corrected for compressibility using the Karman-Tsien formula

$$\frac{P - P_{av}}{P_{t_{av}} - P_{av}} \cong c_p = \frac{c_{pi}}{\sqrt{1-M^2} + \dfrac{c_{pi}}{2} \dfrac{M^2}{1 + \sqrt{1-M^2}}} \qquad (3.26)$$

where P is the static pressure on the blades, $P_{av}$ is the pressure in the middle of the blades,

$$c_{pi} = (w/w_{av})^2 - 1 \qquad\qquad (3.27)$$

the pressure coefficient for incompressible flow obtained from the field plot, where w is the velocity on the blade surface, and finally, M is the relative Mach number in the middle between the blades. The static and total pressures P and $P_t$ of the compressible flow are obtained from the previous calculations and are not equal to the pressures of incompressible flow. $w_{av}$, to be used in Equation (3.27), is the velocity of incompressible flow, which is the same as $w_{av}$ of the compressible flow far upstream only. The Mach number M is the one which was obtained from the calculations of axially symmetric flow and is supposed to exist in the middle between two blades. With all these values known, the pressure at the blade P follows from Equation (3.26). The result $P - P_{av} = \Delta P$ should be compared with the desired result as given by Equation (3.7). In case this pressure difference $\Delta P$ shows peaks, the shape of the inducer leading edge has to be changed until close agreement with the result of Equation (3.7) is reached.

In case of supersonic relative velocities, the flow may be investigated by means of the method of characteristic. This method, as it applies to the present problem, is explained in Reference 3.10.

A detailed discussion of the problems arising here is given in Chapter 3.2.4, "Problems of Supersonic and Transonic Flow in Inducers". Here it may be useful to say that results which are quite near the optimum have been obtained using the simple approach of Chapter 3.2.3.2.

Considering now the conditions at the impeller tip, the deviation between blade angles $\beta_b$ and fluid angles $\beta$ is more pronounced than at the inlet. The deviation at the tip may be found from Section II. The deviation upstream of the tip in the impeller passages can be found from Reference 3.12, where compressible flow calculations were performed and put in such a form that they are useful for all radial-bladed impellers.

This concludes the whole impeller design unless transonic phenomena are of special importance, a topic treated in the next section.

## 3.2.4  Problems of Supersonic and Transonic Flow in Inducers

### 3.2.4.1 Introduction

In radial compressors designed for high pressure ratio without the use of prewhirl, the relative Mach number at the tip may be considerably above 1.0;  if not, the impeller is of a very low specific speed, i.e., if not, a low ratio of inducer diameter to impeller tip diameter is used.  It is known that the efficiencies which can be obtained in the latter case are low.  Low efficiencies have also been encountered with high inducer Mach numbers.  However, in this case, it is felt that improvements are possible, if the flow phenomena are understood.

The purpose of the present chapter is to discuss these flow phenomena and to indicate some design principles which should minimize the losses in the inducer.  This will be done in three steps:  First, relevant known ideas and observations will be presented;  then, we shall discuss how these observations apply to the present problem, and, finally, it will be shown how these phenomena affect the design.

### 3.2.4.2 High-Speed Flow in Conventional Configurations

Straight supersonic diffusion from supersonic to subsonic flow requires that the narrowest cross section is larger than the one necessary for sonic flow.  This narrowest cross section has to be chosen such that the flow can be passed, even when the worst irreversibilities occur before this narrowest cross section.  Otherwise the design flow can never be reached;  the diffuser cannot be started.

Similar conditions exist in a curved channel which has more similarity with a passage formed by blades of a compressor.  Two-dimensional exact solutions leading without shock from supersonic to subsonic flow are known (See Reference 3.13).  Any two neighboring streamlines may be considered as solid boundaries forming a channel leading without shock from supersonic to subsonic flow.  However, when the velocity gradient perpendicular to the streamlines is approximately constant, a narrowest cross section of the channel will occur in the region where the average Mach number is one.  This cross section limits the flow rate and, if larger irreversibilities than per design occur prior to this section, the design flow rate cannot be attained.  Thus, similarly to the straight supersonic diffuser, this shockless transition from supersonic to subsonic flow probably will not occur.

The conditions are very similar in a three-dimensional curved channel:  Unless the streamlines can adjust themselves freely (as in a vaneless diffuser for instance), the shockless passage from average supersonic to average subsonic flow needs a narrowest cross section which does not allow reaching the design mass rate of flow if larger than design irreversibilities occur prior to this cross section.  A shockless transition seems therefore not possible for such a case.

However, if the Mach number average with respect to the whole cross section is below one, an increased channel area can conceivably lead without shocks to subsonic velocities even though locally high supersonic velocities

occur at the beginning. Near an average Mach number of one, the deceleration occurring is very sensitive to any change in area. For instance, in one dimensional flow at M = 1, a 5 per cent increase in area decreases the Mach number to .76. A much larger variation in flow area than the one given above may even be caused by boundary layer growth, partial separation, or simply losses.

### 3.2.4.3   High-Speed Flow in Cascades

A considerable amount of test data on high Mach number flow have been gathered in axial-flow compressor research. A short review of the relevant results is presented here.

When a cascade designed for subsonic flow is used in high Mach number flow, the ratio between maximum velocity on the suction side of the blades and the free stream velocity increases. At a certain free stream Mach number, this local Mach number exceeds one, and the deceleration usually takes place by means of local shock. This shock leads to boundary layer separation when the supersonic expansion over the convex portion of the blade is sufficiently large. Eventually, the cascade becomes choked at less than the flow which would pass when the flow is not separated. This low flow leads to high angles of attack, connected with large supersonic expansion over the blade leading edge, and violent separation.

This limiting free stream Mach number can be increased by limiting the expansion at the blade suction side while maintaining a diffusion rate as large as possible in the entrance section.

Tests on axial-flow rotors show, Reference 3.14, that the free stream Mach number may be as high as 1.4 without reducing the efficiency materially. There are indications that shocks sufficiently near to the leading edge where the boundary layer is thin do not lead to separation, such that the flow behind the shock can be wholly subsonic.

Other experiments, for instance Reference 3.15, show that the losses in high speed flow may be very high, if the blades are poorly designed. Very small differences in blade shape may cause the flow to break down, resulting in a decrease of efficiency from 90 per cent, as in Reference 3.14, to 68 per cent, as in Reference 3.15.

### 3.2.4.4 High-Speed Flow in Radial Flow Compressors

The flow in the entrance section of the inducer is exactly the same as in an axial-flow compressor. However, considering the compressor as a whole, one notices the following difference. The relative velocity head of an axial compressor is a large faction of the total work. Hence any losses in the inducer being equal to, say, the kinetic energy of the relative velocity, result in considerable efficiency drop of the compressor. The same inducer losses are of less significance with a radial-flow compressor since the work input of a radial compressor is so much higher. This may explain why even a primitive design of the inducer region of medium pressure ratio impellers lead to satisfactory efficiency.

In the high pressure ratio radial impeller with an average inducer Mach number near one, the situation may become quite different. It has been mentioned in a previous chapter that a very slight increase in area reduces the velocity considerably. It is common practice that diffusing sections for high Mach number flow should diverge only slightly in order to avoid too sudden deceleration which leads to separation. This practice unfortunately results in premature choking if only small unforeseen losses occur, which in a subsonic design would be quite unconsequential. Consequently, the flow rates do not come up to design, the angle of attack increases, the supersonic expansion near the leading edge is more pronounced and the flow condition is worse yet. This choking condition may produce much larger losses than those caused by the initial supersonic expansion shock and separation. If, in order to avoid this situation, the areas are increased to such an extent that the flow does not choke even when separation occurs, the deceleration rate for unseparated flow would be excessive, and the unseparated flow condition is unlikely to occur. The design of an impeller with such a separated inducer flow will only yield mediocre impeller efficiencies.

3.2.4.5   The Design Criteria

From the above-said it follows that the design criteria should eliminate separation as far as possible when the average Mach number is near one. If separation can be avoided, efficiencies comparable to those obtained in axial flow compressors may result. In view of these remarks, it is perhaps advisable not to decelerate quite as fast as recommended in Figure 3.1b but rather to use a velocity profile more nearly as the one used for the final Supersonic Compressor. In Reference 3.14, Page 19, a similar profile succeeded in avoiding separation in an axial-flow compressor.

3.2.4.6   The Design

With the present state of the art, an accurate calculation of the blades is not possible, especially in the transonic region. It is therefore recommended to disregard the possibility of shocks and to use the method explained previously in Chapter 3.2.3.2. This method leads to good results in the case of axial-flow compressors. It must however, be emphasized that the accuracy and surface finish of the inducer blades should be similar to those used in axial-flow compressors.

As mentioned under 3.2.3.5 of the design procedure, a further analysis of the blade-to-blade flow is desirable. Methods have been developed for calculating the supersonic flow under these circumstances. In Reference 3.2, the method is explained in detail. It assumes that the variation of the stream filament thickness is known. From the present design procedure, or any known procedure, follows the distance of two streamlines in the middle between the blades, but not the variation of this stream filament thickness from blade to blade. In the method of Reference 3.2, it was assumed that this thickness does not vary in tangential direction. This assumption is not correct, but, in absence of further knowledge, is adopted since it simplifies the calculations.

96

Such calculations have been performed for the supersonic radial compressor which was built and tested, and the results will be qualitatively discussed here.

In two-dimensional flow, the suction side of the entrance region of the blade must be straight, in order to avoid incidence shocks, as shown in Figure 3.17a, where the dotted line b-c is a Mach line originating from the suction side of the blade and ending at the leading edge of the neighboring blade. Suppose the blade suction side is curbed as shown in Figure 3.17b. The expansion waves, 1-1', 2-2', etc, originating from this curved surface must be compensated by a shock wave aa' of such a magnitude that the pressure at c is essentially equal to the pressure at a, since we assume that the phenomena at each blade of the inducer are the same. It follows that in two-dimensional flow, the shape of the blade from a-b does not alter the mass rate of flow essentially but modifies the strength of the occurring shock waves which approaches a minimum when the line a-b is straight. This assumes that no boss-wave exists.

The conditions for a real three-dimensional inducer are similar, inasmuch as the shock wave is a minimum for a certain shape of the inducer. The conditions are different, inasmuch as this minimum shock does not occur when the blade surface is straight but when the blade surface has a certain curvature. This is so, due to the compression of the considered stream sheet. In the two-dimensional case, the thickness of the stream sheet remains constant; in the case of a compressor, the stream sheet thickness (as seen in a meridional section) diminishes in direction of the flow. This results in a propagation of compression waves (full lines in Figure 3.17c) which might be neutralized by expansion waves (dotted lines) in Figure 3.17c if the shape of the surface c-b is properly chosen in relation to the change of thickness of the stream sheet.

It is evident that the shape which leads to essentially constant Mach number on the line a-c is a best design. This shape will depend on the Mach number and the hub and shroud contour. Therefore, no generalized result can be given. It is however, interesting to notice that the calculation performed for the test compressor yielded a shape a-b very near to the one obtained from the design procedure of Chapter 3.2.3.2, which was curved as qualitatively shown in Figure 3.17c. If the shape is calculated such that the flow pattern shown in Figure 3.17c, namely, essentially constant Mach number along a-c is possible, there is no guarantee that this flow pattern will occur. For instance, a normal shock ending on the suction surface is likely to occur.

## COMPARISON OF TWO-DIMENSIONAL AND AXIALLY SYMMETRIC FLOWS BETWEEN
## THE SAME BOUNDARY PROFILES

If an axially symmetric flow is cut by a meridional plane, the resulting trace of the streamlines in that plane appears as a two-dimensional flow pattern. Qualitatively, it is clear that the streamlines and potential lines of this meridional flow must resemble those of the plane two-dimensional flow between the same bounding streamlines. Obviously, the bounding streamlines themselves are identical, which forces a strong similarity on the remainder of the flow. Also, the two flows become identical when the bounding streamlines move very far from the axis of rotation.

The method of utilizing the two-dimensional solution in predicting the axisymmetric flow is based on the assumption that the velocity ratios along a normal to the streamlines are the same in two-dimensional and three-dimensional flow. The three-dimensional velocity is then known from the two-dimensional plot up to a multiplying constant K. This constant is determined at every normal from continuity.

$$K \int w_m \rho \, dA = W$$

The question of how accurate this procedure is must be considered. An investigation was conducted at AiResearch in which two analytically known axisymmetric incompressible flows were also computed by the method of the test, and the results compared. The flow geometries are indicated in the upper part of Figure 3.9. The flows were considered as incompressible, but the results are believed to represent compressible flows as well, if the corrections metioned on page 92 are used.

The comparison of the results of the approximate method using the conducting paper analog with the exact solution are shown on the bottom part of Figure 3.9. The plot shows the error in the velocity computed at the inner and outer boundaries as a function of a parameter which expresses the curvature of the flow and the distance of the field from the axis of rotation. If the curvature is small or the region of the flow is small compared to the distance from the axis, then the error would be expected to be small. This is reflected by the parameter $\lambda$.

Admittedly, only two particular cases were investigated, but these cases are believed to be of sufficient interest so that some general conclusions may be drawn. The range of $\lambda$ usually encountered is between $-3 \le \lambda < +3$, which indicates that less than 10 - 12 per cent error is to be expected. It is especially interesting to note that at the upper surface, the approximate method gives velocities which are too high.

DERIVATION OF VORTICITY

The momentum equation in radial direction in which the derivatives with respect to $\psi$ are replaced by a body force $F_r$ is (Ref 3.3, Formula (74a))

$$- \frac{w_u}{r} \frac{\partial (c_u r)}{\partial r} + w_y \left( \frac{\partial w_r}{\partial y} - \frac{\partial w_y}{\partial r} \right) = F_r \qquad (3.28)$$

where $F_r = 0$ for radial blade elements.

The vorticity $\zeta_u = \dfrac{\partial w_r}{\partial y} - \dfrac{\partial w_y}{\partial r}$

becomes $\quad \zeta_u = \dfrac{w_u}{w_y \, r} \dfrac{\partial (r \, c_u)}{\partial r} \qquad (3.29)$

From Figure 3.7, where the symbols $\beta$ and $\gamma$ are defined, it follows immediately that

$$\frac{w_u}{w_y} = \frac{\tan \beta}{\cos \gamma} \qquad (3.30)$$

and hence

$$\zeta_u = \frac{\tan \beta}{r \cos \gamma} \frac{\partial (r \, c_u)}{\partial r} \qquad (3.31)$$

3.1    von Doenhoff A. C., and Tetervin N. Determination of General Relations for the Behavior of Turbulent Boundary Layers. NACA Report 772.

3.2    E. L. Costilow. Application of Characteristic Blade-to-Blade Solution to Flow in a Supersonic Rotor with Varying Stream Filament Thickness. NACA TN 2992.

3.3    C. H. Wu Three-Dimensional Flow in Turbo Machines. NACA TN 2604.

3.4    G. O. Ellis, J. D. Stanitz Comparison of Two- and Three-Dimensional Potential Flow Solutions in a Rotating Impeller Passage. NACA TN 2806.

3.5    Ruden, P. Investigation of Single-Stage Axial Fans. NACA RM 1062.

3.6    J. T. Hamrick, A. Ginsburg, W. M. Osborn. Method of Analysis for Compressible Flow Through Mixed-Flow Impellers of Arbitrary Design. NACA TN 2165.

3.7    J. D. Stanitz, G. O. Ellis. Two-Dimensional Flow on General Surfaces of Revolution in Turbo Machines. NACA TN 2654.

3.8    J. D. Stanitz. Approximate Design Method for High Solidity Blade Elements Compressors and Turbines. NACA TN 2408.

3.9    General Electric Publication. Cat. No. 112L152 g1 and g2. Instructions Analog Field Plotter.

3.10   C. H. Wu and E. L. Costilow. A Method of Solving the Direct and Inverse Problem of Supersonic Flow Along Arbitrary Stream Filaments of Revolution. NACA TN2492.

3.11   G. F. Wislicenus. Fluid Mechanics of Turbomachinery. First Ed. McGraw-Hill Inc. N. Y., London 1947.

3.12   J. D. Stanitz and G. O. Ellis. Two-Dimensional Compressible Flow in Centrifugal Compressors with Straight Blades   NACA Rept 954.

3.13   A. H. Shapiro. Dynamics and Thermodynamics of Compressible Fluid Flow. Vol. 11. p. 783 ff.

3.14   NACA Conference on Jet Engines for Supersonic Propulsion. Oct. 8-9, 1953 p. 11 ff.

3.15   T. J. Golberg, E. Boxer, P. I. Bernot. NACA RM 53 g 16.
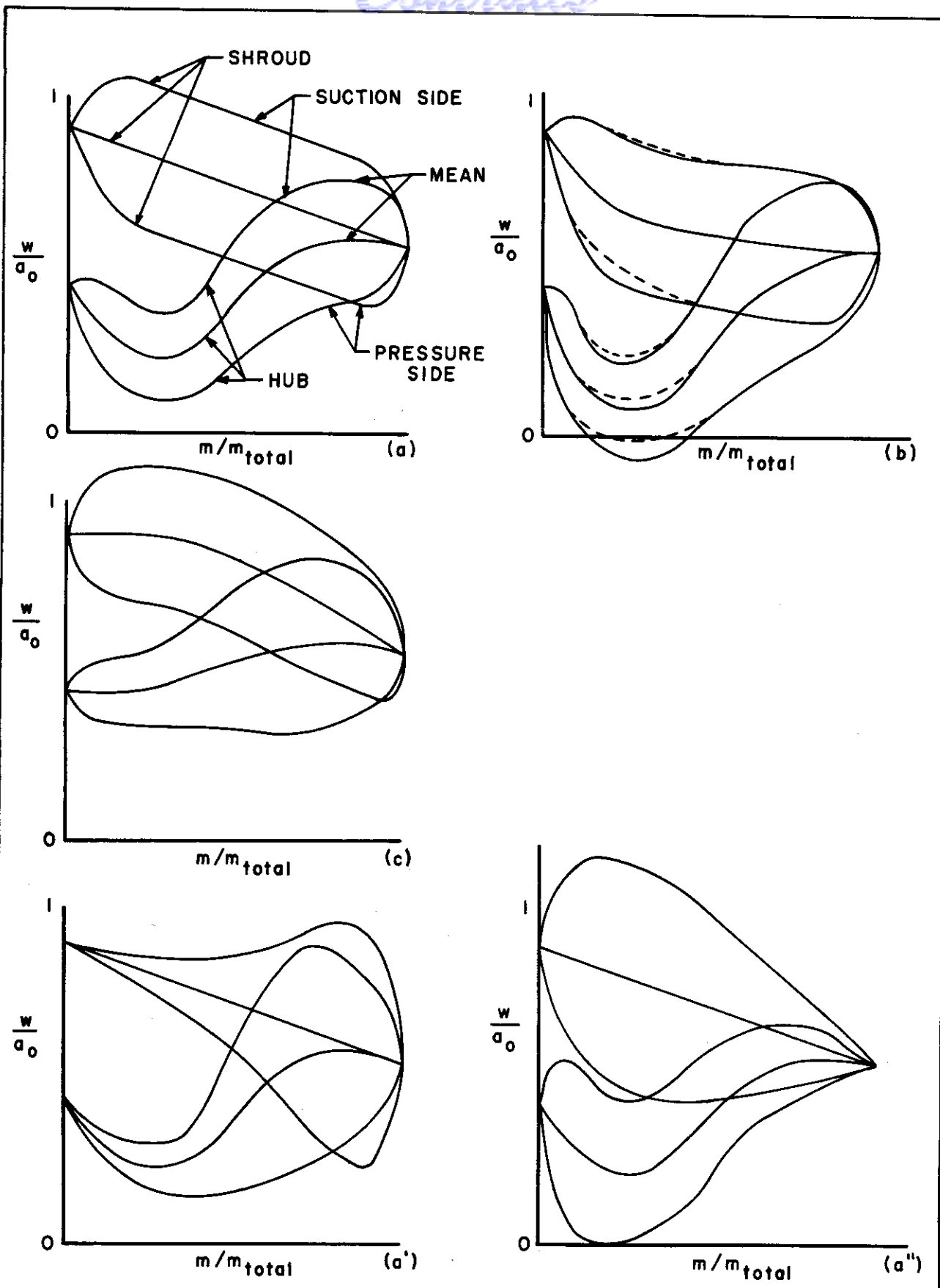
POSSIBLE BLADE LOADING CURVES
AT SHROUD AND HUB

FIG. 3.1

$$\frac{\theta_0}{D_0} = 10^{-3}, \quad H_0 = 1.4$$



FIG. .   TWO DIMENSIONAL BOUNDARY LAYER DEVELOPMENT

The graph shows curves with vertical axis labeled $\frac{w}{a_0}$ marked with values $1$ and $0$, and horizontal axis labeled $m/m_{total}$ with endpoints INLET and OUTLET.
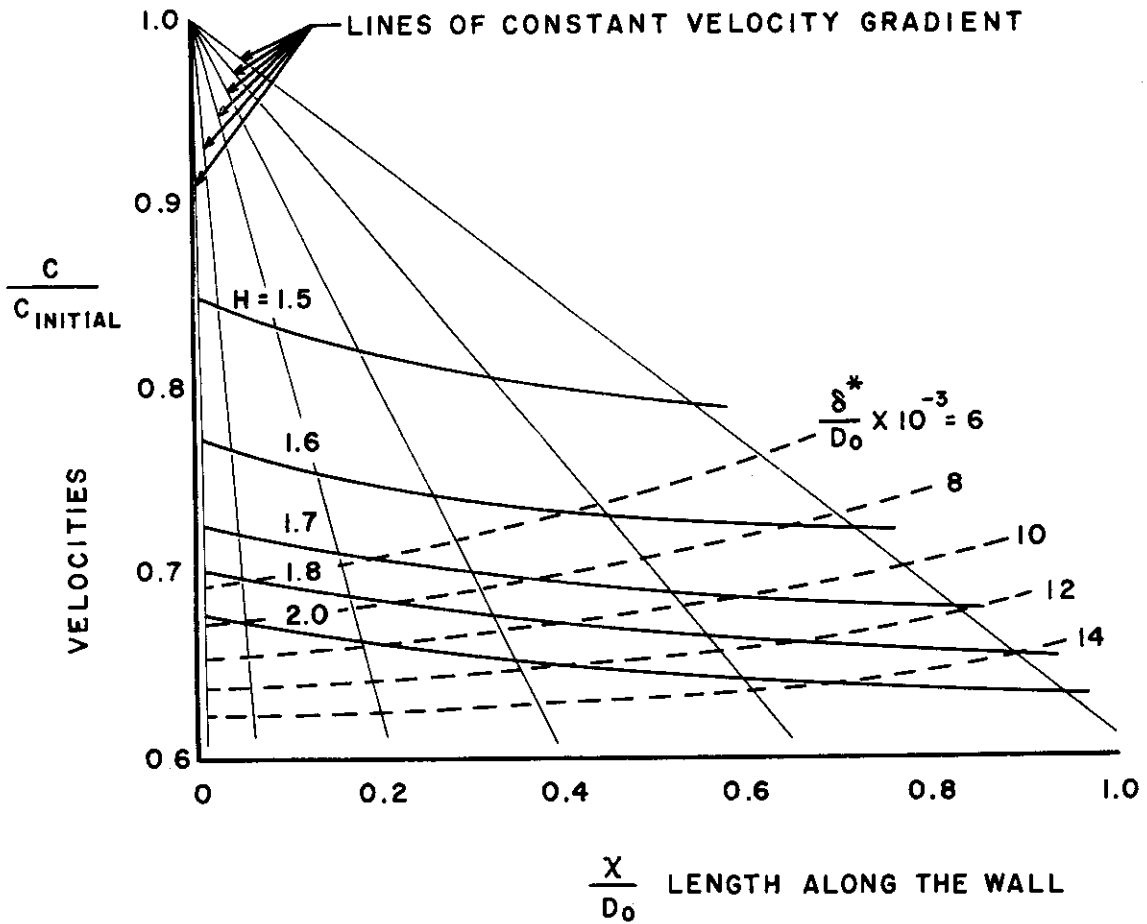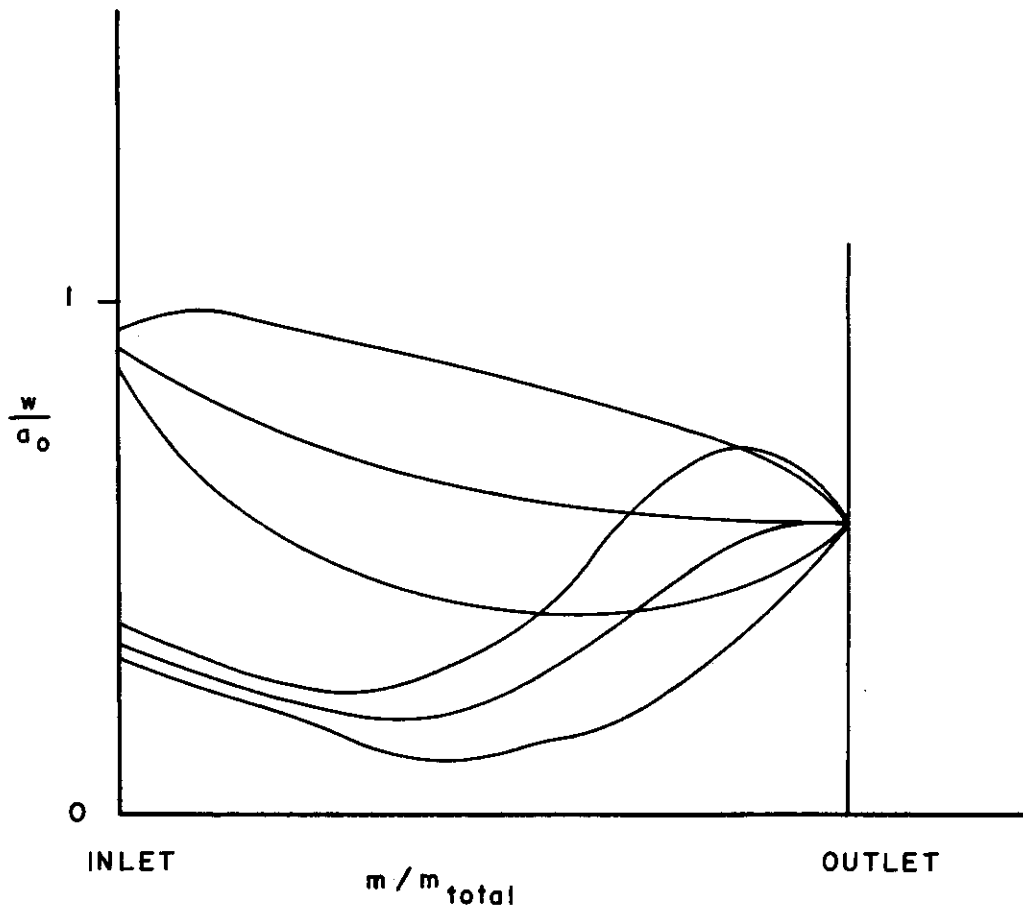
**FIG. .3    DESIRABLE BLADE LOADING CURVE**
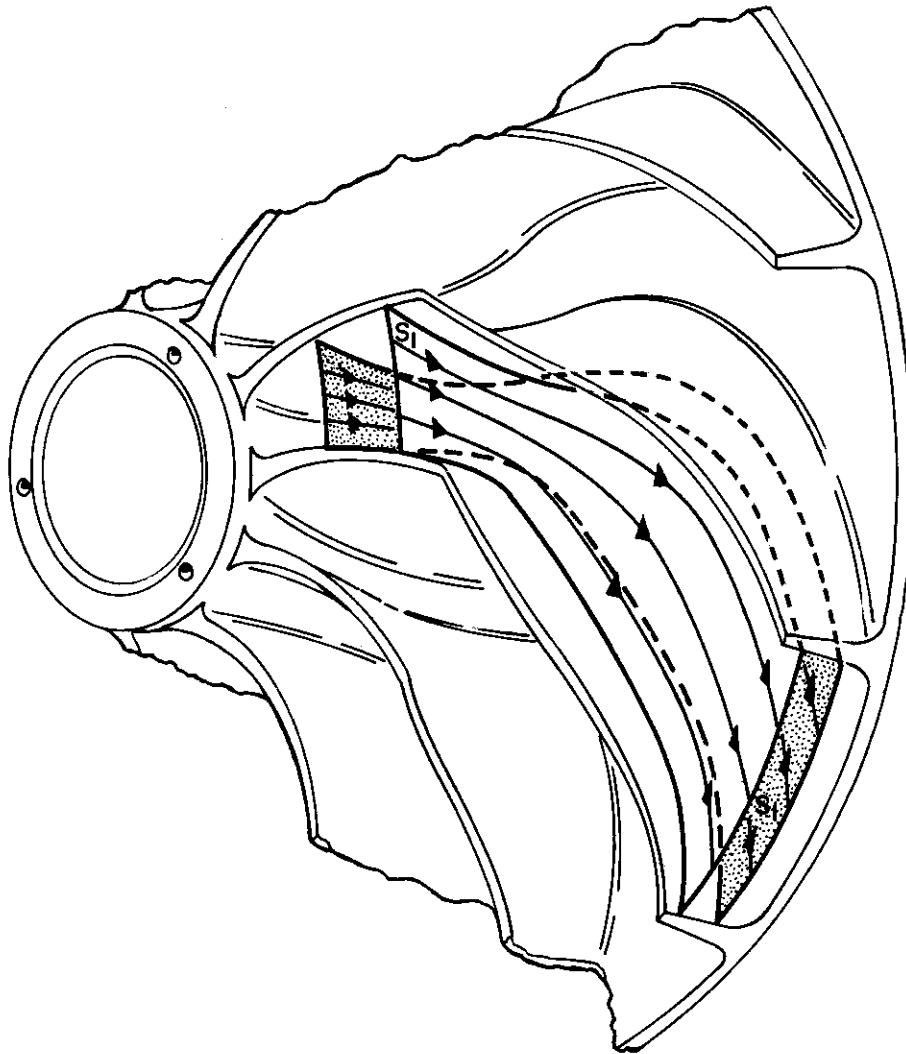
FIG. 3.4     TWO FLUID FLOW SURFACES OF S₁ KIND
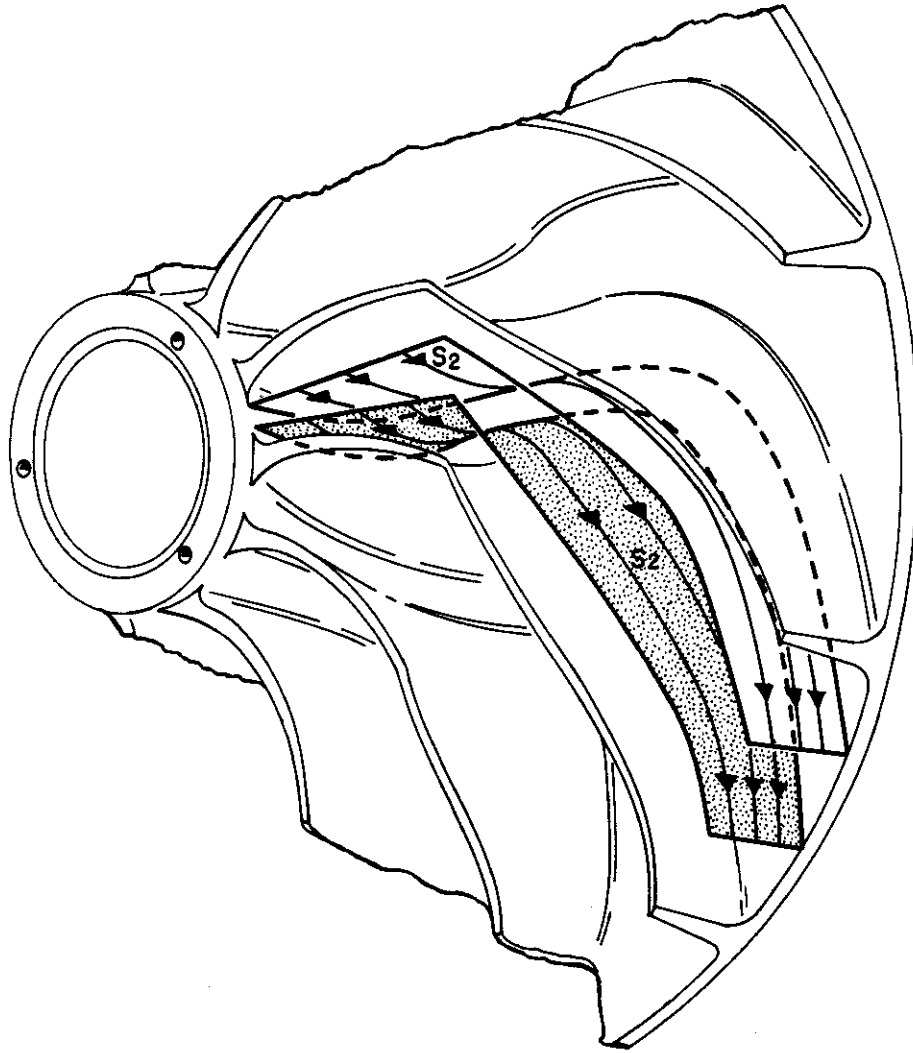
FIG. 3.5　　TWO FLUID FLOW SURFACES OF $S_2$ KIND

DIRECTION OF
IMPELLER ROTATION

IMPELLER TIP

IMPELLER AXIS

32.80°
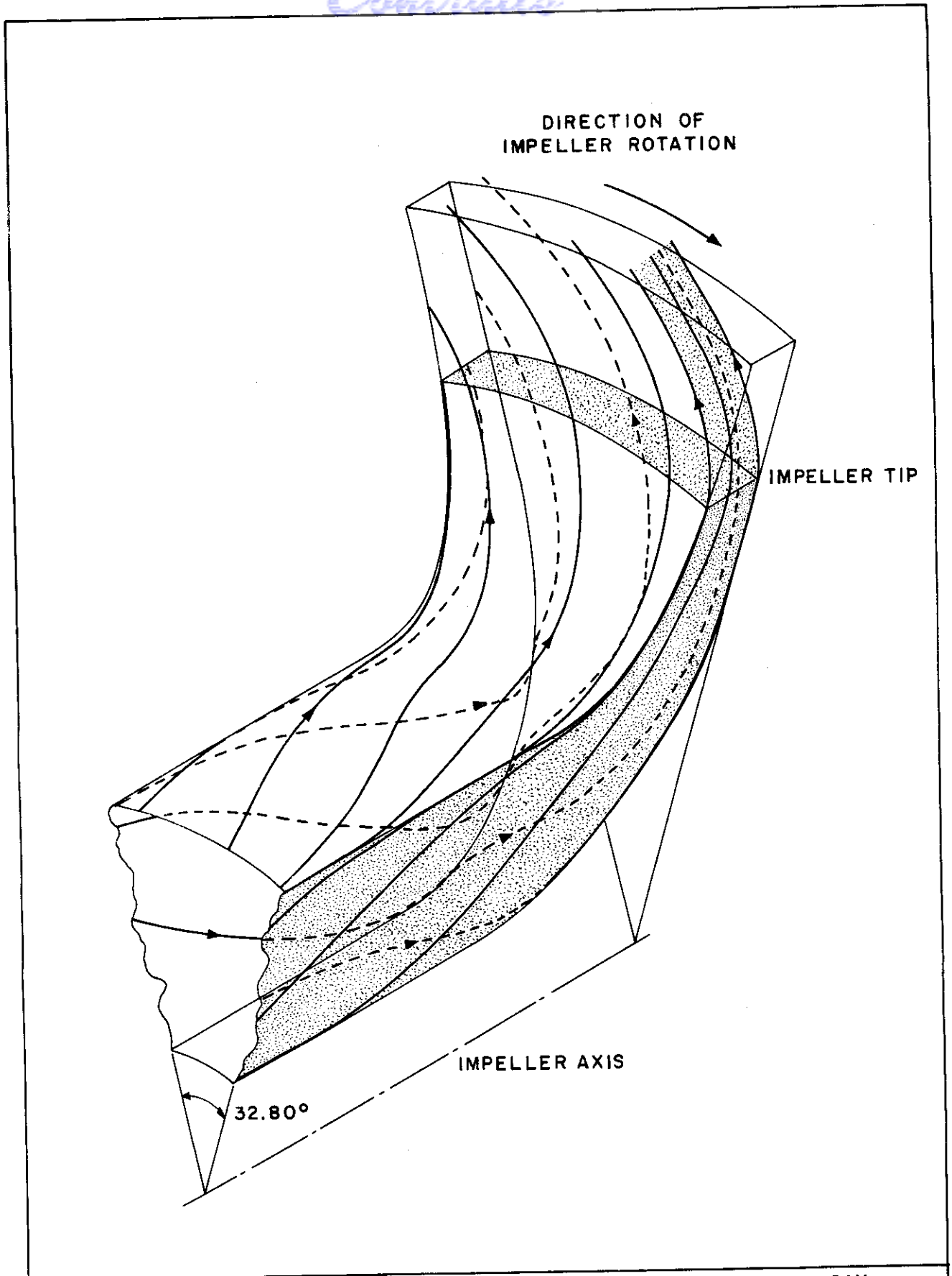
FIG. 3.6   THREE DIMENSIONAL FLOW IN A RADIAL FLOW
COMPRESSOR (FROM REF 3.4)

$$\tan \delta = \frac{\tan \beta_b}{\cos \gamma_t}$$

CYLINDRICAL DEVELOPMENT
OF SECTION A-A

BLADES

AXIS OF ROTATION

CONICAL DEVELOPMENT OF SECTION B-B

FIG. 3.7 BLADE GEOMETRY: δ RAKE ANGLE: $\beta_b$ BLADE ANGLE, $\gamma_t$ CONE ANGLE; THE BLADE CONSISTS OF RADIAL ELEMENT

(a)

(b)
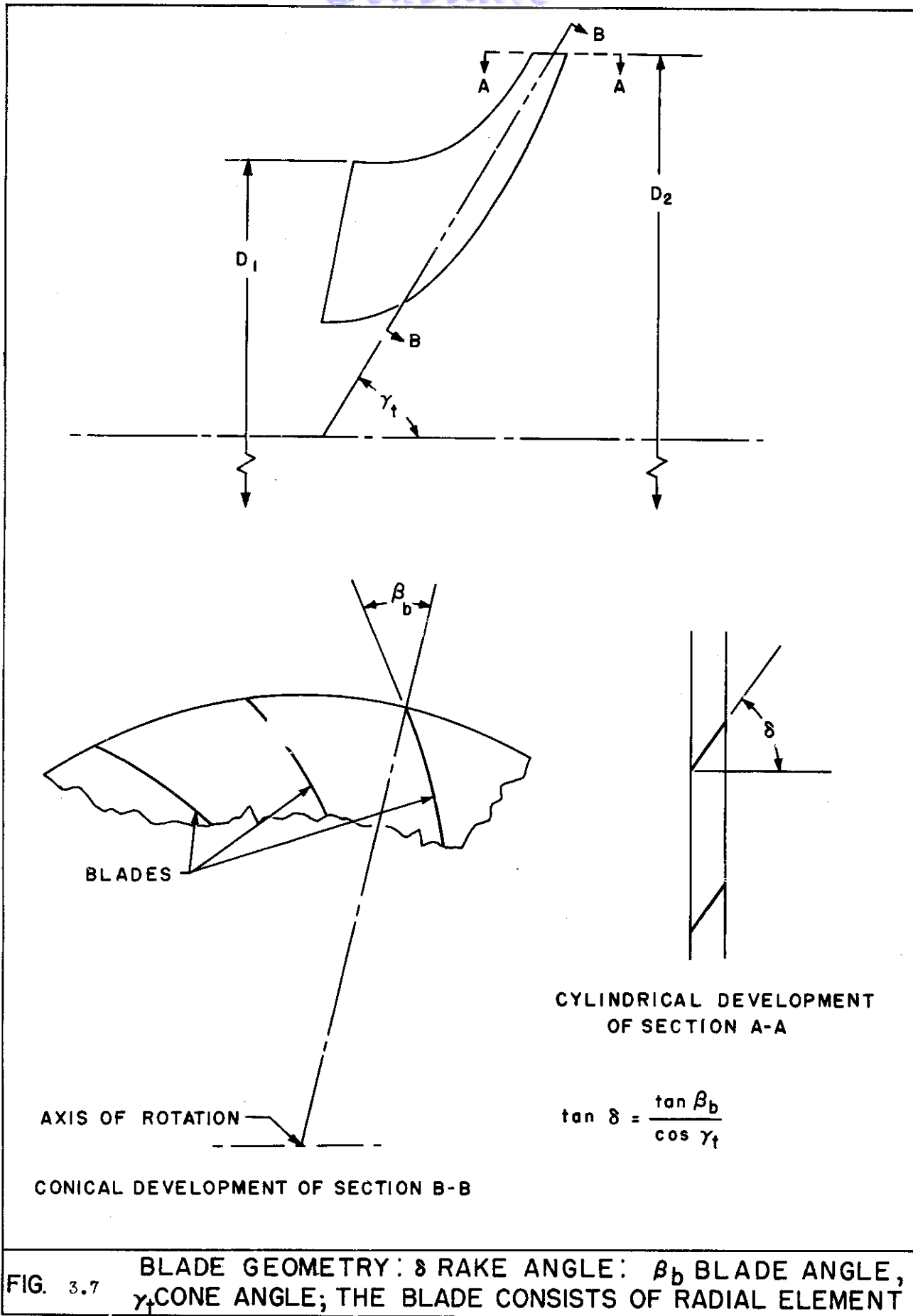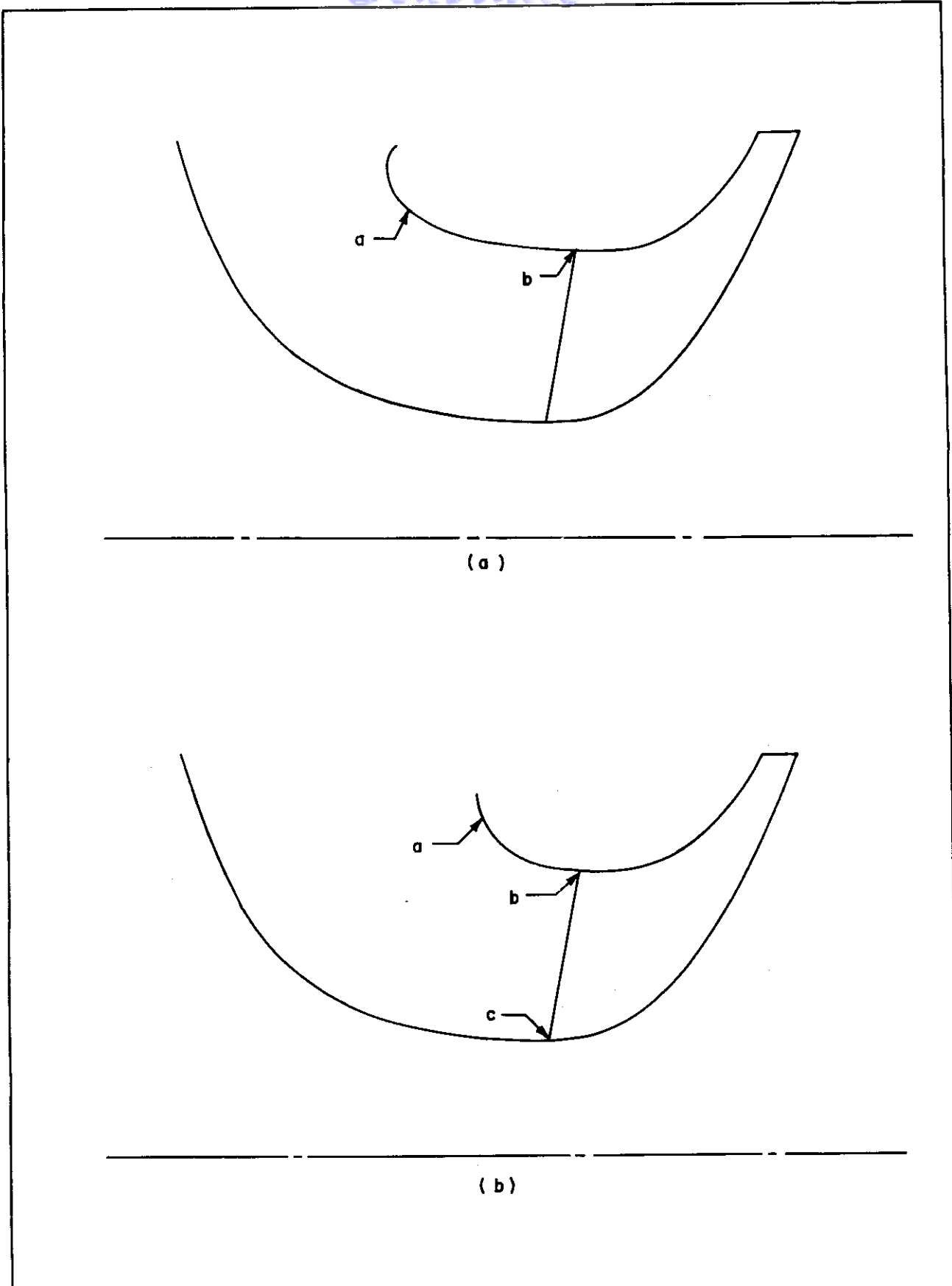
FIG. 3.8          COMPARISON OF TWO INLETS

FIG. 7.9  INLET FORM AND SYMBOLS AND CORRESPONDING VELOCITIES AT SHROUD AND HUB

PRESSURE SIDE

SUCTION SIDE

ROTATION

$\phi$

IMPELLER AXIAL VIEW

SHROUD LINE

5

NORMAL TO STREAMLINES

m

4

n

STATIONS

3

$\gamma$

2

n=0

$\Delta$m

TRACE OF STREAMLINE IN MERIDIONAL PLANE

HUB LINE

IMPELLER MERIDIONAL VIEW
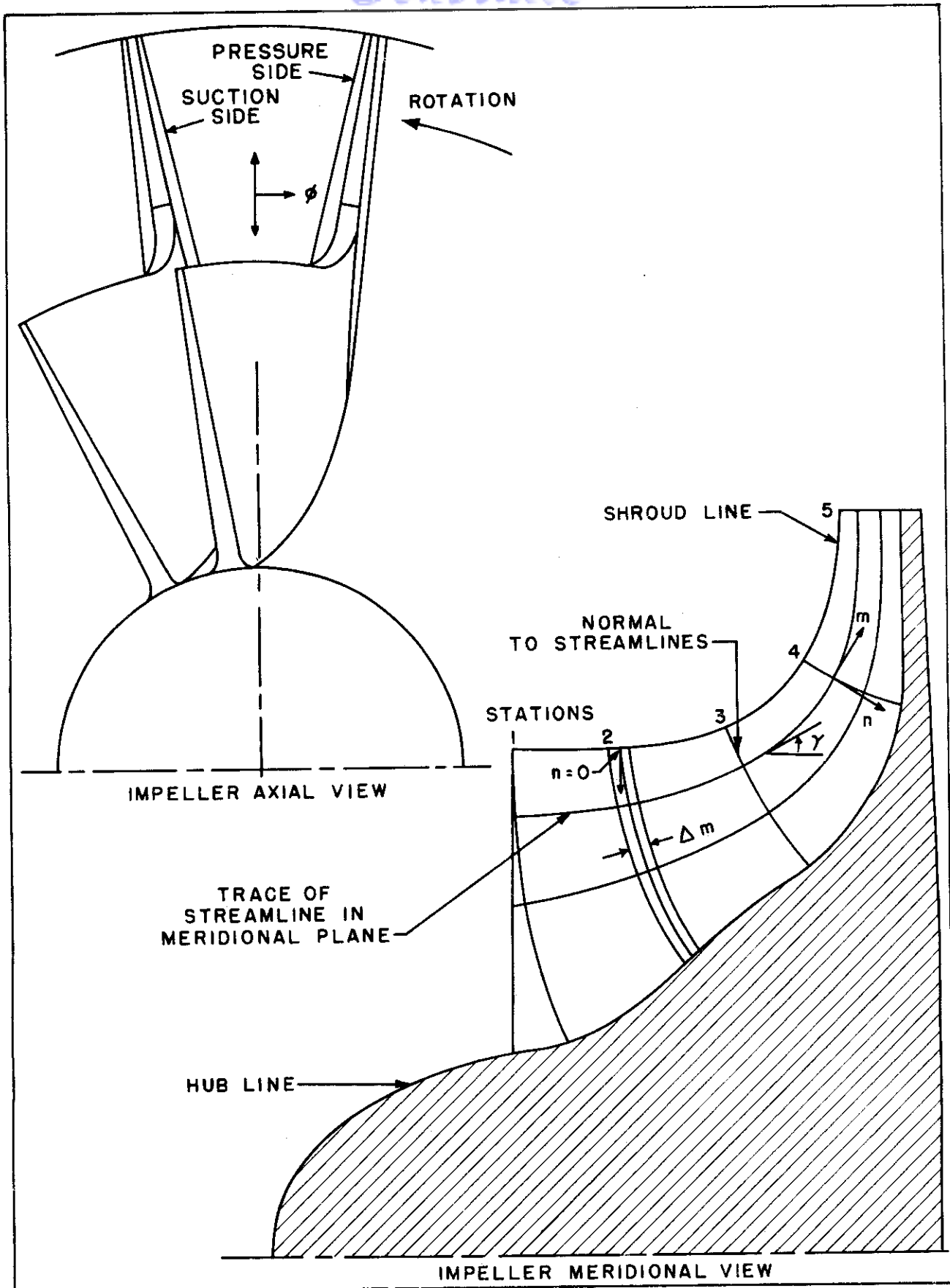
FIG. 3.10    IMPELLER MERIDIONAL AND AXIAL VIEW
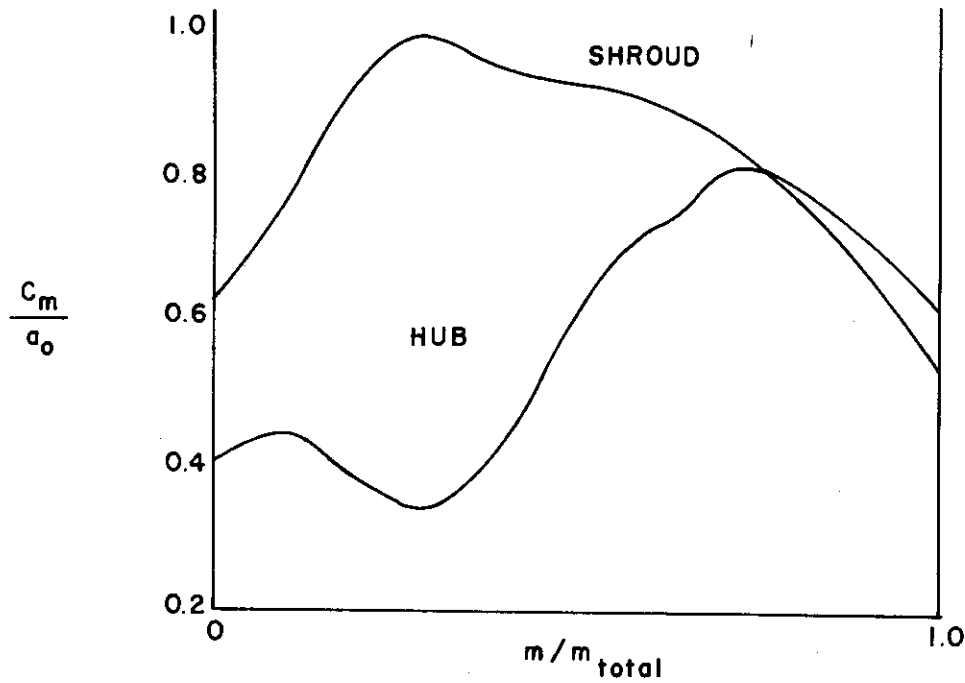
FIRST MERIDIONAL VELOCITIES ALONG HUB
AND SHROUD OF IMPELLER
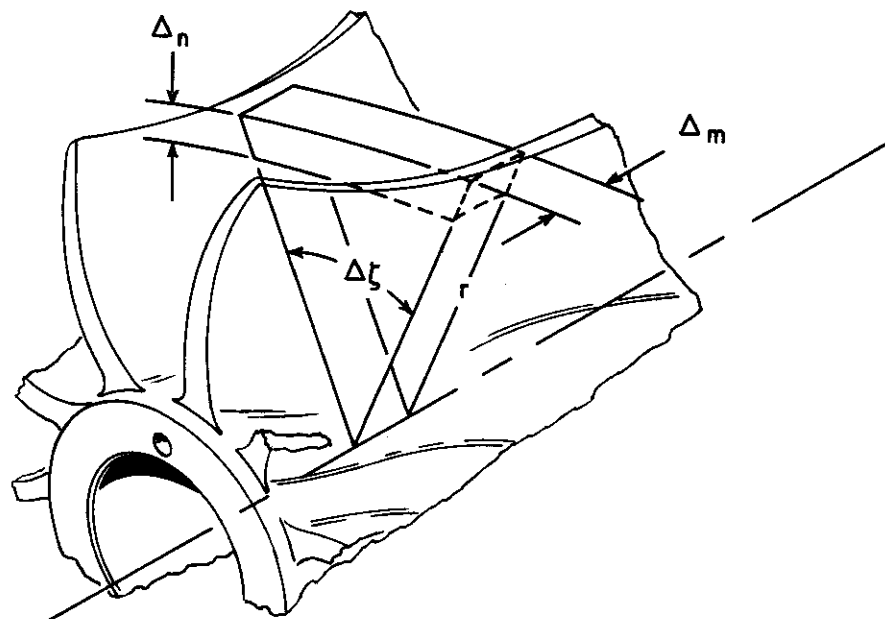


FIG. 3.11, 3.12    FLUID ELEMENT BETWEEN TWO BLADES FOR
THE CALCULATION OF THE BLADE LOADING
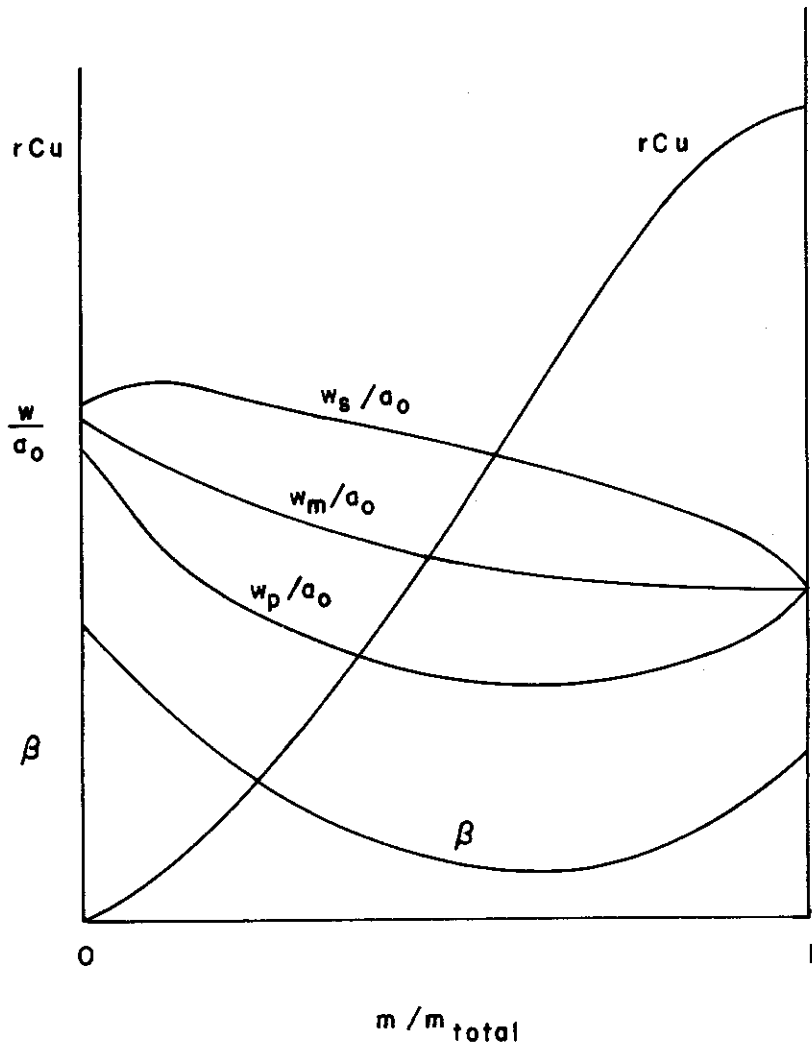
FIG. 3.13

RESULT OF STEP I AND STEP 2
OF IMPELLER CALCULATION

WITH BLADES

NO BLADES

LEADING EDGE
OF IMPELLER BLADES
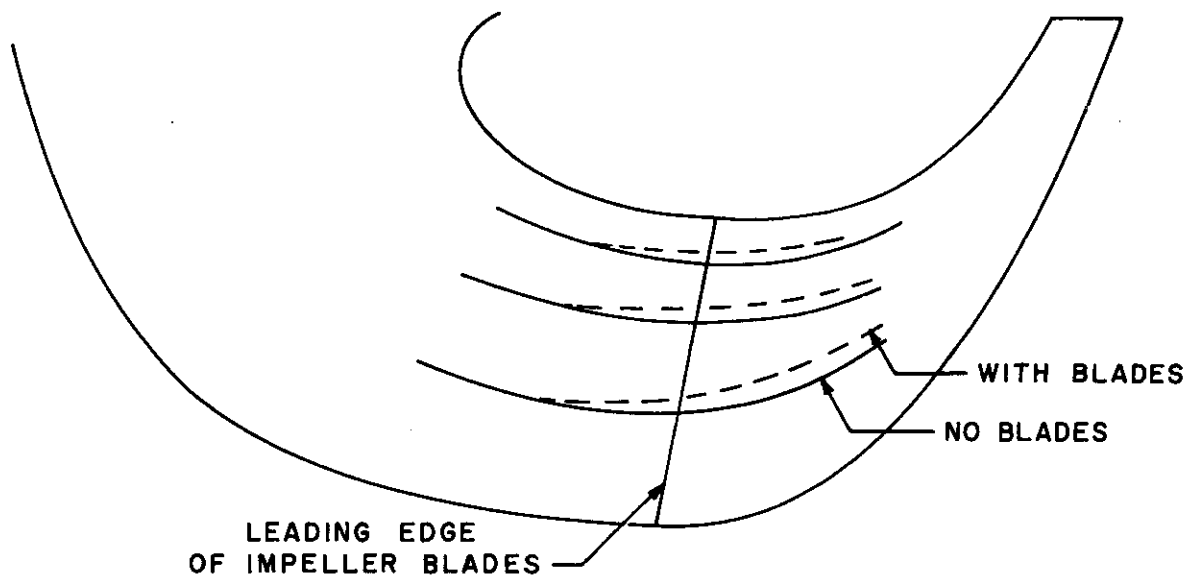
FIG. 3.14    COMPARISON OF STREAMLINE EXISTING WITHOUT
BLADES AND THOSE WITH BLADES

$$\int_0^n C_{m\rho}(2\pi r - zt)\epsilon\, dn$$

$$C_{m\rho}(2\pi r - zt)\epsilon$$

SHROUD        $n \longrightarrow$       HUB
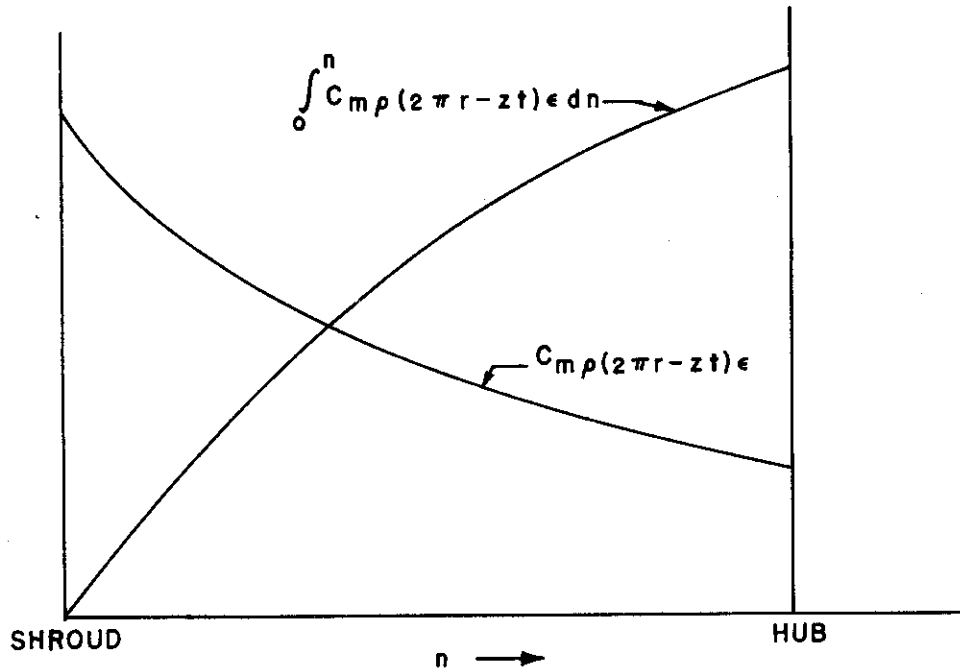
## MASS FLOW DISTRIBUTION ON A NORMAL TO THE STREAMLINE

$\Delta C_{m\zeta}$

$(+)$   $\Delta C_{m_R}$

$0$   $C_{m\rho}\left(\dfrac{1}{R_p} - \dfrac{1}{R}\right)$

$(-)$   $\zeta_u$

SHROUD       $n \longrightarrow$       HUB
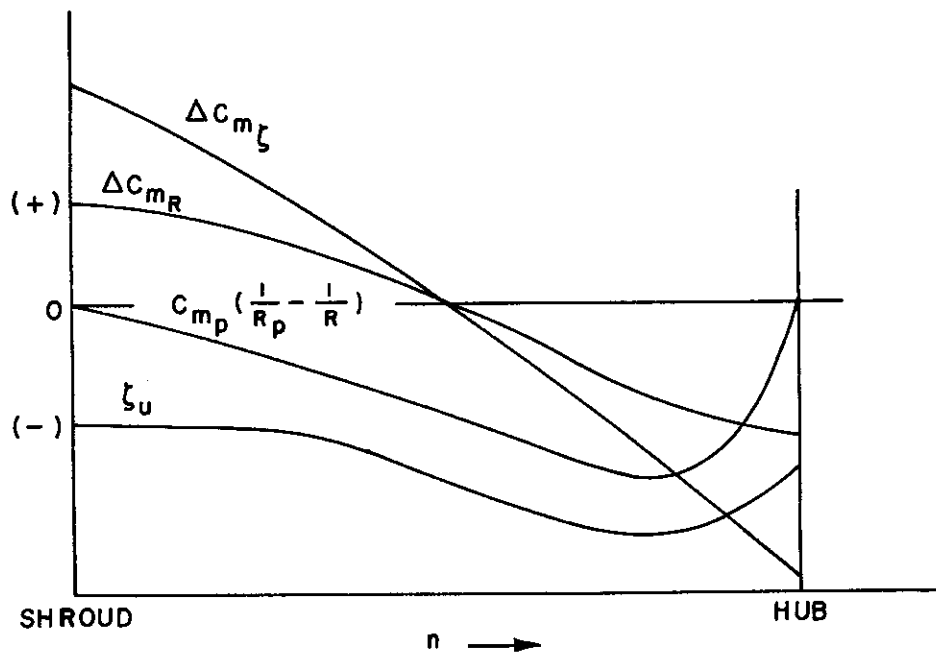
**FIG. 3.15, 3.16**    VORTICITY $\zeta_u$ AND $C_{m\rho}(1/R_p - 1/R)$ AND RESULTING VELOCITIES $\Delta C_{m_R}$ AND $\Delta C_{m\zeta}$

FREE STREAM
VELOCITY  (a)

REGION OF CONSTANT M

(b)

REGION OF ESSENTIALLY
CONSTANT MACH NUMBER

(c)

FREE STREAM
VELOCITY

– – – – – EXPANSION WAVE

——— COMPRESSION WAVE
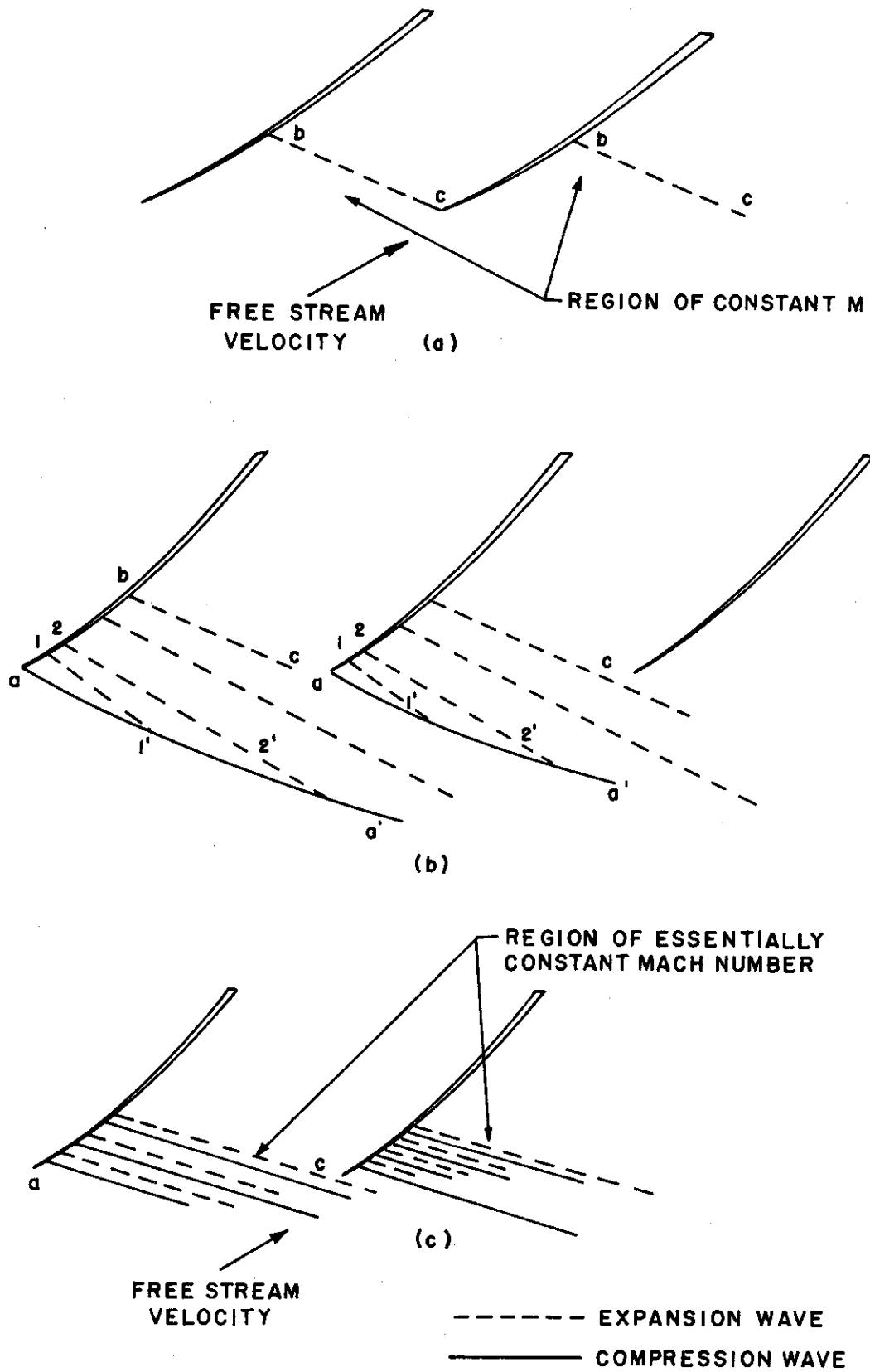
FIG. 3.17    POSSIBLE FLOW IN TWO-DIMENSIONAL (a,b) AND
THREE-DIMENSIONAL (c) CASCADES

**CASE I**          **CASE II**

BOUNDING
STREAMLINES

POTENTIAL
LINE

$R_o$

$R_i$

BOUNDING
STREAMLINES

$r_o$   $r_i$

AXIS OF SYMMETRY
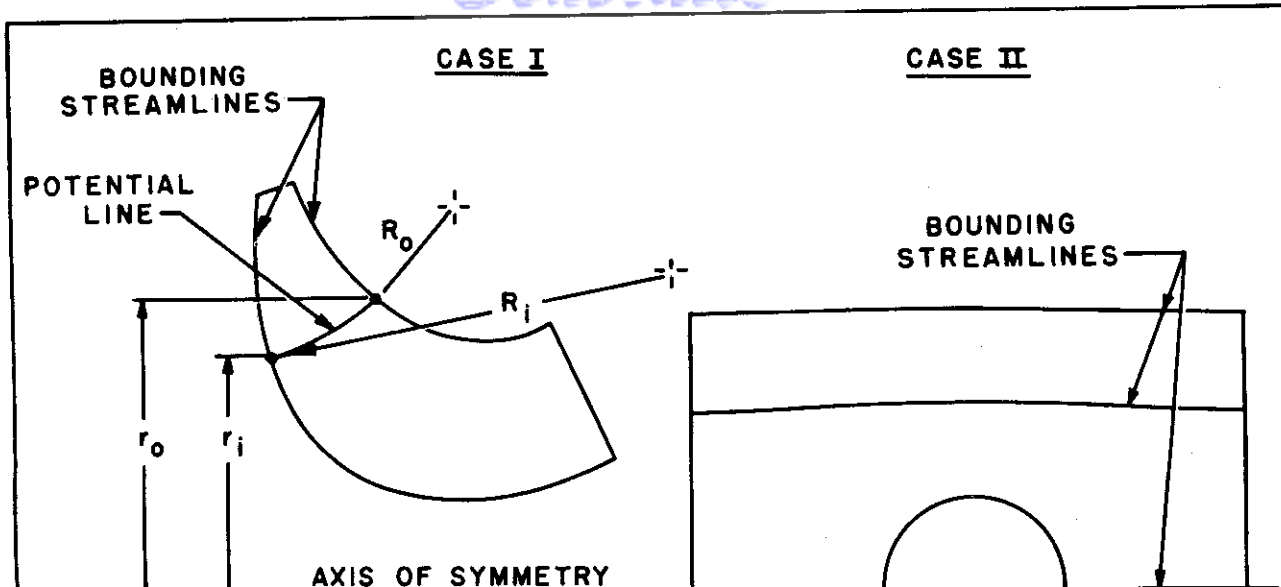
V     VELOCITY OF A PERFECT, INCOMPRESSIBLE FLUID AT A WALL OF AN AXIALLY SYMMETRIC PASSAGE, AS DETERMINED FROM EXACT SOLUTIONS.

$V_a$     VELOCITY OF A PERFECT, INCOMPRESSIBLE FLUID AT A WALL OF AN AXIALLY SYMMETRIC PASSAGE, AS ESTIMATED FROM THE VELOCITY DISTRIBUTION OF A TWO DIMENSIONAL ANALOG.

$\lambda = \dfrac{KC\,(r_o - r_i)^2}{r}$ WHERE $r = r_o$ OR $r = r_i$ FOR INNER OR OUTER WALL, RESPECTIVELY.

$C = \dfrac{1}{R_o} + \dfrac{1}{R_i}$

K     DIRECTIONAL CONSTANT:   K = I AT SUCTION SURFACE
                                      K = -I AT PRESSURE SURFACE

$\text{ERROR} = \dfrac{V_a - V}{V}$

SUCTION SURFACE

.12

.08

.04

O

-4   -3   -2   -1     1   2   3   4

$\lambda$          $\lambda$

PRESSURE SURFACE

-.04

-.08

-.12

**FIG. 3.18**     COMPARISON OF VELOCITIES OBTAINED FROM EXACT SOLUTIONS AND THE APPROXIMATE METHOD

SECTION IV
PREWHIRL

## 4.1 Introduction

It is generally known that the performance of a compressor improves if its specific speed is increased. A compressor of "high specific speed" is characterized by having a high flow rate for its size. Consequently, the inducer diameter is large compared to the tip diameter.

There has been a general tendency, at least in the design of low and medium pressure ratio compressors, to design impellers according to the concept of "high specific speed".

This tendency leads to difficulties with increased pressure ratio. The relative velocity at the inducer eye may become sonic or exceed the sonic value. However, supersonic flow within the compressor passages is as yet not too well understood,and unsatisfactory performance may easily result from lack of knowledge of supersonic blading. In this dilemma the following alternatives present themselves:

a) making the inlet velocity subsonic by resorting to a design of the "low-specific-speed" type.

b) Retaining the high-specific-speed design and partially supersonic flow, and attempting to design the supersonic portion for minimum losses.

c) Retaining the high-specific speed design and eliminating the supersonic flow. This is done by establishing prewhirl by means of guide vanes in front of the inducer which reduces the supersonic flow to subsonic values.
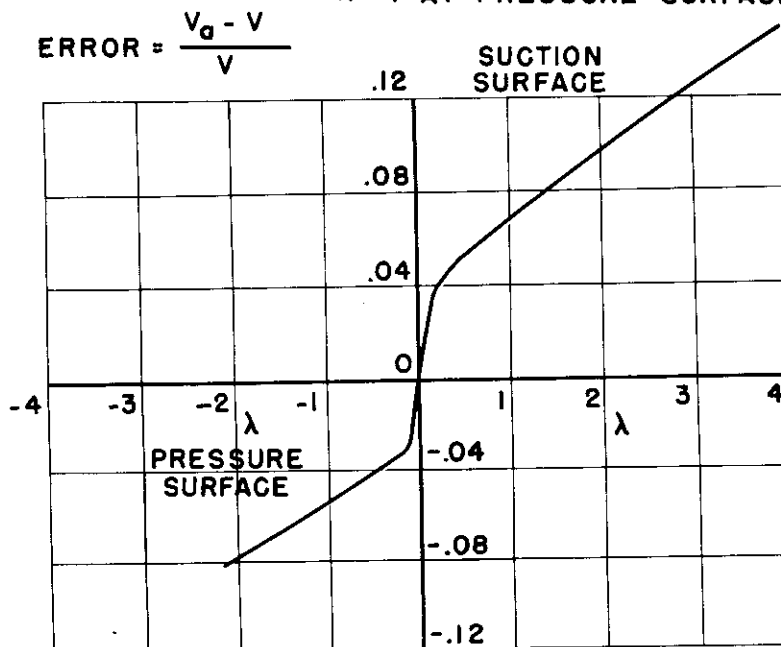
d) Retaining the high-specific-speed design by using prewhirl to reduce relative velocities though not necessarily to subsonic values.

The first of these alternatives will not be discussed here. The second - supersonic inlets without prewhirl - has not been treated heretofore in the literature, but is included in Section II of this report. The third alternative - subsonic prewhirl - has been considered only briefly before (Ref 4.1)and is the subject of this section. The last alternative, a combination of the second and third alternatives, will not be treated here in detail; it combines the characteristics of the other two.

As the term indicates, prewhirl blades impart rotation to the incoming fluid in or against the direction of the rotation of the wheel. For the same through-flow velocity and wheel speed, prewhirl in the direction of rotation reduces the relative velocity. Compared to zero prewhirl, its advantage of reducing the inlet relative Mach number seems obvious. Actually the use of prewhirl requires an increase in wheel speed (to avoid a decrease in head),and this somewhat diminishes the initially apparent gain. A fairly involved analysis is required in order to establish the optimum prewhirl design and the actual benefits.

Pfleiderer has considered free-vortex prewhirl in an excellent paper published in 1950 (Ref 4.2). Unfortunately, the analysis is of limited usefulness in the present case, due principally to the restriction to a single type of prewhirl, the emphasis on volume flow rather than mass flow, and a lack of direct correlation of the prewhirl characteristics to those of the overall compressor, particularly with regard to head.

The most recent study was published in 1953 by Stanitz (Ref 4.1). Stanitz treated the use of prewhirl in mixed-flow compressors in which the conditions at the inlet to a row of axial diffuser vanes are held constant. The objectives of Stanitz' study are quite different from those of this report. His treatment of the problem is therefore not directly useful here, though some use is made of certain detail calculations. In particular, Stanitz was interested in high mass flow per unit frontal area including an axial diffuser, whereas a radial diffuser is assumed here. With refrigeration compressors, frontal area has less significance since the heat exchanger and other apparatus connected with a refrigeration unit are usually much larger than the compressor. However, it is of interest to note that Stanitz concluded that prewhirl is of little value for the case he considered.

## 4.2    Analysis of the Prewhirl

### 4.2.1    General Procedure

In accordance with the Introduction (Section 4.1), the general approach is to establish the conditions for maximum weight flow through a machine with given head. The analysis of three cases will be given. Case I is the conventional zero-prewhirl design, in which the inlet relative Mach number is limited to a value below 1. Cases II and III were mentioned above, namely, zero prewhirl with supersonic inlet and prewhirl with subsonic inlet.

In the analysis, expressions will be derived for tip speed, inducer size, and mass flow. It will be shown that in each case an optimum design exists which is distinguished by a maximum mass flow.

Two important quantities are assumed to be given:

a)  The Euler head $H_{TH} = \dfrac{1}{g} \Delta(u\, c_u)$ in the dimensionless form

$g\, H_{TH}/a_o^2$. Euler head is the work put into the fluid by action

of the impeller and exceeds adiabatic head $H_{ad}$ by an amount determined by certain losses.

b)  the quantity $\lambda = c_{ut}/u_t$, is determined by impeller geometry. It increases with the number of blades and depends also on the amount of backward curvature.

The results of this analysis are expressed in terms of these quantities.

The fluid is assumed to be a perfect gas, and the flow to be homentropic (Ref 4.3) before the entrance to the rotor. This is a good approximation to the actual conditions, since the losses prior to this point are usually small compared to the losses in the impeller and diffuser, and because the entering gas has fairly uniform energy content. In addition, the inlet to the rotor is assumed to be a plane perpendicular to the axis, in which fluid acceleration in the radial direction is negligible.

### 4.2.2 Zero Prewhirl and Subsonic Inlet. Case I

In this case no prewhirl is assumed, and the maximum value of the inlet relative Mach number, $(M_{w_1})_{max}$, is specified. From the definition of $H_{TH}$ as $\frac{1}{g}\Delta(u\, c_u)$ and the definition of $\lambda$ as $\frac{c_{ut}}{u_t}$, one can write an expression for the tip speed. The dimensionless form of the equation in terms of the known quantities $\lambda$ and $gH_{TH}/a_0^2$ is:

$$\left(\frac{u_t}{a_o}\right)^2 = \left(\frac{u_2}{a_o}\right)^2 = \frac{1}{\lambda}\,\frac{g\,H_{TH}}{a_o^2} \tag{4.1}$$

The maximum inlet relative Mach number occurs at the inducer tip when there is no prewhirl. Using geometrical relations from the inducer tip velocity triangle and compressible flow formulas, the equation for the inducer tip radius ratio can be derived in the form:

$$\left(\frac{r_i}{r_t}\right)^2 = \left(\frac{u_i}{u_t}\right)^2 = \left(\frac{a_o}{u_t}\right)^2 \frac{M_{w_i}^2 \sin^2\beta_i}{1+\frac{k-1}{2}M_{w_i}^2 \cos^2\beta_i} \tag{4.2}$$

The mass flow can be found by integrating the meridional component of the mass velocity $\rho\, c_{mi}$ over the inlet area. Without prewhirl, $(\rho\, c_{m_i})$ is a constant and can be found from the tip velocity triangles.

The mass flow can be put in dimensionless form by dividing by an appropriate reference mass flow. The result is

$$\frac{W}{\pi r_t^2 \rho_o a_o} = \left(1 - \frac{r_h^2}{r_i^2}\right)\left(\frac{r_i}{r_t}\right)^2 \frac{M_{w_i}\cos\beta_i}{\left(1+\frac{k-1}{2}M_{w_i}^2\cos^2\beta_i\right)^{\frac{k+1}{2(k-1)}}} \tag{4.3}$$

The tip speed, inducer size, and mass flow have been expressed above in terms of the given parameters $\frac{gH_{TH}}{a_o^2}$, $\lambda$, and $M_{wi}$, the last of these being equal to $(M_{w1})_{max}$ in this case. However, the value of inducer tip relative flow angle $\beta_i$ is also required. This can be eliminated by finding the value of $\beta_i$ which gives maximum mass flow:

$$\cos^2\beta_i = \frac{3 + K M_{w_i}^2}{2 M_{w_i}^2}\left[1 - \sqrt{1 - \frac{4 M_{w_i}^2}{(3 + K M_{w_i}^2)^2}}\right] \qquad (4.4)$$

For $M_{wi} = 0$, this gives $\beta_i = 54.7°$, which agrees with incompressible theory (Ref 4.4, Page 71). For $M_{w_i} = 1.0$ and $k = 1.4$, Eq 4.4 gives $\beta_i = 60.6°$. An approximate theory of Pfleiderer (Ref 4.2), valid for moderate Mach Numbers, give $\beta_i = 57.8°$, which is in reasonable agreement with Eq 4.4.

It is important to note that selecting the value of $\beta_i$ to obtain maximum flow is equivalent to choosing the inducer size $r_i/r_t$. Thus, instead of stating that the optimum value of $\beta_i$ was selected, one could alternatively say that the optimum value of $\frac{r_i}{r_t}$ was selected.

The former point of view is of interest because it will be seen that the optimum value of $\beta_i$ is about $60°$ for all the cases considered herein.

The latter point of view leads to the following conclusion, advanced by Hawthorne (Ref 4.5): for specified head and relative Mach number, the mass flow at first increases with inducer size as one might expect from the increase in flow area. However, for large inducer size, the mass flow actually decreases because the Mach number restriction necessitates a reduction in axial velocity.

4.2.3   Zero Prewhirl and Supersonic Inlet.   Case II

For Case II, no prewhirl is again assumed, but this time Mach numbers are not specified. Instead, the relative velocity ratio $w_t/w_i$ and the impeller outlet flow angle $\alpha_2$ are given. Thus, there are a total of four given quantities: $\dfrac{gH_{TH}}{a_o^2}$, $\lambda$, $\dfrac{w_t}{w_i}$ and $\alpha_2$

The number of independent variables can be reduced from four to two because of the identity

$$\frac{W_i^2}{g H_{TH}} = \frac{\lambda^2 \cot^2 \alpha_2 + (1-\lambda)^2}{\lambda \left(u_t/w_i\right)^2} \tag{4.5}$$

which holds for a radial compressor without prewhirl. The equation can be verified by substituting the definitions of $H_{TH}$ and $\lambda$, and using geometrical relationships from velocity triangles.

The results will therefore be expressed in terms of $\dfrac{g H_{TH}}{a_o^2}$ and $\dfrac{W_1^2}{g H_{TH}}$.

This results in a substantial simplification of the equations without any loss of generality.

Since there is no prewhirl, the relation between tip speed and head is the same as for Case I:

$$\left(\frac{u_t}{a_o}\right)^2 = \frac{1}{\lambda} \frac{g H_{TH}}{a_o^2} \tag{4.6}$$

Using this equation and the geometrical relationships from the inducer tip velocity triangle leads to:

$$\left(\frac{r_i}{r_t}\right)^2 = \left(\frac{u_i}{u_t}\right)^2 = \lambda \frac{w_i^2}{g H_{TH}} \sin^2 \beta_i \tag{4.7}$$

The dimensionless mass flow is found as in Case I, again using tip triangle geometry, and compressible flow formulas:

$$\frac{W}{\pi r_t^2 \rho_o a_o} = \left(1 - \frac{r_h}{r_i^2}\right)\left(\frac{r_i}{r_t}\right)^2 \sqrt{\left(\frac{w_i^2}{g H}\right)\left(\frac{g H_{TH}}{a_o^2}\right)} \left[1 - \frac{K-1}{2}\left(\frac{w_i^2}{g H}\right)\left(\frac{g H_{TH}}{a_o^2}\right)\cos^2 \beta_i\right] \tag{4.8}$$

The parameter $\beta_i$ can again be eliminated by specifying maximum mass flow, leading to

$$2 \sec^2 \beta_i = 3 + \frac{K+1}{2}\left(\frac{w_i^2}{a_o^2}\right)\left(\frac{g H_{TH}}{a_o^2}\right)$$

$$+ \sqrt{\left[3 + \frac{K+1}{2}\left(\frac{w_i^2}{g H_{TH}}\right)\left(\frac{g H}{a_o^2}\right)\right]^2 + 2(3K-1)\left(\frac{w_i^2}{g H_{TH}}\right)\left(\frac{g H_{TH}}{a_o^2}\right)} \tag{4.9}$$

Equation (4.9) gives values which are quite close to those for Case I.

4.2.4    Prewhirl and Subsonic Inlet.    Case III

The analysis of Case III is rather complicated because of the large number of variables involved. For specified head and maximum relative inlet Mach number, the proper combination of the following quantities must be established to give the maximum mass flow:

a)   type of prewhirl (free-vortex, solid-body, etc )

b)   amount of prewhirl, $c_{ui}/\mu_i$

c)   inducer tip relative flow angle, $\beta_i$ .

The analysis is further complicated by nonaerodynamic comsiderations such as impeller stresses and fabrication.

The optimum type of prewhirl will be established first for a compressor using air as a fluid. This is done for simplicity because the selection will be shown to be independent of $\beta_i$ .

Later it will be shown that the result is also valid for a Freon compressor.

In an air compressor for high pressure ratio, stress considerations dictate that the impeller blades must be composed of radial elements. This influences the selection of the type of flow in the annulus following the prewhirl blades, for it must be such that incidence losses at the inducer are not excessive. The following types of flow were considered:

a)   free vortex

b)   constant mass velocity

c)   constant whirl velocity

d)   solid body (also called wheel flow)

e)   radial element

All but the last of these have been described in the literature (Reference 4.1) and are frequently discussed in turbomachine theory. The radial element type appears here for the first time, and must therefore now be defined.

The radial-element prewhirl provides a direction to the flow entering a rotor consisting of a large number of radial-element blades such that there is zero incidence at all radii. The incidence angle is defined as that between the upstream velocity vector and the blade leading-edge tangent, and will be discussed below. This definition implies that:

$$\tan \beta_1 = \frac{r_i}{r_1} \tan \beta_i \qquad (4.10)$$

Equation 4.10 can be alternatively regarded as the defining equation for radial-element prewhirl.

The following conventional differential equation, applicable to all types of prewhirl, is sometimes called the "simple radial equilibrium equation" (Ref 4.1):

$$\frac{Cu_1^2}{r_1} + Cu_1 \frac{dCu_1}{dr_1} + Cm_1 \frac{dCm_1}{dr_1} = 0 \qquad (4.11)$$

Use of this equation is equivalent to making an assumption about the shroud and hub contours. This will be discussed later. Combining Equations 4.10 and 4.11 and using geometrical relations available from the inducer tip velocity triangle leads to the following:

$$\frac{d}{dr_1}\left(\frac{Cu_1}{r_1}\right) - \frac{2\,Cu_1/r_1}{r_1\left[\dfrac{1 - \dfrac{r_i}{u_i}\dfrac{Cu_1}{r_1}}{\dfrac{r_i^2}{r_i\,u_i}\left(\dfrac{Cu_1}{r_1}\right)\tan^2\beta_i} - 1\right]} = 0 \qquad (4.12)$$

This is a first-order, nonlinear differential equation and can be solved completely only by numerical methods.

Though the complete solution of Equation 4.12 (for radial-element prewhirl) cannot be written explicitly, much can be learned by partial solution under restricted conditions. For example, it can be shown that for small amounts of prewhirl (more precisely, for $\dfrac{Cu_1/r_1}{u_i/r_i}$ small), the solution of equation 4.12 with higher-order terms omitted, is

$$\frac{Cu_1}{r_1} = \text{Constant}$$

$$(4.13)$$

which is the equation for solid body prewhirl.

Thus, for small amounts of prewhirl, radial-element prewhirl is very similar to solid-body prewhirl.

Further study of equation 4.12 shows that a singularity occurs in the region of interest $(r \leq 1)$, unless

$$0 \leq \frac{c_{u_i}}{u_i} < \cos^2 \beta_i \qquad (4.14)$$

the singularity can be interpreted physically thus: When $c_{u_i}/u_i$ exceeds the critical value $\cos^2 \beta_i$, reverse flow occurs over part of the flow area.

Therefore one can conclude that the amount of prewhirl of the radial-element type must be limited to the range expressed by Equation 4.14 if undesirable reverse flow is to be avoided. No such limitations exist for the other types of prewhirl which were listed earlier.

The choice of the type of prewhirl is therefore dependent upon the amount of prewhirl required, because of the characteristic limitation of the radial-element type. It happens that radial-element prewhirl is unsuitable for precisely this reason, though the proof is left for a subsequent point in this analysis.

If radial-element prewhirl is momentarily considered to be eliminated, it is evident that some incidence losses must be tolerated. This implies the necessity of a study of the incidence losses associated with the use of each of the types of prewhirl listed earlier, so that these losses can be minimized.

Incidence losses are difficult to determine, but the incidence angle variation is itself a good indication of the losses. Thus, comparison of incidence angle variation can be used to rank the various types of prewhirl with respect to losses.

The incidence angle is the difference between the flow angle $\beta_1$ and the blade angle $\beta_{bl}$. As an example, an expression will now be derived for the incidence angle for the case of solid-body prewhirl with radial-element rotor blading.

From Equation 4.11 and 4.13, an expression can be obtained for absolute inlet velocity as a function of radius. The equation, valid only for solid-body prewhirl is:

$$C_1^2 = C_i^2 \left[ 1 + \frac{1 - \frac{r_1^2}{r_i^2}}{1 + \left(\frac{u_i}{c_{u_i}} - 1\right)^2 \cot^2 \beta_i} \right] \qquad (4.15)$$

Then, from this equation and general geometrical relationships valid for velocity triangles, one can obtain an equation for $\beta_1$ :

$$\tan \beta_1 = \frac{r_1}{r_i} \frac{\tan \beta_i}{\sqrt{1 + 2\left(1 - \frac{r_1^2}{r_i^2}\right)\left(\frac{u_i}{c_{u_i}}\right)^2}} \qquad (4.16)$$

Finally from this and Equation 4.10, the incidence angle can be found

$$\beta_1 - \beta_{b1} = \tan^{-1}\left[ \frac{r_1}{r_i} \frac{\tan \beta_i}{\sqrt{1 + 2\left(1 - \frac{r_1^2}{r_i^2}\right)\left(\frac{u_i}{c_{u_i}} - 1\right)^2}} \right] - \tan^{-1}\left(\frac{r_1}{r_i} \tan \beta_{b1}\right) \qquad (4.17)$$

This equation holds only for solid-body prewhirl used with radial-element rotor blades.

The upper curve of Figure 4.1, based on Equation 4.17, shows incidence angle as a function of radius for one representative case. The strong influence of $\beta_{bi}$ is evident. The lower curve shows the

maximum absolute values of incidence angle plotted versus $\beta_{bi}$ . It

can be seen that there exists an optimum $\beta_{bi}$ , for which incidence

losses are minimized. Further analysis of this sort showed that the prewhirl types listed above ranked in the order given there with respect to incidence losses when used with radial-element rotor blading. Thus it was considered best to use the solid-body type. This is reasonable in view of the afore-mentioned similarity between solid-body prewhirl and radial-element prewhirl, the latter having no incidence losses.

Since the maximum inlet relative Mach number is to be specified, it is necessary to find the radius at which it occurs for solid-body prewhirl.

Equation 4.15 indicates that the maximum absolute velocity always occurs at the hub where $\dfrac{r_1}{r_i}$ has its lowest value. This means that, with solid body whirl a reduction of the absolute velocity caused by a decrease of the whirl component toward the hub is more than offset by the increase of the meridional component.

Using the formulas of compressible flow and Equation 4.15, the inducer Mach numbers (absolute and relative) can be found:

$$\frac{1}{M_{c_1}^{2}} = \frac{\dfrac{1}{M_{c_i}^{2}} + \dfrac{K-1}{2}}{1 + \dfrac{1 - r_1^{2}/r_i^{2}}{1 + \left(\dfrac{u_i}{c_{u_i}} - 1\right)^{2} \cot^{2}\beta_i}} - \frac{K-1}{2} \tag{4.18}$$

$$M_{w_1}^{2} = M_{c_1}^{2}\left[1 - \frac{r_1^{2}}{r_i^{2}}\frac{1 - \left(\dfrac{u_i}{c_{u_i}} - 1\right)^{2}}{\left(\dfrac{u_i}{c_{u_i}} - 1\right)^{2}\cot^{2}\beta_i + 2 - \dfrac{r_1^{2}}{r_i^{2}}}\right] \tag{4.19}$$

Inspection of Equation 4.18 confirms that the maximum absolute Mach number occurs at the hub. But it is by no means obvious from Equation 4.19 just where $(M_{w1})_{max}$ occurs. Detailed analysis of this equation leads to the conclusion that there is a critical value of $c_{ui}/u_i$ such that for values less than critical, $(M_{w_1})_{max}$ occurs at the tip, while for values greater than critical, $(M_{w_1})_{max}$ occurs at the hub. If $c_{ui}/u_i$ is equal to the critical value, the inlet relative Mach number is the same at all radii, a somewhat surprising fact.

The equation for the critical value of $c_{ui}/u_i$ , for which the inlet relative Mach number is constant, is

$$\frac{c_{u_i}}{u_i} = \frac{1}{1 + \sqrt{2 + \dfrac{K-1}{2}M_{w_1}^{2}}} \qquad \left[\text{HERE } M_{w_1} = M_{w_i} = \left(M_{w_1}\right)_{MAX}\right] \tag{4.20}$$

Equation 4.20 is independent of $\beta_i$. For $k = 1.4$ and $(M_{w1})_{max} = 1.0$, the critical value of $c_{ui}/u_i$ is 0.403.

After the optimum prewhirl type has been established as solid-body and its Mach number characteristics have been determined, the optimum amount of prewhirl and the optimum inducer tip relative flow angle can be determined. When prewhirl is used in a compressor the required tip speed is no longer a function of the head alone: it also depends on the prewhirl characteristics. In addition, if the rotor has a constant-diameter exit, the head may vary from one streamline to another. In the case presented here it is assumed that the rotor exit is designed to give constant head and is therefore not of constant diameter.

Using the definitions of $H_{TH}$ and $\lambda$, and triangle geometry, expressions for the tip speed and inducer size can be derived:

$$\lambda \frac{u_t^2}{a_o^2} = \frac{g H_{TH}}{a_o^2} \cdot \frac{c_{ui}/u_i}{\left(1 - \frac{c_{ui}}{u_i}\right)^2} \cdot \frac{M_{wi}^2 \sin^2\beta_i}{1 + \frac{k-1}{2} M_{c_i}^2} \qquad (4.21)$$

$$\frac{r_i^2}{r_t^2} = \left(\frac{u_i}{u_t}\right)^2 = \frac{a_o^2}{u_t^2} \frac{1}{\left(1 - \frac{c_{ui}}{u_i}\right)^2} \frac{M_{wi}^2 \sin^2\beta_i}{1 + \frac{k-1}{2} M_{c_i}^2} \qquad (4.22)$$

The mass flow can be obtained by integrating the through-flow component of the mass velocity. In integral form the equation is:

$$W = \int_{r_h}^{r_i} \frac{\rho_o a_o}{\left[1 + \frac{k-1}{2} M_{c_i}^2\right]^{\frac{k+1}{2(k-1)}}} \sqrt{M_{c_i}^2 + \left(1 - 2\frac{r_i^2}{r_i^2}\right) \frac{M_{wi}^2 \sin^2\beta_i}{\left(\frac{u_i}{c_{ui}} - 1\right)^2}} \times \qquad (4.23)$$

$$\left[1 - \frac{k-1}{2} M_{c_i}^2 \frac{1 - \frac{r_i^2}{r_i^2}}{1 + \left(\frac{u_i}{c_{ui}} - 1\right)^2 \cot^2\beta_i}\right]^{\frac{1}{k-1}} 2\pi r_1 dr_1$$

Two approximations were made at this point for ease of integration.

The bracketed term was expanded by means of the binomial theorem, with only the first two terms retained. Since the second term within the brackets is small compared to the first, this is a good approximation.

The lower limit of the integral was changed from $r_h$ to zero and a factor $1 - \dfrac{r_h^2}{r_i^2}$ was added. This procedure is exact if $\dfrac{r_h}{r_i}$ is zero or unity, and is a very good approximation for intermediate values with the present integrand.

With these two approximations the final dimensionless expression for the mass flow is:

$$
\frac{W}{\pi r_t^2 \rho_o a_o} = \frac{1}{3}\left(1 - \frac{r_h^2}{r_i^2}\right)\left(\frac{r_i}{r_t}\right)^2 \frac{M_{c_i}}{\left(1 + \frac{\kappa-1}{2}M_{c_i}^2\right)^{\frac{\kappa+1}{2(\kappa-1)}}} \frac{\left(\frac{u_i}{c_{u_i}} - 1\right)^3 \cot^3 \beta_i}{\sqrt{1 + \left(\frac{u_i}{c_{u_i}} - 1\right)^2 \cot^2 \beta_i}} \times
$$

$$
\left\{\left[1 + \frac{2\tan^2 \beta_i}{\left(\frac{u_i}{c_{u_i}} - 1\right)^2}\right]^{\frac{3}{2}}\left[1 + \frac{1}{10}M_{w_i}^2 \cos^2 \beta_i - \frac{3}{10}\frac{M_{c_i}^2}{1 + \left(\frac{u_i}{c_{u_i}} - 1\right)^2 \cot^2 \beta_i}\right] \right. \tag{4.24}
$$

$$
\left. -1 - \frac{1}{10}M_{w_i}^2 \cos^2 \beta_i \right\}
$$

From the equations above one can see that where formerly it was necessary to specify the inducer tip relative flow angle $\beta_i$, one must now specify two quantities, $\beta_i$ and $\dfrac{c_{ui}}{u_i}$, despite the fact that only solid-body prewhirl was considered. In Cases I and II, $\beta_i$ was determined by specifying that the mass flow should be a maximum for given tip diameter. It happens that in the present case, specifying maximum mass flow determines both $\beta_i$ and $M_{c_i}$, though in a more arbitrary manner, which will now be described.

Figure 4.2 presents mass flow versus $r_i/r_t$ for various values of the ratio $c_{u_i}/u_i$, and for representative values of the head and maximum relative Mach number, which are held constant. The following procedure was used in obtaining these values.

a) values of $\frac{g H_{TH}}{a_o^2}$, $(M_{w_i})_{MAX}$, $\beta_i$ and $c_{u_i}/u_i$ were selected

b) critical value of $c_{u_i}/u_i$ were determined from Eq 4.20

c) for $\dfrac{c_{u_i}}{u_i}$ less than (or equal to) critical, $M_{w_i} = (M_{w_1})_{max}$. $M_{oi}$ was found from Eq 4.19.

d) for $\dfrac{c_{ui}}{u_i}$ greater than critical, $M_{wh} = (M_{w1})_{max}$. $M_{oh}$ was found from Eq 4.19, and $M_{oi}$ was found from Eq 4.18.

e) inducer size and mass flow were determined using Eqs 4.21, 4.22, and 4.24.

For each curve of Figure 4.2, the flow varies approximately quadratically with inducer tip radius. This is logical since the flow area varies in this manner. However, it is important to note that each curve has a maximum. The curve for $\dfrac{c_{u_i}}{u_i} = 0$ corresponds to zero prewhirl (Case I), and it can be verified that the maximum flow occurs at the point where $\beta_i = 60.6°$, the value given by Eq 4.4.

The case of constant relative Mach number is also shown on Fig. 4.2. It can be seen that in the range shown, this case gives the greatest mass flow.

Using Figure 4.2 one can state that for the given values of $H_{TH}$ and $(M_{w1})_{max}$ the maximum flow can be obtained at Point A, for which

a) $c_{ui}/u_i$ has the value giving constant relative Mach number.

b) $\dfrac{r_i}{r_t} = 0.9\sqrt{\lambda}$ which corresponds to $\beta_i = 80°$

For other values of head and/or lower values of the maximum relative Mach number it can be shown that the same conclusion is reached except that the value of $\beta_i$ may be slightly different.

It is impractical to construct an inducer for $\beta_i$ greater than about 60°, hence this value is herein arbitrarily chosen as being the optimum. For maximum flow with $\beta_i$ = 60°, the value of $c_{u1}/u_1$ giving constant relative Mach number should be retained. This can be seen from Fig. 4.2 by noting the dotted line which connects points at which $\beta_i$ = 60°. The point of maximum mass flow on this line is point B, which is also on the curve for constant $M_{w1}$.

The mass flow at point B, the arbitrarily selected optimum, is only slightly less than that at point A.

It was previously stated that radial-element prewhirl should be discarded because of the limitation in the amount which can be obtained; this will now be verified. Here Eq 4.14 becomes:

$$\frac{c_{ui}}{u_i} < 0.25 \tag{4.25}$$

Since $\dfrac{c_{u_i}}{u_i}$ is about 0.40 at point B in Fig. 4.2, it is evident why radial-element prewhirl was discarded: the flow at point B would not have been attained.

It has now been established that for an air compressor which is to have minimum incidence losses, the optimum prewhirl type is solid-body, and the optimum amount of prewhirl is that giving constant relative Mach number, while the optimum inducer tip relative flow angle is 60°. It is of interest to know the incidence angle variation for these optimum conditions. The prewhirl example chosen for Fig. 4.1, which was discussed earlier, is the optimum case just described. It can be seen from Fig. 4.1 that if the optimum tip blade angle $\beta_{bi}$ (about 53°) is used, the incidence angle variation is about $\pm 7°$, with positive incidence at the tip and negative incidence at the hub.

This incidence range is not excessive, but can be reduced further if necessary by designing the impeller inlet face differently from the heretofore assumed plane perpendicular to the axis. Unfortunately, this method of further reducing the losses leads to an overhang of the tip of the inducer (swept-forward leading edge), which may be objectionable from a stress standpoint, though a compromise may be desirable. Another possible compromise solution consists of letting the rotor blades depart slightly from the radial-element configuration.

## Application of Prewhirl to the Freon Compressor

In principle, one could establish the optimum prewhirl for a Freon compressor by examining all possibilities and selecting the particular combination which gives the maximum mass flow. This procedure would differ from that already used for an air compressor only in that incidence angles could be assumed to be zero in all cases, since stresses do not dictate rotor blade configuration. The rotor blades can be designed to match the prewhirl.

Actually, it is far simpler to examine the criteria for the optimum prewhirl for air compressors and show that they are also optimum for Freon, provided the proper value of k is used. To repeat, the criteria for air compressors are:

a) Prewhirl with constant relative Mach number. This implies solid-body prewhirl with

$$\frac{c_{u_i}}{u_i} = \frac{1}{1 + \sqrt{2 + \frac{k-1}{2} M_{w_i}^2}} \tag{4.26}$$

b) $\beta_1 = 60°$

It is assumed that if individual variation of the quantities $\beta_1$, $\frac{M_{wi}}{M_{ci}}$, or type of prewhirl does not lead to an increase of mass flow, then no combination of these quantities will do so either. For "smooth" analytical functions, this is a good assumption. Therefore, since changes of $\beta_1$ and $c_{u_i}/u_i$ have already been treated, only changes in the type of prewhirl need be considered. The change in the values of k is already accounted for in Eq 4.26.

Stanitz (Reference 4.1) has calculated the radial distribution of mass velocity $\rho_1 c_{m_1}$ for various types of prewhirl with fixed inducer radius. The inducer tip velocity triangle which was used in his computations corresponds very nearly to the present optimum for an air compressor with prewhirl. Therefore, the effect of a change of the prewhirl type on the mass flow can be estimated from Stanitz' calculations, considering that the mass flow is the integral of $\rho_1 c_{m_1}$. Figure 4.3 gives Stanitz' curves, and it is immediately evident that the area under the curve which represents the mass flow is greatest for the case of solid-body prewhirl.

Unfortunately, two of the conditions selected by Stanitz for his calculation prevent the conclusion at this point that solid-body prewhirl is the optimum type; namely, that

    a)  the inducer size does not change with prewhirl type.

    b)  the relative Mach number at the inducer tip does not change with the prewhirl type.

However, it can be shown that the inducer is given by Eq 4.22 regardless of the prewhirl type. Also, some analysis of solid-body and free-vortex prewhirl (the two extremes) indicates that it is reasonable to assume that for a fixed maximum relative Mach number near 1.0, the mass flow for each type of prewhirl obtained from Figure 4.2 cannot be exceeded. Thus solid-body prewhirl gives maximum mass flow.

It will be recalled that in the case of the air compressor, consideration of both rotor stresses and aerodynamic incidence losses led to selection of solid-body prewhirl. It is interesting to note that, as shown above, in the case of the Freon compressor, where rotor stresses do not influence aerodynamic design, the same selection of prewhirl type is required. Furthermore, the previous amount of prewhirl and inducer tip flow angle (Eq 4.26) are also optimum here, provided the proper value of $\mathcal{X}$ is used.

## Inlet Hub and Shroud Contours

It was stated earlier that use of the simple radial equilibrium equation (Eq 4.11) is equivalent to making an assumption about shroud and hub contours. Actually, the equation is valid only if the shroud and hub are long cylinders at the inducer - which they generally are not. Thus a much more complicated equation should have been used, the form of which would depend upon the actual hub and shroud contours. The contours however, are not considered as given in this general study, hence the simplest contours were selected.

The effect of the contours was roughly estimated by going to the extreme of entirely removing the radial equilibrium requirement. It was estimated that the greatest increase in mass flow could then be obtained by using a flow distribution in the inducer which approached constant $M_{w1}$ and constant $C_{u1} r_1$ near the tip and constant $M_{w1}$ and constant $C_{u1}/r_1^2$ near the hub. This is not too unlike the optimum distribution which had been given before (constant $M_{w1}$ and constant $C_{u1}/r_1$); hence the increase in mass flow would be small.

Thus it seems reasonable to conclude that the mass flow obtainable with the optimum prewhirl and axial inlet could only be slightly increased by careful design of hub and shroud contours. It should be emphasized, however, that improper design could, of course, have a strong adverse effect.

## 4.3    Comparisons Of The Three Cases

### 4.3.1    General Comparison

In the following comparisons of the results of the analysis of the three cases, it shall be assumed that (1) the inlet gas conditions ($\rho_o$ and $a_o$) are fixed, and that (2) the Euler head is the principal independent variable.

The factor $\lambda$, defined as the ratio of exit whirl velocity to tip speed will also be assumed to be constant for most of the following comparisons.

Figure 4.4 shows the variation of the inducer tip flow angle with head for each of the three cases. (The actual examples chosen for each case are described on the figures.) The angle $\beta_i$ does not vary appreciably in the range shown, and is about $60°$ for each case. This corresponds to the findings of Pfleiderer (Ref 4.2).

Figure 4.5 gives a comparison of the ratio of the relative velocities. For Case II, this ratio is an independent variable, and is therefore constant in this comparison. For Cases I and III, the ratio $w_t/w_i$ increases with head. In general, the higher the value of this ratio the better. In the comparison shown, the prewhirl case has the most favorable values.

Figure 4.6 gives the comparison of maximum inlet relative Mach numbers. This parameter is of great importance, since higher values generally imply greater losses. In Cases I and III, $(M_{wi})_{max}$ is an independent variable and therefore a constant in this comparison. Case II gives high values (hence the name "supersonic inlet") which increase with head. The region where $(M_{wi})_{max}$ occurs is shown in the auxiliary table in Figure 4.6. For no prewhirl (Cases I and II), it occurs at the inducer tip whereas with optimum prewhirl, the same relative Mach number is found at all radii.

Figure 4.7 gives the maximum inlet absolute Mach number $(M_{c1})_{max}$. It is of less importance than $(M_{w1})_{max}$, but it is of interest to note that the prewhirl case has the highest value of $(M_{c1})_{max}$, that it is subsonic, and that it occurs in the region of the inducer hub.

Figure 4.8 compares tip speeds for the three cases. The fact that higher tip speed is required with prewhirl is clearly shown. As much as 30 per cent higher tip speed is required in the range shown, though the percentage decreases with head. In all cases, tip speed increases with head.

Figure 4.9 gives optimum inducer sizes. The size of the inducer has been shown to be an important factor in determining the mass flow, and this can be seen by comparing Figure 4.9 and 4.10, the latter giving mass flow.

### 4.3.2. Comparison for Equal Tip Diameter

Figure 4.10, which gives dimensionless mass flow, shows that for constant tip diameter the mass flow comparison is quite similar in general appearance to the inducer size comparison of Figure 4.9. The compressor with prewhirl has the largest mass flow (and inducer diameter) at low head, while at very high head, the supersonic-inlet machine has the highest value. The transition occurs at $\dfrac{gH_{TH}}{a_o^2}$ equal to about 2.2 for the examples shown.

The data shown in Figures 4.9 and 4.10 are sufficient for an indication of the shape of the impeller, for the impeller exit width is proportional to the mass flow. Figure 4.11 gives sketches of impeller shapes for various cases in which the rotor diameter and $\lambda$ are held constant. The disadvantages of the Case I compressor at high head are clearly evident from its shape, which is of the "low-specific-speed" type. It should be emphasized that these sketches are based on optimum inducer diameters.

### 4.3.3 Comparison for Equal Mass Flow

A typical design problem is the selection of the type of compressor to be used for a given value of flow as well as of head. Figure 4.12 and 4.13 give tip diameter and rotational speed comparisons for this case. Case II has the lowest impeller size at high head, as expected from the foregoing discussion. Case III has the highest rpm over most of the range of head shown except for very high head.

Approximate impeller shapes for the important case of equal mass flow (and equal $\lambda$ ) are shown in Figure 4.14. In the case of prewhirl, the approximate shape of the impeller exit required to keep constant head on all stream surfaces is shown. For low head the largest machine is the one with supersonic inlet, and the smallest is the one with prewhirl. In this range, the prewhirl compressor tends to approach an axial compressor in appearance.

For very high heads, Figure 4.14 again shows the undesirable shape of the Case I compressor impeller, which is now the largest. The smallest machine is the supersonic-inlet compressor. Both Case II and Case III have desirable impeller shapes in this range. From Figures 4.8 and 4.13 one can see that the prewhirl machine has the highest tip speed, but a lower rotational speed than the supersonic-inlet compressor.

## 4.4    Use of Freon

Most of the computations described above were made for air compressors. It is therefore important to consider the effect of substituting Freon as the working fluid.    With Freon the value of k is in the range of 1.1 to 1.2, compared to the value of 1.4 for air.

In general, there is little change in dimensionless mass flow and dimensionless tip speed when Freon is used instead of air. The greatest change is in rotor geometry, particularly inducer size, which is greater for Freon.

## 4.5    Discussion of Certain Changes

The effect of a change in $\lambda$ can be found from the curves in most cases, or from the equations given earlier. The effect of changes in the values of maximum relative Mach number, outlet flow angle, relative velocity ratio, and inducer hub ratio, can also be found from the equations.

It may be necessary to compromise some of the advantages of the optimum prewhirl design. One such compromise was mentioned earlier in connection with incidence angles in an air compressor. As another example, the shape of the impeller exit (see Figure 4.14) may appear undesirable. Using a different type of prewhirl (say constant velocity or even constant mass velocity) will result in a more nearly constant exit diameter, but the mass flow will be decreased and the incidence losses increased.

## 4.6    Summary

A rather extensive investigation of various types of prewhirl, including the effects of radial equilibrium, has been conducted. The optimum prewhirl has been found to be solid-body, and to have a constant relative Mach number and an inducer tip relative flow angle of $60^\circ$.

The advantages of the two alternatives to the compressor with subsonic inlet relative velocities (namely, zero prewhirl and supersonic inlet and prewhirl and subsonic inlet) can be summarized thus:

Zero prewhirl and supersonic inlet provides

   a) greater simplicity

   b) lower tip speed

   c) smaller size at very high head

d)  lower inlet absolute Mach number

e)  lower incidence angles for air compressors

Its disadvantage is the necessity of dealing with supersonic flow within the inducer.
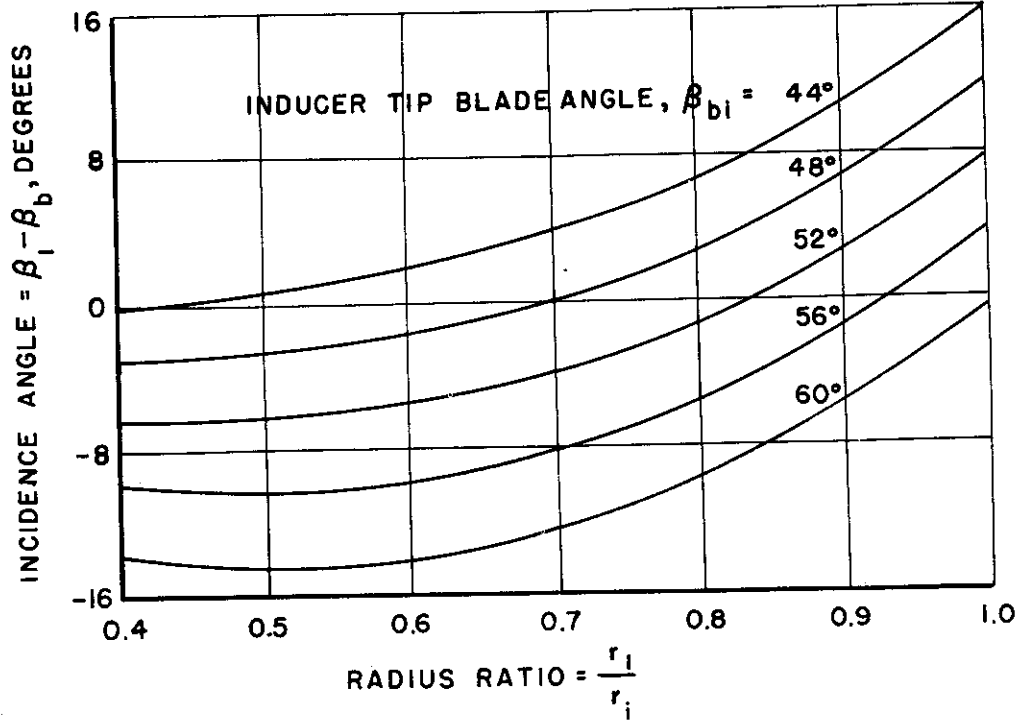
Prewhirl and subsonic inlet provides

a)  lower inlet relative Mach number

b)  more favorable relative velocity ratio

c)  lower rotational speed at very high head

The choice between the alternatives obviously depends on the relative weight of these advantages.  It appears, however, that the use of prewhirl and subsonic inlet is, in general, not sufficiently advantageous, unless the problems associated with the supersonic inlet without prewhirl prove to be insurmountable.

4.1    Stanitz, J. D.  Design Considerations for Mixed-Flow Centrifugal
Compressors with High Weight-Flow Rates per Unit Frontal Area.
NACA RM E53A15.  1953.

4.2    Pfleiderer, C.  Die Uberschallgrenze Bei Kreiselverdichtern.
Zeitschrift des Verienes Deutscher Ingenieure.  Vol.  92.  p129.  1950.

4.3    Howarth, L.  Modern Developments in Fluid Dynamics.  High Speed Flow.
Vols. I and II.  Oxford.  1953.

4.4    Eck, Bruno.  Ventilatoren.  Second Edition.  Berlin:  Springer-Verlag.  1952

4.5    Hawthorne, W. R.  Factors Affecting the Design of Jet Turbines.
SAE Journal.  Vol. 54, No. 7.  p347.  1946.
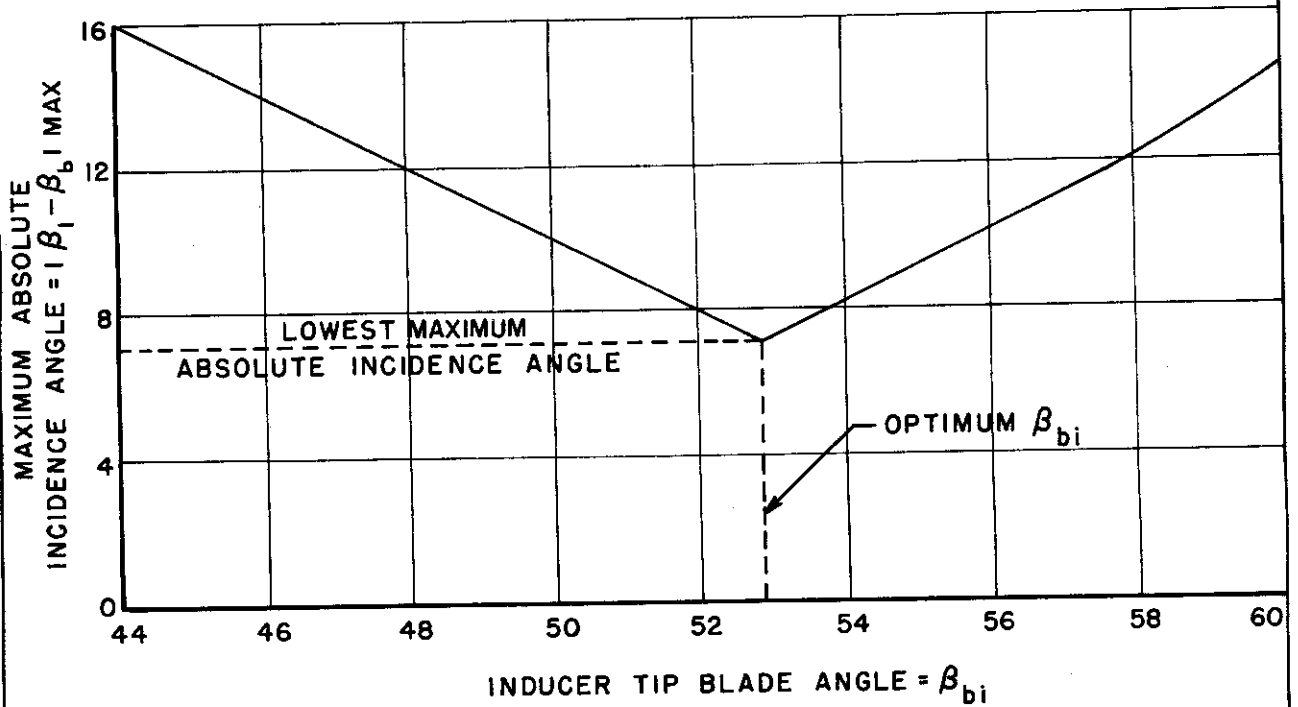
FIG. 4.1        INCIDENCE ANGLES FOR A TYPICAL CASE

INDUCER TIP VELOCITY TRIANGLE
(EXAMPLE SHOWN IS POINT B)

POINT A (MAX. MASS FLOW)

POINT B
(ARBITRARY OPTIMUM)

AMOUNT OF PREWHIRL:

$\dfrac{C_{ui}}{U_i} = 0.5$

$\dfrac{C_{ui}}{U_i} = 0.403$ (CONSTANT $M_{wi}$)

$\dfrac{C_{ui}}{U_i} = 0.3$

$\dfrac{C_{ui}}{U_i} = 0$ $\left(\begin{array}{c}\text{ZERO}\\\text{PREWHIRL}\end{array}\right)$

$\beta_i = 60°$

NOTES:
1. SOLID-BODY PREWHIRL
2. $(M_{wi})$ MAX = 1.0
3. $r_h / r_i = 0.4$
4. $gH_{th}/a_0{}^2 = 2.0$

DIMENSIONLESS INDUCER SIZE $= \dfrac{1}{\sqrt{\lambda}}\ \dfrac{r_i}{r_h}$

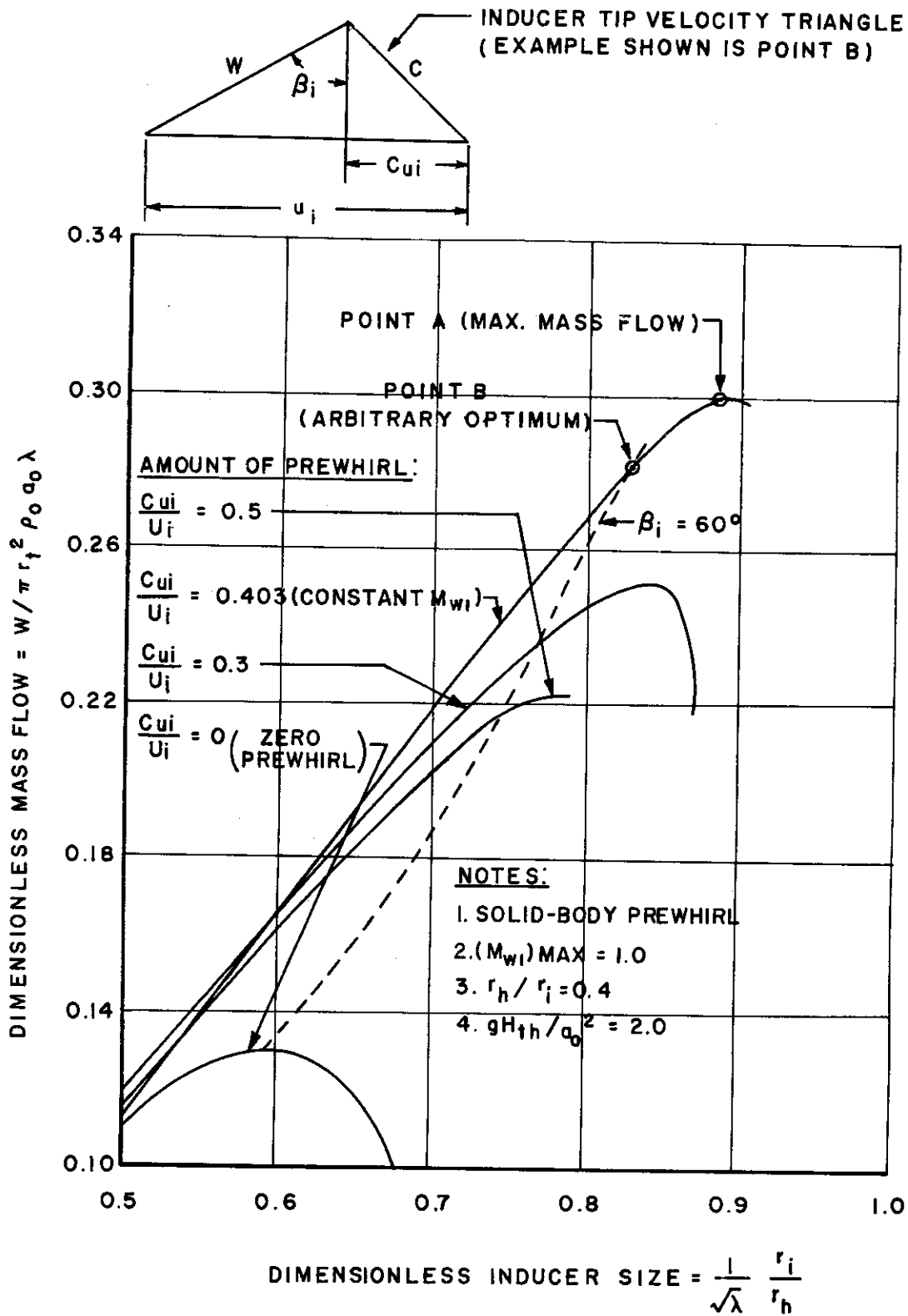DIMENSIONLESS MASS FLOW $= W/\pi\, r_t{}^2\, \rho_0\, a_0\, \lambda$

FIG. 4.2      INFLUENCE OF AMOUNT OF
PREWHIRL FOR A TYPICAL CASE

BASED ON FIG.3(b)OF NACA RM E53A15,
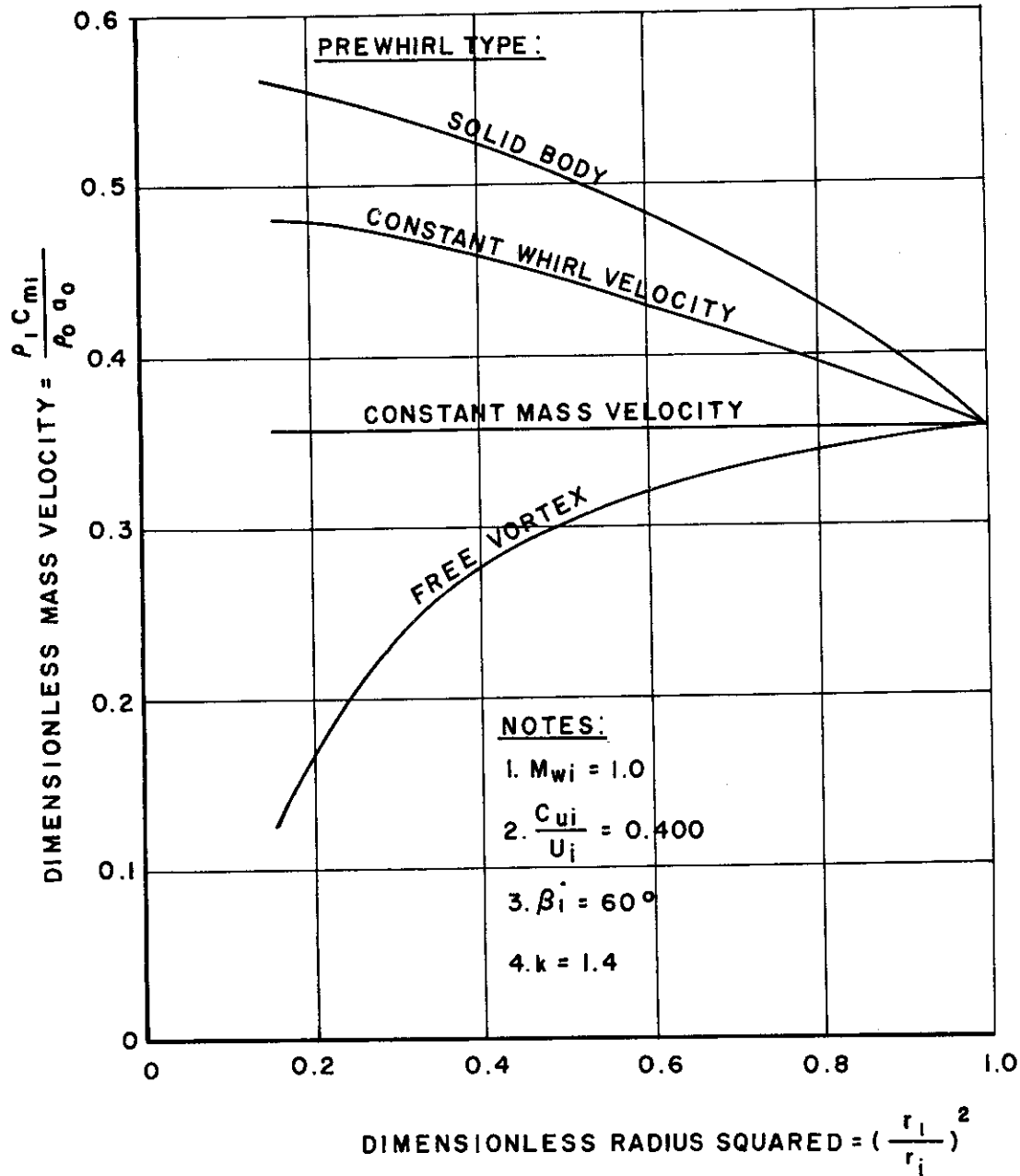EXCEPT FOR CORRECTION OF THE
SOLID-BODY CURVE.
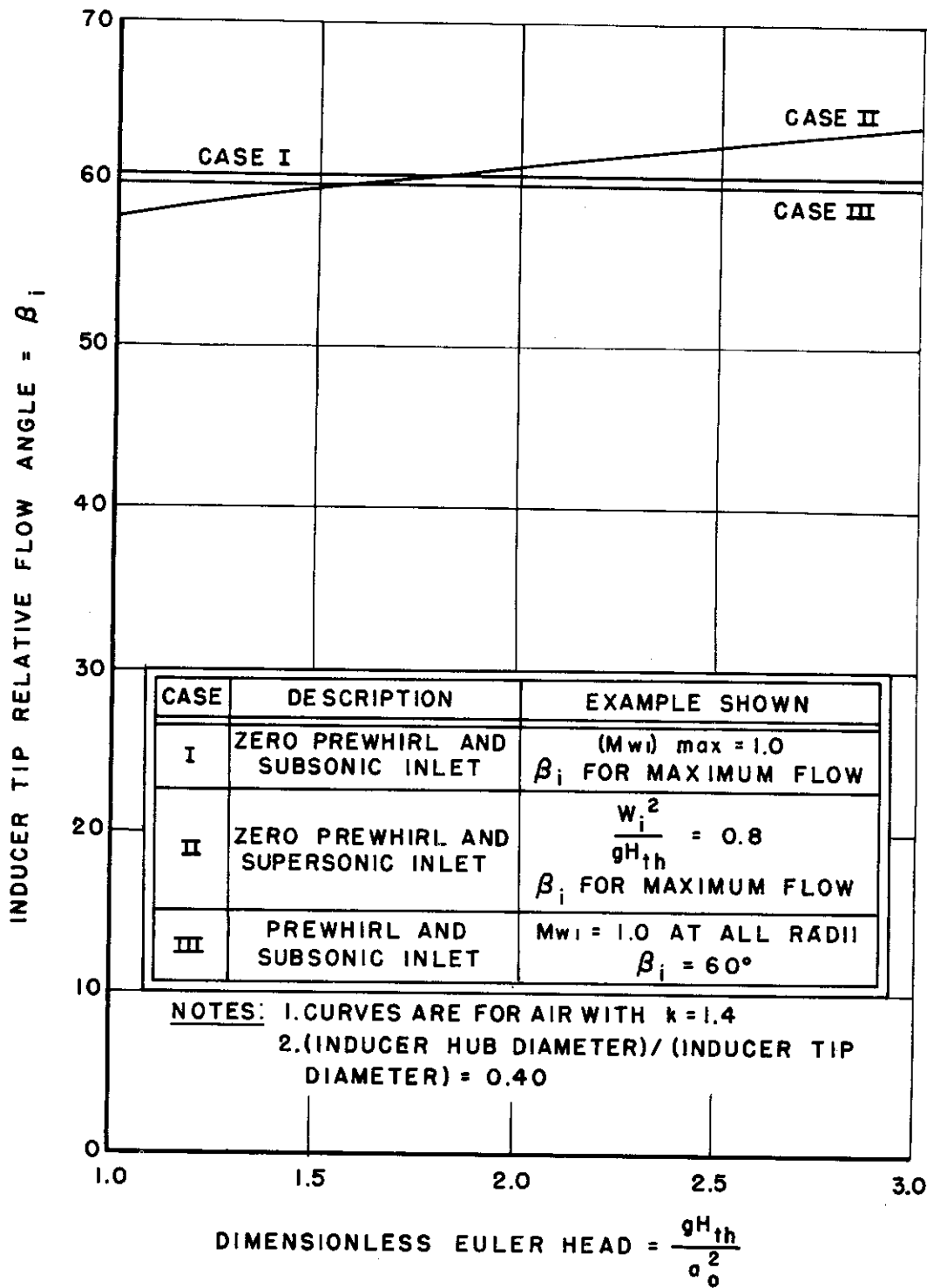


**FIG. 4.3    EFFECT OF PREWHIRL TYPE ON MASS VELOCITY**

INDUCER TIP RELATIVE FLOW ANGLE = $\beta_i$

70

CASE II

CASE I

60

CASE III

50

40

30

20

10

0

| CASE | DESCRIPTION | EXAMPLE SHOWN |
|------|-------------|---------------|
| I | ZERO PREWHIRL AND SUBSONIC INLET | $(M_{Wi})$ max = 1.0<br>$\beta_i$ FOR MAXIMUM FLOW |
| II | ZERO PREWHIRL AND SUPERSONIC INLET | $\dfrac{W_i^2}{gH_{th}}$ = 0.8<br>$\beta_i$ FOR MAXIMUM FLOW |
| III | PREWHIRL AND SUBSONIC INLET | $M_{Wi}$ = 1.0 AT ALL RADII<br>$\beta_i$ = 60° |

NOTES: 1. CURVES ARE FOR AIR WITH $k$ = 1.4

2. (INDUCER HUB DIAMETER)/(INDUCER TIP DIAMETER) = 0.40

1.0          1.5          2.0          2.5          3.0

DIMENSIONLESS EULER HEAD = $\dfrac{gH_{th}}{a_o^2}$

FIG. 4.4          COMPARISON OF TIP RELATIVE FLOW ANGLES

| CASE | DESCRIPTION | EXAMPLE SHOWN |
|------|-------------|---------------|
| I | ZERO PREWHIRL AND SUBSONIC INLET | $(M_{w_i})\,max = 1.0$ <br> $\beta_i$ FOR MAXIMUM FLOW |
| II | ZERO PREWHIRL AND SUPERSONIC INLET | $\dfrac{W_i^2}{gH_{th}} = 0.8$ <br> $\beta_i$ FOR MAXIMUM FLOW |
| III | PREWHIRL AND SUBSONIC INLET | $M_{w_i} = 1.0$ AT ALL RADII <br> $\beta_i = 60°$ |
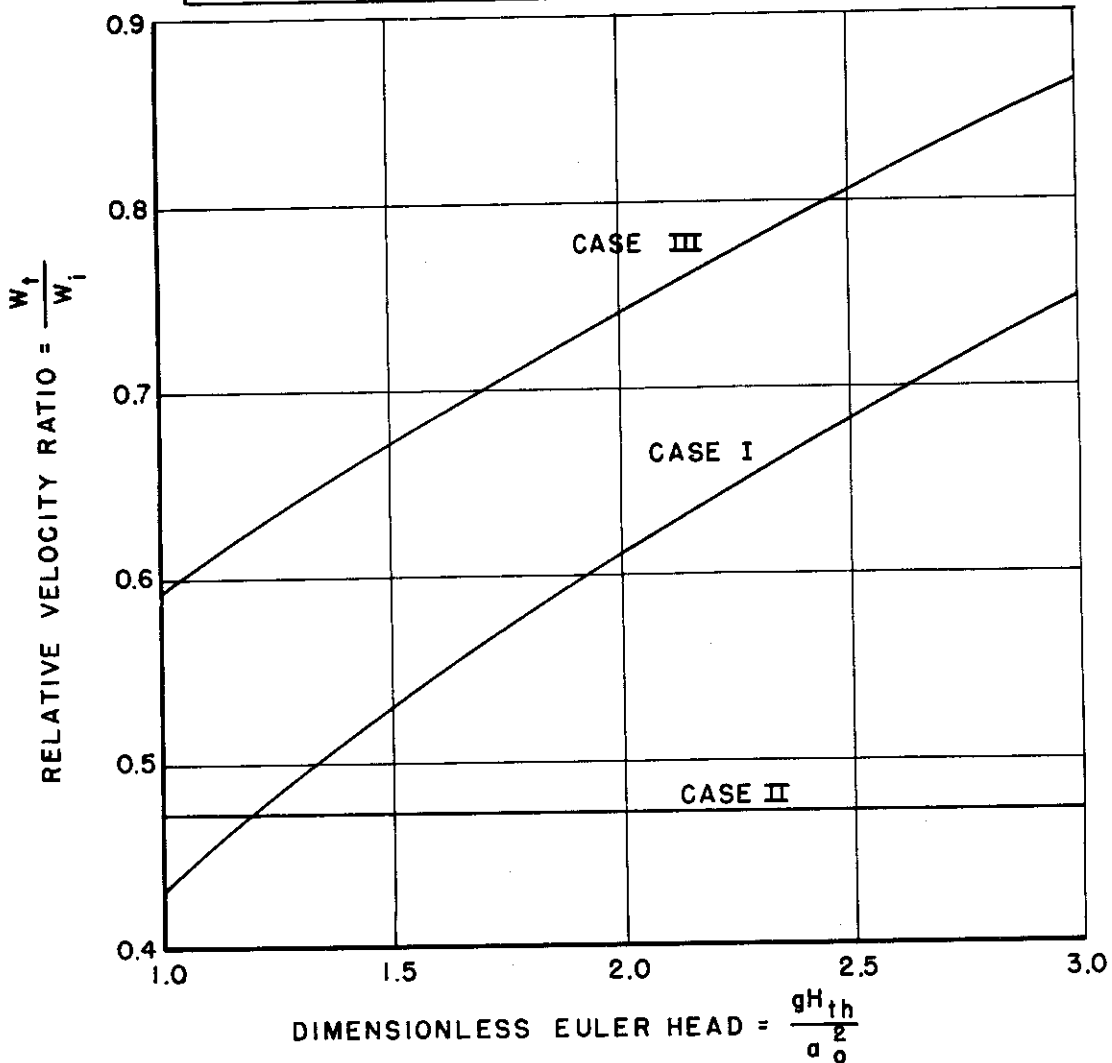


NOTES: 1. CURVES ARE FOR AIR WITH $k = 1.4$
2. (INDUCER HUB DIAMETER)/(INDUCER TIP DIAMETER) $= 0.40$
3. IMPELLER EXIT FLOW ANGLE $\alpha_t$ ASSUMED TO BE $68.2°$
4. FACTOR $\lambda$ ASSUMED TO BE $0.8$

FIG. 4.5       COMPARISON OF RELATIVE VELOCITY RATIOS

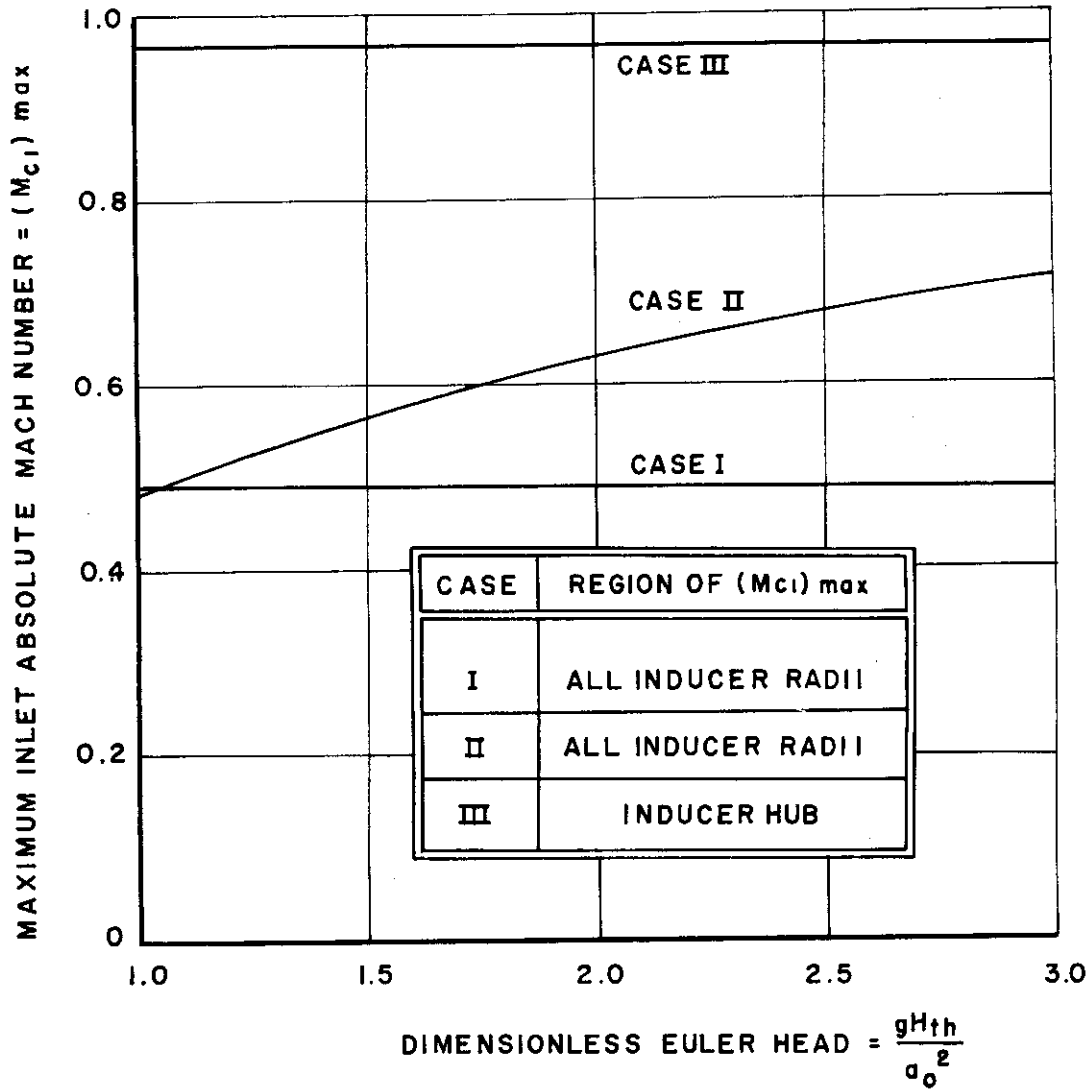| CASE | DESCRIPTION | EXAMPLE SHOWN |
|------|-------------|---------------|
| I | ZERO PREWHIRL AND SUBSONIC INLET | $(M_{wi})\,max = 1.0$<br>$\beta_i$ FOR MAXIMUM FLOW |
| II | ZERO PREWHIRL AND SUPERSONIC INLET | $\dfrac{W_i^2}{gH_{th}} = 0.8$<br>$\beta_i$ FOR MAXIMUM FLOW |
| III | PREWHIRL AND SUBSONIC INLET | $M_{wi} = 1.0$ AT ALL RADII<br>$\beta_i = 60°$ |



| CASE | REGION OF $(M_{wi})\,max$ |
|------|---------------------------|
| I | INDUCER TIP |
| II | INDUCER TIP |
| III | ALL INDUCER RADII |

CASE II

CASE I AND CASE III

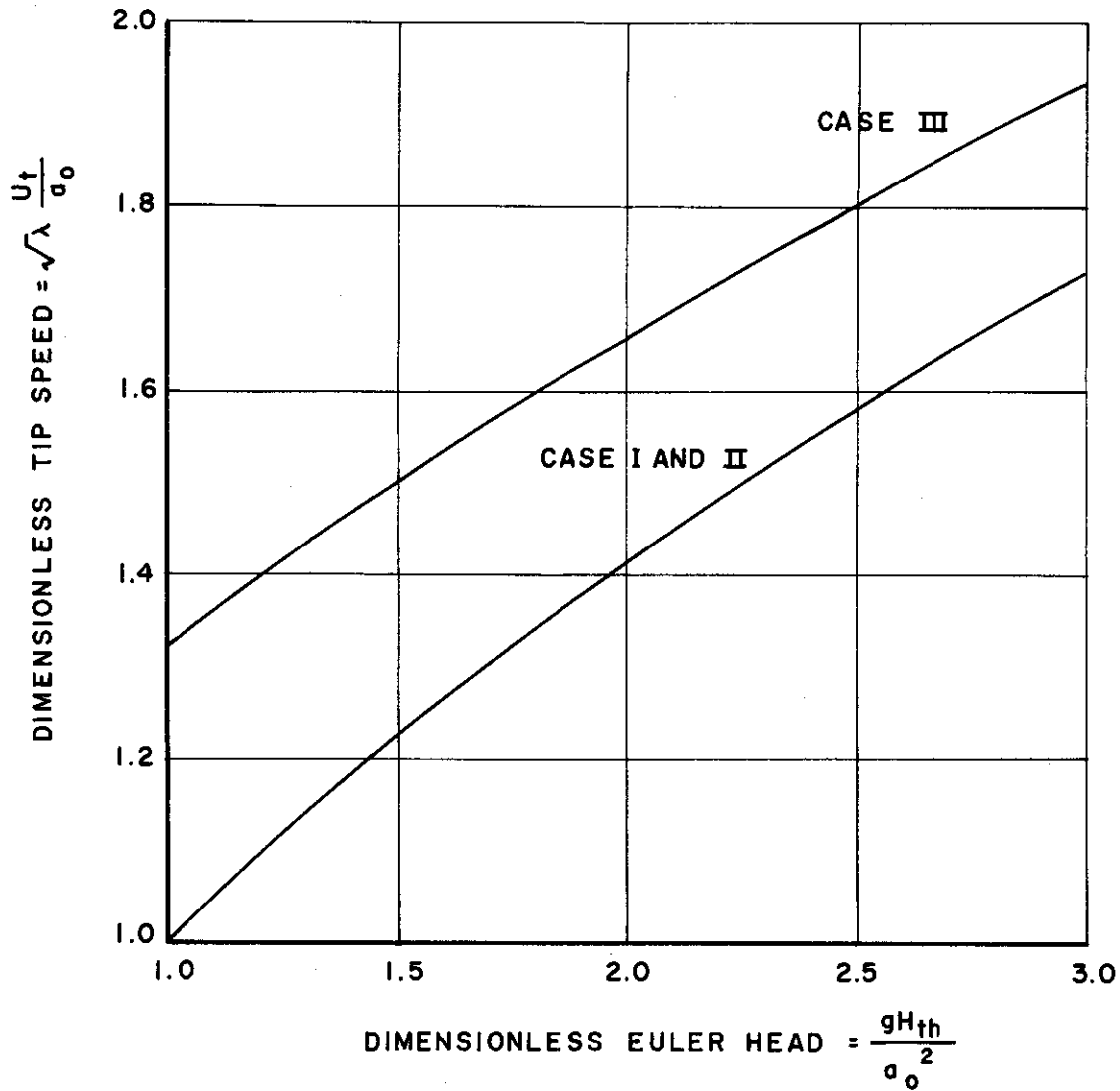DIMENSIONLESS EULER HEAD $= \dfrac{gH_{th}}{a_0^2}$
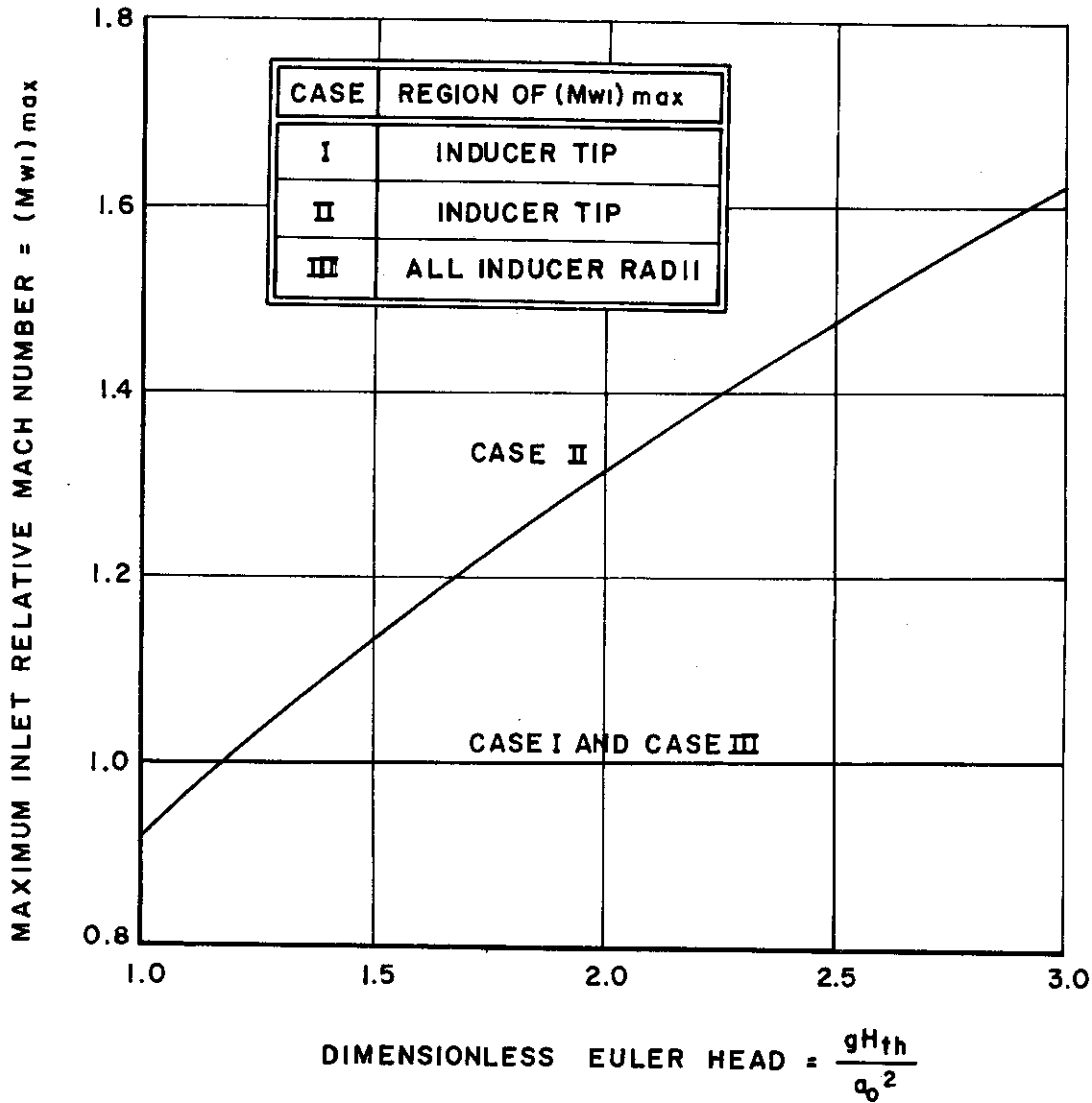
NOTES: 1. CURVES ARE FOR AIR WITH $k = 1.4$

2. (INDUCER HUB DIAMETER)/(INDUCER TIP DIAMETER) $= 0.40$

FIG. 4.6     COMPARISON OF MAXIMUM INLET RELATIVE MACH NUMBERS

| CASE | DESCRIPTION | EXAMPLE SHOWN |
|------|-------------|---------------|
| I | ZERO PREWHIRL AND SUBSONIC INLET | $(M_{wi})$ max $= 1.0$ <br> $\beta_i$ FOR MAXIMUM FLOW |
| II | ZERO PREWHIRL AND SUPERSONIC INLET | $\dfrac{W_i^2}{gH_{th}} = 0.8$ <br> $\beta_i$ FOR MAXIMUM FLOW |
| III | PREWHIRL AND SUBSONIC INLET | $M_{wi} = 1.0$ AT <u>ALL</u> RADII <br> $\beta_i = 60°$ |

CASE III

CASE II

CASE I

| CASE | REGION OF $(M_{ci})$ max |
|------|--------------------------|
| I | ALL INDUCER RADII |
| II | ALL INDUCER RADII |
| III | INDUCER HUB |

MAXIMUM INLET ABSOLUTE MACH NUMBER $= (M_{ci})$ max

DIMENSIONLESS EULER HEAD $= \dfrac{gH_{th}}{a_0^2}$

NOTES: 1. CURVES ARE FOR AIR WITH $k = 1.4$

2. (INDUCER HUB DIAMETER)/(INDUCER TIP DIAMETER) $= 0.40$

FIG. 4.7     COMPARISON OF MAXIMUM INLET ABSOLUTE MACH NUMBERS

| CASE | DESCRIPTION | EXAMPLE SHOWN |
|------|-------------|---------------|
| I | ZERO PREWHIRL AND SUBSONIC INLET | $(M_{w1})_{max} = 1.0$ <br> $\beta_i$ FOR MAXIMUM FLOW |
| II | ZERO PREWHIRL AND SUPERSONIC INLET | $\dfrac{W_i^2}{gH_{th}} = 0.8$ <br> $\beta_i$ FOR MAXIMUM FLOW |
| III | PREWHIRL AND SUBSONIC INLET | $M_{w1} = 1.0$ AT $\underline{ALL}$ RADII <br> $\beta_i = 60°$ |



NOTES: 1. CURVES ARE FOR AIR WITH $k = 1.4$

2. (INDUCER HUB DIAMETER)/(INDUCER TIP DIAMETER) $= 0.40$

FIG. 4.8      COMPARISON OF TIP SPEEDS

**DIMENSIONLESS INDUCER SIZE** $= \dfrac{1}{\sqrt{\lambda}} \dfrac{r_i}{r_t}$

CASE III

CASE II

CASE I

**DIMENSIONLESS EULER HEAD** $= \dfrac{gH_{t\,h}}{a_0^2}$

| CASE | DESCRIPTION | EXAMPLE SHOWN |
|---|---|---|
| I | ZERO PREWHIRL AND SUBSONIC INLET | $(M_{w_i})\,max = 1.0$ $\beta_i$ FOR MAXIMUM FLOW |
| II | ZERO PREWHIRL AND SUPERSONIC INLET | $\dfrac{w_i^2}{gH_{th}} = 0.8$ $\beta_i$ FOR MAXIMUM FLOW |
| III | PREWHIRL AND SUBSONIC INLET | $M_{w_i} = 1.0$ AT <u>ALL</u> RADII $\beta_i = 60°$ |

NOTES: 1. CURVES ARE FOR AIR WITH $k = 1.4$
2. (INDUCER HUB DIAMETER)/(INDUCER TIP DIAMETER) = 0.40

**FIG.** 4.9     **COMPARISON OF INDUCER SIZES**

| CASE | DESCRIPTION | EXAMPLE SHOWN |
|------|-------------|---------------|
| I | ZERO PREWHIRL AND SUBSONIC INLET | $(M_{wi})_{max} = 1.0$<br>$\beta_i$ FOR MAXIMUM FLOW |
| II | ZERO PREWHIRL AND SUPERSONIC INLET | $\dfrac{W_i^2}{gH_{th}} = 0.8$<br>$\beta_i$ FOR MAXIMUM FLOW |
| III | PREWHIRL AND SUBSONIC INLET | $M_{wi} = 1.0$ AT ALL RADII<br>$\beta_i = 60°$ |

NOTES: 1. CURVES ARE FOR AIR WITH k = 1.4
2. (INDUCER HUB DIAMETER)/(INDUCER TIP DIAMETER) = 0.40

CASE III

CASE II

CASE I

DIMENSIONLESS MASS FLOW $= W/\pi r_t^2 \rho_0 a_0 \lambda$
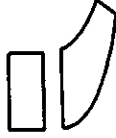
DIMENSIONLESS EULER HEAD $= \dfrac{gH_{th}}{a_0^2}$
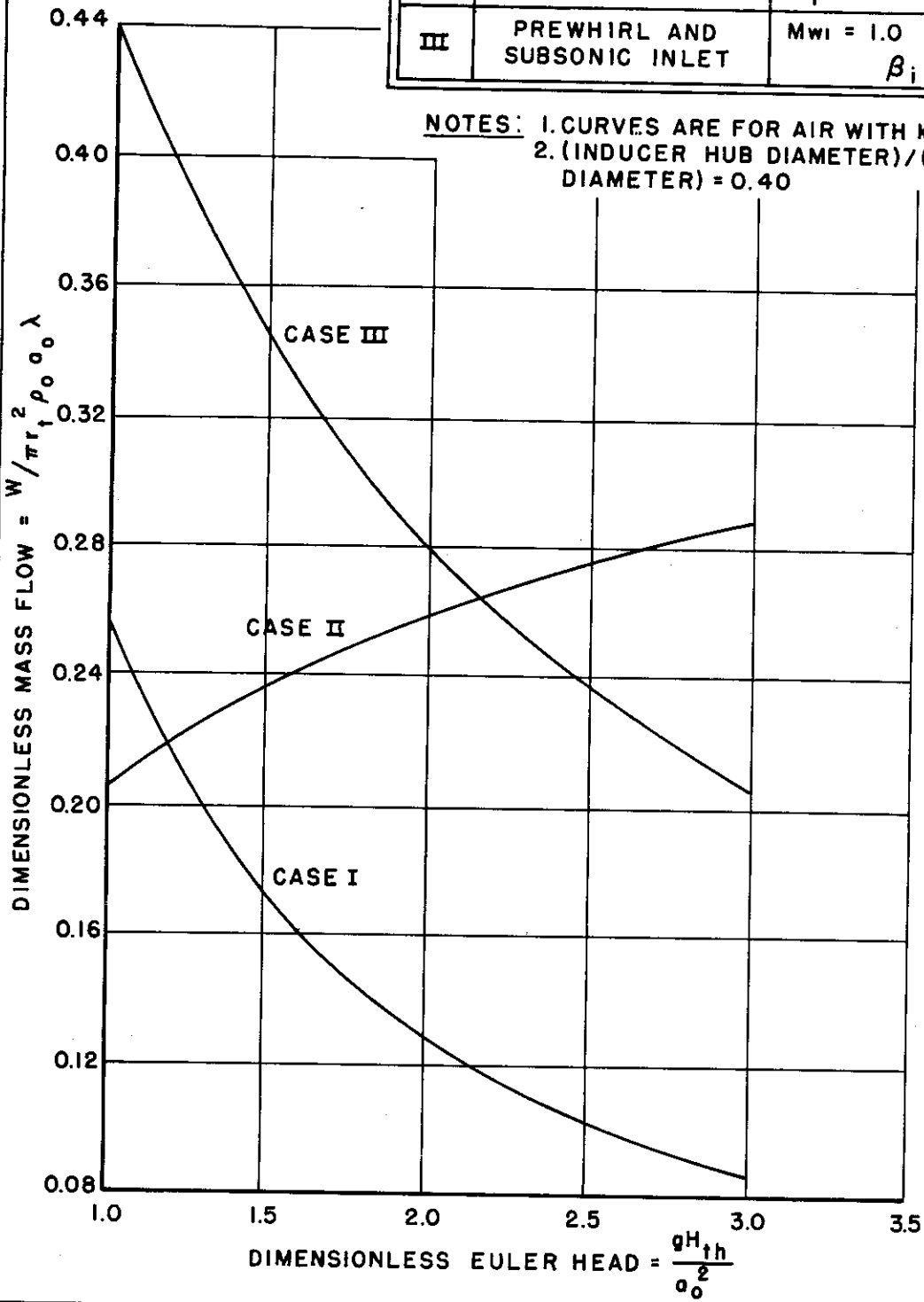
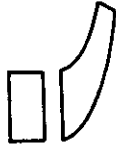FIG. 4.10     COMPARISON OF MASS FLOWS

| DIMENSIONLESS EULER HEAD | CASE I ZERO PREWHIRL AND SUBSONIC INLET | CASE II ZERO PREWHIRL AND SUPERSONIC INLET | CASE III PREWHIRL AND SUBSONIC INLET |
|---|---|---|---|
| $\dfrac{gH_{TH}}{a_o^2} = 1$ | | | |
| $\dfrac{gH_{TH}}{a_o^2} = 2$ | | | |
| $\dfrac{gH_{TH}}{a_o^2} = 3$ | | | |

NOTE: BASED ON FIGURES    AND    WITH  $\lambda = 0.8$

**APPROXIMATE IMPELLER SHAPES FOR TIP DIAMETER AND EQUAL $\lambda$.**

FIG. 4.11

NOTE:

BASED ON FIGURE ____ , ASSUMING EQUAL MASS
FLOW AND EQUAL $\lambda$.



RATIO OF TIP DIAMETERS FOR
EQUAL MASS FLOW AND EQUAL $\lambda$

FIG. 4.12

FIG. 4.13     RPM RATIO FOR EQUAL MASS FLOW AND EQUAL $\lambda$

The chart plots on the vertical axis $\dfrac{N \text{ WITH LIMITED MACH PREWHIRL (CASE III)}}{N \text{ WITH UNLIMITED MACH, NO PREWHIRL (CASE II)}}$ from 0.8 to 2.0, versus the horizontal axis DIMENSIONLESS EULER HEAD $= \dfrac{gH_{th}}{a_0^2}$ from 1.0 to 3.0.

NOTE: BASED ON FIGS.     AND
ASSUMING EQUAL MASS FLOW
AND EQUAL $\lambda$

| DIMENSIONLESS EULER HEAD | CASE I ZERO PREWHIRL AND SUBSONIC INLET | CASE II ZERO PREWHIRL AND SUPERSONIC INLET | CASE III PREWHIRL AND SUBSONIC INLET |
|---|---|---|---|
| $\dfrac{gH_{TH}}{a_o^2} = 1.0$ | | | |
| $\dfrac{gH_{TH}}{a_o^2} = 2.0$ | | | |
| $\dfrac{gH_{TH}}{a_o^2} = 3.0$ | | | |

NOTE:
BASED ON FIGURES       AND       ASSUMING

$$\frac{W}{\pi r_t^2 \rho_o a_o \lambda} = 0.26 \quad \text{AND} \quad \lambda = 0.8$$

FIG. 4.14     APPROXIMATE IMPELLER SHAPES FOR EQUAL MASS FLOW AND EQUAL $\lambda$.

## 5.1  Summary of Diffuser Studies

Studies of diffusers have been directed to the problem of viscous flow in the vaneless type as well as in the guide vane type.

A design procedure was developed for vaneless diffusers. It was subsequently applied to investigate conditions of optimum performance. The problem of viscous flow also was attacked and is shown to be amenable to a solution, if the flow is divided into a core and a boundary layer. The viscous effect appears clearly in the curvature of the streamlines in the region of the diffuser wall.

In attacking the problems of guide vane diffusers relatively thick boundary layers had to be considered, differing from those commonly found in experimental diffuser setups.  The studies were centered around the development of a semiempirical procedure which allows the calculation of the growth of the boundary layer in conical diffusers.  For that purpose, the flow in the conical diffuser is divided into a region with a potential core and a quasi-steady region in which separated flow is present.  With this method, the maximum deceleration that can be achieved without separation for any given initial condition can be determined.

Incorporating these data into the calculation of the performance of separated diffuser flow  allows an estimate of the optimum performance of conical diffusers as a function of the inlet conditions.

Results of the boundary layer studies are then applied to establish a system of loss coefficients which can be used for the performance prediction of centrifugal machines.  They also present some indications as to the amount of deceleration to be prescribed in the design of guide vanes and particularly as to the magnitude of the flow factor, which is one of the main parameters in the design of guide vanes.

A simplified method based on viscous consideration is presented for the design of subsonic guide vanes.

## 5.2 Vaneless Diffuser

### 5.2.1 Introduction

Vaneless diffusers have been widely used in centrifugal and mixed-flow compressors to provide a wide range of operation. With the advent of high pressure ratio compressors, they are found to present the important advantage of a shock-free deceleration from supersonic to subsonic flow.

Investigations on the performance of vaneless diffusers have been carried out ever since the building of centrifugal pumps, starting from incompressible flow consideration and progressing into compressibility and viscous effects. Most investigations have been confined to parallel wall diffusers(Refs 5.1, 5.3). When a variable shape is considered, it is generally introduced in conjunction with a low efficiency impeller to improve the velocity profile at the impeller exit.

With the wealth of experimental results and analytical work presently available on vaneless diffusers, it appeared possible to establish a shape that would give an optimum performance for a given entrance condition, taking fully into account the viscous problems.

The presented study is aiming at these objectives.

### 5.2.2 Design Procedure for Vaneless Diffusers

The diffusion that occurs in a vaneless diffuser can be determined when the velocity at every radius of the diffuser is known. In case of compressibility, the knowledge of the Mach number lends itself to the same purpose. Thus it is proposed to prescribe the Mach number along the radius.

### 5.2.2.1 Theory

Consider a vaneless diffuser which has the geometry shown on Figure 5.1.

The one-dimensional approach assumes that the flow has a constant velocity $c$ across the width $b$ and that it follows a path in the plane $z = o$ as shown on Figure 5.1. The flow in the vaneless space is then governed by the following relations:

Continuity $\qquad RB\rho c_r = \rho_i\, c_{r_i}$ (5.1)

Momentum $\qquad \dfrac{d(Rc_u)}{Rc_u} = -\dfrac{r_i}{b_i}\,\dfrac{fdR}{B\cos\alpha}$ (5.2)

Experimental data $\qquad f = \dfrac{\tau_o}{\dfrac{1}{2}\rho c^2}$ (5.3)

Equation of state $\qquad P = R\rho T$ (5.4)

These fundamental relations have been established in Refs 5.1, 5.2 and 5.3. The contribution of the present study consists in putting these relations into a working form for design analysis.

Expression for Pressure Loss

On the basis of one-dimensional compressible flow, the loss in total pressure along an incremental path, dl, is given by Ref 5.4 where the hydraulic diameter is taken equal to 2b.

$$- \frac{dP_T}{P_T} = \frac{kM^2}{2} \frac{2f}{b} \, dl \tag{5.5}$$

The geometry of the path gives

$$dl = \frac{dr}{\cos} \tag{5.6}$$

Combining (5.5) and (5.6) and introducing the dimensionless parameters R and B yields

$$\frac{dP_T}{P_T} = \frac{(-)kfr_i}{b_i} \frac{M^2 \, dR}{B \cos \propto} \tag{5.7}$$

$$B = \frac{b}{b_i} \quad R = \frac{r}{r_i}$$

From the geometry of the path we have

$$\theta_r = c \, \cos \propto \tag{5.8}$$

The continuity equation is then written in the form

$$RB \frac{\cos \propto}{\cos \propto_i} \frac{\rho c}{\rho_1 c_1} = 1 \tag{5.9}$$

With the introduction of compressible flow relations as tabulated in gas tables Ref 5.5, Equation (5.9) can be calculated. As an identity we have

$$\frac{\rho c}{\rho_1 c_1} = \frac{\rho_T a_T}{\rho_{T_i} a_{T_i}} \frac{M \left( \frac{a}{a_T} \right) \left( \frac{\rho}{\rho_T} \right)}{M_i \left( \frac{a}{a} \right) \frac{a}{a_{T_i}}} \tag{5.10}$$

In the present case where there is no heat loss, the total temperature in the diffuser is constant.

$$T_T = T_{T_i} = \text{constant}$$

As a consequence, we also have the relations

$$\frac{a_T}{a_{T_i}} = 1 \tag{5.11}$$

$$\frac{\rho_T}{\rho_{T_i}} = \frac{P_T}{P_{T_i}} \tag{5.12}$$

Combination of the Equations **(5.9)**, **(5.10)**, **(5.11)** and **(5.12)** give for B cos$\alpha$ the expression:

$$\frac{1}{B \cos\alpha} = \frac{\dfrac{P_T}{P_{Ti}}}{\cos\alpha_i} \quad R \quad \frac{M\left(\dfrac{a}{a_T}\right)\left(\dfrac{\rho}{\rho_T}\right)}{M_i\left(\dfrac{a}{a_T}\right)_i\left(\dfrac{\rho}{\rho_T}\right)_i} \tag{5.13}$$

Substitution of **(5.13)** in **(5.7)** gives the dimensionless expression for the loss in total pressure:

$$-\frac{d\left(\dfrac{P_T}{P_{T_i}}\right)}{\left(\dfrac{P_T}{P_{T_i}}\right)^2} = \frac{kf}{\cos\alpha_i} \quad \frac{r_i}{b_i} \quad \frac{M^3\left(\dfrac{a}{a_T}\right)\left(\dfrac{\rho}{\rho_T}\right)}{M_i\left(\dfrac{a}{a_T}\right)_i\left(\dfrac{\rho}{\rho_T}\right)_i} \; RdR \tag{5.14}$$

We now define the integral $I_1(R)$ as:

$$I_1(R) = \int_1^R M^3\left(\frac{a}{a_T}\right)\left(\frac{\rho}{\rho_T}\right) RdR \tag{5.15}$$

and integrate Equation **(5.14)** to obtain:

$$\frac{1}{\left(\dfrac{P_T}{P_{T_i}}\right)} = 1 + \frac{kf}{\cos\alpha_i} \quad \frac{r_i}{b_i} \quad \frac{I_1(R)}{M_i\left(\dfrac{a}{a_T}\right)_i\left(\dfrac{\rho}{\rho_T}\right)_i} \tag{5.16}$$

Expression for the Component Mach Numbers and Flow Angle

We define the integral $I_2(R)$ as

$$I_2(R) = \int_1^R \frac{1}{B \cos \alpha} \, dR \qquad (5.17)$$

and integrate the momentum equation, (5.2), to obtain:

$$\frac{c_u}{c_{u_i}} = \frac{1}{R} \exp\left[-f \frac{r_i}{b_i} I_2(R)\right] \qquad (5.18)$$

With the definition of the tangential and radial Mach numbers as:

$$M_u = \frac{c_u}{a} \, , \quad M_r = \frac{c_r}{a}$$

We obtain from (5.18)

$$M_u = M_{u_i} \left(\frac{a}{a_T}\right)_i \frac{1}{R\left(\frac{a}{a_T}\right)} \exp\left[-f \frac{r_i}{b_i} I_2(R)\right] \qquad (5.19)$$

The flow angle and the radial component of the Mach number are given respectively by

$$\sin \alpha = \frac{M_u}{M} \qquad (5.20)$$

$$M_r = M \cos \alpha \qquad (5.21)$$

The useful relations for the calculation procedure are now collected in the following order:

Equations (5.15), (5.16), (5.13), (5.17), (5.19), (5.20), and (5.21).

Examination of these relations shows that, if a function $M(R)$ is given, these equations yield the width distribution of the diffuser and the flow properties. For such a radial distribution of Mach number we find the total pressure distribution from (5.15) and (5.16). The results obtained are used to give the distribution of $B \cos \alpha$ from (5.13). The distribution of the tangential component of the Mach number is then obtained from (5.17) and (5.19). Equation (5.20) gives the flow angle distribution. The width distribution is then obtained from (5.20) and (5.13). The distribution of the radial component is given by (5.21).

The procedure outlined above has the advantage of prescribing the Mach number distribution which makes full use of readily available compressible gas tables.

It avoids the process of solving the differential equations in a stepwise fashion as used in Ref (5.2).

It permits the direct calculation of the diffuser efficiency in an early phase of the calculation procedure as soon as Equation (5.16) is calculated. Therefore, if in the investigation an unrealistic efficiency appears, the calculation can be discontinued. It can, therefore, be used readily for the investigation of an optimum flow path.

This method is applicable to pure radial diffusers and can be extended to conical or mixed-flow diffusers.

It is useful in the design of the combination of vaneless and vaned diffusers where, in general, a prescribed Mach number at the entrance to the vanes is desired. The vaneless diffuser is then to be designed for given inlet and exit Mach numbers.

The disadvantage of the method is that the ordinary criterion of boundary layer separation based on the velocity gradient cannot be applied directly, though the Mach number distribution is also a measure of this velocity gradient.

In reality, the stagnation pressure varies across the width of the diffuser. This may produce phenomena which are essentially different from those occurring in one-dimensional flow. Whether the present one-dimensional approach is still of value can only be judged from the results of experiments.

### 5.2.2.2 Applications

The design procedure of 5.2.2 is now applied to some numerical examples to illustrate the effects of the main parameters - for example, the flow deceleration, the initial flow angle, and the variation of the mass rate of flow.

## Effect of the Deceleration Rate

The effect of the flow deceleration on the diffuser performance can be seen through the radial distribution of the Mach number. Conditions were selected for the design which represented closely those of the experimental supersonic compressor.

$$M_i = 1.15 \quad \alpha_i = 70^\circ \qquad b_i/D_i = 0.04$$

$$M_f = .80 \text{ at } R = 1.4 \qquad f = .008, \text{ friction factor}$$

The comparison was based on the vaneless diffuser efficiency which is defined as:

$$\eta = \frac{\text{Rise in enthalpy based on inlet static and outlet total pressure}}{\text{Entering Kinetic Energy}}$$

Two reasonable Mach number distributions designated by I and II on Figure 5.2 are selected. The resulting flow characteristics and diffuser shapes are calculated.

Figure 5.3 shows that in order to obtain the deceleration prescribed by Mach number distribution I, the diffuser width has to remain nearly constant for a short distance from the inlet. The radial distribution of the flow angle, $\alpha$, as represented on Figure 5.4, shows that for distribution I the flow begins nearly with a logarithmic spiral path ($\alpha$ = constant) then straightens out toward the radial direction.

The variation of the flow angle $\alpha$ for distribution II indicates that it follows a path that is shorter than that of distribution I. One would expect that a shorter path would give a higher efficiency if the flow were at low speed; however, as seen in Figure 5.5, the efficiency of the diffuser with distribution I is higher, which must be attributed to the effect of high-speed flow. A considerable shortening of the path would be required to offset this effect.

The distribution of the tangential and radial components of the Mach number $M_u$ and $M_r$, represented on Figure 5.6, shows that the deceleration rate has little effect on $M_u$, which is to be expected, whereas most of the deceleration is shown through the variation of $M_r$. Distribution II indicates an increase of the radial component of the velocity $M_r$ near the inlet, whereas distribution I has a small decrease in $M_r$.

An improvement in performance of vaneless diffusers, especially those operating at high-speed flow is, therefore, to be expected through a greater deceleration beginning immediately at the inlet. Referring again to Figure 5.2, we see that a higher deceleration rate than distributions I and II may be advantageous,

the limit being dictated only by the flow conditions in the boundary layer, which this theory does not account for. In addition, the gain in efficiency by changing from distribution II to I (which are quite different from each other), is not much, particularly if the vaneless diffuser is short.

The above-outlined method should not be generalized to vaneless diffusers comprising larger diameter ratios than used in the calculation.

## Effect of the Initial Flow Angle or Variation in Mass Rate of Flow

In this series of numerical examples, the following conditions are considered:

$$M_i = 1.15 \qquad \alpha_1 = 65^\circ \qquad b_i/D_i = .04$$

$$M_f = 0.8 \text{ at } R = 1.4$$

$$f = .008 \text{ (friction factor)}$$

The decrease in the initial angle can also be interpreted as a change in mass rate of flow through the diffuser. For distribution Ia, which is the same as distribution I of Figure 5.2, the results of the calculation, Figure 5.5, show a definite gain in efficiency. This is to be expected from vaneless diffusers operating with a smaller value of $\alpha_i$, since the flow path is

shorter. Considering the possible improvements in efficiency due to stronger deceleration, the distributions III and IV, Figure (5.2), were investigated. The higher deceleration rate has a pronounced effect on the radial distribution of $M_r$, Figure 5.6. The distributions III and IV require, as shown on Figure 5.3, a

divergence of the walls. The efficiency of the diffusers calculated with these distributions appears to be a little better than distribution Ia. For the given conditions, distribution IV is most satisfactory, as it combines a relatively large deceleration and a high efficiency.

## Effect of the Friction Factor

Experimental results on vaneless diffusers, Ref (5.6), reveal a wide range in the value of the friction factor, $f$, as can be seen on Figure 5.7. The numerical value $f = 0.008$ has been adopted for the present investigation, but it should be noted that the presented theory also allows a variable friction factor.

## 5.2.2.3 Conclusion

The optimum performance of a vaneless diffuser having a good velocity profile at the entrance is obtained when the flow is decelerated fast right at the beginning of the diffuser. This performance corresponds to a slight divergence of the wall with increasing radius. Short vaneless diffusers, as they are used between impeller tip and guide vanes, do not warrant generally any contouring of the walls because the potential efficiency gains are small.

Considerable gains in efficiency can be expected, if the velocity vector from the impeller is directed more towards the radial direction, which is particularly advisable in vaneless diffusers of large diameter ratio.

## 5.2.3 Prediction of the Performance of the Vaneless Diffuser of the Experimental Supersonic Radial Compressor

The presented design procedure does not lend itself to the treatment of the direct problem: i.e., to determine the performance from a given vaneless diffuser geometry.

In order to predict the performance of the parallel-walled diffuser of the experimental supersonic compressor, it appeared more convenient to use the method of Ref (5.2).

The design conditions for the supersonic compressor are:

Entering Mach number $M_i$ = 1.2

Entering flow angle $\alpha_i$ = 68.2°

Physical width $b_i$ = .515

The boundary layer is assumed to occupy a fraction of the width. The ratio of effective width to physical width used in the calculation is:

$$\frac{b_{effective}}{b_{physical}} = 0.875$$

It is shown in Chapter 3.4.2 that the ratio of boundary layer width to total width does not change much in this example. The use of constant blocking seems therefore justified. Through a study of the variation of the friction factor f, Ref (5.3), a distribution of f with the radius is selected. The results of the calculation predict a distribution of Mach number, and efficiency as shown on Figure 5.8.

As to be expected, a large radius is needed in order to bring the velocity down to a small value. The efficiency based on total pressure varies steeply at the beginning of the diffuser and remains nearly constant at larger radii.

## 5.2.4 Approximate Solution of Two-Dimensional Flow with Friction in a Radial Vaneless Diffuser

### 5.2.4.1 Theory

We consider the viscous flow in a vaneless diffuser with non-uniform entrance conditions. Due to the impeller inefficiency, the non-uniform conditions extend over the tangential and axial directions. In the present study, non-uniformity in the tangential direction is neglected. A simplified approach may be used for the treatment of this problem. It consists of dividing the flow into separate layers.

Figure 5.9 shows the physical model for this approach. The flow entering the vaneless diffuser is assumed to be made up of two parts.

a. The main core flow has a velocity V

b. The boundary layer flow has a velocity c

The main core flow is treated on the basis of the theory given in the previous chapter. The boundary layer flow is the subject of this study.

Let us consider the forces acting on the boundary layer flow shown in Figure 5.9.

The control volume is located in the boundary layer. The pressure gradient in the boundary layer is assumed to be the same as in the main flow. If the slope $\frac{dz}{dr}$ of the boundary line that separates the main flow from the boundary layer is small, the relative flow can be seen on a plane z = constant, according to Figure 5.10.

With $\tau_o$ and $\tau_m$ defined as:

$\tau_o$ = shear stress on wall

$\tau_m$ = shear stress due to main flow

The stress acting on the control volume can also be seen on the same figure. Summing up, the shear stresses in the r and $\phi$ direction are given by

$$\sum \tau_r = \tau_m \cos \gamma - \tau_o \cos \alpha \qquad (5.22)$$

$$\sum \tau_\phi = \tau_m \sin \ - \tau_o \sin \alpha \qquad (5.23)$$

The governing equations of the flow are then

$$2\pi r \delta \rho c_r = \text{constant} \qquad (5.24)$$

$$c_r \frac{dc_r}{dr} - \frac{c_u^2}{r} = \frac{1}{\rho} \frac{dP}{dr} + \frac{\sum \tau r}{\rho} \qquad (5.25)$$

$$c_r \frac{dc_u}{dr} + \frac{c_u c_r}{r} = \frac{\sum \tau_\phi}{\rho \delta} \qquad (5.26)$$

$$\tau_o = f \frac{\rho c^2}{2}, \ f = \text{constant} \qquad (5.27)$$

$$\tau_m = f_m \frac{\rho c^2}{2}, \ f_m = \text{constant} \qquad (5.28)$$

$$\frac{dP}{dr} \quad \text{given by main flow} \tag{5.29}$$

$$\rho = \rho_i = \text{constant, incompressible flow} \tag{5.30}$$

A more accurate approach to the problem using, for instance,

$$\tau_o \propto c^2 \tag{5.31}$$

$$\tau_m \propto w^2 \tag{5.32}$$

could be introduced.

Introducing the dimensionless numbers

$$R = \frac{r}{r_i} \qquad C_u = \frac{c_u}{a_o} \tag{5.33}$$

$$C = \frac{c}{a_o} \qquad C_r = \frac{c_r}{a_o} \tag{5.34}$$

the previous equations yield the system:

$$\frac{\delta}{\delta_i} = \frac{Cr_i}{RC_r} \tag{5.35}$$

$$C_r \frac{dC_r}{dR} - \frac{C_u^2}{R} = -\frac{1}{k} \frac{\rho_{oi}}{\rho_i} \frac{dP/P_{oi}}{dR}$$

$$+ (f_m \cos \gamma - f \cos \alpha) \frac{\left(\dfrac{V}{a_{oi}}\right)^2}{2} \frac{r_i}{\delta_i} \frac{RC_r}{Cr_i} \tag{5.36}$$

$$C_r \frac{dC_u}{dR} + \frac{C_u C_r}{R} = (f_m \sin \gamma - f \sin \alpha) \frac{\left(\dfrac{V}{a_{oi}}\right)^2}{2} \frac{r_i}{\delta_i} \frac{RC_r}{Cr_i} \tag{5.37}$$

$$\tan \alpha = \frac{C_u}{C_r} \tag{5.38}$$

$$\tan \gamma = \frac{V_u - C_u}{V_r - C_r} \tag{5.39}$$

k = Specific heat ratio, 1.4 for air

For a given radial variation of $V$, $\frac{dP}{dr}$, for fixed values of $f$, $f_m$, and for initial values of $c_u$, $c_r$, the system is solved numerically.

The present approach does not solve the problem entirely, since it requires that the values of $f$ and $f_m$ still be selected properly. Also, the presented theory does not allow for negative meridional components of velocity which have been observed in vaneless diffusers. Nevertheless, it is believed that the theory describes in a qualitative manner relevant phenomena in a vaneless diffuser.

## 5.2.4.2 Application of the Theory

For a typical example, a main core flow is selected. The inlet conditions and the radial variation of Mach number are shown on Figure 5.11. Application of the procedure of Chapter 5.2.4.1 gives the radial width distribution of the main core flow (Figure 5.12).

The initial thickness of each boundary layer, Figure 5.12, is taken as 0.075 of the initial main core flow. For simplification, the initial tangential components of the velocity in the main core flow and in the boundary flow are considered equal. This assumption is supported by experimental results of a study of the velocity profile at the impeller exit. The initial radial component of this velocity within the boundary is half of that in the main flow.

The value of the friction coefficient at the interface between the main flow and the boundary flow is taken as 0.008, the value which is used in the determination of the main core flow. The friction coefficient between the boundary flow and the wall of the diffuser is taken as 0.010, assuming that the internal shear in a fluid flowing between parallel plates increases approximately in a linear fashion with distance from the mid-plane.

It may be noted that the above-selected values of the friction factor vary somewhat with the degree of diffusion (Ref 5.6).

The differential equations that govern the flow were solved and resulted in a flow path in the boundary layer region as shown in Figure 5.13. As can be expected, this flow path is curved more than that of the main flow.

The above results also give the width distribution of the boundary layer, which is to be added to that of the given main flow in order to obtain the final shape of the vaneless diffuser as is done in Figure 5.12.

## 5.2.4.3 Conclusion

The two-dimensional viscous problem of the vaneless diffuser can be approximately solved, by making up the flow with a large number of layers. The calculation indicates a large variation in the stream paths from one layer to the other. Losses involved in the diffusion process could be materially reduced if means could be found to reduce the variation in stream paths and especially to avoid the presence of stream paths that approach a circle, thereby not contributing to the diffusion process.

## 5.3 Vaned Diffuser

### 5.3.1 Review of Design Procedures for Vaned Diffuser

Vaned diffusers are used in radial and mixed-flow compressors to obtain an efficient diffusion in a short distance. Investigations have been made to improve its performance but they are mostly directed towards an over-all approach and limited to subsonic flow.

A review of design methods for subsonic vaned diffusers of radial and mixed-flow compressors may be appropriate. At present, the design of subsonic vaned diffusers for radial and mixed-flow compressors is based mainly on the following methods:

a. Channel Approach - The flow in the diffuser is treated on a one-dimensional basis. The number of blades and their thickness distribution are determined in such a way that the blade channel has an area distribution equivalent to that of a conical or two-dimensional diffuser. The design criterion consists of using an equivalent optimum cone angle which ranges between $4^\circ$ and $10^\circ$. Ref (5.7) presents such an approach.

b. Airfoil Approach - The airfoil approach to the design problem consists in generating the diffuser blades so as to avoid boundary layer separation. The separation depends on the velocity distribution along the diffuser blades. At present, a good design criterion for estimation of the separation point within the diffusers of radial and mixed-flow compressors seems to be lacking.

The airfoil approach to the design problem treats the flow on a two-dimensional and three-dimensional basis. In general, design methods for vaned diffusers can be considered as a particular application of the methods used for impellers.

Within the group of two-dimensional theories, Ref (5.8) considers the flow in a circular cascade of blades as due to a distribution of sources and sinks. The velocity along the blades is calculated accordingly.

Ref (5.9) uses the method of conformal transformation which derives the flow of circular cascades from the flow in rectangular cascades of existing compressor blades. Relations are established for the lift coefficients, solidities, pressure and velocity distributions of the blades in circular and rectangular cascades. The method consists then in selecting a plain cascade that gives a circular cascade having a desired lift coefficient.

All these methods are for incompressible flow. In the case of compressible flow, the circular cascade is treated in Ref (5.10), where the method of "initial value" is applied. Suitable flow properties are prescribed on an arbitrary streamline, and the blade shapes are calculated accordingly.

The three-dimensional approach to the aerodynamic design of diffuser vanes is presented in Ref (5.11). The velocity distribution is prescribed along the blade element located on a specified surface of revolution. The blade camber and thickness distribution are then calculated with compressibility effects. Ref (5.12) considers also the three-dimensional effect by giving a design procedure for blades located on a stream filament of revolution. It specifies the blade thickness distribution, and the camber of the blade is calculated with compressible flow. The three-dimensional aspect to the design problem is also considered by Ref (5.13), which uses the force field concept. It determines a mean-stream surface of the compressible flow neglecting friction in the diffuser. To account for the finite spacing, a series expansion is used to determine the flow in the neighborhood of the mean-stream surface. The force field concept proves to be a particular case of the initial value problem in Ref (5.10).

None of these design procedures takes into consideration the viscosity effect in a rational manner.

c. Viscosity Effect - Viscosity effects naturally make the problem more complicated. An effort is made in Ref (5.9) to account for the viscosity in the design of diffuser blades. This method presents design criteria aimed at the reduction of the secondary flow caused by the boundary layer.

In consideration of the extensive amount of work devoted to frictionless flow in the guide vanes, and of the relatively small effort devoted to the actual viscous problem, it was felt that the present studies should largely be concerned with the viscosity effect in vaned diffusers.

Since the deceleration of the flow is accompanied by boundary layer growth and loss in energy, this latter being due to the wall friction, or mixing of the flow if separation prevails, an accurate prediction of the performance of guide vanes must take these phenomena into consideration.

## 5.3.2 The Boundary Layer Concept as Applied to the Guide Vane Channel

Adopting the terminology of axial-flow machines, the guide vanes in centrifugal and mixed-flow compressors have a low aspect ratio. The problem arises then as to the nature of the flow in the space between two consecutive guide vanes. Is it a "channel" flow where unsteadiness and mixing occurs, or is it a flow where the commonly accepted concept of boundary layer is applied? Depending on the flow at the impeller exit, both of these concepts are applicable. In good impellers where there is a uniform distribution of the velocity at the impeller exit, the boundary layer concept may be used. The flow consists of a potential core, and a thick boundary layer on the side walls of the diffuser, whereas at the stagnation point on the leading edge of the diffuser blades, the flow starts with an infinitesimal layer.

This physical picture of the flow in the guide vanes is supported by measurements as indicated on Figure 5.14. The standard boundary layer concept is different from the one used here since the layer thickness in guide vaned diffusers is large, as compared to the total flow area, and therefore has a large direct influence on the flow area and pressure distribution.

### 5.3.3  Flow in Guide Vanes and Conical Diffusers

Since we have adopted the boundary layer concept for the guide vane calculation, we have to determine the growth of the boundary layer on the walls that make the guide vanes. The complicated three-dimensional viscous flow in guide vanes is now replaced by the simplified one-dimensional approach which consists in establishing an average clogging effect due to the boundary layer growth.

At first thought it appears that a rectangular section diffuser may represent the flow in guide vanes rather faithfully; however, very little experimental work on diffusers of rectangular cross section has been done which could be applied to our problem. The initial boundary layer on these diffusers, for instance, does by no means represent the infinitesimal thickness at the leading edge of a guide vane. In addition, results are generally given on an over-all basis, and information on the behavior of the flow in the diffuser itself is relatively scarce as compared to that of conical diffusers.

Generally, for the purpose of studying the development of boundary layer growth in guide vanes the following equivalent diffusions were considered:

a.    Diffusion on a two-dimensional basis like that of a two-dimensional diffuser or airfoils with high aspect ratio.

b.    Diffusion in conical diffusers where the energy exchange from the main flow to the boundary layer approaches that of the guide vanes. A multitude of experimental results are available. On the basis of one-dimensional flow, it is shown in the (Appendix C) that, for the same initial conditions, the growth of the boundary layer in the guide vanes is the same as that in a conical diffuser having the same velocity distribution.

c.    Diffusion in rectangular cross section diffusers which closely resembles the flow in guide vanes but where little information is available at the present time.

Considering all these factors, the diffusion in conical diffusers appeared to be most promising and was therefore selected.

### 5.3.4  Calculation of the Development of the Turbulent Boundary Layer in a Conical Diffuser

Since the performance of a diffuser is mainly affected by the development of the boundary layer which reduces the area available for diffusion, a procedure for the prediction of this boundary layer  is desirable.

### 5.3.4.1  Physical Representation of the Flow in a Conical Diffuser

a.    It may be assumed that the flow in a conical diffuser consists of a core flow having no viscosity and a boundary layer region. (Figure 5.9.)

b.  The flow that enters a conical diffuser has a boundary layer which
can be of the laminar or turbulent type.  When the laminar boundary layer is
subject to a large positive pressure gradient, such as the one usually ob-
served at the entrance of the conical diffuser, Ref (5.14), it becomes turbulent.
Therefore, any practical consideration of the boundary layer in a conical
diffuser generally will deal with the turbulent type.

c.  It has been observed, Ref (5.15), that in the vicinity of the separation
region, the boundary layer presents some instability phenomena indicated by the
shedding of vortices along the wall.  Diffusion is still possible if the scale
of these vortices is small.  If instabilities of larger magnitude arise, the
turbulent fluctuation of the flow can be carried upstream and the entering
velocity profile may be affected, Ref(5.24.).

## 5.3.4.2  The Existing Theories for Turbulent Boundary Layers

A multiplicity of calculating procedures for turbulent boundary layers
with a pressure gradient is available in the literature.  Ref (5.16) gives a
critical review of the existing methods.

In general, the calculation consists of determining the displacement
thickness and the momentum thickness through two relations.  One of them is
based on the momentum equation;  the other is based either on the energy
equation or the moment of momentum equation.  All make use of empirical data
for shear stress and turbulence effects.  An application of the commonly known
procedures to some typical cases does not yield satisfactory results.

The Doenhoff and Tetervin method, Ref (5.17), supported by data on airfoils,
fails in predicting the growth of the displacement thickness in conical diffusers
according to calculations made by Rupert and Persh, Ref (5.18).

The data of Ref (5.18), which incorporates information on turbulence
effects and wall shear stress, has been subjected to our investigation.  The
experimental data were obtained from NACA studies of conical diffusers, Ref (5.19).
The boundary layer growth has been calculated and is shown in Figure 5.16.
Figure 5.16 indicates that the method of Ref (5.18) gives a good approximation
for the momentum thickness.  However, the displacement thickness, which is the im-
portant factor in conical diffuser performance, is not too well represented.

The possible explanation for these failures is that the mechanism of the
turbulent flow in the boundary layer has not as yet been fully understood.
Since empirical data must be used, some inaccuracy is therefore to be expected.
For instance, Rupert and Persh do not give a good correlation for the data on
the turbulent normal shear stress, and von Doenhoff uses a wall shear stress
which does not vanish when separation is approached.

## 5.3.4.3 Basis of the Present Approach

In establishing a calculation procedure for the boundary layer in vaned diffusers of centrifugal and mixed-flow machines, the following facts have to be emphasized:

a. The boundary layer is generally thick as compared to the diffuser width.

b. The flow outside the boundary layer is compressible, the Mach number being as high as 0.8.

It is also recognized that the existing methods for the calculation of turbulent boundary layer make little use of the information on flow in conical diffusers. Though there is basically no difference between the turbulent boundary layer flow in a cone, and the flow in a two-dimensional channel, it is conceivable that the chances of success for any calculation procedure are greater if one restricts oneself to the use of conical diffuser data.

Since most of the calculating procedures fail, or do not attempt to treat the separated flow region, it is thought that the task of obtaining a calculation procedure is made easier if one method is first established for the flow up to the vicinity of the separated flow region. Another method would have to be conceived for the quasi-separated flow and its possible reattachment. In fact, this can be justified when one considers that a pronounced effect of stream turbulence and mixing is observed in the quasi-separated region.

## 5.3.4.4 Calculation Procedure for the Boundary Layer

The boundary layer is characterized by the displacement thickness, the momentum thickness, and the shape parameter. They are defined as:

$$\delta^* = \int_0^\delta \left(1 - \frac{u}{U}\right)\left(1 - y/r\right)\, dy \tag{5.40}$$

$$\theta = \int_0^\delta \left(1 - \frac{u}{U}\right)\left(\frac{u}{U}\right)\left(1 - \frac{y}{r}\right)\, dy \tag{5.41}$$

$$H = \delta^*/\theta \tag{5.42}$$

For small values of $y/r$, i.e., for a boundary layer which is thin as compared to the diffuser radius, the previous expressions are reduced to that of the two-dimensional flow.

It is also assumed here that the following empirical relation for a skin friction factor $c_f$ under a pressure gradient is applicable to a conical diffuser.

$$c_f = \frac{\tau_0}{\frac{1}{2}\rho U^2} = 0.246\, e^{-1.561 H}\, R_\theta^{-.268} \tag{5.43}$$

For two-dimensional flow, this relation (which is due to Ludwig-Tillman) has been verified recently by Ref (5.20). A question may arise as to its validity when used with $\kappa^*$ and $\theta$ as defined previously, which can only be settled by a direct measurement. But for small values of $y/r$, Equation (5.43) is perfectly valid, since the axially-symmetric boundary layer will then behave like a two-dimensional one, as can be seen physically. Further argument in favor of the full validity of the previous expression for $c_f$ is based on consideration of the internal structure of the boundary layer. The boundary layer is divided into the laminar sublayer and the outer semiviscous region. As $c_f$ depends on the flow at the wall, it is governed mainly by the laminary sublayer. Since this latter has a small thickness in either case, axially symmetric or two-dimensional, the expression for $c_f$ should be valid everywhere. Ref (5.21) contemplates the same problem, but unfortunately obtains the values of $c_f$ for a conical diffuser through the momentum equation, which is in doubt in the separated flow region.

## The Momentum Equation

Using the assumptions common to the boundary layer theory, the application of the momentum theorem (Appendix A) to the control volume of Figure 5.15 yields, for incompressible flow, the equation

$$\frac{d\theta}{dx} + \frac{\theta}{R}\frac{dR}{dx} + (2 + H)\frac{\theta}{U}\frac{dU}{dx} = \frac{c_f}{2} + A , \qquad (5.44)$$

which is like that of a two-dimensional boundary layer.

Investigation by Ref (5.22) shows that, for a given velocity gradient, the compressibility effect on the results of this equation is negligible up to Mach number $M = 1$.

Recent investigation by Rashis, Ref (5.25) and Newman, Ref (5.26), attributes an additional term A to the right-hand member of Equation (5.44) to account for turbulent effects and the variation in static pressure across the boundary layer. Since the present calculation procedure is limited to a nonseparated flow region where turbulence fluctuations are small, this term can be neglected.

## Approximations

An approximation of Equation (5.44) is desirable for engineering purposes.

The main feature of the momentum equation is its insensitivity to the variation of H, (Ref 5.27). This fact will now be applied. It provides also the explanation that, in general, there is little error involved in the calculation of the momentum thickness of the boundary layer. With H maintained constant, A negligible, and $c_f$ given by Equation (5.43), integration of Equation (5.44) as carried out in Appendix A yields:

$$\frac{\theta}{\theta_i} \left(\frac{R}{R_i}\right)^{1.268} \left(\frac{R_\theta}{R_{\theta_i}}\right)^{0.268} \left(\frac{U}{U_i}\right)^{C_1} = 1 + C_2 \quad I \tag{5.45}$$

where

$$C_1 = 1.268 \ (2 + H) - 0.268 \tag{5.46}$$

$$C_2 = 0.1423 \ e^{-1.561 \ H} \ R_{\theta_i}^{-0.268} \tag{5.47}$$

$$I = \int_0^{\frac{x}{\theta_i}} \left(\frac{U}{U_i}\right)^{C_1} \left(\frac{R}{R_i}\right)^{1.268} \ d\frac{x}{\theta_i} \tag{5.48}$$

### The Approximate Momentum Thickness Relation for Incompressible Flow

With the hypothesis that integral I is small, Equation (5.45) is reduced to:

$$\frac{\theta}{\theta_i} \left(\frac{R}{R_i}\right)^{1.268} \left(\frac{R_\theta}{R_{\theta_i}}\right)^{0.268} = \left(\frac{U_i}{U}\right)^{C_1} \tag{5.49}$$

In neglecting I and in assuming H constant, the exponent $C_1$ is to be determined from experimental data. The results on Figure 5.17, show that exponent $C_1$ can be taken equal to 5.17.

The experimental data show that, for incompressible flow, the variation of $\theta$ as given by Equation (5.49) is acceptable for future calculation; they show further that exponent $C_1$ is not a sensitive function of the initial Reynolds number, as the data available on Figure 5.17, covers the range of $1 \times 10^3$ to $5 \times 10^4$. This is observed to be in line with the theoretical value of $C_1$ given by Equation (5.45).

The result can be compared to the relations proposed by Ref (5.28), which gives a momentum thickness relation similar to Equation (5.49), but with an exponent dependent on the initial Reynolds number.

### Effect of Compressibility in a Conical Diffuser

The compressibility effect on the flow in a conical diffuser is equivalent to a higher deceleration rate (large $-\frac{dU}{dx}$). Since Equation (5.49) has been tested for incompressible flow only, it was anticipated that it may not be valid for higher deceleration rates.

In addition, one observes considerable acceleration of the flow right before the entrance, as shown on Figure 5.18. As a result, the inlet conditions to a conical diffuser are not so well defined.

To verify the application of Equation (5.49) to the compressible case, one may consider the experimental data using as inlet conditions:

(a)  The conditions that exist at the point where acceleration starts, Figure 5.18.

(b)  The conditions where the velocity is a maximum, Figure 5.18.

The results using inlet conditions (b) are represented on Figure 5.19. They show a deviation from Equation 5.49. A similar study was made using inlet condition (a) and no better agreement was obtained. Hence, it is concluded that the effect of a high deceleration rate needs to be taken into account.

## Approximate Momentum Thickness Relation for High Subsonic Flow or Flow with a High Velocity Gradient

The effect of the velocity gradient is introduced with integral I of Equation (5.45). Using as an initial condition the one that corresponds to the maximum velocity, Figure 5.18, the momentum equation is written:

$$\frac{\theta}{\theta_i} \left(\frac{R}{R_i}\right)^{1.268} \left(\frac{R_\theta}{R_{\theta_i}}\right)^{0.268} \left(\frac{U}{U_i}\right)^{C_1} = 1 + C_2 \int_0^{\frac{x}{\theta_i}} \left(\frac{U}{U_i}\right)^{C_1} \left(\frac{R}{R_i}\right)^{1.268} d\left(\frac{x}{\theta_i}\right) \quad (5.50)$$

Evaluation of the experimental data shows that $C_1$ and $C_2$ can be taken as:

$C_1 = +5.17$

$C_2 = -0.015$

## The Auxiliary Equation

The auxiliary equation linking the shape parameter H to other parameters of the boundary layer provides an additional relation to complete a system of three equations in three unknowns, $\theta$, $\delta^*$, H, that characterize the boundary layer. In general, it is obtained through,

(a)  dimensional analysis

(b)  the use of the energy equation of the boundary layer, Ref (5.18), or the moment of momentum equation, Ref (5.16).

The auxiliary equations obtained with the procedures of Refs (5.16) and (5.18) are known to present little difference, according to Ref (5.25). They all need an empirical relation for the wall shear stress and the distribution of the shear stress across the boundary layer.

In the present study, a dimensional analysis of the momentum equation is made to bring out the parameters of the auxiliary equation (Appendix B). The analysis gives for the auxiliary equation:

$$\theta R_\theta^{0.268} \quad \frac{dH}{dx} = f(H)\Gamma + g(H) \tag{5.51}$$

where:

$$\Gamma = \frac{-0.246}{c_f} \quad \frac{\theta}{U} \quad \frac{dU}{dx} \tag{5.52}$$

If the free-stream Mach number is used,

$$\Gamma = \frac{0.246}{k\, c_f} \quad \frac{\theta}{M^2} \quad \frac{dP}{Pdx} \tag{5.53}$$

The functions of $f(H)$ and $g(H)$ are now to be determined with experimental data taken only from conical diffusers.

The task of evaluating the functions of $f(H)$ and $g(H)$ from experimental data involves a most time-consuming, yet inaccurate process. For a given set of data, curves representing the variation of $\theta R_\theta^{0.268} \frac{dH}{dx}$ with H are plotted. Also the variation of $\Gamma$ with H is obtained. Some typical representations are shown on Figures (5.20) and (5.21). By cross-plotting, the variation of $\theta R_\theta^{.268} \frac{dH}{dx}$ with $\Gamma$, for H = constant, is obtained. The simplest relations are used for this purpose. From Figure (5.22), the function $g(H)$ is determined by extrapolating the curve to the value of $\Gamma = 0$. The function $f(H)$ is determined by considering the variation of $\theta R_\theta^{.268} \frac{dH}{dx}$ with H at $\Gamma = 1$.

The functions of $f(H)$ are presented on Figure 5.23, where their analytical expressions are also given.

A Comparative Study of the Auxiliary Equation

The auxiliary equation (5.51) differs from the Von Doenhoff equation which is applied to two-dimensional flow over an airfoil, Reference 5.17, by the use of a skin friction coefficient which vanishes asymptotically toward the separation point. It uses the same parameters as Reference 5.17. It differs from this latter:

(a) in the sources of empirical data

(b) in the possibility of obtaining a large value of $\Gamma$, i.e., large deceleration.

Large values of $\Gamma$ have been obtained in cones of relatively small cone angle with flow at high Mach numbers. Using data from tests with free-stream Mach numbers as high as 0.8 also serves the purpose of coming closer to our goal of designing vaned diffusers for high subsonic flow.

## The Separation Point

Theoretically, the separation point is the point where the gradient $\frac{\partial u}{\partial y}$ vanishes.

Examination of the velocity profiles measured with pitot static probes is subject to question in the determination of the exact location of the separation, for the presence of the probe may cause a disturbance having an effect on the separation point. Indirect methods such as Schlieren could avoid the disturbances.

Since the separation can be practically determined from the velocity profile, it would be more rational to say that the flow is separated if the velocity $u/U$ reaches a defined value at a very small distance from the wall, for instance:

$$u/U = .05 \text{ at } y/\delta = .01$$

In order to determine the location $x$ of the separation point in this calculation procedure, one has to extrapolate the curve $(c_f, x)$ to find the distance $x$ where $c_f$ would vanish, Figs. 5.24 b, c. This is due to the fact that the analytical expression for $c_f$ vanishes only asymptotically. For the purposes of the calculation, the question arises as to where the extrapolation should start.

The following alternatives are considered: extrapolation for $c_f$ is to start:

(i) at a fixed value of $H$

(ii) at a location where $u/U$ when extrapolated reaches a finite value on the wall of the boundary layer.

(iii) at a sufficiently small value of $c_f$.

Alternative (i) is eliminated, for $H$ is known to be as high as 2.4 without a separation.

Alternative (ii) is now considered. Theoretically, the velocity $u$ is zero at the wall. Therefore, any velocity profile must appear as shown on Figure 5.24 a. The region of the laminar sublayer is, in general, small, so that the turbulent velocity profile can be extrapolated as shown in Figure 5.24a. From the experimental data, such an extrapolation is carried out to find the location $x$ at which $\frac{u_{wall}}{u} = 0.2$ and $0.1$. The curves marked $\frac{u_{wall}}{U} = 0.2$ and $0.1$ on Figs. 5.24 b, c, give the location $x$. Unfortunately, in our calculation procedure, the velocity profile is not known, unless the assumption is made that all the profiles are of the power type.

Alternative (iii) seems to be the most acceptable, for it corresponds to the physical phenomenon of the vanishing of the wall shear stress. The value from which extrapolation is to start is, according to Figure 5.24b and Figure 5.24c, in the range:

$$0.0004 < c_f < 0.0006$$

Therefore, in the present procedure, alternative (iii) is adopted.

## Summary

For a given velocity distribution $U(x)$ and the inlet conditions, the momentum and displacement thicknesses in a turbulent boundary layer of a conical diffuser can be calculated with the following relations:

$$\frac{d\theta}{dx} + \frac{\theta}{R}\ \frac{dR}{dx} + (2 + H)\ \frac{\theta}{U}\ \frac{dU}{dx} = \frac{c_f}{2} \qquad (5.54)$$

$$c_f = 0.246\ e^{-1.561\ H}\ R_\theta^{-0.268} \qquad (5.43)$$

$$\theta R_\theta^{0.268}\ \frac{dH}{dx} = f(H)\sqrt{\ } + g(H) \qquad (5.51)$$

$$\sqrt{\ } = -\frac{0.246}{c_f}\ \frac{\theta}{U}\ \frac{dU}{dx} \qquad (5.52)$$

$f(H)$ and $g(H)$ are given by Figure 5.23 or analytically by:

$f(H)$ and $= 0.100 - 3.08(H-1.5)\ (H-2.0)\ (H-1.289) + 0.761\ (H-1.596)$ for $H \gtrless 1.55$

$\quad = 0.100 - 3.08(H-1.5)\ (H-2.0)\ (H-1.289) + 2.33\ (H-1.286)\ (H-1.587)$
$\qquad\qquad\qquad\qquad\qquad\qquad\qquad\qquad (H-0.011)$ for $H \lessgtr 1.55$
$\qquad\qquad\qquad\qquad\qquad\qquad\qquad\qquad\qquad\qquad (5.55)$

$g(H) = -0.761\ (H-1.596)$ for $\gtrless 1.55$

$\quad = -2.330\ (H-1.286)\ (H-1.587)\ (H-0.011)$ for $H \lessgtr 1.55 \qquad (5.56)$

When an approximation of the momentum equation is used, the thickness $\theta$ is given by:

(a) $\qquad \dfrac{\theta}{\theta_i}\ \left(\dfrac{R}{R_i}\right)^{1.268}\ \left(\dfrac{R_\theta}{R_{\theta_i}}\right)^{0.268} = \left(\dfrac{U_i}{U}\right)^{5.17} \qquad (5.57)$

for small pressure gradients that correspond to incompressible flow in conical diffusers of less than 15 degrees included angle, and by:

(b) $\qquad \dfrac{\theta}{\theta_i}\ \left(\dfrac{R}{R_i}\right)^{1.268}\ \left(\dfrac{R_\theta}{R_{i_\theta}}\right)^{0.268}\ \left(\dfrac{U}{U_i}\right)^{5.17} = 1 - 0.015 \int_0^{\frac{x}{\theta_i}} \left(\dfrac{U}{U_i}\right)^{5.17}\left(\dfrac{R}{R_i}\right)^{1.268} d\left(\dfrac{x}{\theta_i}\right)$

$\qquad\qquad\qquad\qquad\qquad\qquad\qquad\qquad\qquad\qquad\qquad\qquad (5.58)$

for a large pressure gradient that corresponds to compressible flow in conical diffusers.

It should be emphasized that the auxiliary equation as established above uses only data of decelerated flow in conical diffusers. Its application to accelerated flow in nozzles is therefore questionable.

## Application of the Boundary Layer Calculation to the Study of Conical Diffuser Performance

### The Present Experimental Studies of Conical Diffusers and Domain of Application of the Boundary Layer Calculations

Most of the experiments carried out to study the diffusion process in diffusers were concerned only with the over-all approach in establishing the angle of divergence necessary for optimum performance, and many disregarded the influence of the inlet conditions. Even where the inlet boundary layer conditions were taken into consideration, the test conditions often do not correspond to those to be met in centrifugal compressors, nor were the results presented on a uniform basis, Ref (5.33).

The boundary layer calculation procedure mentioned previously will be used to determine the approximate location of the point where the flow separates from the walls. Knowledge of the separation point, even in an approximate way, is considered to be important in the design of guide vanes; for beyond separation, the flow will have to be handled with care - for instance, separated flow does not allow any efficient turning. The calculation procedure will permit the establishing of the maximum deceleration rate up to the separation point for any given initial condition, as a function of the diffusion rate.

Extending this investigation to various initial conditions allows us to establish a chart of maximum diffusion.

### The Maximum Diffusion Chart

A chart will be established giving the maximum diffusion that can be achieved without separation for different entrance conditions.

As can be seen from the study of the boundary layer equations, the separation point depends on the inlet conditions governed by the following parameters:

a.  the Reynolds number that measures the effect of viscosity.

b.  the dimensionless thickness which is necessary to show how soon the boundary layer will fill up the diffuser.

c.  the shape parameter which measures the state of the velocity profile with respect to separation.

The influence of these factors will be studied separately.

The following data are needed for the boundary layer calculation:

a.  the distribution of the velocity of the potential core flow that gives the pressure distribution outside the boundary layer.

b.  the variation of the radius which corresponds to the actual physical boundary of the flow (i.e., the radius that includes the core flow as well as boundary thickness).

If the boundary layer growth in a conical diffuser is to be determined (direct problem), the calculation procedure will require an iteration process. For this, an assumption will be made for the potential core flow from which the boundary layer growth is calculated. Having now established the physical boundary of the diffuser, the potential core flow is recalculated and the iteration is repeated.

Next, the solution of the inverse problem is given. It consists of determining the boundary layer growth for a given distribution of the velocity of the potential flow. To simplify the calculation, the previous requirement  b.  is assumed to be given approximately by the variation of the radius that corresponds to the potential core flow. As compressibility has an effect on the variation of the radii with the potential flow, the Mach number is selected so that it covers the range of the subsonic guide vanes operations.

From these considerations, a series of potential flow distributions, I, II and VI, are assumed as shown on Figure 5.25. They are selected with simplicity in mind and considering that they approximate the one-dimensional distribution of the velocity in good subsonic guide vanes. The inlet velocity corresponds to a Mach number of 0.857 ($\frac{U}{a_o}$ = 0.800). An isentropic compression corresponds to each velocity and the area is given by continuity. The variation of the radii is then derived from that of the area.

### Effect of the Initial Reynolds Number on the Separation

The Reynolds number $R_{\theta_i}$ that is commonly found in the guide vane diffuser ranges between 20,000 and 140,000. Among all the factors that influence the separation point, it is thought that the Reynolds number has the smallest effect. To support this idea, a calculation was made to find the separation point for velocity distributions III and IV. The initial thickness $(\theta/d)_i$ and shape parameter $H_i$ being maintained constant, the variation of $c_f$ vs $(\frac{x}{d})_i$ is shown on Figure 5.26. Assuming that imminent separation takes place at $c_f$ = 0.0005,

the results of the calculation show that, despite the change in $R_{\theta_i}$, $c_f$ reaches

0.0005 at approximately the same value of $(x/d)_i$ for each case, i.e., at the same $(V/a_o)$ for each velocity distribution.

As a consequence, the effect of $R_{\theta_i}$ can be neglected for the considered

range of $R_{\theta_i}$. The influence of the other parameters $(\theta/d)_i$ and $H_i$ is calculated

using a constant $R_{\theta_i}$ = 20,000.

### Effect of the Initial Thickness and Shape Parameter on the Separation

The influence of the initial thickness and the shape parameter on separation was calculated for different inlet conditions and is shown on Figure 5.27. An examination of Figure 5.27 indicates:

a. When the initial boundary layer is in a state that approaches separation, there exists an optimum rate of deceleration which will give the maximum diffusion.

b. With a good initial boundary layer ($H_i < 1.5$), the line of $c_f = 0.0005$ which indicates imminent separation changes considerably with increasing thickness.

Following the line of $c_f = 0.0005$, one finds that the maximum diffusion is obtained with the largest diffusion rate. However, a calculation shows that the displacement thickness would be many times that of the potential core. This is unrealistic since the flow would have filled up the diffuser. The boundary layer concept, together with all of the assumptions, is therefore no longer valid.

Thus, a limit beyond which the calculation procedure does not apply should be set. Such a limiting condition occurs when the boundary layer entirely fills the diffuser as shown in Figure 15a. With a given type of velocity profile, for instance the power type, the relation between the displacement thickness and the radius of the potential core which is equivalent to filling up the physical area can be calculated. At present this limit is assumed to occur when $\delta/r = 1$. In this case, the displacement thickness occupies the outer half of the circular cross section of the diffuser. On Figure 5.27, the line of $\delta/r = 1$ is shown. The maximum diffusion ratio is taken as that given by the intersection of lines $\delta/r = 1$ and $c_f = 0.0005$. This maximum could have been given by the intersection of the line $\delta/r = 1$ with line $(x/d) = 0$, i.e., at an infinite diffusion rate. However, for the calculation procedure presented here, a finite diffusion rate was used, though this choice may be subject to question.

The results of Figures 5.27a, b, c, are combined in Figure 5.28 and show the effect of $(\theta/d)_i$ and $H_i$ on the maximum diffusion rate of a conical diffuser, before separation starts.

On a comparative basis, it can be seen that when the boundary layer is near separation ($H_i > 1.5$), there is little effect of the initial thickness.

The asymptotic character of the curves of Figure 5.28 is to be noted. For low values of $H_i$, the initial thickness effect is considerable.

## Estimate of the Maximum Performance of Conical Diffusers in View of its Application to the Design of Guide Vanes

In view of the simplification introduced in the representation of the flow in guide vanes by that of conical diffusers, prediction of the performance of conical diffusers as a function of the entrance conditions would have been desirable. Many analytical attempts have been made without much success. Experimental results, which would have been useful, unfortunately, cover a range of inlet conditions which are not applicable to the guide vanes of centrifugal compressors.

The basis of the present approach can be stated as follows: the conical diffuser is to be divided into two parts - the nonseparated flow region and the quasi-steady flow region. This physical concept of the flow picture is introduced in an attempt to represent the flow as faithfully as possible. For a given inlet condition, the assumption is made that the highest performance is obtained when the maximum diffusion is achieved in the nonseparated flow region. Further diffusion is allowed in the separated flow region. This subdivision of the flow in conical diffusers in two distinct parts may be subject to question as there is a transition region from one part to the other.

The performance of the two parts is now considered separately.

## Nonseparated Flow Region

From the results of Figure 5.28, the maximum diffusion that can be achieved up to imminent separation is obtained. The study of maximum diffusion yields also the distance $x/d_i$ which is needed to accomplish the diffusion (Figure 5.27).

On the basis of one-dimensional flow in the diffuser, the state of the fluid at the imminent separation is determined by the velocity $V_s$ as shown in Figure 5.30, to which is associated a total pressure $p_o$. This pressure is found from the static pressure rise in the nonseparated part which will be obtained through the energy equation. The loss coefficient $\zeta_1$, which measures the loss in total pressure, and is defined in Appendix D, is given by

$$\zeta_1 = (4f)\left(\frac{x}{d_i}\right)\frac{U_m^2}{U_i^2} \; ; \qquad 2U_m^2 = U_i^2 + U_s^2 \qquad (5.59)$$

where $f$ is the friction factor in fully developed turbulent pipe flow. $\zeta_1$, together with the velocity ratio $U_i/U_s$, permits the determination of the efficiency based on static pressure of the nonseparated flow region.

## Quasi-steady Flow Region

When the region of imminent separation is reached, further recovery is possible. However, in the quasi-steady flow region, diffusion must be accomplished with a divergence smaller or, at most, equal to that of the nonseparated flow. The maximum decrease in divergence is the reduction of the divergence to zero, i.e., the addition of a straight pipe. The maximum pressure recovery lies probably not too far from that obtained with the straight pipe. In the absence of any test results in the separated flow region, it is on the conservative side to take as optimum performance of the quasi-steady flow that a straight pipe is added to the downstream of the conical diffuser.

## Analysis of Peters' Experiments

Experimental study of the quasi-steady flow is practically nonexistent. A survey of literature shows that the experiments of Peters (Ref 5.35) offer some useful interpretation, and an analysis of these experiments is necessary.

The performance of the quasi-steady flow region can be obtained from Peters data as follows. The tests were conducted over a wide range of

$$(\theta/d)_i \text{ and } H_i$$

$$H\left(\frac{\theta}{d}\right)_i < .04 \qquad H_i < 1.48$$

For each of these initial conditions, Peters ran tests on many conical diffusers to obtain the one with optimum performance. For $\frac{L}{d_i} = 30$, which corresponds to $\left(\frac{\theta}{d}\right)_i = .025$, this optimum is obtained with a divergence of $5.2^{\circ}$. The corresponding physical area ratio is 2.34. The effective area for diffusion is smaller. For the previous initial conditions, the boundary layer calculation gives a deceleration ratio up to the separation point of 1.7, which would place the region of imminent separation around the end of the conical part of the Peters' diffuser.

The largest additional pressure $\Delta\eta_2 = \dfrac{\Delta P}{\frac{1}{2}\rho U_i^{\ 2}}$ obtained by diffusion of the quasi-steady flow is at least that given by Peters in the straight section. Figures 21, 23 of Ref 5.35 give

$$\Delta P / \frac{1}{2}\rho U_i^{\ 2} = 0.16 \tag{5.60}$$

In order to obtain other points for different $(\theta/d)_i$ and $H_i$, we can refer to Figure 23 of Ref 5.35. The divergence obtained is rather large; that is, the separation occurs earlier than right at the end of the conical part of the Peters diffuser. The recovery pressure $\Delta P / \frac{1}{2}\rho U_i^{\ 2}$ as given may be conservative. Utilizing all of the experimental results, the curve of maximum additional pressure recovery is drawn (Figure 5.29).

$$\Delta\eta_2 = \frac{\Delta P}{\frac{1}{2}\rho U_i^2} = f\left[\left(\frac{\theta}{d}\right)_i, H_i\right] \tag{5.61}$$

From Peters' experiments it is possible to obtain the value of the length $L/d_i$ necessary for maximum additional pressure recovery. As is seen in Figure 5.30, this length is quite insensitive to the diffuser divergence; so a mean value may be used.

The irreversibility involved in the additional recovery is measured by the loss coefficients $\zeta_2$, $\zeta_u$, which are defined in Appendix D. Following Peters, they can be taken as:

$$\zeta_2 = 4f\, x^1/d_i\, \frac{U_s^2}{U_i^2}\,, \qquad \text{loss due to wall friction.} \tag{5.62}$$

$$\zeta_u = (0.08)\left(1 - \frac{U_f^2}{U_i^2}\right), \qquad \begin{array}{l}\text{loss due to the shrinking of the}\\ \text{quasi-steady flow. (Ref 5.26).}\end{array} \tag{5.63}$$

Since $U_f$ is not known a priori, we reference the previous formula by a mean value of $\frac{U_f}{U_i}$, and $\zeta_u$ becomes:

$$\zeta_u = (0.08)\left(1 - C\,\frac{U_s^2}{U_i^2}\right) \tag{5.64}$$

where $\quad C = 0.85 \qquad\qquad$ for $\left(\frac{\theta}{d}\right)_i = 0.02$,

$\qquad\qquad\quad .65 \qquad\qquad\qquad \left(\frac{\theta}{d}\right)_i = 0.04$,

$\qquad\qquad\quad .53 \qquad\qquad\qquad \left(\frac{\theta}{d}\right)_i = 0.06$.

## Chart of Maximum Performance of Conical Diffusers

The previous method of estimate is applied to the determination of the optimum performance of conical diffusers. The calculation procedure is explained in the appendix.

Results for three different values of the friction factor are available and are presented on Figure 5.31. From these, the following conclusions can be drawn. For good entering velocity profiles ($H_i < 1.05$), the efficiency for various values of friction factor varies only slightly, independent of the initial boundary layer thickness.

This result is in agreement with experimental studies which indicate an optimum angle of diffusion independent of the inlet conditions. The experimental studies were generally made with conical diffusers having good inlet conditions. The effects of the initial boundary layer are larger with bad inlet conditions. Comparison with experimental data of Ref 5.33 for instance, confirms these numerical results.

## 5.4   Design of Subsonic Guide Vanes

In the following, the design method used at AiResearch is presented.

### 5.4.1 General Principles

A survey of the flow phenomena from experiments leads to the formulation of the following principles:

a. The velocity distribution along the wall of the diffuser is to be controlled such that the growth of the boundary layer is to be kept within limits. Separation of the flow is to be avoided in the entrance part of the diffuser channel.

b. Chapter 5.3.4.4 shows that even in the simple case of a conical diffuser there is a limit beyond which the diffusion process without any boundary layer control is very inefficient. The loss in total pressure increases past this limit, whereas the static pressure does not rise and even decreases in many cases. For a good impeller design, this limit lies in the vicinity of a velocity deceleration of

$$U_1/U_f = 3.$$

Further diffusion is possible through the use of boundary layer controls such as splitter vanes, tandem blades or sudden change in the wall shape.

c. Often the question arises as to the most desirable type of velocity distribution. The velocity distribution commonly encountered along the blade midsection of the existing vaned diffusers is as shown on Figure 5.32a. It is characterized by a large deceleration on the suction side with a tendency for early separation in the throat of the diffuser channel. The acceleration on the pressure side does not contribute to the diffusion. In cases of high subsonic entrance velocities, the effect of supersonic flow is avoided by using a small loading at the tip of the blades, Figure 5.32b, which corresponds to a small diffusion. This is not desirable as the high-speed flow contributes to higher losses. Moreover, the study of the influence of inlet conditions on boundary layer development shows considerable gains by diffusing rapidly at the beginning. The boundary layer theory also reveals that with the proposed limiting deceleration ratio there always exists imminent separation in the guide vanes. Handling of the quasi-steady flow requires a relatively larger length for diffusion than nonseparated flow. This leads to the design concept of a light loading in the trailing edge region as shown on the figures. The above considerations would favor as the most desirable velocity distribution the one shown on Figure 5.32c, which is characterized by an initial deceleration as rapid as is compatible with supersonic effects and separation requirements.

d. The above-discussed velocity distribution can be accomplished in many fashions, one of which is to use parallel walls and introduce turning in the flow. However, the diffusion within a curved channel tends to introduce crossflow in the boundary layer region, which is shown to be detrimental to the diffuser, Ref 5.9. Diffusion should therefore be accomplished with little turning, as is done by diffusion in the meridional plane. It may be pointed out that along the walls that constitute the meridional shape, the initial conditions of the boundary layer are much more unfavorable than at the leading edge of the blade section. The velocity gradient in the middle of the channel, along the above walls, is less severe than that of the blade section where separation may occur earlier. This situation favors then the diffusion in the meridional plane.

e. Phenomena of unsteady flow have not yet been studied; however, the experimental results of Ref 5.34, indicate that a small number of blades is desirable. This requirement coincides with that of a high loading of the blade at the entrance of the guide vanes as previously advocated.

f. In order to meet the incidence introduced with the nonuniform conditions across the passage width caused by the impeller performance and the boundary layer effect, the diffuser blades have to be twisted, or in the simplest case, slanted and scalloped.

## 5.4.2  Calculation Procedure

The problem is to determine the meridional shape and the blade shape that will produce a prescribed velocity distribution at the mid-blade section. The procedure described in Section III for use in designing impellers is fully applicable here, since the diffuser can be considered a stationary impeller.

The calculation is done in four steps:

a. A meridional shape is selected, generally on the basis of simplicity. Two diverging conical surfaces (Figure 5.33) are frequently used.

b. The clogging factor $\epsilon$ is estimated. A correct estimate of the clogging factor in a diffuser is much more crucial than in the impeller. An overoptimistic estimate of $\epsilon$ will not provide sufficient area for the diffusion process. A conservative estimate provides too large diffusion ratio with subsequent separation. On the basis of an assumed initial condition (Chapter 2.4.7) and an average diffusion corresponding to the mean velocity deceleration, the boundary calculation yields the growth of the displacement thickness from which $\epsilon$ is calculated up to the separation. Since diffusion in vaned diffusers is carried beyond separation, the estimate of $\epsilon$ in the quasi-steady flow region can be made on the basis of the value of $\epsilon$ at the proximity of the separation.

c. After the meridional shape and the clogging factor are determined, the channel theory (Chapter 3.2.3.2.2) is applied to find the blade thickness and turning angle of the blade that satisfies the prescribed velocity

distribution along the blade section made on surfaces of Figure 5.33. An iterative process is needed for this purpose. The channel theory is known to be valid inside the diffuser vanes. The question arises as to its application to the entrance of the vaned diffuser, particularly when most of the deceleration is already accomplished at the entrance to the guide vanes. An approximate approach is proposed for this case - particularly when the number of blades is reduced to a small value. The solution consists in determining the incompressible flow that would go through the circular cascade up by the mid-blade sections. For engineering purposes, a field plotter may be used as pointed out in Chapter 3.2.3.5. The Karman-Tsien compressibility correction is then introduced. This approximate solution is valid for relatively small Mach numbers, $M < .85$. Since the Karman-Tsien correction can not give a local Mach number larger than 1, it is subject to question in the case of higher subsonic flow.

d.  The calculation procedure considers only the velocity distribution on surface S, Figure 5.33. Twisted blades and curved meridional shapes introduce three-dimensional effects, and the velocity distributions along other blade sections cannot be neglected. However, compressors of the type considered here have diffuser vanes of such small height that the blades need not generally be twisted. The calculation procedure can therefore be restricted to steps (a), (b) and (c).

# THE MOMENTUM EQUATION

Momentum Balance in the Boundary Layer

The control volume ABCD Figure 5.15 is considered. In the following derivation, the usual assumption of zero pressure gradient across the boundary layer is removed $\frac{\partial P}{\partial y} \neq 0$ and the turbulence effect is considered.

Continuity:

Mass entering control volume along AB

$$W = 2\pi \int_0^\delta \rho \ rudy$$

Mass leaving along CD

$$W + \frac{dW}{dx} \ dx$$

Continuity gives the mass entering along BC

$$\frac{dW}{dx} \ dx$$

Momentum balance in the x direction:

Entering momentum flux along AB

$$m = 2\pi \int_0^\delta \rho u^2 rdy$$

Outgoing momentum flux along CD

$$m = \frac{dm}{dx} \ dx$$

Entering momentum flux along BC

$$U \frac{dW}{dx} \ dx + (0) \ dx^2$$

Shear force at wall

$$\gamma_o \ 2\pi \ Rdx + (0) \ dx^2$$

Pressure force along AB

$$F = \int_0^\delta 2\pi\, p\, r\, dy$$

Pressure force along CD

$$F + \frac{dF}{dx}\, dx$$

Pressure force along BC

$$P\, \frac{d}{dx} \int_0^\delta 2\pi\, r\, dy\, dx + (0)\, dx^2$$

The momentum theorem yields:

$$\frac{dm}{dx}\, dx = U\, \frac{dW}{dx}\, dx - 2\pi R\, \mathcal{T}_o\, dx - \frac{d}{dx} \int_0^\delta 2\pi\, p\, dy\, dx + P\, \frac{d}{dx} \int_0^\delta 2\pi\, r\, dy\, dx$$

$$+ (0)\, dx^2$$

Upon neglecting second order terms and simplifying

$$\int_0^\delta \rho r u^2\, dy = U \int_0^\delta \rho r u\, dy - \mathcal{T}_o R - \frac{d}{dx} \int_0^\delta p r\, dy + P\, \frac{d}{dx} \int_0^\delta r\, dy \qquad (5.65)$$

or

$$\int_0^\delta \rho r u^2\, dy - U \int_0^\delta \rho r u\, dy + \frac{dP}{dx} \int_0^\delta r\, dy = -\mathcal{T}_o R + \frac{d}{dx} \int_0^\delta (P - p)\, r\, dy$$

The turbulence effect is introduced with

$$u = \bar{u} + u'$$

$$p = \bar{p} + p'$$

Upon taking the time average with the rules of Ref 5.30 for averaging, the
momentum equation yields:

$$\frac{d}{dx} \int_0^\delta \rho r \bar{u}^2\, dy - U \int_0^\delta \rho r\, \bar{u}\, dy + \frac{dP}{dx} \int_0^\delta r\, dy \qquad (5.66)$$

$$= -\mathcal{T}_o R + \frac{d}{dx} \int_0^\delta (P - \bar{p})\, r\, dy - \frac{d}{dx} \int_0^\delta \rho r\, \overline{u'\, u'}\, dy$$

With the definition of the displacement and momentum thickness as:

$$RU\delta^* = \int_0^\delta (U - \bar{u})\, r\,dy$$

$$RU\theta = \int_0^\delta (U - \bar{u})\bar{u}\, r\,dy$$

one obtains:

$$\int_0^\delta \rho r u^2 dy = -RU^2 (\delta^* + \theta) + U^2 \int_0^\delta r\,dy \qquad (5.67)$$

In addition, at the edge of the boundary layer the pressure, P, is related to the velocity, U, by

$$\frac{dP}{dx} = -\rho U \frac{dU}{dx} \qquad (5.68)$$

With (5.68) and (5.67) the left hand number of Eq (5.66) becomes:

$$-\frac{d}{dx} RU^2 (\delta^* + \theta) + \frac{d}{dx} U^2 \int_0^\delta r\,dy + U \frac{d}{dx} \int_0^\delta \rho(U - \bar{u})\, r\,dy$$

$$-U \frac{d}{dx}\left(U \int_0^\delta r\,dy\right) - U \frac{dU}{dx} \int_0^\delta r\,dy = -\frac{d}{dx}\left[\rho R U^2 (\delta^* + \theta) + U \frac{d}{dx} \rho\, UR\, \delta^*\right.$$

$$= -\rho U^2 \frac{d}{dx} R\theta - \left(\frac{\delta^*}{\theta} + 2\right) R\theta \rho U \frac{dU}{dx}$$

The momentum Equation (5.66) is then reduced to:

$$\frac{d}{dx} R\theta + \left(\frac{\delta^*}{\theta} + 2\right) \frac{R\theta}{U} \frac{dU}{dx} = \frac{\mathcal{T}_0^R}{\rho U^2} + A \qquad (5.69)$$

where 
$$A = \frac{1}{\rho U^2} \frac{d}{dx} \int_0^\delta \rho\, \overline{u'u'}\, r\,dy - \frac{1}{\rho U^2} \frac{d}{dx} \int_0^\delta (P - \bar{p})\, r\,dy$$

Integration of the Simplified Momentum Equation

With the common assumption for boundary layer studies, the pressure gradient $\frac{\partial P}{\partial y}$ is taken equal to zero, then

$$P = \bar{p}$$

Far from the separated flow region the turbulence effect is small. There-
fore A is neglected. The momentum equation is reduced to the standard form.

$$\frac{d\theta}{dx} + \frac{\theta}{R}\frac{dR}{dx} + (2 + H)\frac{\theta}{U}\frac{dU}{dx} = \frac{\tau_o}{\rho U^2} = \frac{c_f}{2} \tag{5.70}$$

In the following, H is assumed to be constant. With the skin friction
coefficient $c_f$ given by

$$c_f = 0.246 \ e^{-1.561\ H} \ R_\theta^{-0.268} \tag{5.43}$$

and the transformation of variables as given by Ref (5.30)

$$X(x) = \theta U^{C_1} r^{1.268} R_\theta^{0.268} \tag{5.71}$$

$$C_1 = 1.268 (2 + H) - 0.268$$

The simplified momentum equation is reduced to:

$$\frac{dX}{dx} = 0.156 \ U^{C_1} r^{1.268} \ e^{-1.561\ H} \tag{5.72}$$

Upon integrating, the momentum equation with constant H yields:

$$\frac{\theta}{\theta_i}\left(\frac{R}{R_i}\right)^{1.268}\left(\frac{R_\theta}{R_{\theta_i}}\right)^{0.268}\left(\frac{U}{U_i}\right)^{C_1} = 1 + C_2 \int_0^{\frac{x}{\theta_i}} \left(\frac{U}{U_i}\right)^{C_1}\left(\frac{R}{R_i}\right)^{1.268} d\,\frac{x}{\theta_i} \tag{5.45}$$

$$C_2 = 0.1423 \ e^{-1.561\ H} \ R_{\theta_i}^{-0.268}$$

## THE AUXILIARY EQUATION

The Auxiliary Equation 
$$\theta R_\theta{}^{0.268} \frac{dH}{dx} = f(H)\Gamma' + g(H) \tag{5.51}$$

The following analysis is carried out to establish a dimensionally correct form of the auxiliary equation.

The momentum equation gives

$$\frac{d\theta}{dx} = \frac{c_f}{2} - (2 + H) \frac{\theta}{U} \frac{dU}{dx} - \frac{\theta}{R} \frac{dR}{dx} \tag{5.70}$$

The following transformation used in two-dimensional case by Maskell, Ref (5.27) is carried out for axially symmetric flow.

$$\Theta = \theta \, e^{pH} \, R_\theta{}^q \tag{5.73}$$

$$\Gamma' = \frac{\Theta}{U} \frac{dU}{dx} \tag{5.74}$$

$$\int = \frac{c_f}{2} \, e^{pH} R_\theta{}^q \tag{5.75}$$

p, q are constants.

From the definition of $\Theta$ one obtains:

$$e^{pH} R_\theta{}^q \frac{d\theta}{dx} = \frac{d\Theta}{dx} - p \Theta \frac{dH}{dx} - e^{pH} \theta q R_\theta{}^{q-1} \frac{dR_\theta}{dx} \tag{5.76}$$

The last term is now calculated:

$$e^{pH} \theta q R_\theta{}^{q-1} \frac{dR_\theta}{dx} = q e^{pH} R_\theta{}^q \left[ \frac{\theta}{U} \frac{dU}{dx} + \frac{d\theta}{dx} \right]$$

or with the use of (5.70), (5.73), (5.74), (5.75), gives

$$e^{pH} \theta q R_\theta{}^{q-1} \frac{dR_\theta}{dx} = q \left[ \int -(H + 1)\Gamma' - e^{pH} R_\theta{}^q \frac{\theta dR}{Rdx} \right] \tag{5.77}$$

Substitution of (5.77) in (5.78) yields:

$$p \, \Theta \frac{dH}{dx} = \frac{d\Theta}{dx} - (1 + q)\left[\int + \left(H - \frac{2 + q}{1 + q}\right)\Gamma - \frac{\Theta}{R} \frac{dR}{dx}\right]$$  (5.78)

The previous form suggests a variety of combinations for the auxiliary equation giving the variation of H with x. It can be seen a simple form can be taken as:

$$\theta R_\theta^{0.268} \frac{dH}{dx} = f(H)\Gamma + g(H)$$  (5.51)

$$\Gamma = -\frac{0.246}{c_f} \frac{\theta}{U} \frac{dU}{dx}$$  (5.52)

## Transformation of the Parameter $\Gamma$

The parameter $\Gamma$, which is the main factor in the auxiliary equation, has been defined previously.

In cases where the free stream is given by the Mach number, it is transformed into:

$$\Gamma = \frac{0.246}{c_f} \frac{\theta}{RM^2} \frac{dp}{pdx}$$  (5.53)

$$k = 1.4 \text{ for air}$$

as can be seen in the following:

$$\Gamma = -\frac{0.246}{c_f} \frac{\theta}{2\frac{\rho U^2}{2}} \frac{\frac{\rho dU^2}{2}}{dx}$$

$$= \frac{0.246}{c_f} \frac{1}{2} \frac{\theta}{\frac{k}{2}M^2 p} \frac{dP}{dx}$$

$$= \frac{0.246}{c_f} \frac{\theta}{kM^2} \frac{dP}{Pdx}$$  (5.53)

DEVELOPMENT OF THE BOUNDARY LAYER IN A TRUNCATE DIFFUSER

In order to approach the boundary layer flow in a real guide vane channel, we consider a truncate diffuser and its control volume as shown in Figure 5.34. This diffuser has an axis of symmetry, and its boundary layer characteristics are assumed to be constant along the dimensions a and b. In addition, the standard assumptions for boundary layer studies apply.

The mass and momentum flux entering the control volume at $x = x_o$

$$\text{Mass} \quad W = \oint \int_o^\delta \rho u \, dy \, ds$$

$$\text{Momentum} \quad m = \oint \int_o^\delta \rho u^2 \, dy \, ds$$

where $\oint ds$ means integration around the truncate section.

The momentum flux that enters the control volume along dx is $U \dfrac{dm}{dx} dx$, and the pressure force acting on the control volume at $x = x_o$ is:

$$\oint \int_o^\delta P \, dy \, ds$$

The incremental pressure force acting on the control volume along dx is:

$$P \frac{d}{dx} \oint \int_o^\delta dy \, ds$$

The shear force on the wall is calculated with

$$\tau_o \left[ a + b + \frac{d}{dx} (a + b) \right] dx$$

Application of the momentum equation theorem to the control volume yields:

$$\frac{dm}{dx} \quad U \frac{dw}{dx} - \frac{d}{dx} \quad P \oint \int_o^\delta dy \, ds - \tau_o \left[ (a + b) + \frac{d}{dx} (a + b) \right] + P \frac{d}{dx} \oint \int_o^\delta dy \, ds \quad (5.79)$$

The momentum displacement thicknesses and shape parameters are introduced as:

$$U \delta^* = \int_o^\delta (U - u) \, dy$$

$$U^2 \theta = \int_o^\delta (U - u) u \, dy \qquad H = \delta^*/\theta$$

After subscripts a and b are used whenever quantities are taken along a and b, respectively, the momentum equation is then reduced to the simplified form:

$$a \left[ \frac{d}{dx} \theta_a + \left(2 + H_a + \frac{1}{a} \frac{da}{dx}\right) \frac{\theta_a}{U} \frac{dU}{dx} \right]$$
$$+ b \left[ \frac{d}{dx} \theta_b + \left(2 + H_b + \frac{1}{b} \frac{db}{dx}\right) \frac{\theta_b}{U} \frac{dU}{dx} \right] = \frac{\tau_o}{\rho U^2} (a + b) \tag{5.80}$$

In the case where $b = 0$, this equation is reduced to that of the boundary layer in a two-dimensional diverging channel as given by Ref (5.31).

For $a = b$, the equation is identical to the previous case. Due to the assumption of symmetry, the boundary layer behaves in this case as in a two-dimensional channel.

Even in this simple case, the boundary layer is only defined if there exists two additional relations such as:

$$c_f = c_f (H, R_\theta) \tag{5.81}$$

$$\theta R_\theta \frac{dH}{dx} = f'(H) \sqrt{\phantom{7}} + g'(H) \tag{5.82}$$

Since the shear stress depends mainly on the inner part of the boundary layer, it would be the same whether the diffuser is conical or two-dimensional. However, the second relation that gives the growth of the shape factor is completely different. This is due to the fact that the energy exchange from the main stream to the boundary layer is influenced by the three-dimensional effect in the case of the truncate diffuser; for instance, at the corners of the wall $\theta_a$ and $\theta_b$ are interrelated.

## Comparison between the Growth of the Boundary Layer in the Truncate Diffuser and the Conical Diffuser

An attempt is made to determine the conditions under which the growth of the boundary layer is the same in the truncate and conical diffusers. The boundary layer is governed by the following equations:

in the truncate diffuser:

$$\frac{d}{dx} \theta_2 + \left(2 + H_a + \frac{1}{a} \frac{da}{dx}\right) \theta_a \frac{dU}{dx} = c_f \tag{5.83}$$

$$H_a = \delta^*_a / \theta_a \qquad c_f = c_f (H, R_{\theta_i}) \tag{5.84}$$

$$\theta R_\theta \frac{dH}{ax} = f'(H) \sqrt{\phantom{7}} + g'(H) \tag{5.85}$$

in the conical diffuser:

$$\frac{d}{dx}\theta + \left(2 + \frac{1}{\Gamma}\frac{d\Gamma}{dx}\right)\frac{\theta}{V}\frac{dV}{dx} = \frac{c_f}{2} \tag{5.83a}$$

$$H = \delta^*/\theta; \quad c_f = c_f(H, R_{\theta_i}) \tag{5.84a}$$

$$\theta R_\theta \frac{dH}{dx} = f(H)\Gamma + g(H) \tag{5.85a}$$

a.  A comparison is possible only if relation (5.85) is known.

b.  The problem of equivalence can also be formulated by finding the conditions that would give the same solution for the system (5.83), (5.84), and (5.85) and the system (5.83a), (5.84a), and (5.85a). In the absence of a known relation for (5.85), we consider the case where (5.85) and (5.85a) are identical. Equations (5.84) and (5.84a) have already been shown to be identical. There remains to determine the conditions under which (5.83) and (5.83a) would give the same solution.

For the case where the initial conditions $\theta_i$, $R_{\theta_i}$, and $H_i$ are the same in both systems, Equations (5.83) and (5.83a) show that their solution would be the same if

$$\frac{1}{a}\frac{da}{dx}\frac{1}{U}\frac{dU}{dx} \quad \text{is equal to} \quad \frac{1}{\Gamma}\frac{d}{dx}\frac{1}{U}\frac{dU}{dx}$$

In the case of incompressible flow, the continuity gives

$$\frac{1}{a}\frac{da}{dx}\frac{dU}{dx} = \frac{1}{2U}\frac{dU}{dx}$$

$$\frac{1}{\Gamma}\frac{d\Gamma}{dx}\frac{dU}{dx} = \frac{1}{2\Gamma}\frac{dV}{dx}$$

and the previous equivalence condition becomes:

$$\frac{1}{U}\left(\frac{dU}{dx}\right)^2 = \frac{1}{V}\left(\frac{dV}{dx}\right)^2$$

Thus, with the assumptions of this analysis, the equivalence condition is fulfilled if we make:

$$U(x) = V(x)$$

i.e., the velocity distribution should be the same in both types of diffusers.

## CALCULATION OF THE CHART OF MAXIMUM PERFORMANCE
## FOR CONICAL DIFFUSERS

Application of the results of the studies in Chapter 5.3.4.4 is shown in the calculation of the charts of maximum performance of conical diffusers. For a given inlet condition characterized by $(\theta/d)_i$ and $H_i$, we propose to estimate the highest performance of a conical diffuser having a Reynolds number $\frac{\rho V d}{\mu}_i$ and a corresponding friction factor $f$ taken from data for fully developed pipe flow. Illustration is by way of a numerical example.

a. Relation between the conical diffuser loss coefficients and efficiencies.

On the basis of integrated values, the state of the fluid at the diffuser entrance $i$, the beginning of the quasi-steady flow region $s$, the end of the diffuser $f$ is represented on the h-s diagram of Figure 5.35.

The diffuser efficiency based on static pressure is defined by:

$$\eta_{ST} = \Delta h_{fs-i} \Big/ \Delta h_{oi-i}$$

$$= \left(\frac{P_f}{P_i}\right)^{\frac{k-1}{k}} - 1 \Big/ \frac{k-1}{2} M_i^2 \qquad (5.86)$$

Since the diffuser flow is divided into two parts, the contributions of the nonseparated flow and quasi-steady flow to the diffuser efficiency can be introduced as:

$$\Delta\eta_1 = \Delta h_{ss-i} \Big/ \Delta h_{oi-i} \qquad \text{contribution of the non-separated flow} \qquad (5.87)$$

$$\Delta\eta_2 = \Delta h_{fs-ss} \Big/ \Delta h_{oi-i} \qquad \text{contribution of the quasi-steady flow} \qquad (5.88)$$

The diffuser efficiency based on total pressure is defined by:

$$\eta_{total} = \Delta h_{ofs-i} \Big/ \Delta h_{oi-i}$$

$$= \frac{\left(P_{of}\Big/P_i\right)^{\frac{k-1}{k}} - 1}{\frac{k-1}{2} M_i^2} \qquad (5.89)$$

The over-all loss coefficient $\zeta$ is defined by:

$$\zeta = 1 - \eta_{total} = \Delta h_{oi - ofs} \Big/ \Delta h_{oi - i} \tag{5.90}$$

The components $\zeta_1$, $\zeta_2$, $\zeta_\mu$ of $\zeta$ are such that

$$\zeta = \zeta_1 + \zeta_2 + \zeta_\mu \tag{5.91}$$

$$\zeta_1 = \Delta h_{oi - oss} \Big/ \Delta h_{oi - i} \tag{5.92}$$

When the assumption $\Delta h_{of - f} = \Delta h_{ofs - fs}$ is made,

The relation between $\eta_{static}$ and is given by:

$$\eta_{static} = 1 - \zeta - \left(\frac{c_f}{c_i}\right)^2 \tag{5.93}$$

For a given $c_f/c_i$, $\eta_{static}$ varies linearly with $\zeta$ and the graph relating these quantities is as shown on Figure 5.36.

b. <u>Conical diffuser performance</u>, numerical example:

given $\left(\dfrac{\theta}{d}\right)_i = 0.04 \qquad H_i = 1.4$

$R_e = \dfrac{\rho c_i d}{\mu} \qquad \lambda = 0.014$

the deceleration ratio of the nonseparated flow is obtained from Figure 5.28.

$c_i / c_s = 1.50$

From data of Figure 5.27a, the necessary length $(x/d_i)$ which is necessary for this diffusion is obtained

$x/d_i = 2.14$

Equation (5.59) for the loss coefficient $\zeta_1$, gives:

$\zeta_1 = .021$

The static pressure rise in the nonseparated flow region is determined by $c_i/c_s$ and $\zeta_1$. The contribution $\Delta\eta_1$ of this flow can be determined using Figure 5.36, which gives

$$\Delta\eta_1 = .53$$

The contribution $\Delta\eta_2$ of the quasi-steady flow region is given by the studies of Page 179 and Figure 5.29 as:

$$\Delta\eta_2 = .21$$

and the maximum efficiency based on static pressure is:

$$\eta_{static} = \Delta\eta_1 + \Delta\eta_2 = .74$$

Calculation of the value of the loss coefficient $\zeta_2$ is made with equation (5.62), using the length $x/d_i$ of Figure 5.30:

$$x/d_i = 6.0 \qquad \zeta_2 = 0.037$$

The coefficient $\zeta_\mu$ is calculated from Eq (5.64) as:

$$\zeta_u = .0567$$

Thus, the total loss coefficient $\zeta$ and, consequently, the value of the efficiency based on total pressure are obtained

$$\zeta = .115 \qquad \eta_{total} = .885$$

Using the chart of Fig. (5.36), the results of $\eta_{static}$ and $\zeta$ the value $c_i/c_f$ can be determined as:

$$\zeta = .115$$

$$\eta_{static} = .74 \qquad c_i/c_f = 2.6$$

The length necessary to obtain this performance is given by:

$$x/d_i + x'/d_i = 8.14$$

Thus, for the given inlet conditions, the conical diffuser that gives the best performance is defined.

By changing the inlet conditions, the results can be put into a working chart such as Figure 5.31, calculated for

$$\lambda = 0.014$$
$$0.017$$
$$0.020$$

Remarks:

1.   The estimate of maximum performance is based on one single conical
     diffuser.  Further diffusion-like cascading has not been considered.
     Since the performance is given as a function of the initial conditions,
     the effect of cascading can be estimated by the successive use of the
     charts.

5.1    Polikovsky, V., Nevelson, M.  The Performance of A Vaneless Diffuser Fan.,
       NACA TM 1038. December, 1942.

5.2    Stanitz, J. D.  One-Dimensional Compressible Flow in Vaneless Diffusers of
       Radial and Mixed-Flow Centrifugal Compressors, Including Effects of Friction,
       Heat Transfer and Area Change. NACA TN 2610. January, 1952.

5.3    Faulders, C. R., Experimental and Theoretical Study of Vaneless Diffusers Flow
       with Supersonic Entry.  Gas Turbine Laboratory, M.I.T., June, 1952.

5.4    Shapiro, A. H., Hawthorne, W. R., Edelman G. M.  The Mechanics and Thermo-
       dynamics of Steady One-Dimensional Gas Flow with Tables for Numerical
       Solutions.  Meteor Report, M.I.T.  December 1947.

5.5    Emmons, H. W.  Gas Dynamics Tables for Air. Dover Publications, N. Y.  1947.

5.6    Brown, W. B.  Friction Coefficients in a Vaneless Diffuser. NACA TN 1311, 1947.

5.7    Campbell K., and Talbert J. E.  Some Advantages and Limitations of Centrifugal
       and Radial Compressors SAE Journal.  October 1945.

5.8    Hudimoto, Busuke  Theory of Wing Lattice, Technical Report, Engineering
       Research Institute, Kyoto University. Japan. March, 1951.

5.9    Faulders, C. R.  An Aerodynamic Investigation of Vaned Diffusers for Centri-
       fugal Compressors.  Gas Turbine Laboratory, M)I.T., January, 1954.

5.10   Giraud, F. L.  Determination of Solutions of the Hydrodynamical Equations as
       an initial Value Problem.  Gas Turbine Laboratory, M.I.T., Unpublished Notes.

5.11   Wu, C. H., Brown C.  A Method of Designing Turbomachine Blades With a
       Desirable Thickness Distribution for Compressible Flow Along an Arbitrary
       Stream Filament of Revolution.  NACA 2455. September 1951.

5.12   Stanitz, J. D.  Approximate Design Method for High-Solidity Blade Elements
       in Compressors and Turbines.  NACA TN 2408. July 1951.

5.13   Reissner, H. J., Bloom, M.  The Design of Circular Three-Dimensional Blade
       Systems for Steady Compressible Isentropic Flow. Brooklyn Polytechnic
       Institute, Department of Aeronautical Engineering. November, 1949.

5.14   Copp, Martin R.  Effects of Inlet Wall Contour on the Pressure Recovery of a
       10 Degree 10-Inch Inlet Diameter Conical Diffuser.  NACA RM L51E 11a.

5.15   Margoulis, W. Recherches  Expérimentales and Théoriques Effectuées de 1930
       à 1933, Sur la Mécanique de Fluides et la Transmission de la Chaleur dans
       les Fluides en Mouvement,  Technique Aéronautique. 1933.

5.16 Granville, P. S.  A Method for the Calculation of the Turbulent Boundary Layer in a Pressure Gradient.  ATI 105712, Navy Dept., May 1951.

5.17 Von Doenhoff A. C.  and Tetervin N., Determination of General Relations for the Behavior of Turbulent Boundary Layers.  NACA Report 772.

5.18 Rupert, F. K., and Persh, J. A., A Procedure for Calculating the Development of Turbulent Boundary Layers Under the Influence of Adverse Pressure Gradient. NACA TN 2478.

5.19 Little, B. H.  and Wilbur, S. W., High Subsonic Performance Characteristics and Boundary Layer Investigations of a 12 Degree, 10-Inch Inlet Diameter Conical Diffuser.  NACA RM L50C O2a.

5.20 Sandborn, V. A.  Preliminary Experimental Investigation of Low Speed Turbulent Boundary Layers in Adverse Pressure Gradient.  NACA TN 3031.

5.21 Shaw, R. R.  The Turbulent Boundary Layer in Diffusing Ducts, Aeronautical Research Council, Fluid Motion Sub-Committee, Great Britain.  Reprinted by Armed Services Technical Information Agency.  AD 8811.

5.22 Tetervin, N.  Approximate Formulas for the Computation of Turbulent Boundary Layer Momentum Thickness in Compressible Flows.  NACA, ACR NO. L6A22.

5.23 Polzin, J.  Flow Investigation in a Two-Dimensional Diffuser. R.T.P. Translation No. 1286, British Ministry of Aircraft Production  (In. Archiv, Bd 11, Heft 5. Oct. 1940)

5.24 Reid, E. G.  Performance Characteristics of Plane Wall Two-Dimensional Diffusers. NACA TN 2888.

5.25 Rashis, B.  An Analytical Investigation of the Effect of the Rate of Increase of Turbulent Kinetic Energy in the Stream Direction of the Development of Turbulent Boundary Layers in Adverse Pressure Gradients.  NACA TN 3049.

5.26 Newman, B. G.  Skin Friction in a Retarded Turbulent Boundary Layer Near Separation.  Aeronautical Research Council, Australia. Report A73. Nov. 1950.

5.27 Maskell, E. C.  Approximate Calculation of the Turbulent Boundary Layer in Two-Dimensional Incompressible Flow, Royal Aircraft Establishment, Farmborough, Hanks.  Aero Report 2463.  November 1951.

5.28 Ross, D.  Robertson, J. M.  An Empirical Method for Calculation of the Growth of a Turbulent Boundary Layer.  Readers Forum, Journal of the Aeronautical Sciences.  May, 1954.

5.29 Tetervin, N. and Lin C. C.  A General Integral Form of the Boundary Layer Equation for Incompressible Flow with an Application to the Calculation of the Separation Point of the Turbulent Boundary Layer. NACA TN 2158.

5.30   Eskinazi, S. J., Flagle, C. D., Kuetenik, J. R., Weske, J. R.  A Problem in
Retardation of a Turbulent Boundary Layer.  John Hopkins University,
Mechanical Engineering Department Internal Flow Research., A.T.I., 149078.

5.31   Schlichting, H.  Grenzschicht - Theorie.; Verlag, G. Braun. Karlsruhe.

5.32   Copp, Martin R., Klevatt, P. L.  Investigation of High Subsonic Performance
Characteristics of a 12 Degree 21-Inch Conical Diffuser, Including the Effects
of Change in Inlet Boundary Layer Thickness. NACA RM L9H10.

5.33   Ross, D., Robertson, J. M.  Effect of Entrance Conditions on Diffuser Flow.
A.S.C.E. Proceedings. Vol.78 No. 141.

5.34   Cheshire, L. J.  Design and Development of Centrifugal Compressors For
Aircraft Gas Turbines, War Emergency  Issue No. 12.  Institute of Mechanical
Engineers, London.

5.35   Peters, H.  Conversion of Energy in Cross-Sectional Divergences Under
Different Conditions of Inflow. NACA TM 737.
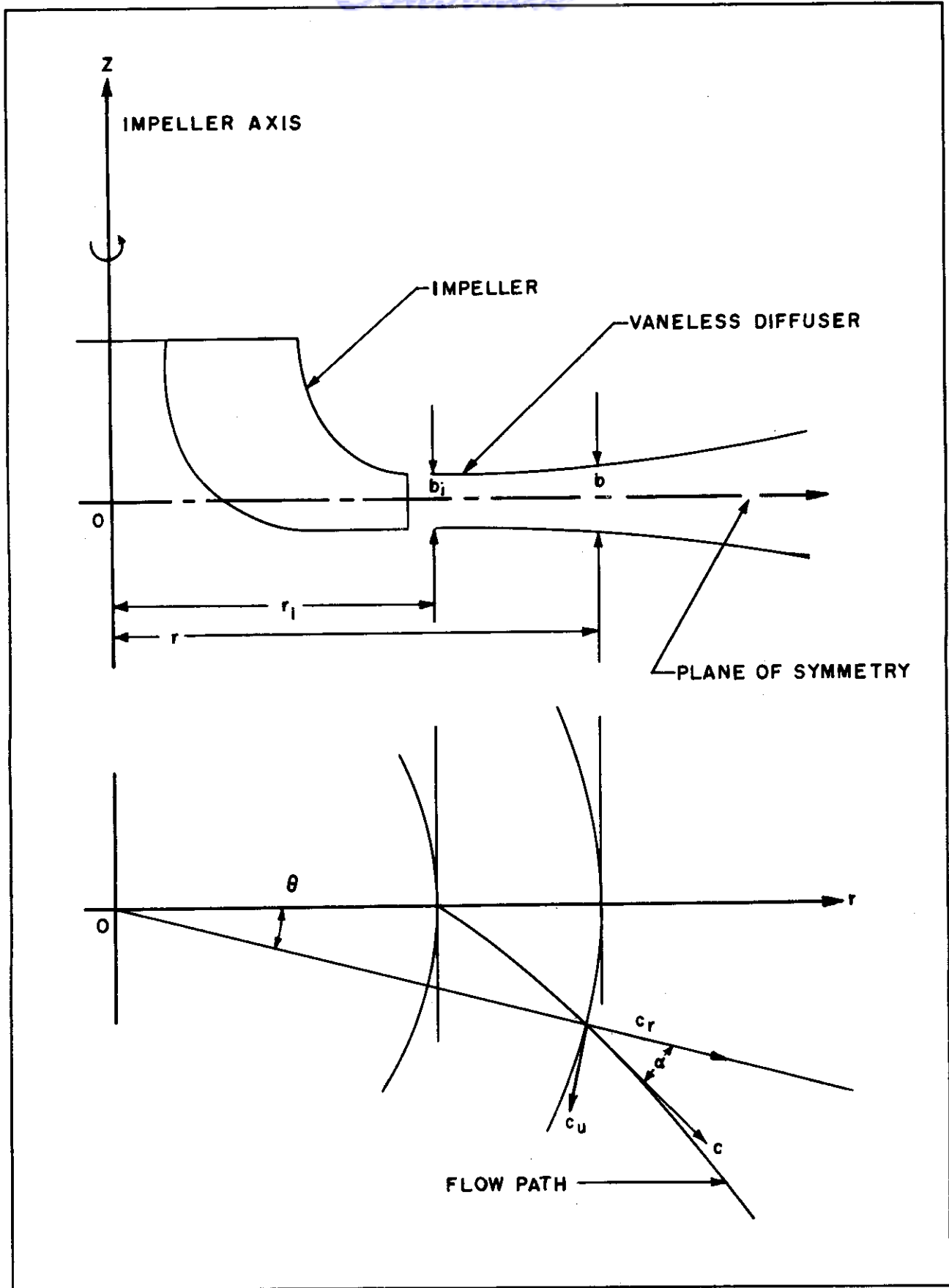
FIG. 5.1     GEOMETRY OF VANELESS DIFFUSER AND FLOW PATH
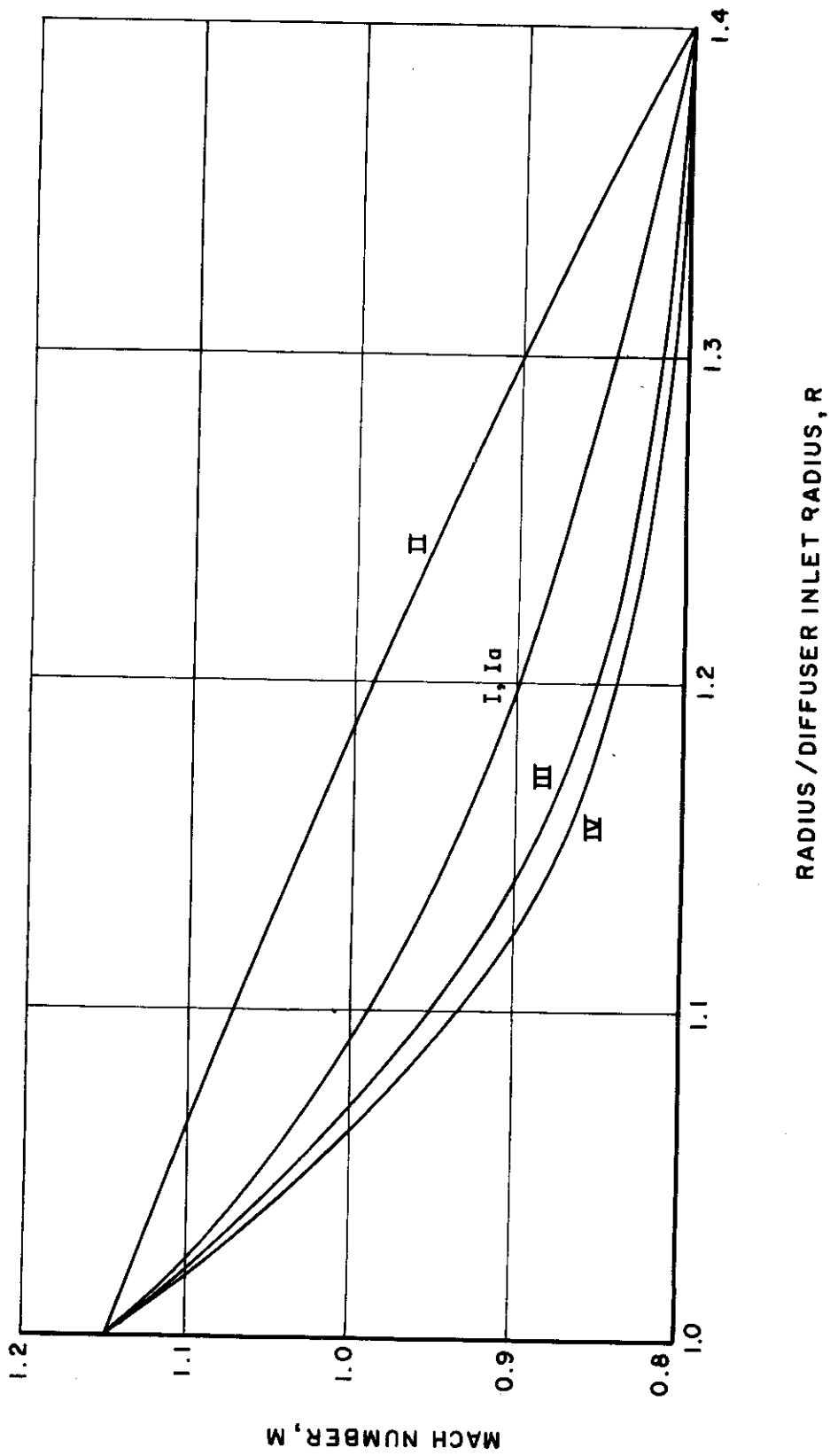
FIG. 5.2     RADIAL VARIATION OF MACH NUMBER
IN VANELESS DIFFUSER

INITIAL CONDITIONS

$M_i = 1.15$

$\alpha_i = 70°$ FOR I, II
$= 65°$ FOR III, IV, Ia

PRESCRIBED VARIATION OF MACH
NUMBER I···IV, FROM FIGURE 5.2

$f = 0.008$

RADIUS/DIFFUSER INLET RADIUS, R

WIDTH/DIFFUSER INLET WIDTH, B
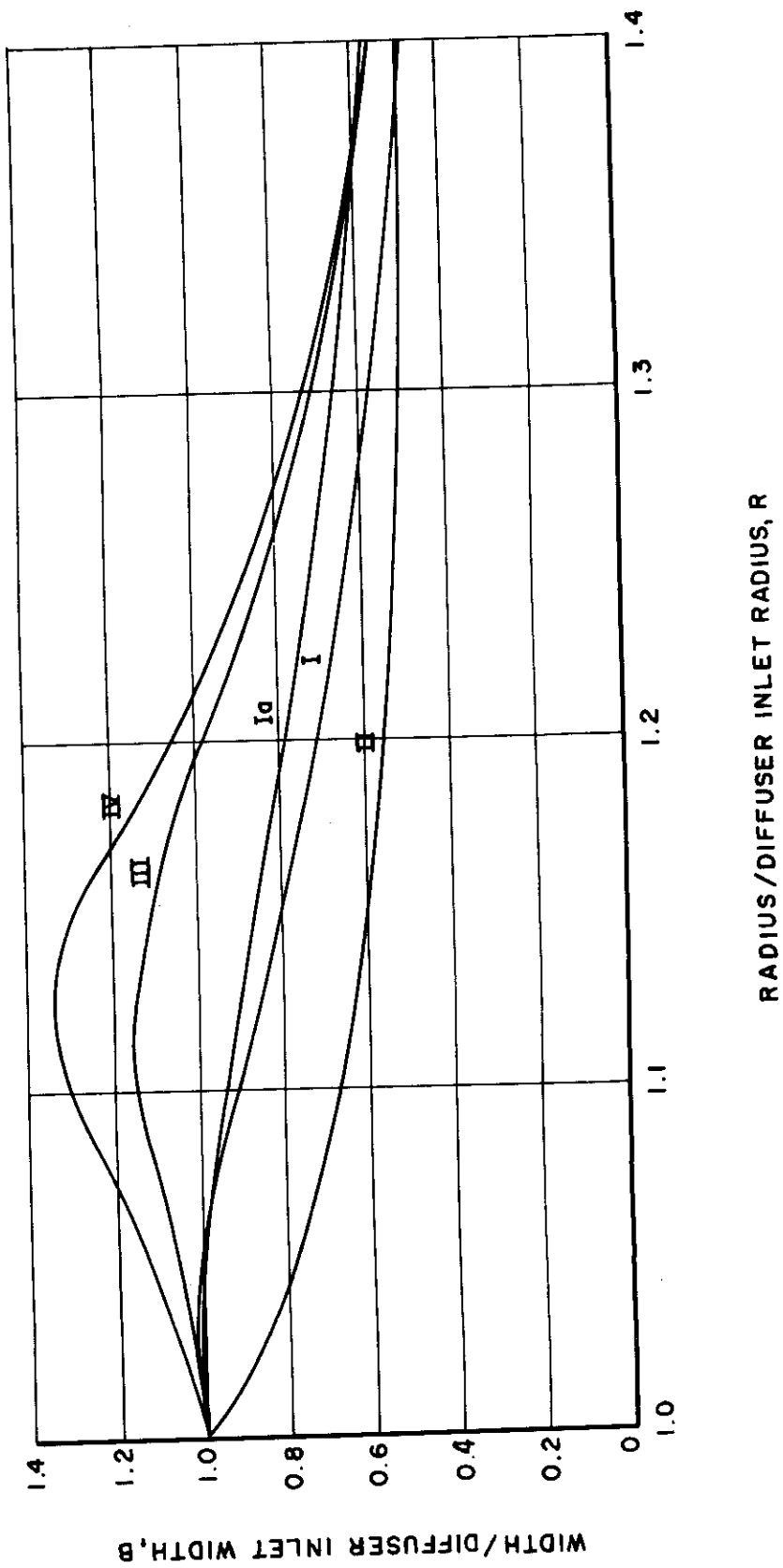
FIG. 5.3          VANELESS DIFFUSER WIDTH VARIATION
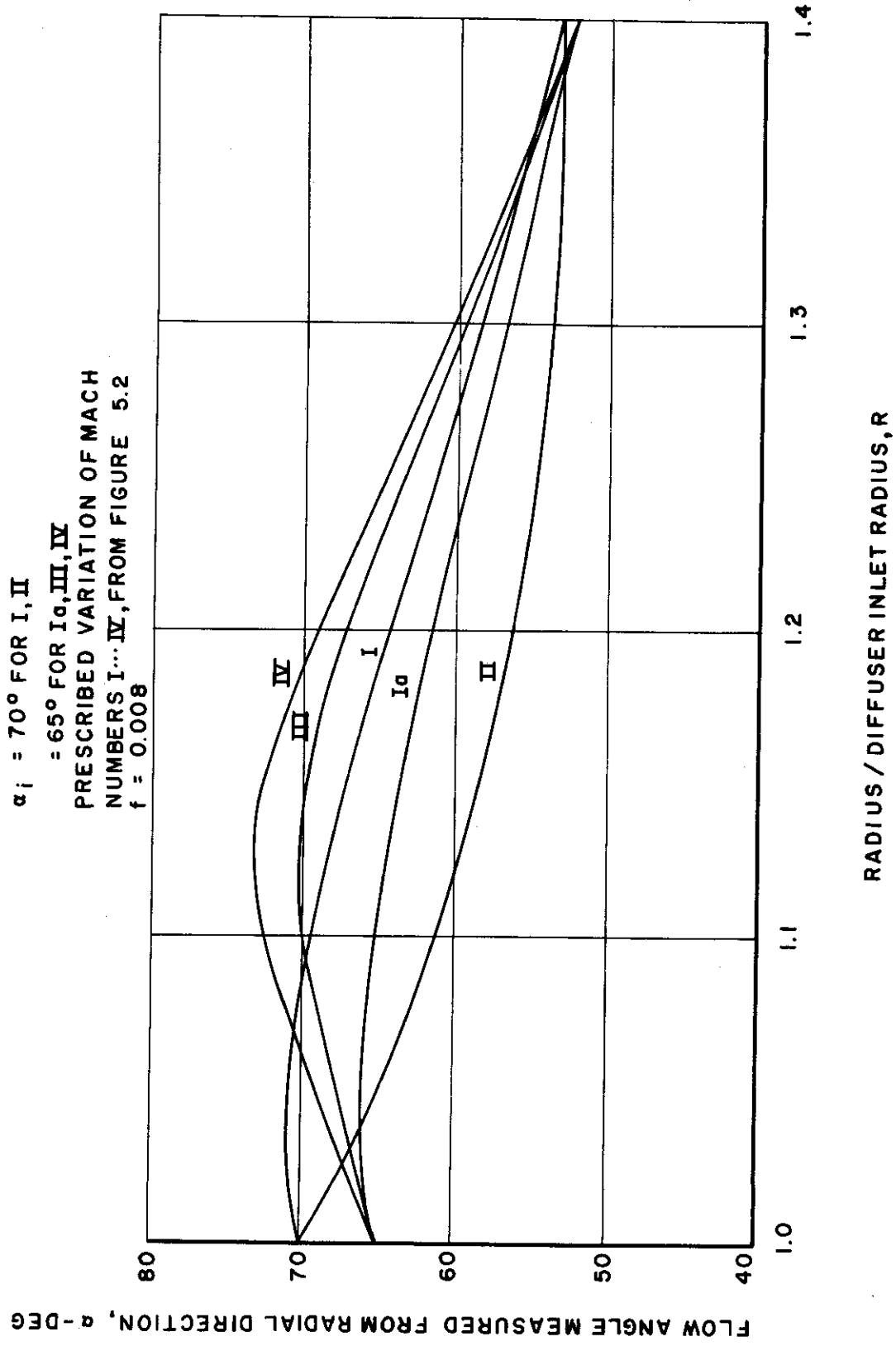
FIG. 5.4    FLOW ANGLE VARIATION IN VANELESS DIFFUSER

INITIAL CONDITIONS

$M_i = 1.15$

$\alpha_i = 70°$ FOR I, II

$= 65°$ FOR III, IV, Ia

PRESCRIBED MACH NUMBER
VARIATION I···IV, FROM FIG. 5.2

$$\eta = \frac{\text{ENTHALPY RISE FOR ISENTROPIC COMPRESSION BETWEEN INLET STATIC AND EXIT TOTAL PRESSURES}}{\text{ENTERING KINETIC ENERGY}}$$

RADIUS/DIFFUSER INLET RADIUS, R
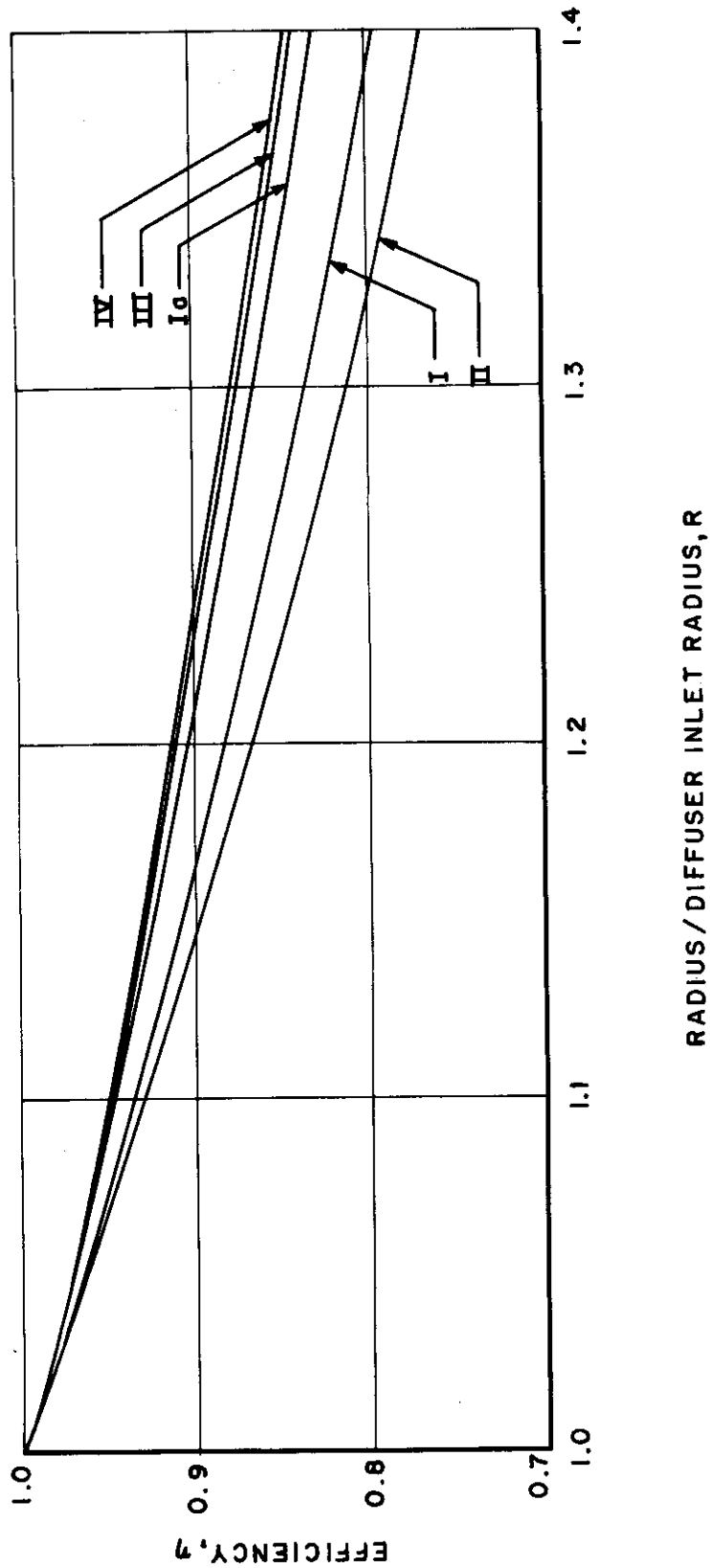
EFFICIENCY, $\eta$

RADIAL VARIATION OF EFFICIENCY
IN VANELESS DIFFUSER

FIG. 5.5
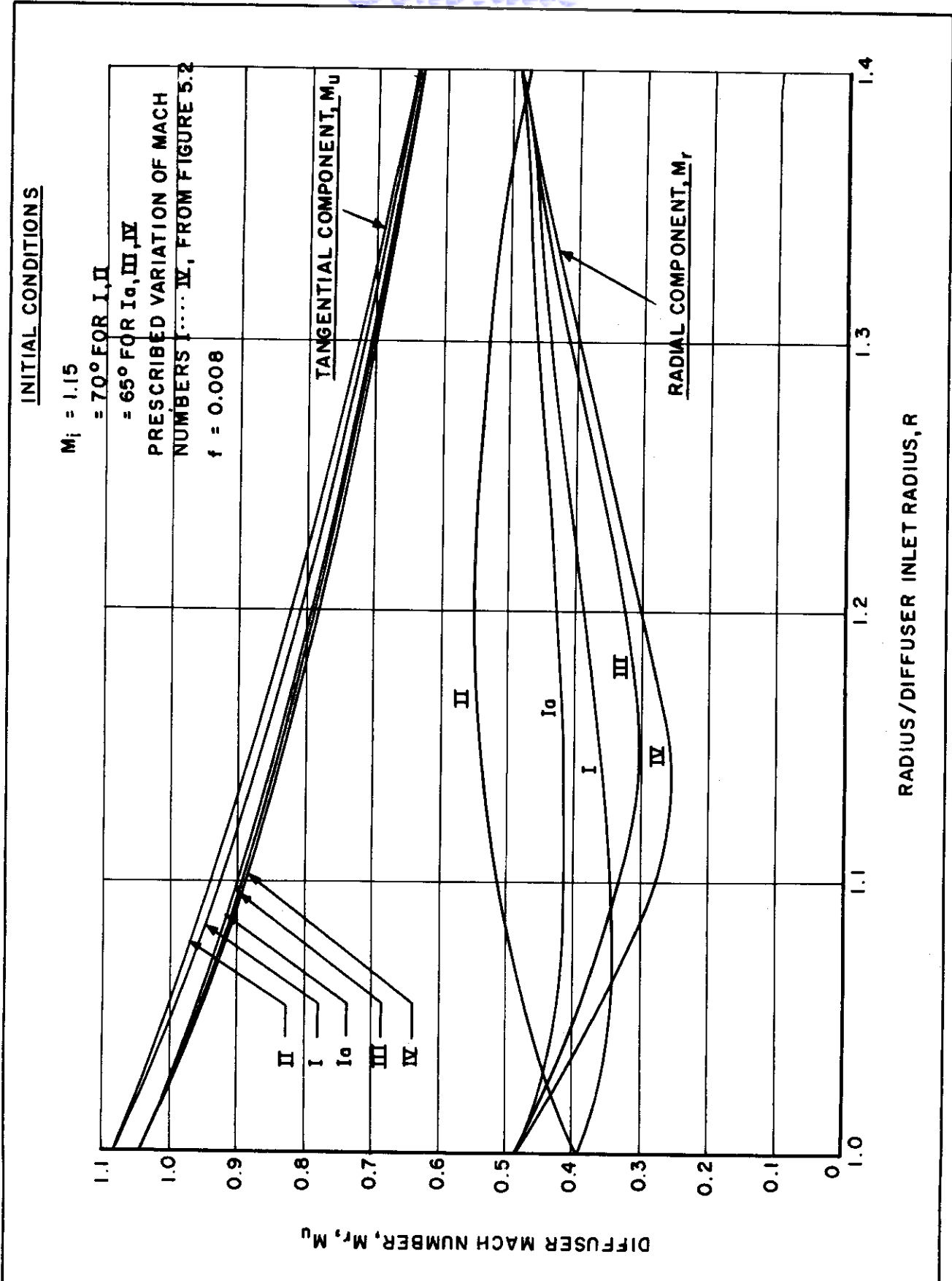
FIG. 5.6    VARIATION OF TANGENTIAL AND RADIAL MACH
NUMBERS IN VANELESS DIFFUSER

$$f = \frac{\tau_0}{\frac{1}{2}\rho V^2}$$

$\tau_0 \equiv$ WALL SHEAR STRESS

DATA FROM REF. 5.9

BLADING V (SUBSONIC)

BLADING T (SUPERSONIC)

$M_i = .70$

$M_i = 1.05$

RADIUS / DIFFUSER INLET RADIUS, R
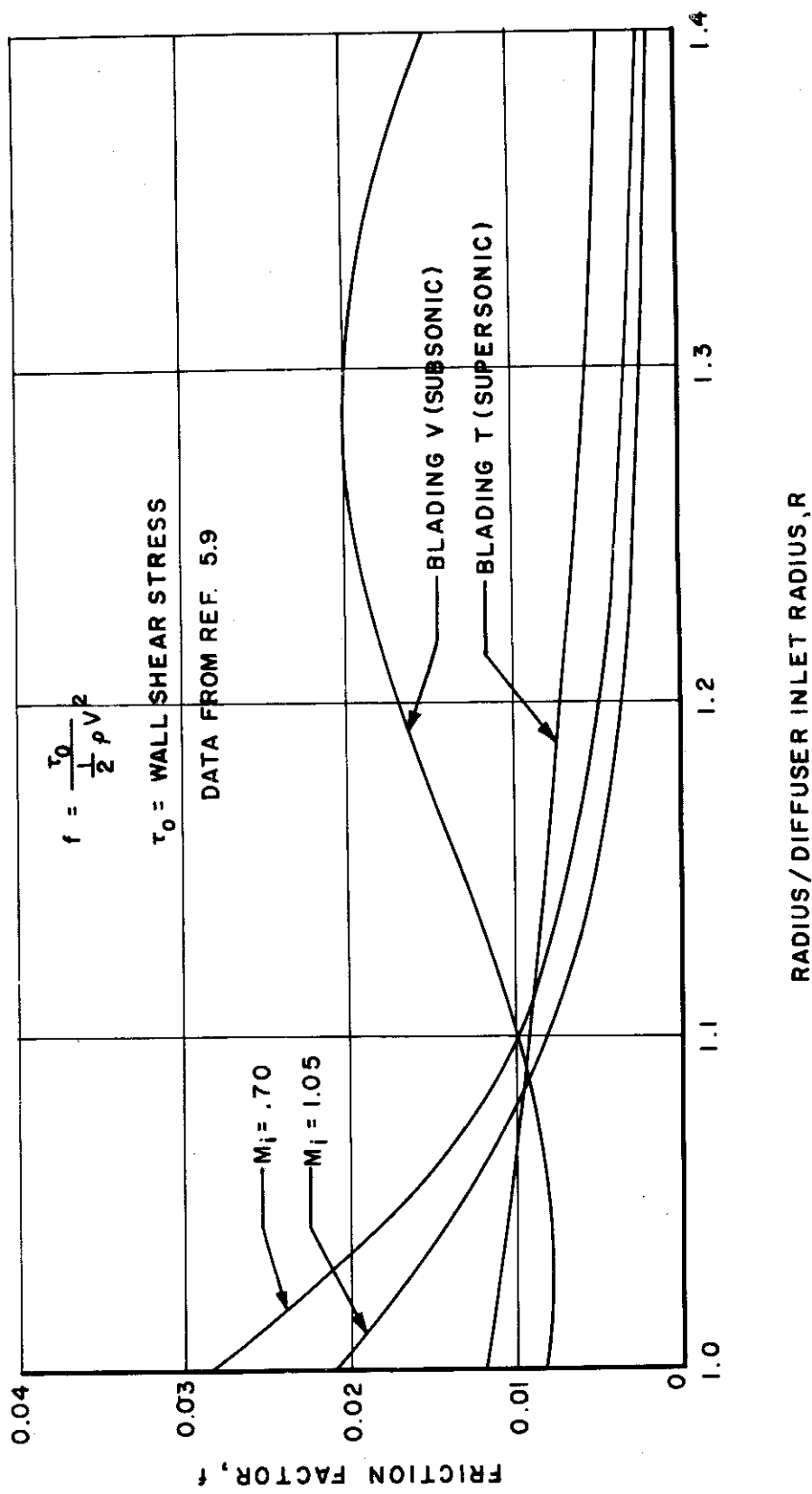
FRICTION FACTOR, f

**FIG. 5.7      FRICTION FACTOR VARIATION IN VANELESS DIFFUSER**
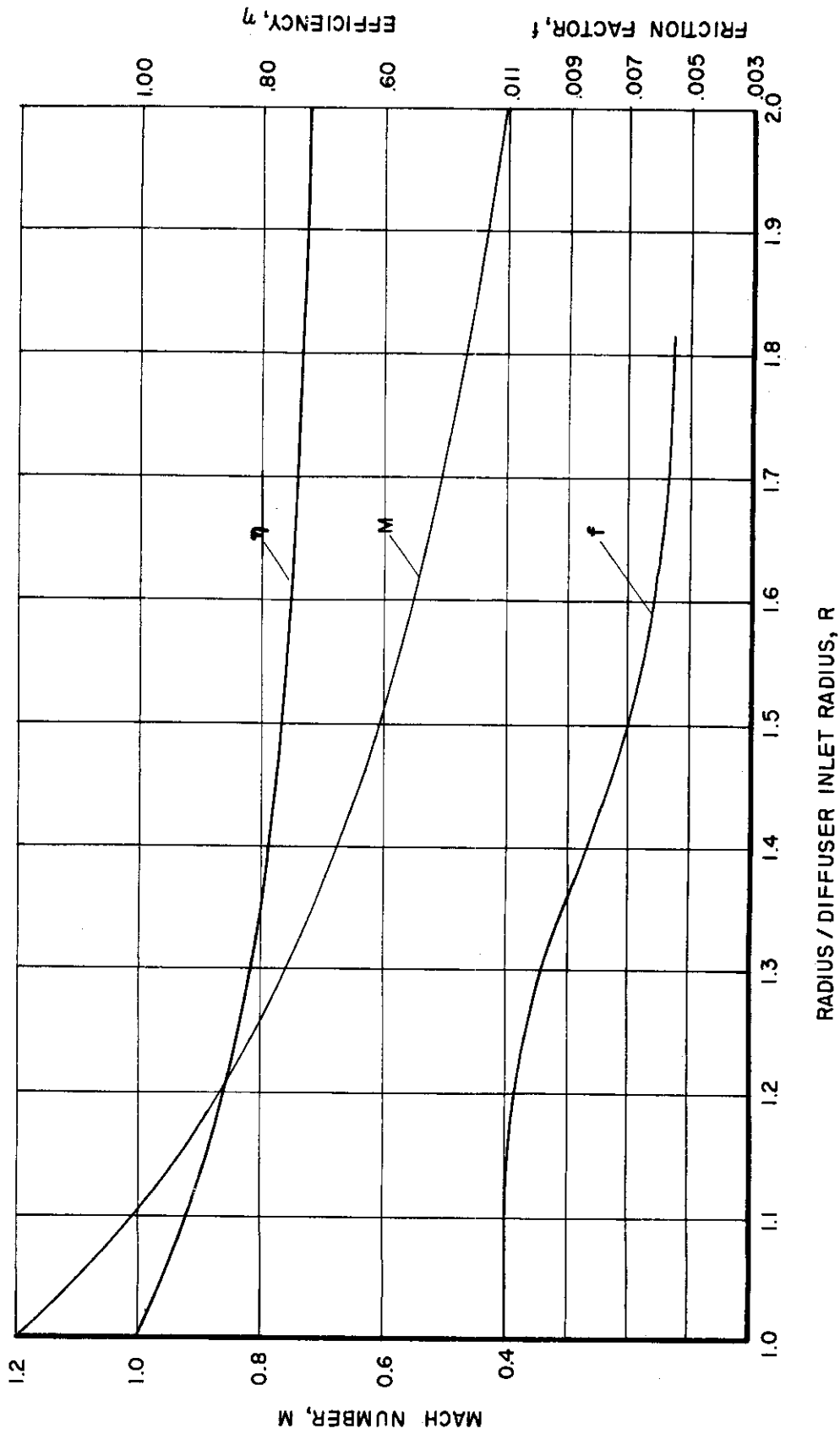
FIG. 5.8　PREDICTED PERFORMANCE OF SUPERSONIC
RADIAL COMPRESSOR VANELESS DIFFUSER

BOUNDARY LAYER

MAIN CORE FLOW

$z$

$r$

$V$

$c$
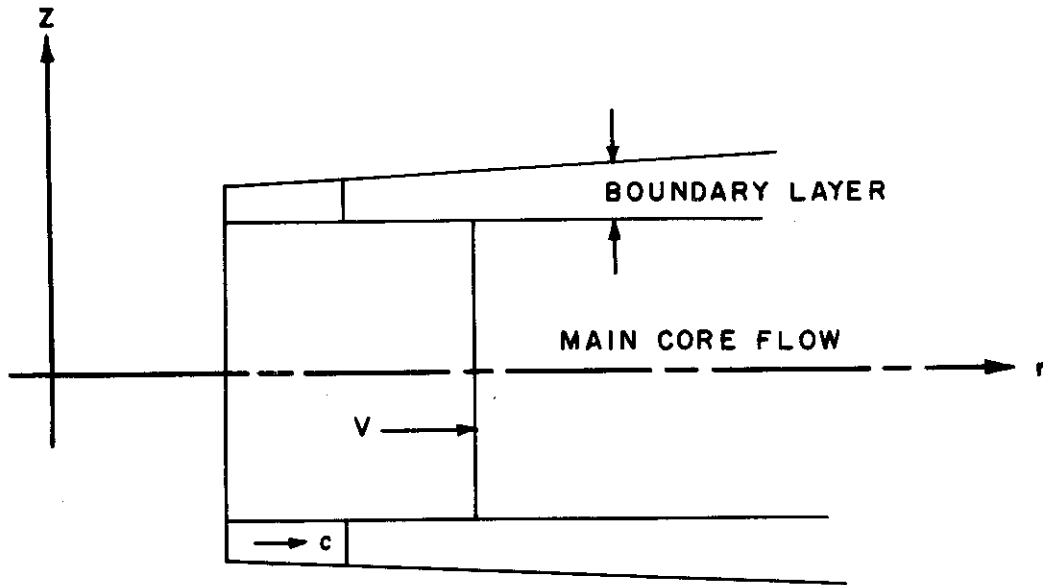
VELOCITY PROFILES AT
DIFFUSER ENTRANCE

$z$

$\delta$

$\tau_o$

$c$

$\tau_m$

$V$

$r$
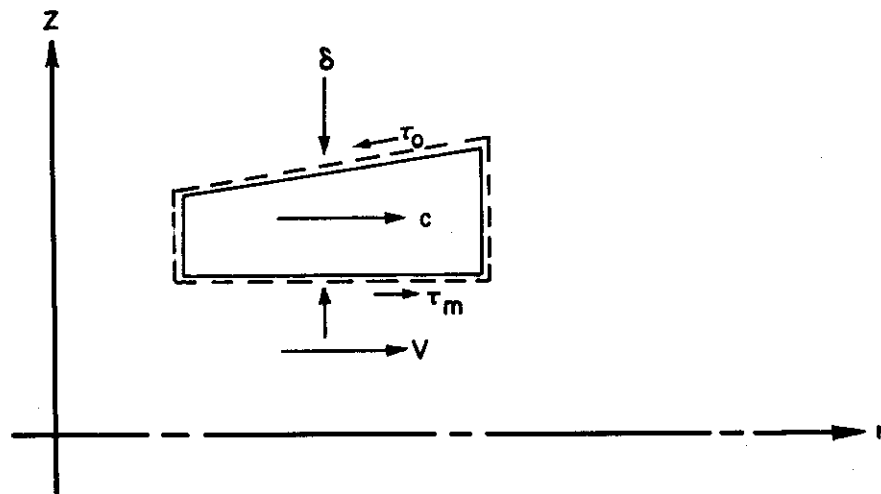
FIG. 5.9     CONTROL VOLUME IN THE BOUNDARY LAYER

VELOCITY
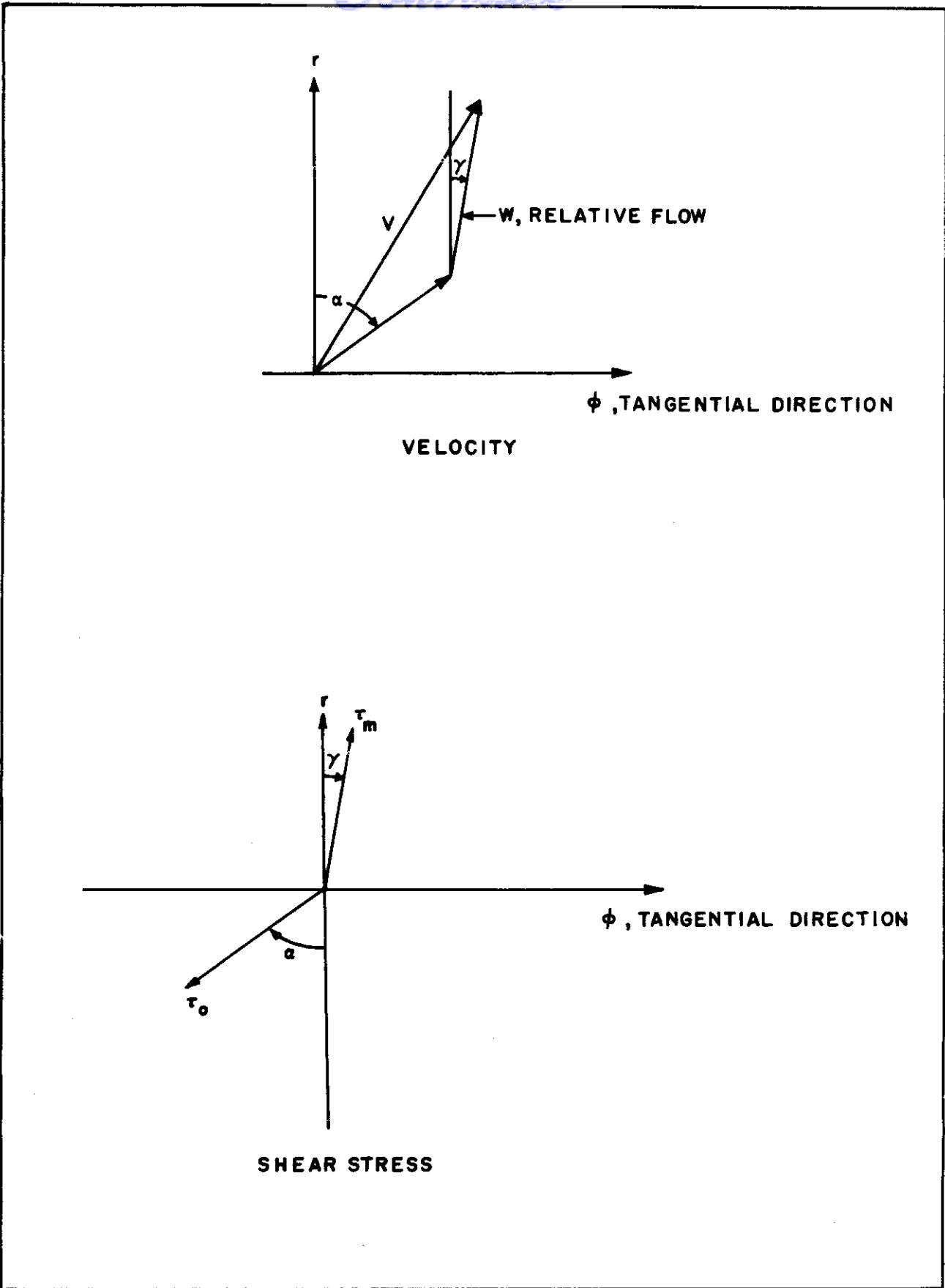


SHEAR STRESS

FIG. 5.10 | VELOCITY AND SHEAR STRESS IN PLANE Z = CONSTANT

INLET CONDITIONS: $r_i/b_i = 12.67$

$a_i = 68.2°$

$M_i = 1.07$

FRICTION FACTOR $f = 0.008$



MACH NUMBER, M

TANGENTIAL COMPONENT
OF MACH NUMBER, $M_u$

PRESSURE DISTRIBUTION, $p/p_0$

MACH NUMBER, PRESSURE RATIO—M, $M_u$, $p/p_0$

RADIUS / DIFFUSER INLET RADIUS, R
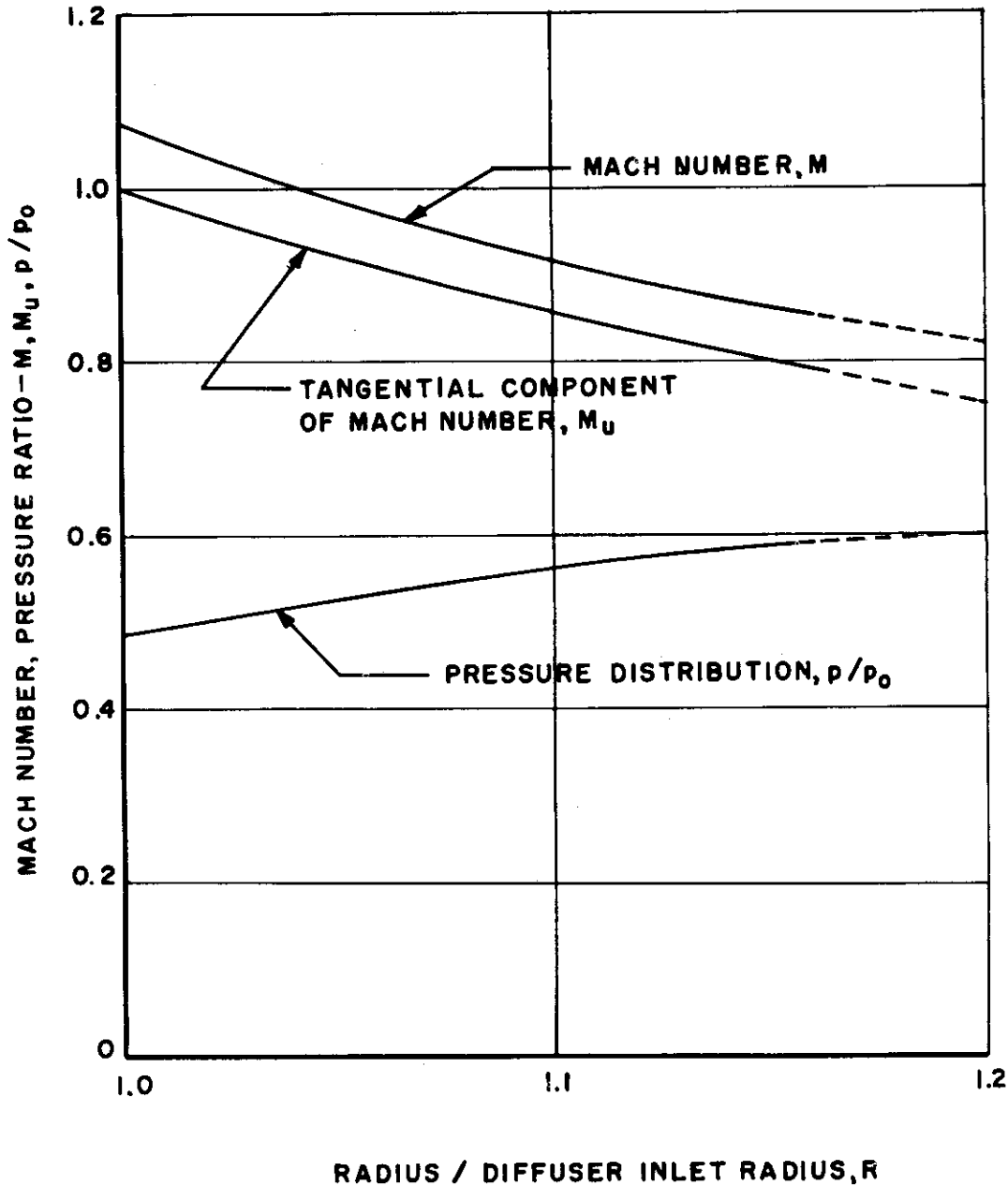
FIG. 5.11

CHARACTERISTIC OF MAIN CORE
FLOW IN VANELESS DIFFUSER

DIFFUSER WIDTH BASED ON MAIN
CORE FLOW AND BOUNDARY LAYER FLOW

BOUNDARY LAYER FLOW
ENTRANCE CONDITIONS

$C_{u_i} = .908$     $M_i = 1.019$

$C_{r_i} = .188$     $\alpha_i = 78.2°$

$\delta_i = .075$

$\delta$ BOUNDARY
LAYER THICKNESS

f = 0.010

DIFFUSER WIDTH BASED
ON MAIN CORE FLOW

f = 0.008

MAIN CORE FLOW
EXIT

$M_e = 0.85$

$\eta = 0.91$

MAIN CORE FLOW
ENTRANCE CONDITIONS

$M_i = 1.07$

$\alpha_i = 68.2°$

$C_{u_i} = .908$

$C_{u_i} = .377$

B = DIFFUSER WIDTH / INLET WIDTH BASED ON
MAIN CORE FLOW

$\delta$ = BOUNDARY LAYER THICKNESS / INLET WIDTH
BASED ON MAIN CORE FLOW

B / 2

RADIUS / DIFFUSER INLET RADIUS, R

FIG. 5.12     VARIATION OF DIFFUSER WIDTH
IN VANELESS DIFFUSER

MAIN CORE FLOW PATH

BOUNDARY LAYER FLOW PATH

1.25

1.0

α

α

10°

DIFFUSER EXIT R=1.16

DIFFUSER INLET R=1.0
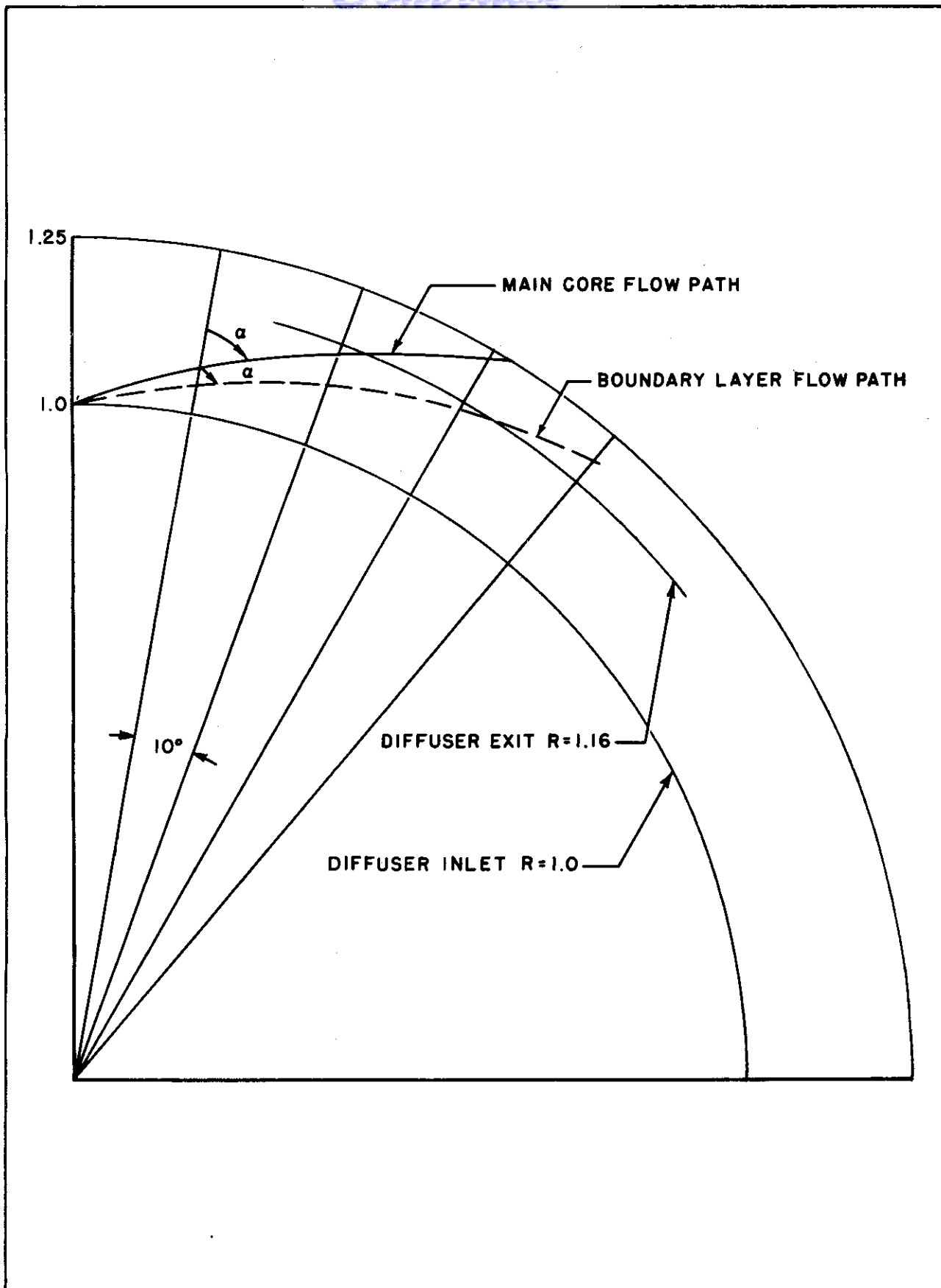
FIG. 5.13 VANELESS DIFFUSER FLOW PATH

Y = 16.7% PITCH — CURVE A
= 50.0% PITCH — CURVE B
= 83.3% PITCH — CURVE C

FLOW

$\left(\dfrac{V}{V_\mathbb{C}}\right)^2$

Z
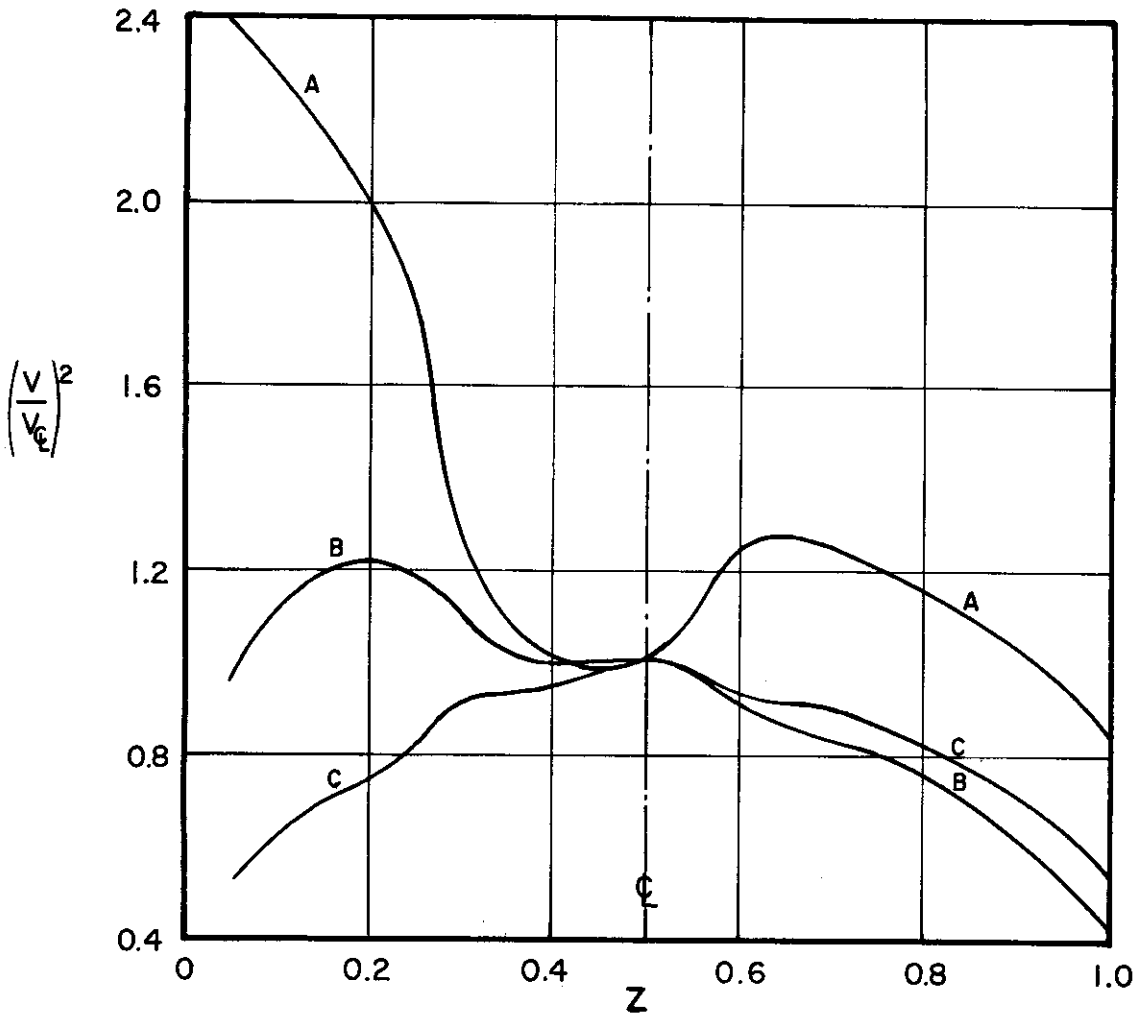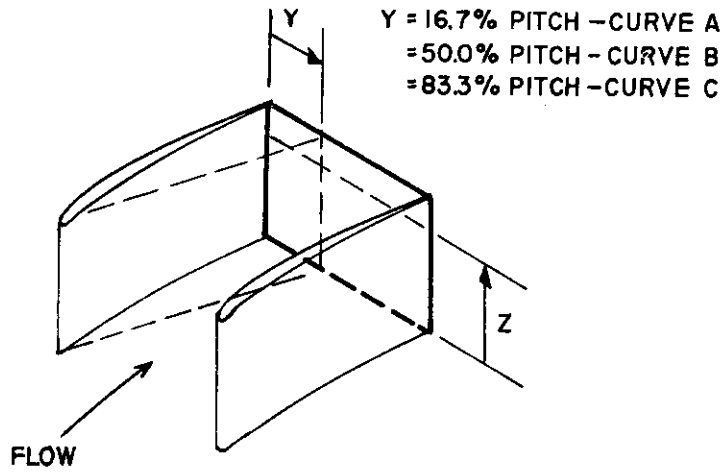
FIG. 5.14    MAP OF VELOCITY AT PLANE OF DIFFUSER EXIT

QUASI STEADY
FLOW

NON-SEPARATED
FLOW

U

U

(a)

POTENTIAL CORE

THE FLOW IN CONICAL DIFFUSER

U

U

(b)

$\delta^*$

DISPLACEMENT THICKNESS

PHYSICAL REPRESENTATION

X

$\tau_0 D$

A

u

B

U

C

R

r

Y

(c)

AXIS OF SYMMETRY

WALL OF CONICAL DIFFUSER

CONTROL VOLUME
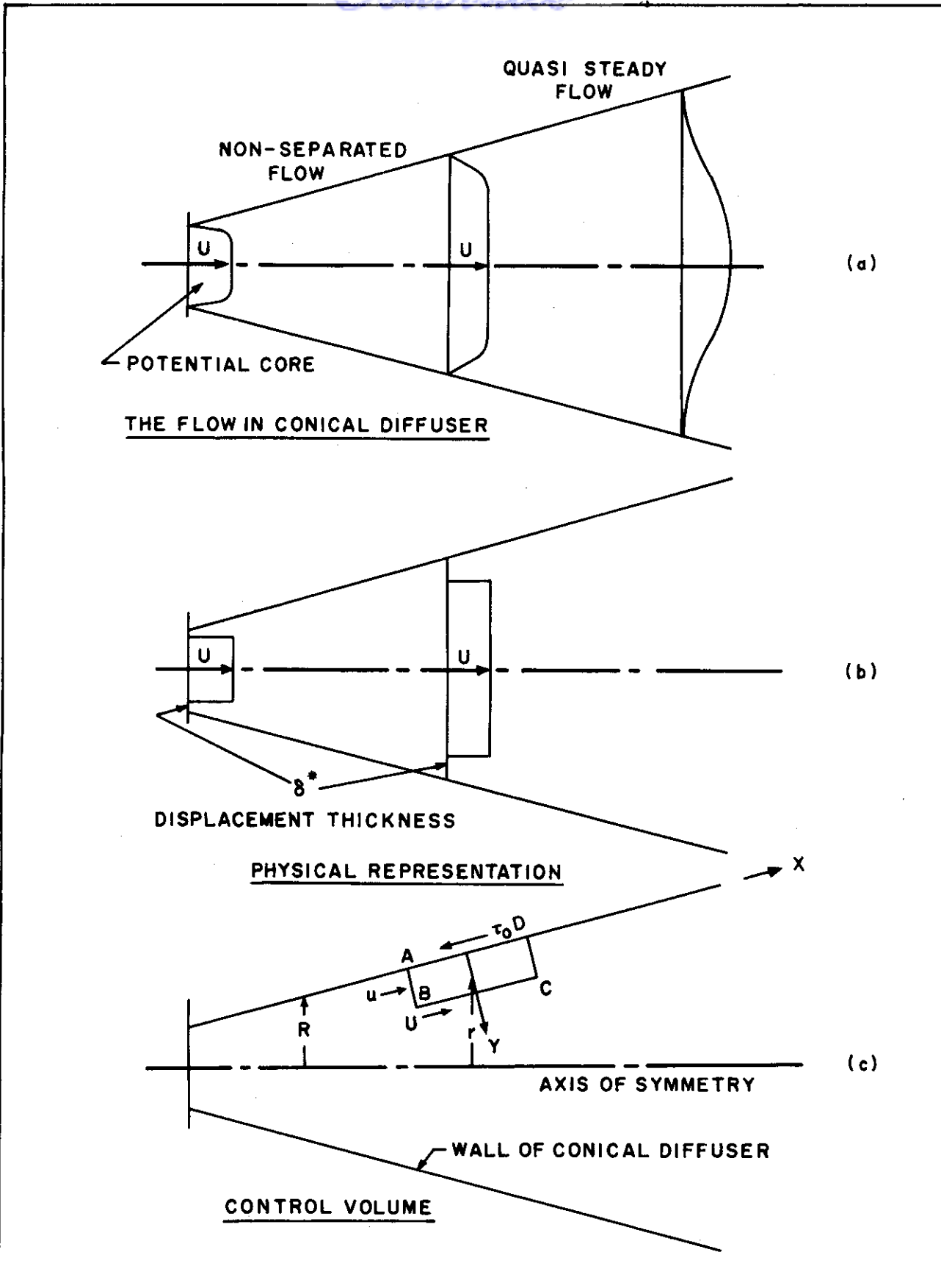
FIG. 5.15          THE FLOW IN A CONICAL DIFFUSER
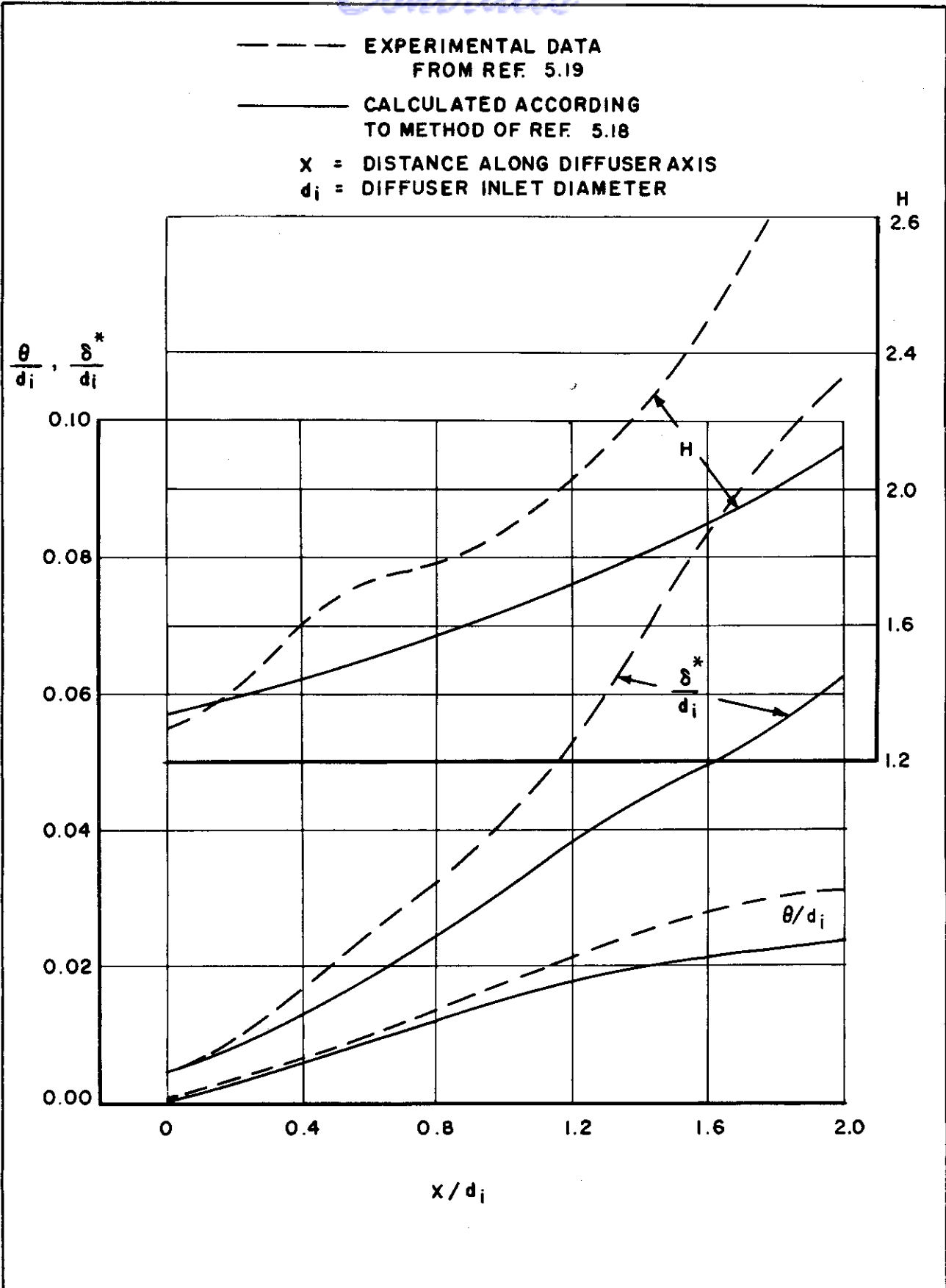
BOUNDARY LAYER CHARACTERISTICS
IN A 12° CONE DIFFUSER
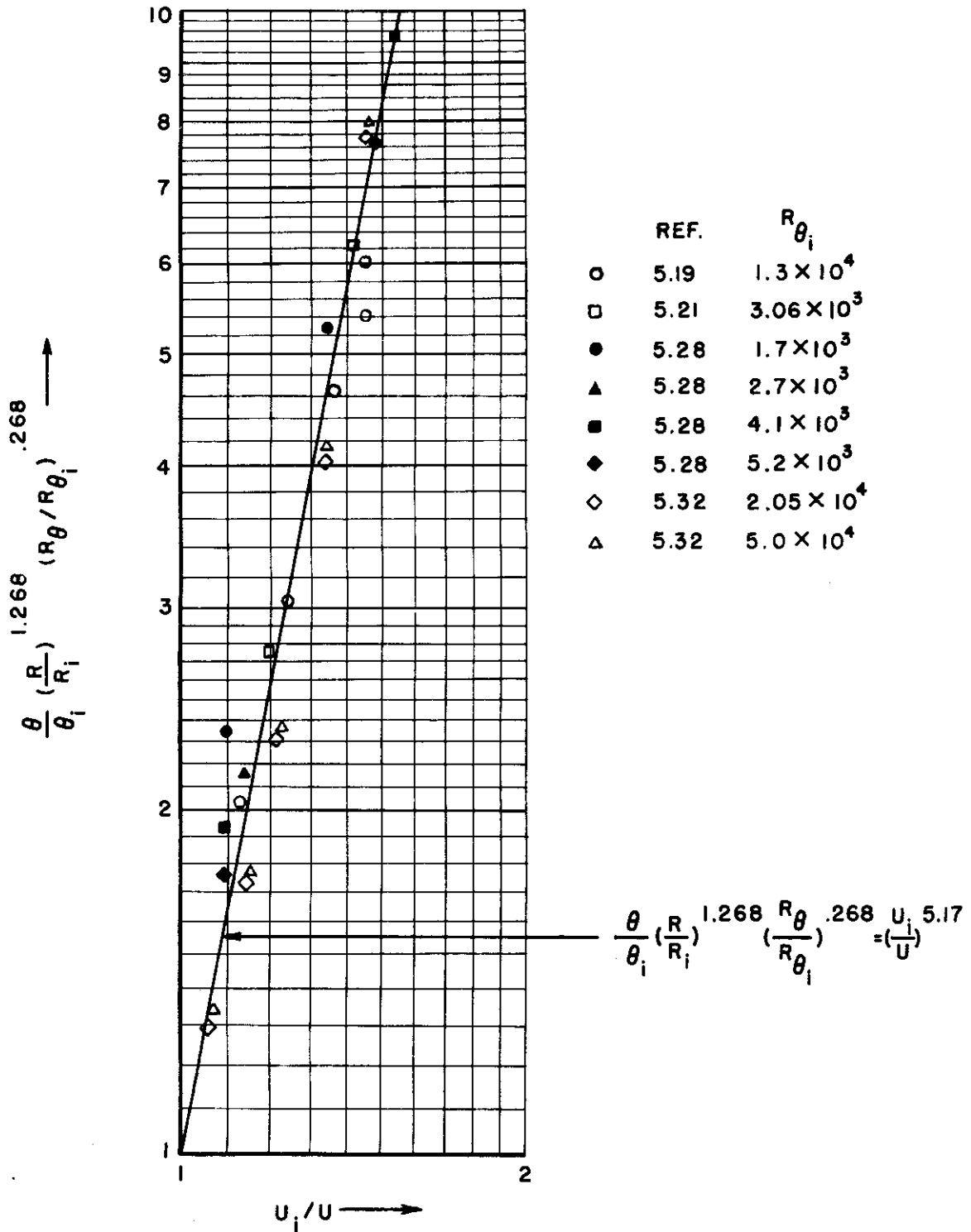
FIG. 5.16

CORRELATION FOR MOMENTUM THICKNESS IN CONICAL DIFFUSERS

FIG. 5.17

DIFFUSER AXIS

DIFFUSER WALL

LOW SPEED FLOW

HIGH SPEED FLOW

PRESSURE

MAXIMUM VELOCITY

ACCELERATION STARTS

DISTANCE ALONG DIFFUSER AXIS
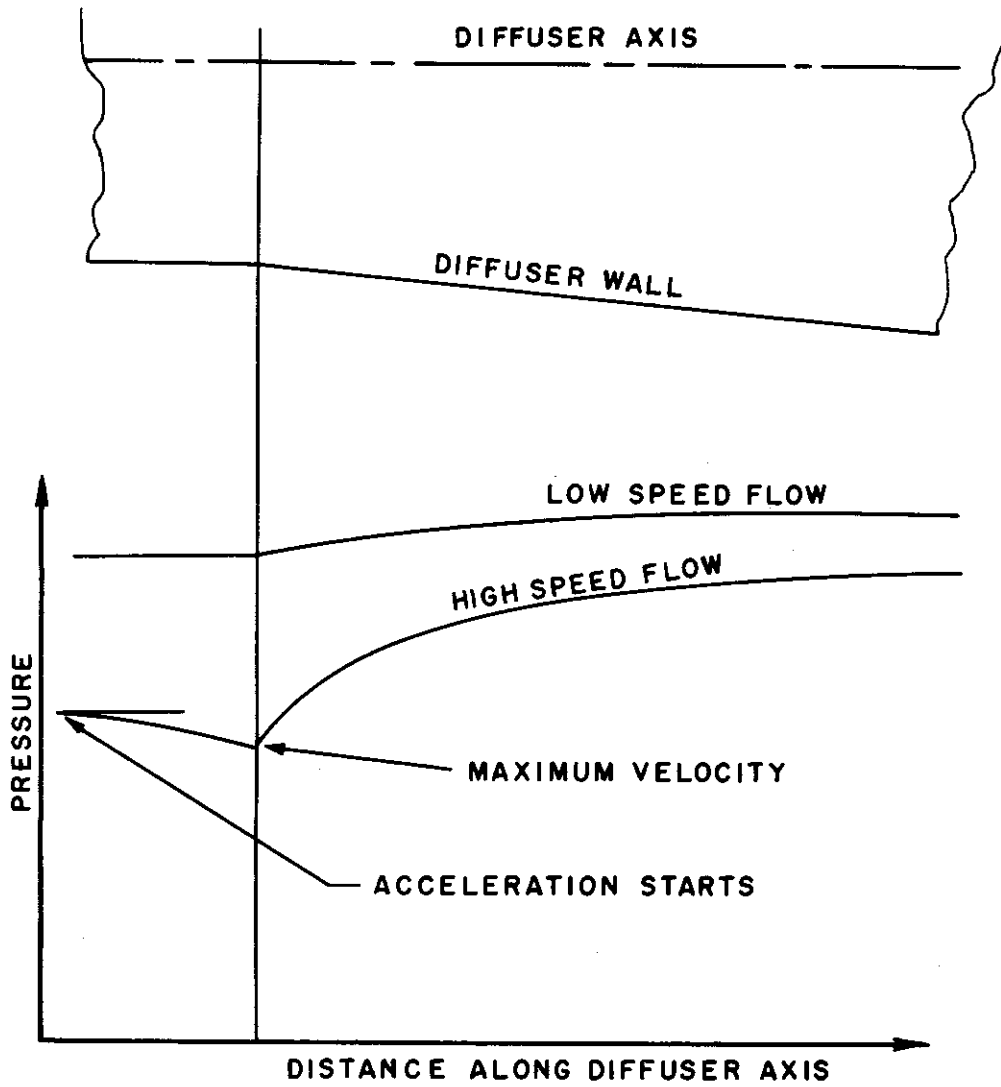
FIG. 5.18    INLET CONDITIONS TO CONICAL DIFFUSER

| REF. | $M_i$ |
|------|-------|
| □ 5.19 | 0.645 |
| ◇ 5.19 | 0.853 |
| △ 5.19 | 0.931 |
| ● 5.32 | 0.262 |
| ■ 5.32 | 0.500 |
| ◆ 5.32 | 0.671 |
| ▲ 5.32 | 0.765 |
| × 5.32 | 0.830 |
| ▼ 5.32 | 0.900 |

$$\frac{\theta}{\theta_i}\left(\frac{R}{R_i}\right)^{1.268}\left(\frac{R_\theta}{R_{\theta_i}}\right)^{.268} = \left(\frac{U_i}{U}\right)^{5.17}$$
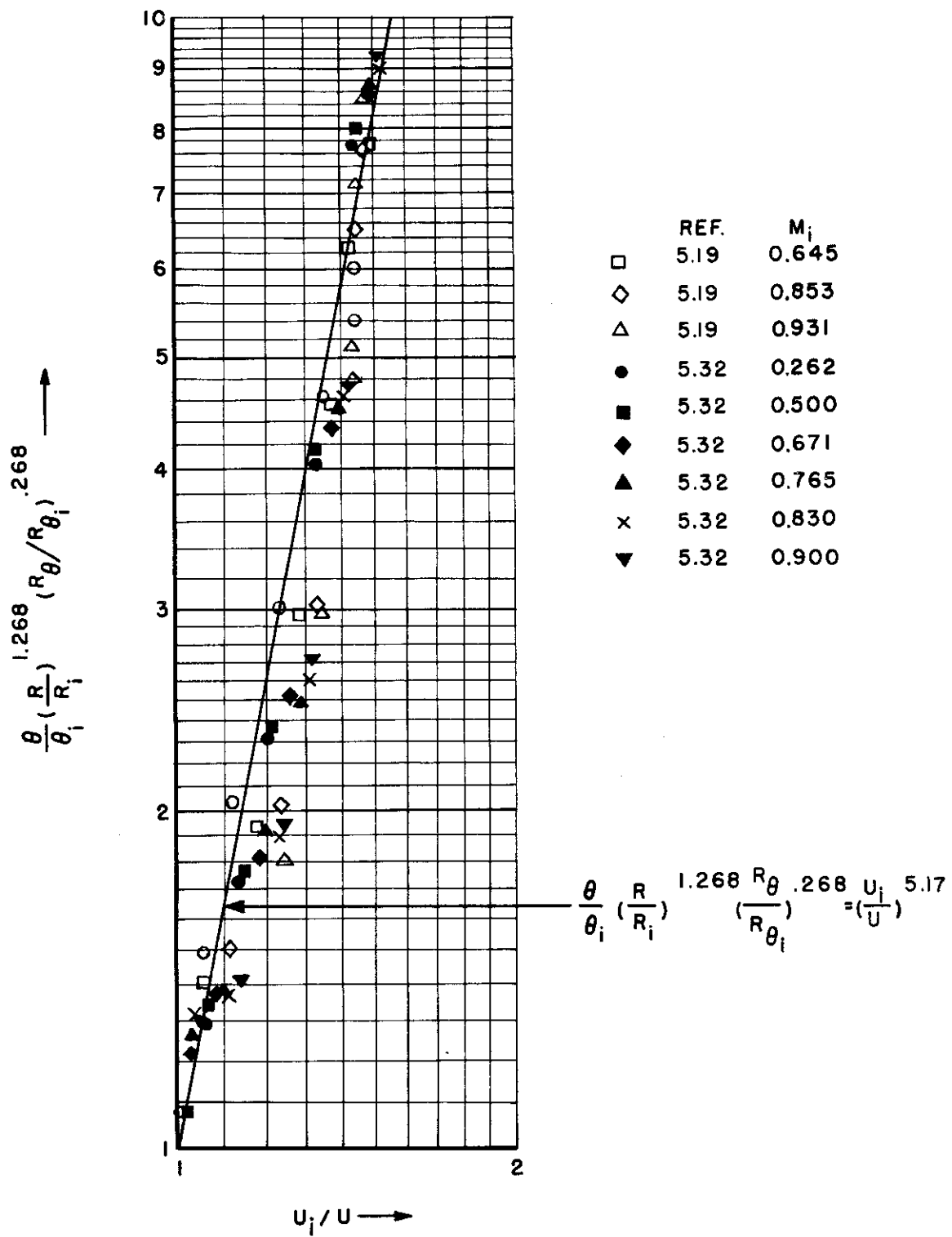
**FIG. 5.19**   **EFFECT OF LARGE PRESSURE GRADIENT ON MOMENTUM THICKNESS IN CONICAL DIFFUSERS**

$$\Gamma = \frac{-0.246}{c_f} \; \frac{\theta}{U} \; \frac{dU}{dX}$$

**TYPICAL VARIATION OF $\Gamma$ WITH H
IN A CONICAL DIFFUSER**

FIG. 5.20

DATA FROM REF. (5.32)
(THICKER BOUNDARY LAYER)

$P_i/H_o$

| | |
|---|---|
| ○ | 0.953 |
| □ | 0.855 |
| ◇ | 0.753 |
| △ | 0.692 |
| ▽ | 0.644 |
| × | 0.598 |
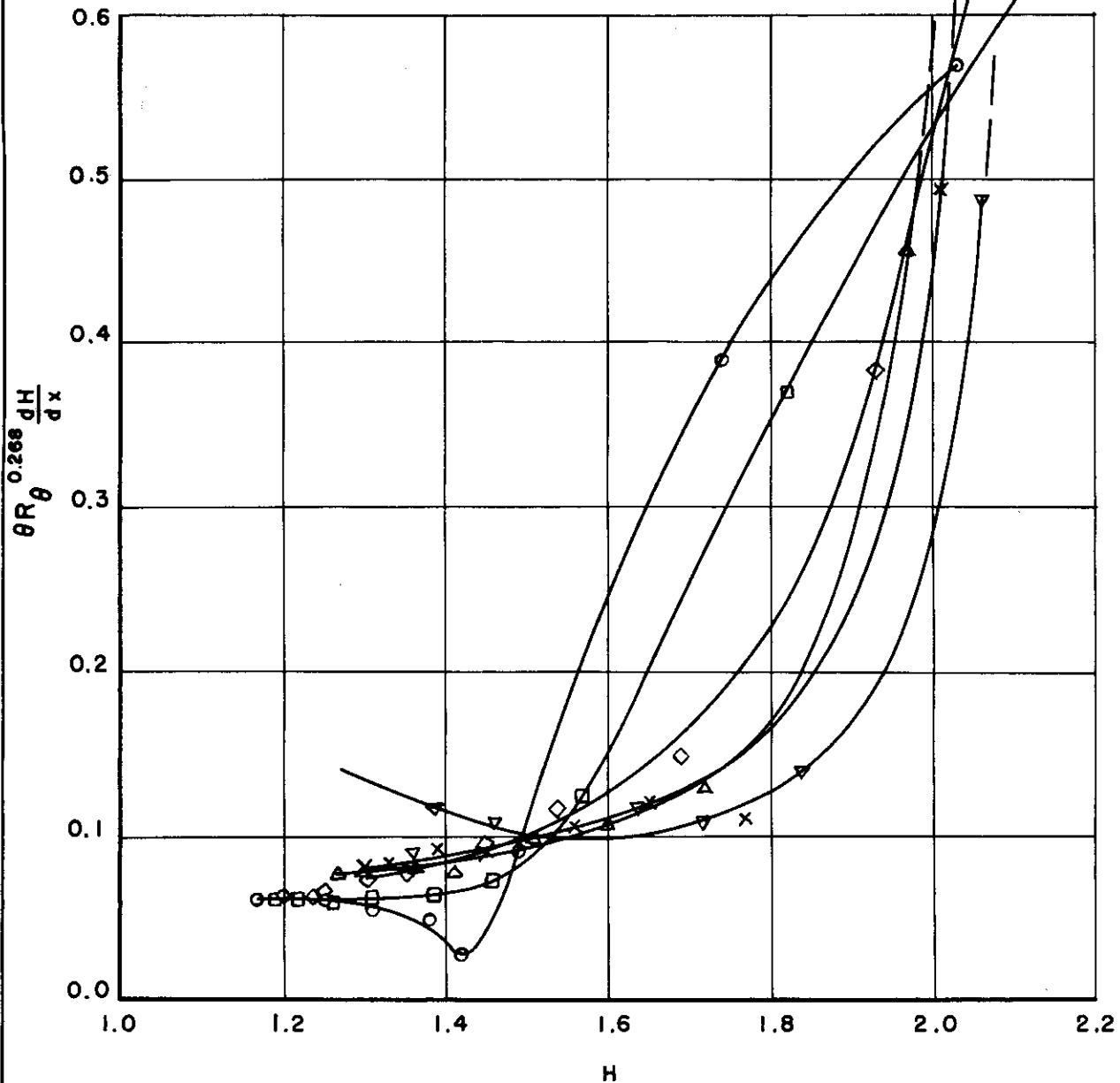
FIG. 5.21  TYPICAL VARIATION OF $\theta R_\theta^{0.268} \frac{dH}{dx}$ WITH H IN A CONICAL DIFFUSER
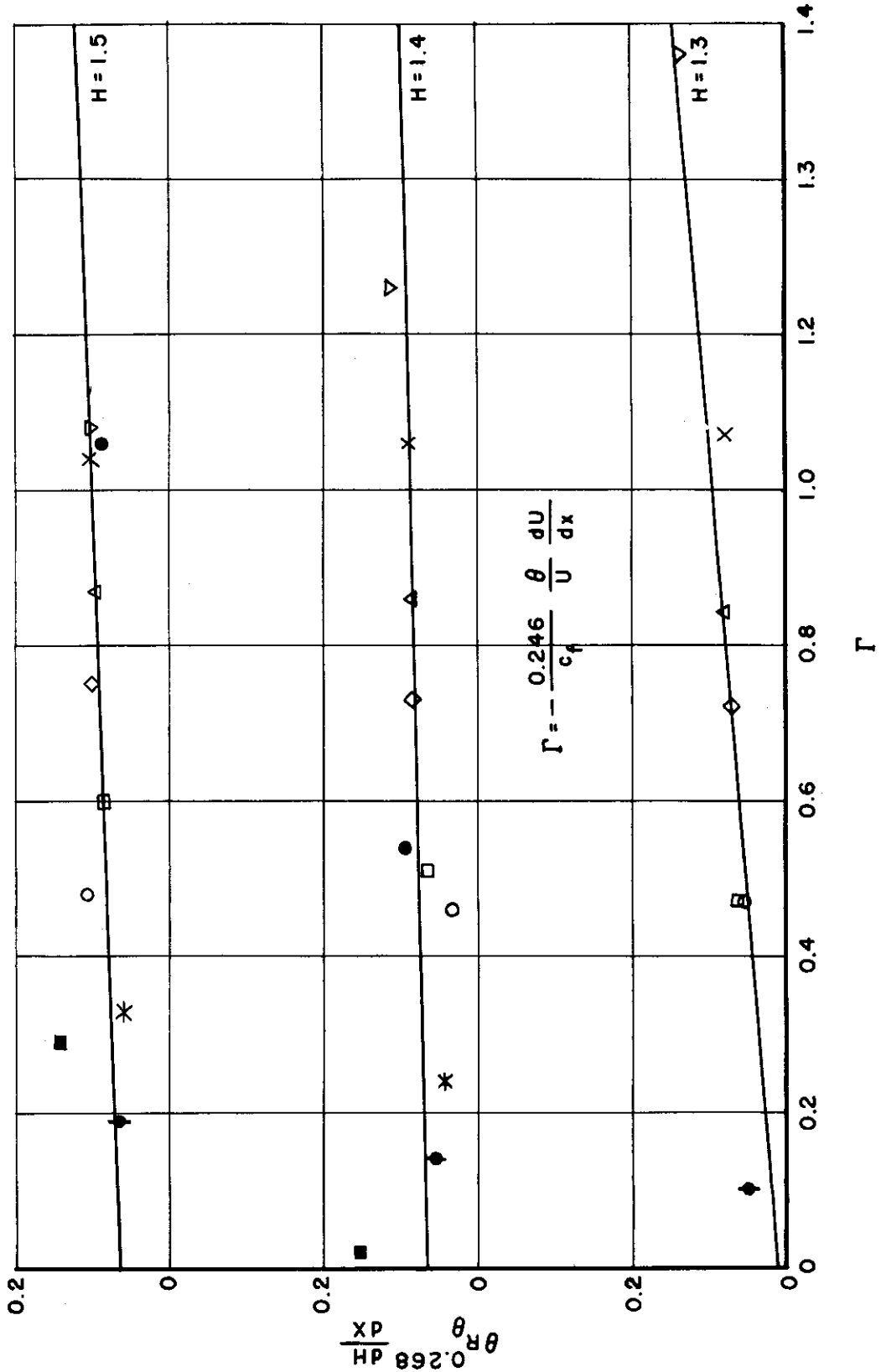
FIG. 5.22a   VARIATION OF $\theta R_\theta .268 \frac{dH}{dx}$ WITH $\Gamma$,
FOR CONSTANT SHAPE PARAMETER H

$$\Gamma = -\frac{0.246}{c_f}\frac{\theta}{U}\frac{dU}{dx}$$

FIG. 5.22b

VARIATION OF $\theta R_\theta \, 0.268 \frac{dH}{dx}$ WITH $\Gamma$

FOR CONSTANT SHAPE PARAMETER H

$H \geq 1.55 \quad f(H) = 0.100 - 3.08(H-1.5)(H-1.289)(H-2.0)$
$+ 0.761 (H-1.596)$

$H \leq 1.55 \quad f(H) = 0.100 - 3.08(H-1.5)(H-2.0)(H-1.289)$
$+ 2.33(H-1.286)(H-1.587)(H-0.011)$

$\theta R_\theta^{0.268} \dfrac{dH}{dX} = f(H)\Gamma + g(H)$

$\Gamma = -0.246 \dfrac{\theta}{c_f} \dfrac{1}{U} \dfrac{dU}{dX}$

$c_f = 0.246 \, e^{-1.561H} R_\theta^{-0.268}$

f(H)

g(H)

$H \geq 1.55 \quad g(H) = -0.761(H-1.596)$

$H \leq 1.55 \quad g(H) = -2.330(H-1.286)(H-1.587)(H-0.011)$

H ⟶

0.40
0.30
0.20
0.10
0
−0.10
−0.20
−0.30

1.3  1.4  1.5  1.6  1.7  1.8  1.9

f(H),
g(H)
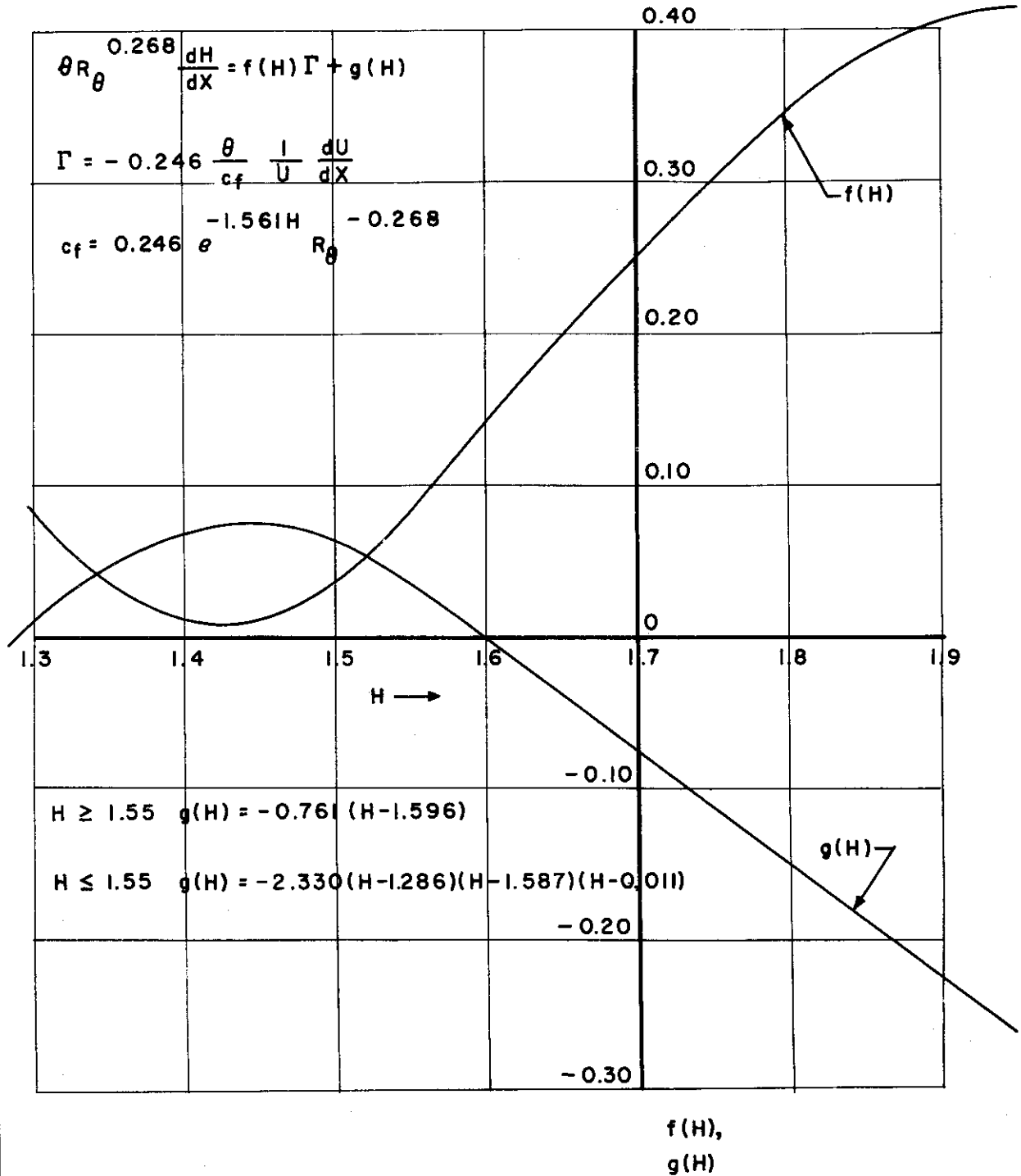
FIG. 5.23  THE FUNCTION $\theta R_\theta^{0.268} \dfrac{dH}{dX} = f(H)\Gamma + g(H)$
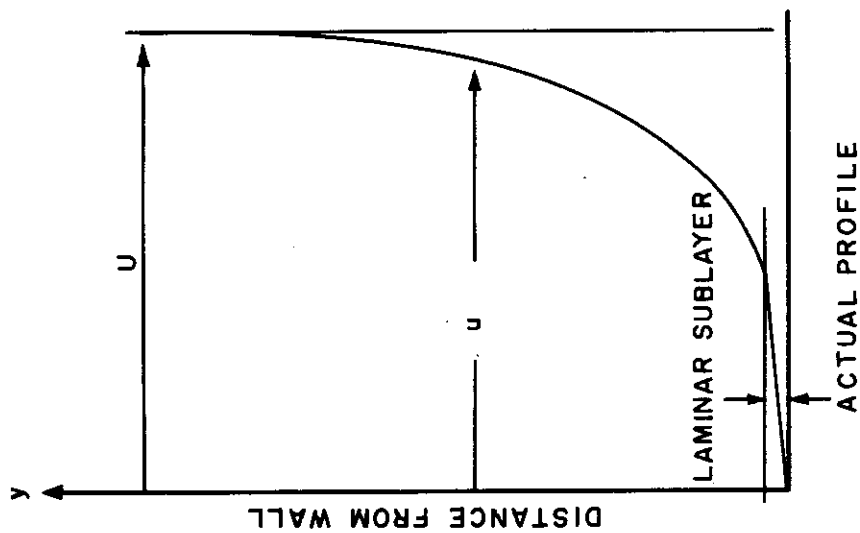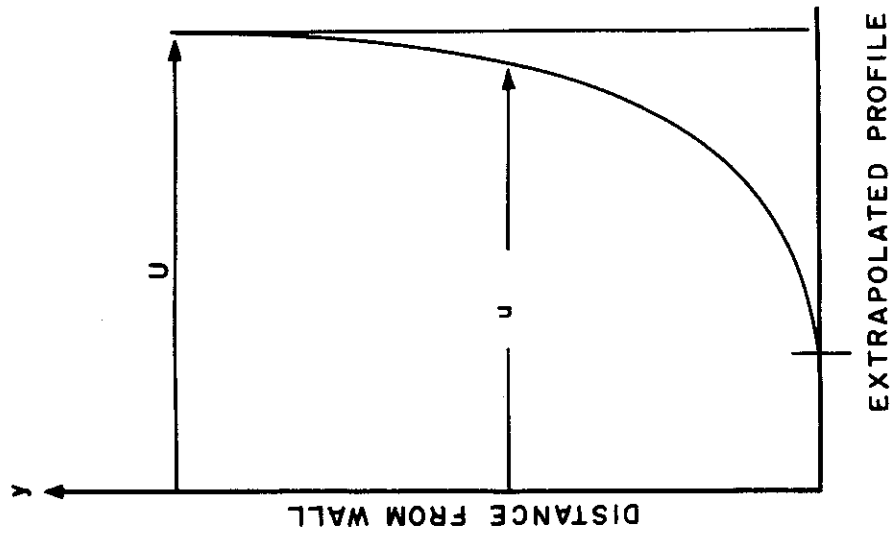
VELOCITY PROFILE IN TURBULENT
BOUNDARY LAYERS

FIG. 5.24a

| $10^{-4}R_\theta$ | $R_i/H_o$ | $U_i/U$ | $\Gamma$ | $H$ | $U_i/U$ | $\Gamma$ | $H$ | $H_i$ |
|---|---|---|---|---|---|---|---|---|
| 2.31 | 0.953 | 1.48 | 0.64 | 1.82 | 1.50 | 2.17 | 1.96 | 1.20 |
| 3.78 | 0.855 | 1.41 | 1.25 | 1.70 | 1.48 | 1.30 | 1.90 | 1.24 |
| 4.62 | 0.753 | 1.39 | 0.92 | 1.70 | 1.48 | 1.60 | 1.90 | 1.26 |
| 5.15 | 0.692 | 1.39 | 1.09 | 1.72 | 1.48 | 1.60 | 1.90 | 1.30 |
| 5.45 | 0.644 | 1.40 | 1.12 | 1.75 | 1.49 | 1.46 | 1.90 | 1.34 |
| 5.64 | 0.598 | 1.37 | 1.20 | 1.78 | 1.48 | 1.42 | 1.91 | 1.40 |

$(\frac{\theta}{d})_i = 0.0075$
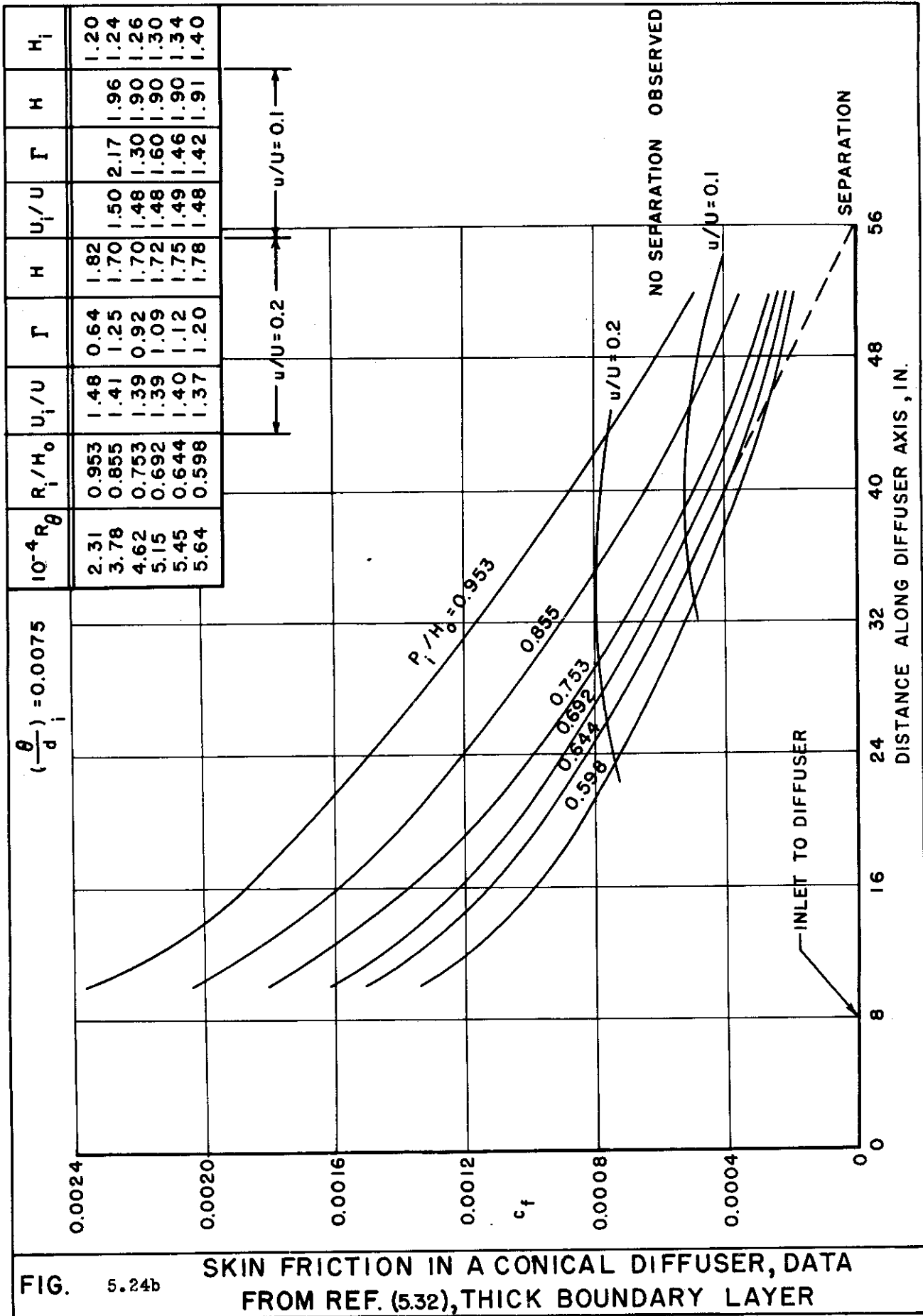
**FIG.** 5.24b  SKIN FRICTION IN A CONICAL DIFFUSER, DATA
FROM REF. (5.32), THICK BOUNDARY LAYER

| $10^{-4} R_{\theta_i}$ | Pref/$H_o$ | $U_i/U$ | H | $U_i/U$ | $H_i$ |
|---|---|---|---|---|---|
| | | u/U = .2 | | u/U = .1 | |
| .57 | .965 | 1.39 | 2.1 | 1.41 | 2.6 | 1.34 |
| 1.00 | .723 | 1.50 | 2.1 | 1.77 | 2.6 | 1.41 |
| 1.09 | .646 | 1.38 | 2.6 | 1.76 | 2.40 | 1.53 |

$\left(\dfrac{\theta_i}{d_i}\right) = .0032$

$c_f$
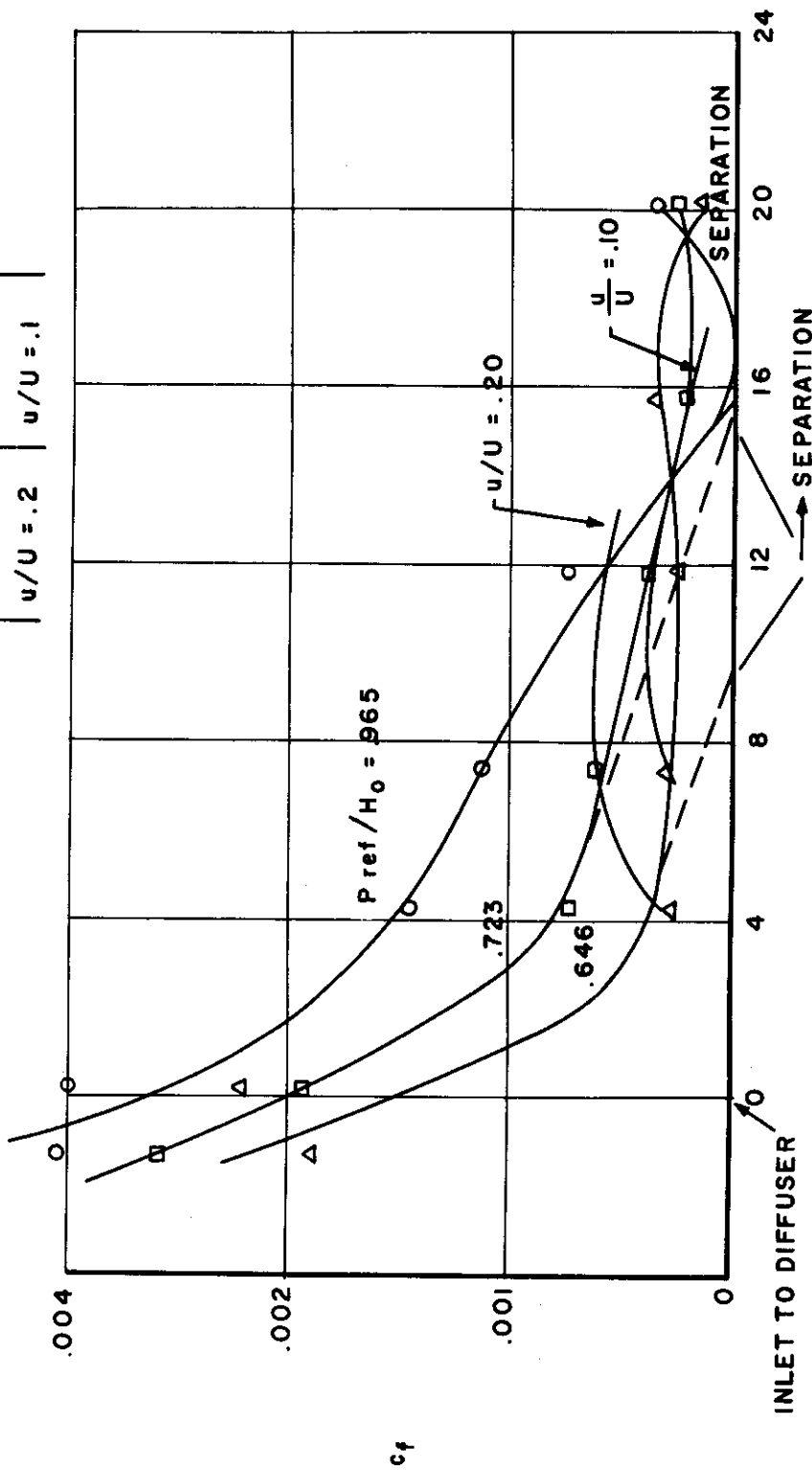
DISTANCE ALONG DIFFUSER AXIS, INCHES

INLET TO DIFFUSER

FIG. 5.24c   SKIN FRICTION IN A CONICAL DIFFUSER, DATA FROM REF (5.32), THICK BOUNDARY LAYER
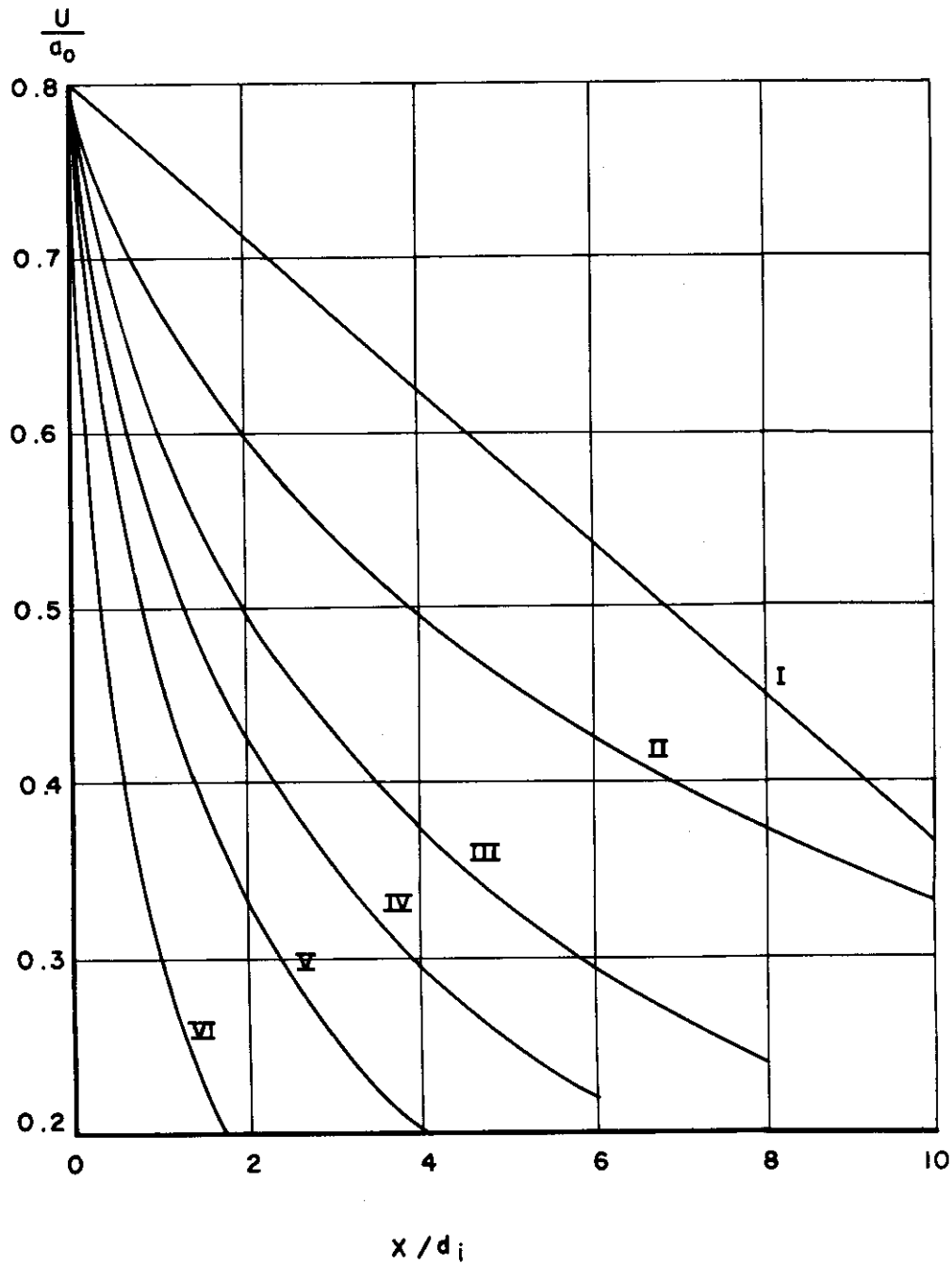
VARIATION OF THE VELOCITY IN THE
POTENTIAL CORE OF CONICAL DIFFUSER

FIG. 5.25

$H_i = 1.4$
$(\theta/d)_i = .04$
DIST. III

$R_{\theta_i} = 20,000$

$R_{\theta_i} = 70,000$

$H_i = 1.4$
$(\theta/d)_i = 0.04$
DIST. IV

$R_{\theta_i} = 20,000$

$R_{\theta_i} = 70,000$
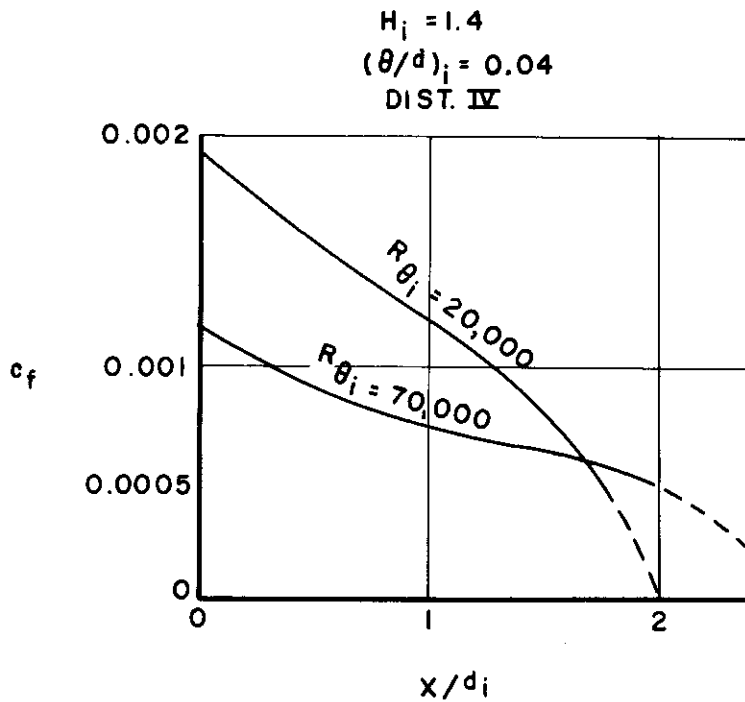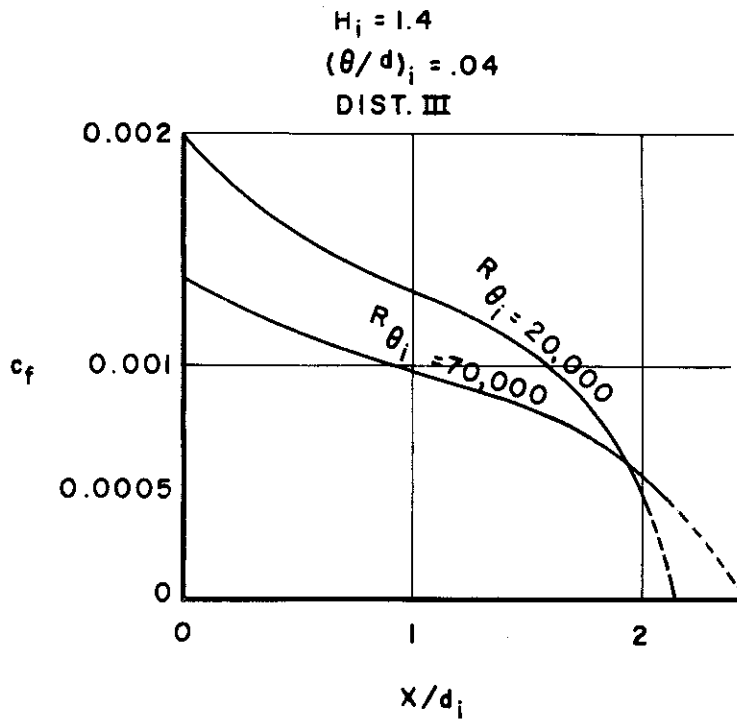
FIG. 5.26    EFFECT OF THE INITIAL REYNOLDS
NUMBER ON THE SEPARATION

INITIAL MOMENTUM THICKNESS $(\frac{\theta}{d})_i = 0.02$

LINES OF IMMINENT SEPARATION $c_f = 0.0005$

WITH INITIAL SHAPE PARAMETER $H_i$

$H_i$

1.6

1.5

1.4

MAXIMUM DIFFUSION LINES

LINE OF $\frac{\delta}{R} = 1$

B.L. FILLS THE CHANNEL

I

II

III

IV

V

VI

$U/a_0$

$X/d_i$
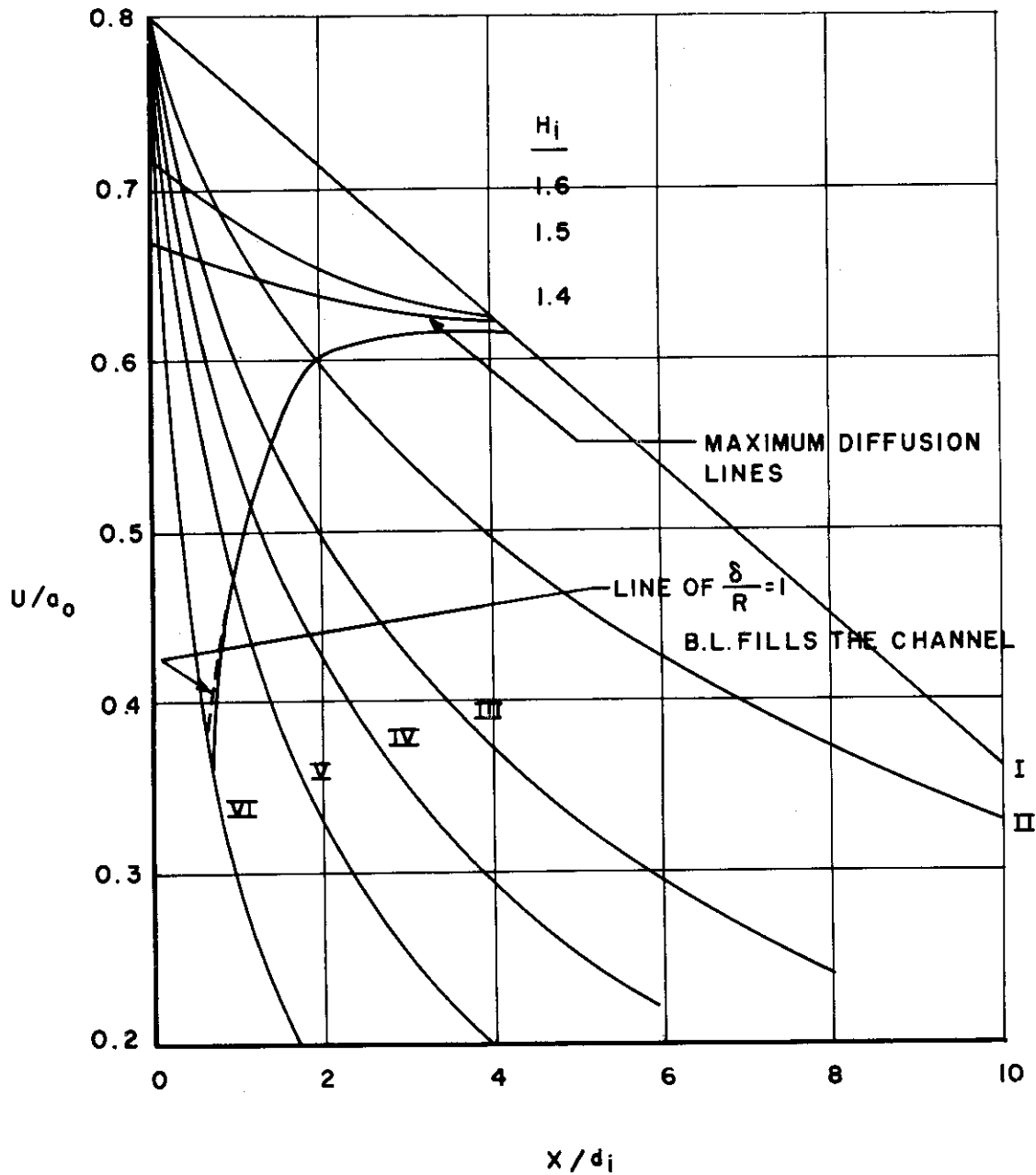
FIG. 5.27a

IMMINENT SEPARATION FOR INITIAL MOMENTUM THICKNESS $(\theta/d)_i = 0.02$

INITIAL MOMENTUM THICKNESS $(\frac{\theta}{d})_i = 0.04$

LINE WITH IMMINENT SEPARATION $c_f = 0.0005$

WITH INITIAL SHAPE PARAMETER $H_i$



$\frac{U}{a_o}$

$\frac{H_i}{}$
1.6
1.5
1.4

MAXIMUM DIFFUSION LINES

LINE OF $\frac{\delta}{R} = 1$
BOUNDARY LAYER FILLS CHANNEL

I
II
III
IV
V
VI

$\frac{X}{d_i}$
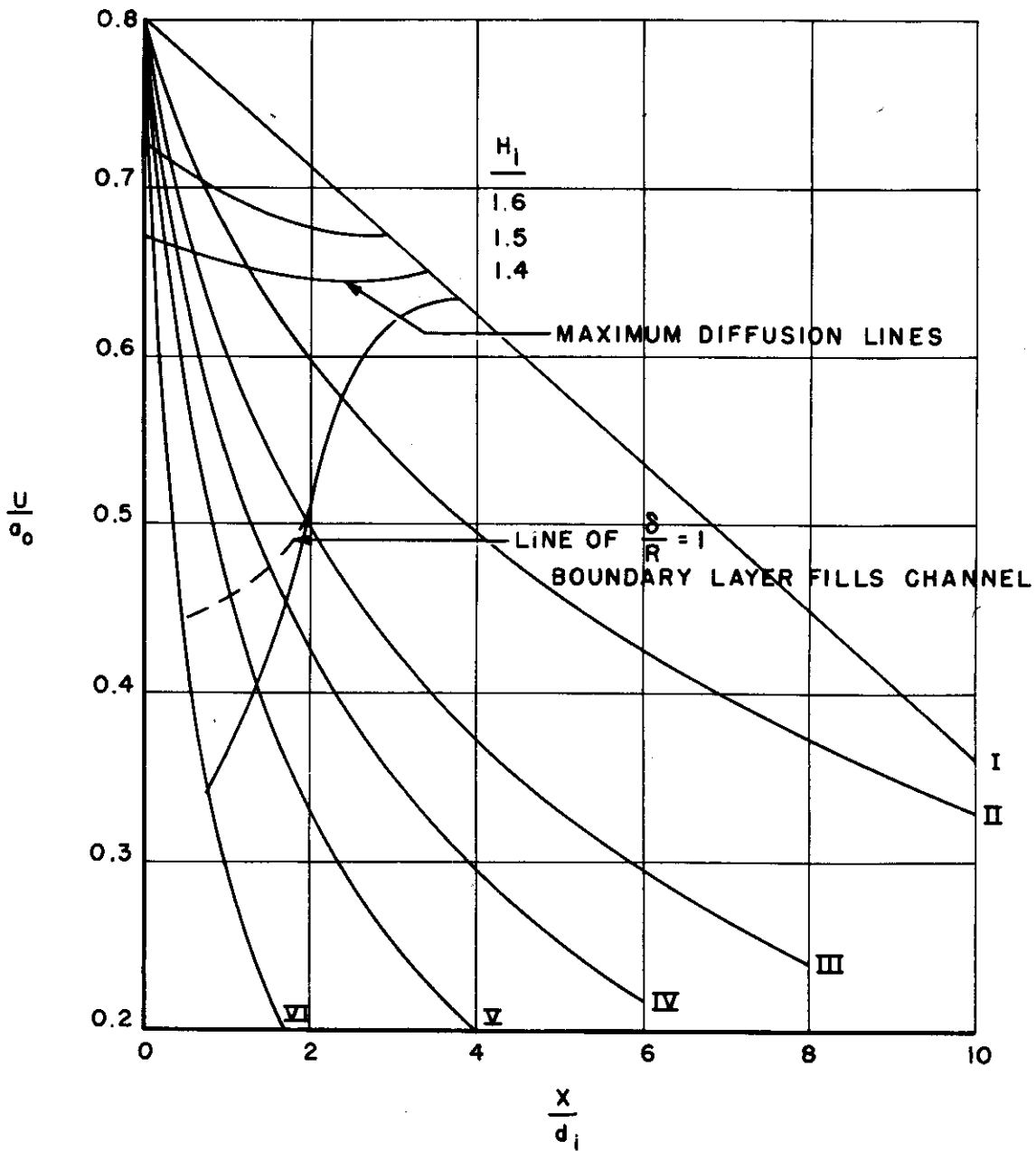
FIG. 5.27b

IMMINENT SEPARATION FOR INITIAL
MOMENTUM THICKNESS $(\theta/d)_i = 0.04$

INITIAL MOMENTUM THICKNESS $(\frac{\theta}{d})_i = 0.06$

LINES OF IMMINENT SEPARATION $c_f = 0.0005$
WITH INITIAL SHAPE PARAMETER $H_i =$

1.6

1.5

1.4

LINE OF $\frac{\delta}{R} = 1$
BOUNDARY LAYER FILLS CHANNEL
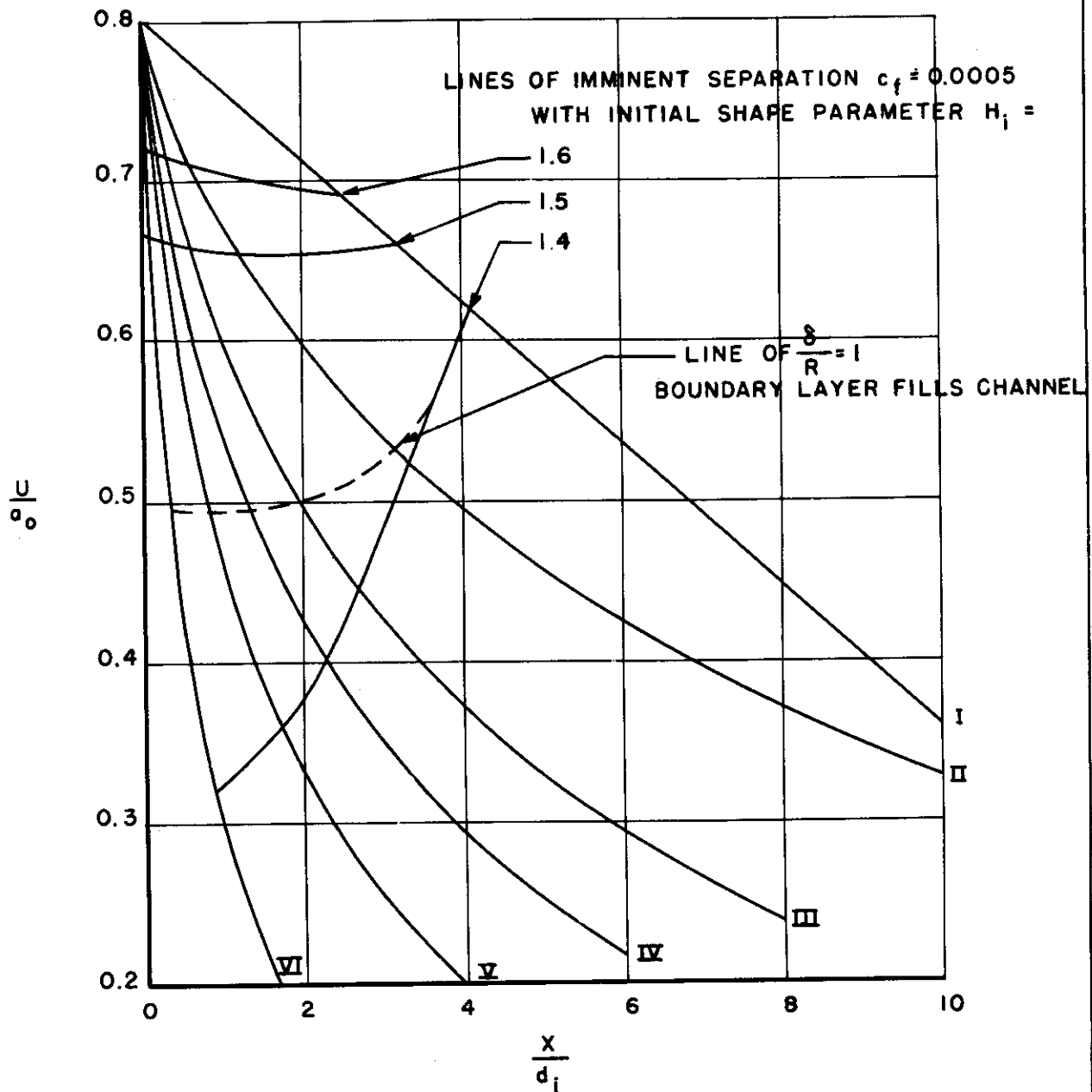
FIG. 5.27c

IMMINENT SEPARATION FOR INITIAL
MOMENTUM THICKNESS $(\theta/d)_i = 0.06$

$V_i$ = INLET VELOCITY

$V_s$ = VELOCITY AT WHICH SEPARATION
IS IMMINENT, $c_f$ = 0.0005
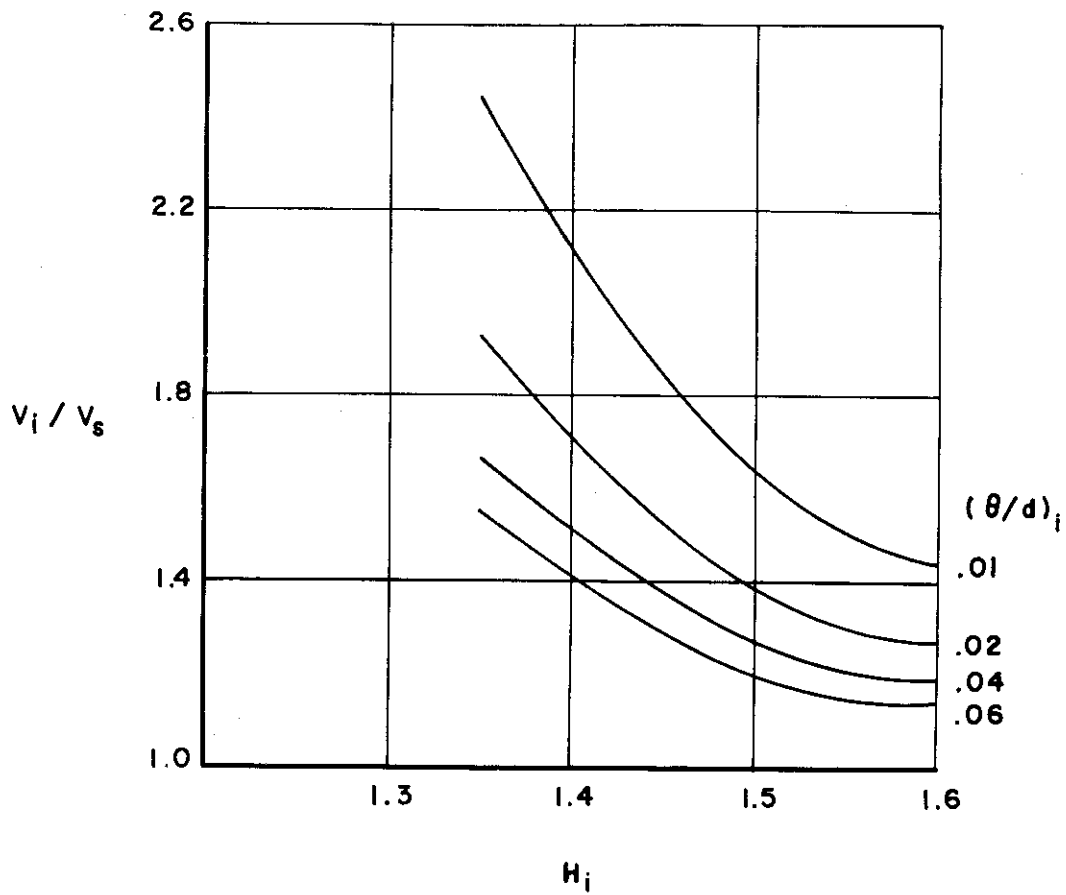
FIG. 5.28    MAXIMUM DECELERATION FOR CONICAL DIFFUSERS

QUASI STEADY FLOW

$\Delta P = P_f - P_s$

$\Delta \eta_2 = \dfrac{\Delta P}{\frac{1}{2} V_1^2}$

$H_i = 1.4$

$H_i = 1.5$

DATA FROM REF 5.35

$\left( \dfrac{\theta}{d} \right)_1$
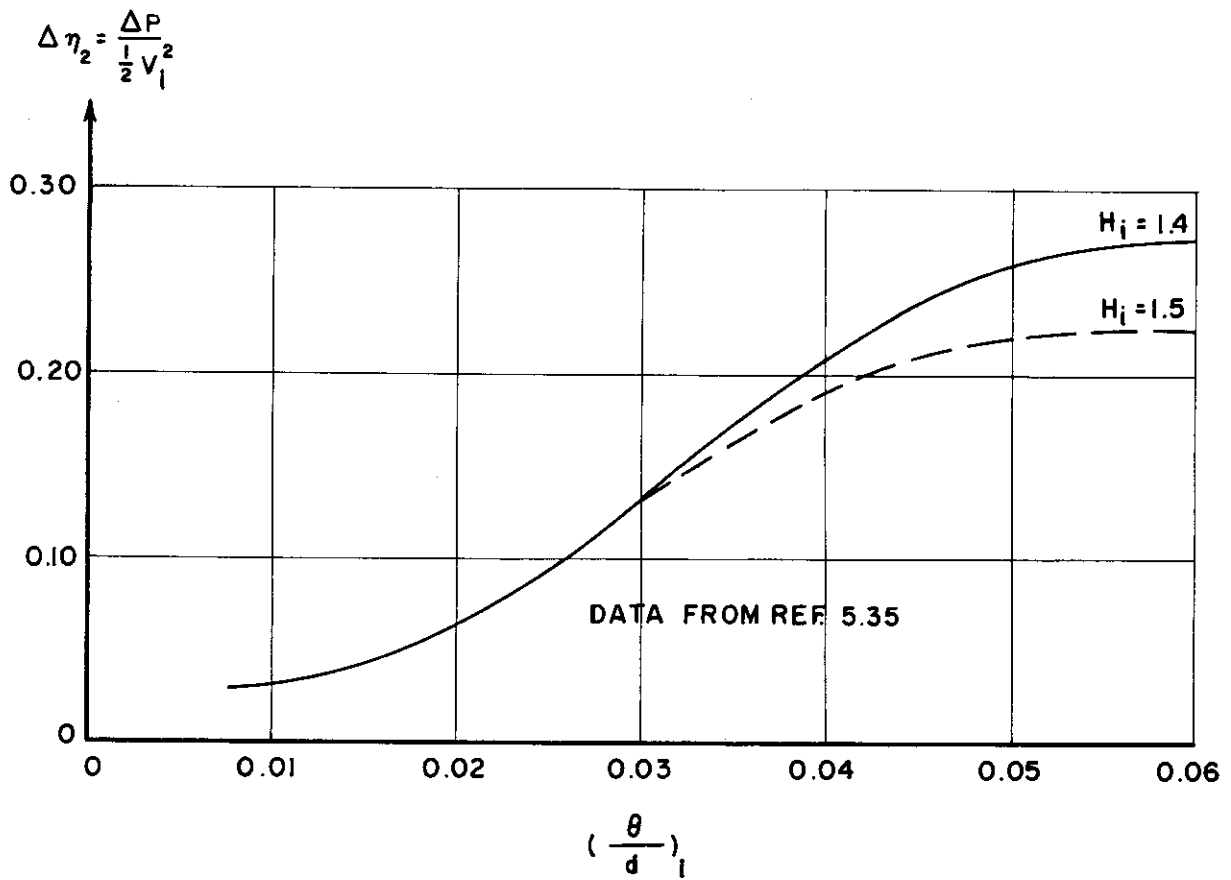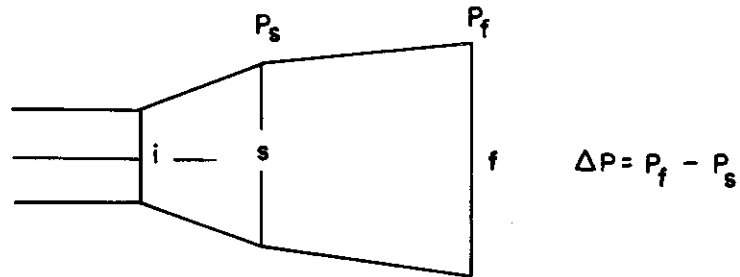
FIG. 5.29    PRESSURE RECOVERY IN QUASI STEADY FLOW

QUASI - STEADY FLOW

MEAN VALUE

$L/d_i$

DATA FROM REF. 5.35

$\alpha = 7.5°$

$\alpha = 2.5°$

$(\frac{\theta}{d})_i$
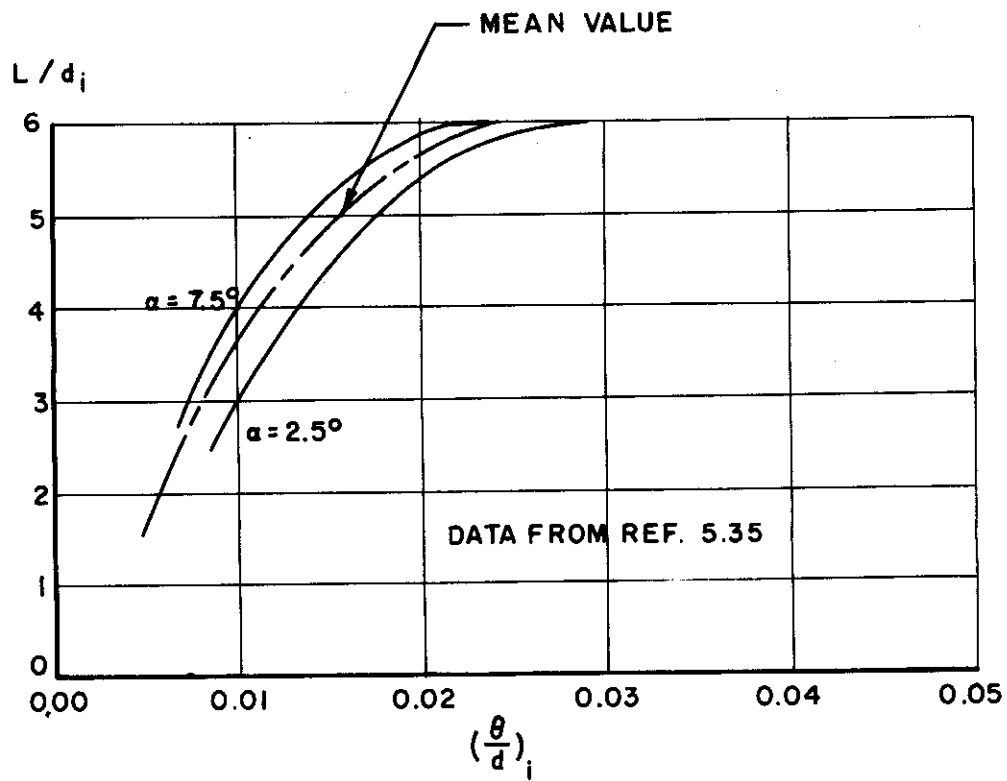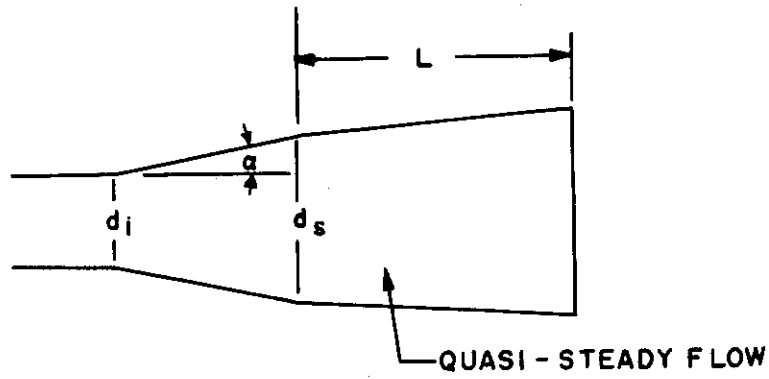
LENGTH FOR DIFFUSION OF
QUASI STEADY FLOW
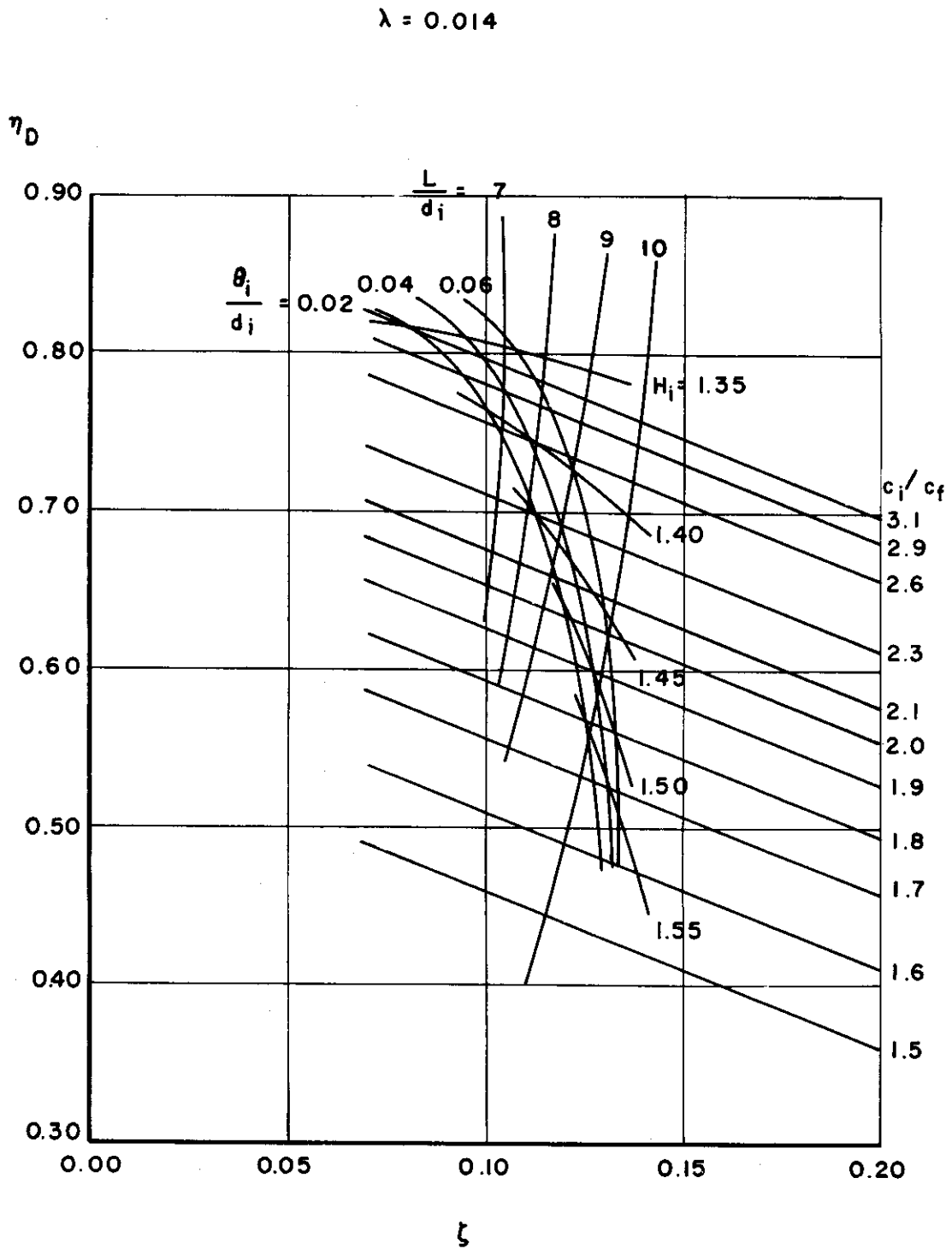
FIG. 5.30

$\lambda = 0.014$

INFLUENCE OF INLET CONDITIONS ON
CONICAL DIFFUSER PERFORMANCE

FIG. 5.31a

$$\lambda = 0.017$$



FIG. 5.31b    INFLUENCE OF INLET CONDITIONS ON CONICAL DIFFUSER PERFORMANCE

$$\lambda = 0.020$$
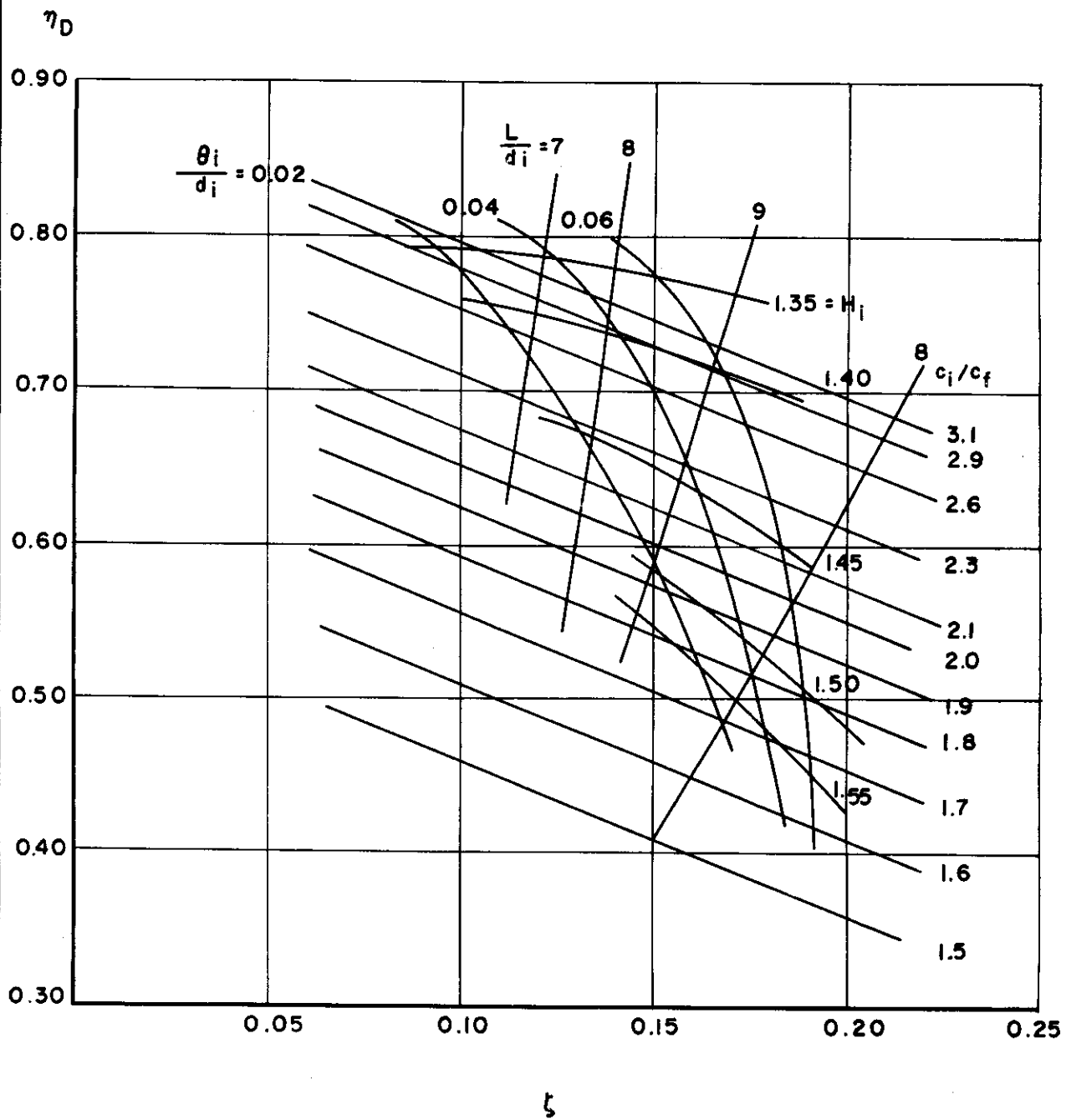
FIG. 5.31c    INFLUENCE OF INLET CONDITIONS ON
CONICAL DIFFUSER PERFORMANCE

(a)

(b)

(c)

POSSIBLE SEPARATION
LOCATED IN ENTRANCE
PART OF THE BLADE

DISTANCE ALONG BLADE

SMALL DIFFUSION RATE

DISTANCE ALONG BLADE

DISTANCE ALONG BLADE
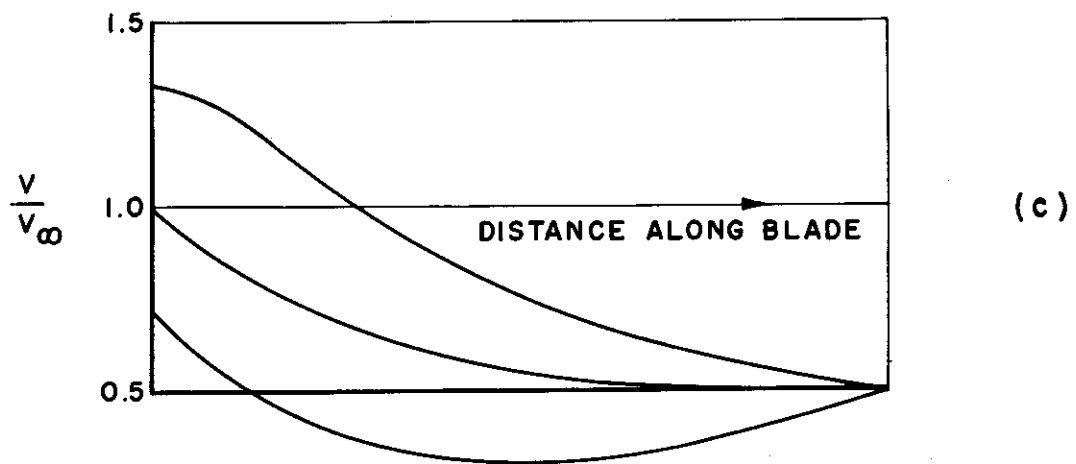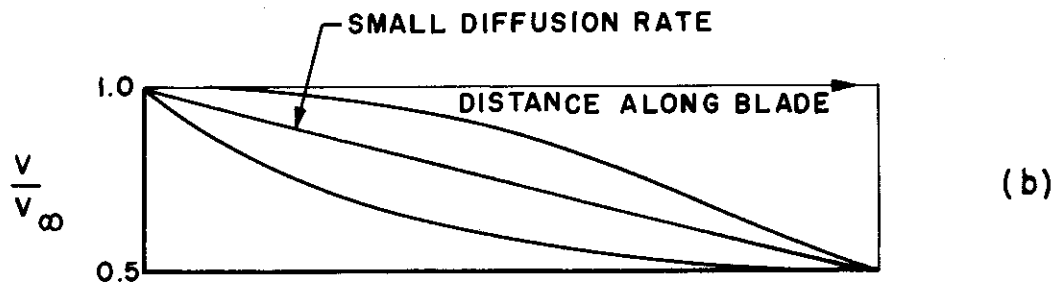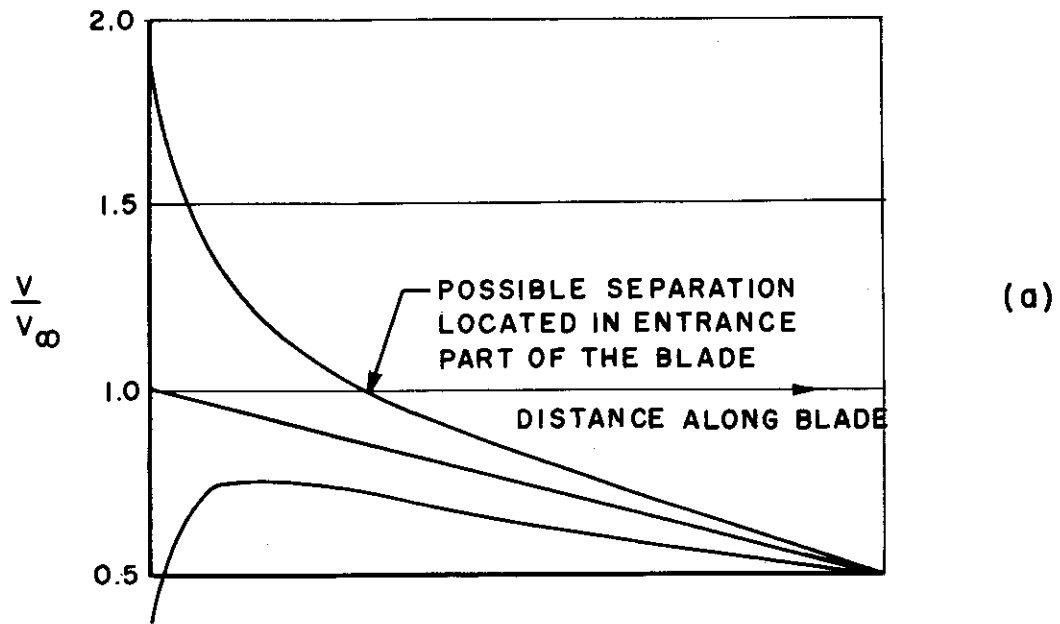
VELOCITY DISTRIBUTIONS ALONG
GUIDE VANE SECTIONS

FIG.  5.32

S

VANED DIFFUSER

IMPELLER

AXIS
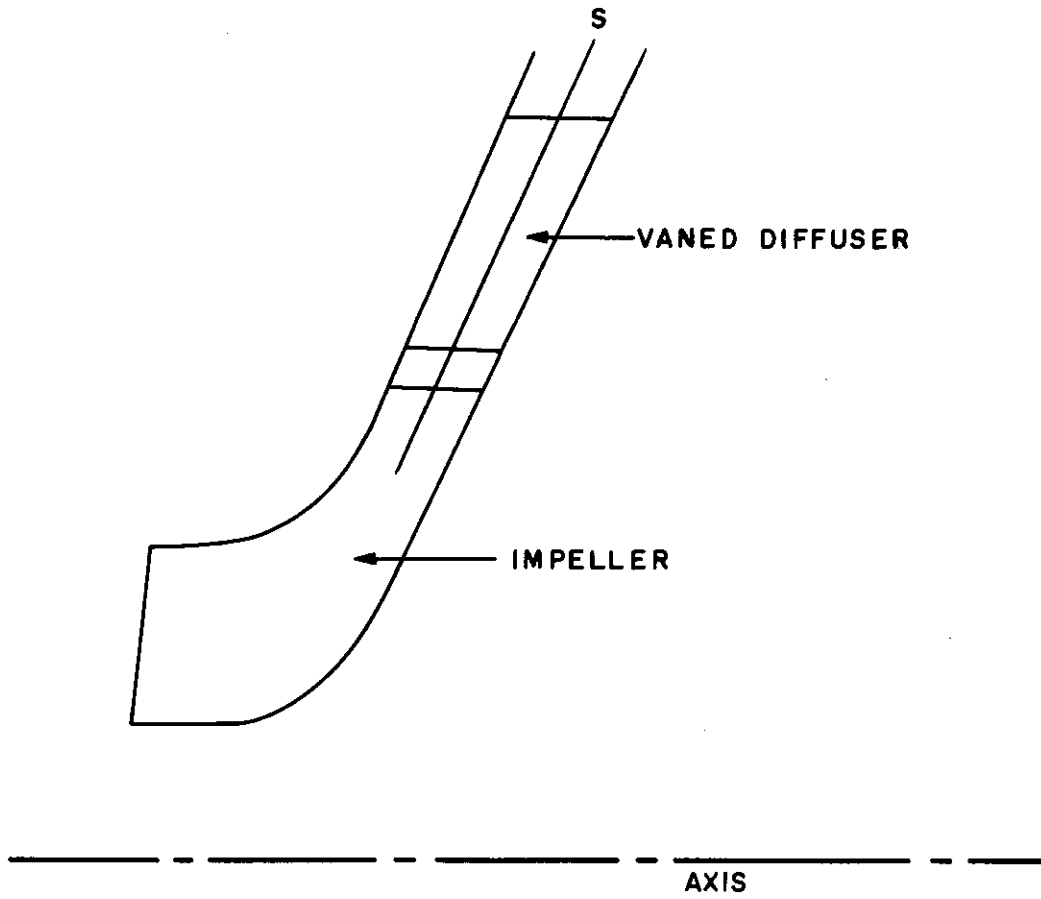
FIG. 5.33

SURFACE OF REVOLUTION S ON
WHICH BLADE SECTION IS MADE
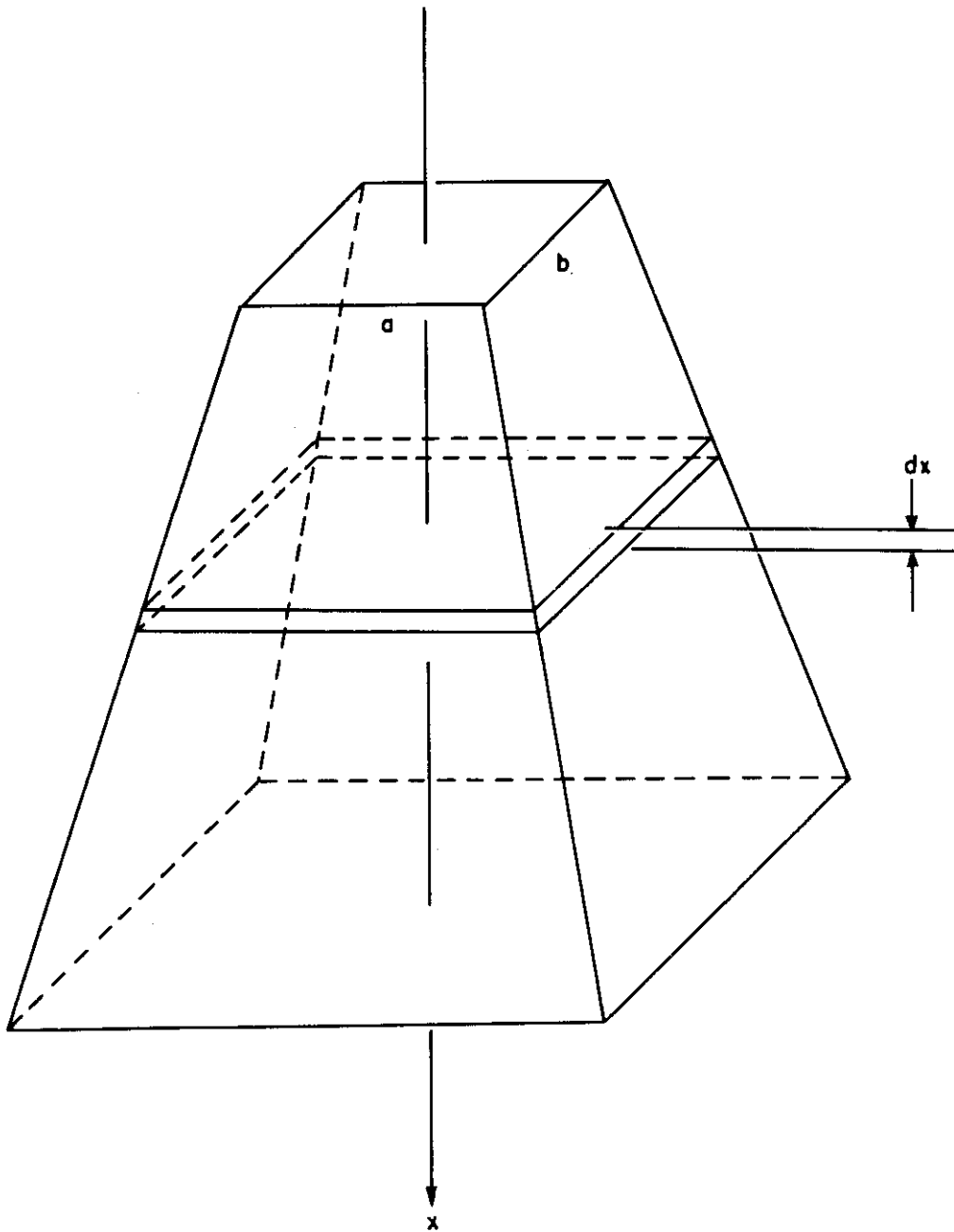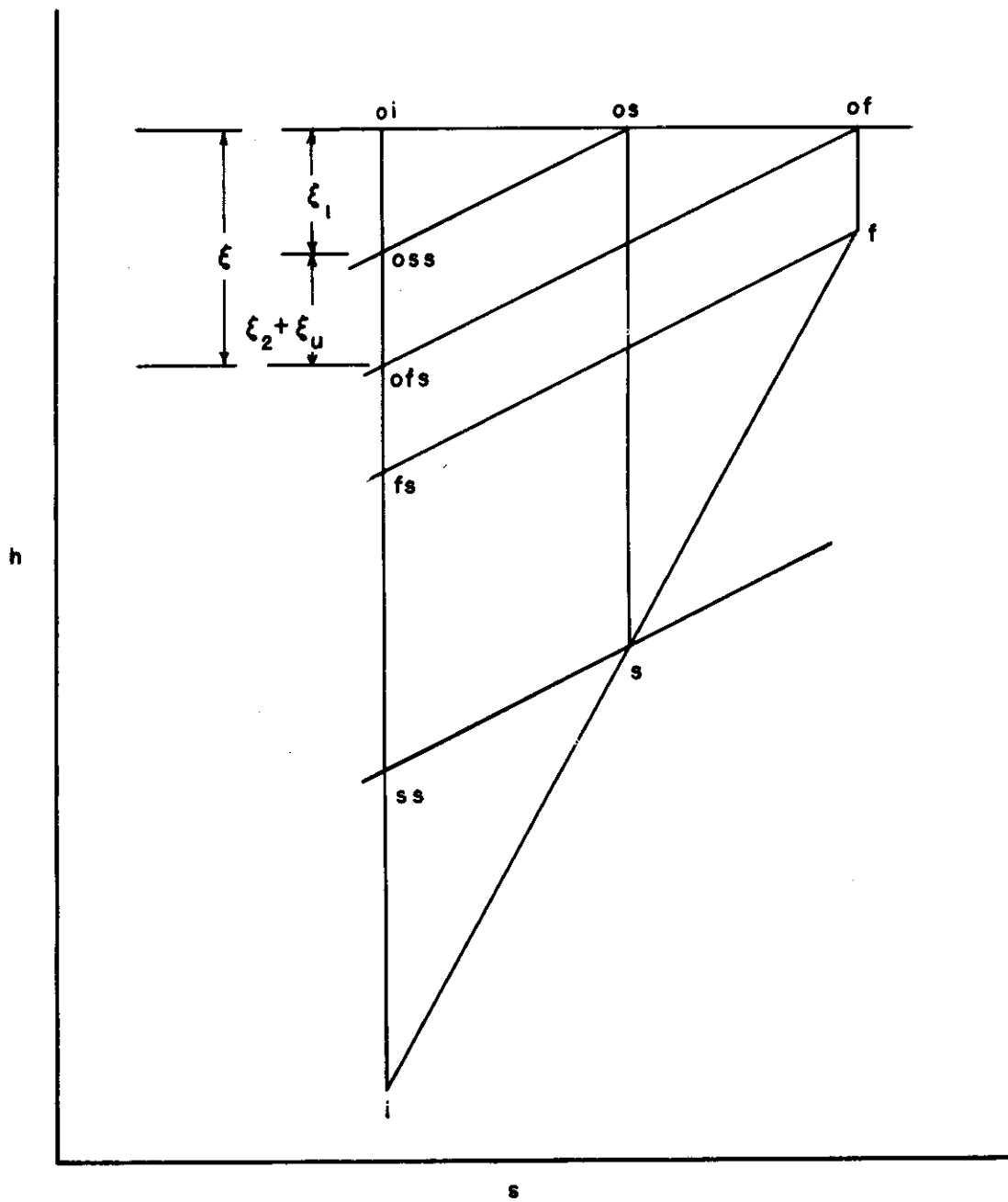
FIG. 5.35    DEFINITION OF LOSS COEFFICIENT AND
EFFICIENCY OF A CONICAL DIFFUSER

$\eta_D$, DIFFUSER EFFICIENCY BASED ON STATIC PRESSURE

$\zeta$, LOSS COEFFICIENT

REHEAT FACTOR = 1

$$\eta_D = 1 - \zeta - \left(\frac{c_f}{c_i}\right)^2$$
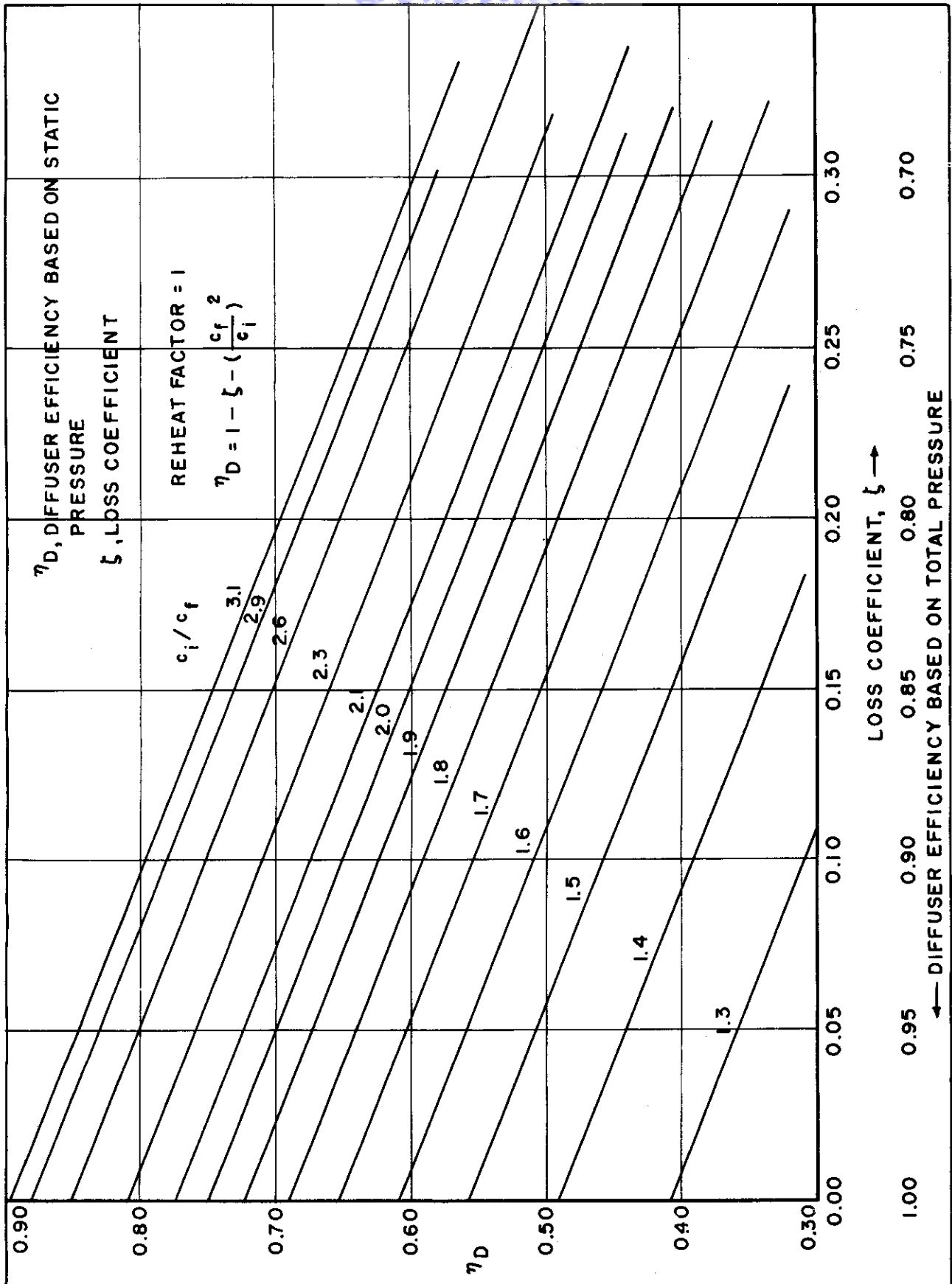
RELATION BETWEEN DIFFUSER EFFICIENCIES AND VELOCITY DIFFUSION

FIG. 5.36

# DESIGN, FABRICATION, AND TESTING OF THE SUPERSONIC RADIAL COMPRESSOR

## 6.1 The Design of the Compressor

In compliance with the development program required in the Exhibit, a single-stage compressor of the radial type operating at Mach numbers in the transonic and supersonic regime had to be built and tested. A relatively small size typical of aircraft auxiliary turbomachinery was to be selected.

In order to meet these requirements, the following design philosophy was adopted.

(1) The compressor should correspond as nearly as possible to one which would actually be used for aircraft pressurization in the near future.

(2) The unknown aerodynamic characteristics should be stressed, i.e., a compressor design should be chosen which promised the largest advancement of the art within the limits of achieving an actual operating unit.

Study of the problems of cabin pressurization indicated that a pressure ratio of 6:1 in a single stage would be desirable. This pressure ratio is actually representative of design requirements for pressurization of the B-52 airplane at high altitudes. Those pressure ratios can be obtained with tip speeds ranging between 1800 and 2000 ft per second. At these high tip speeds, the impeller blades must, for stress reasons, consist of radial elements and, consequently, in a radial-flow machine, an outlet blade angle of $\beta_2 = 0^\circ$ had to be chosen. Though not required in the exhibit, thoughts were also given to a slightly mixed-flow design, which would have allowed backward-curved blading though maintaining radial blade elements. Such a design might have led to some improvements in efficiency as compared to the radial impeller, though the higher inducer relative Mach number connected with this design might be a drawback. But preliminary designs already showed that the required higher tip speeds would make the impeller heavier and might lead to mechanical problems. The radial-bladed impeller was, therefore, considered the best solution aerodynamically and stresswise. The following other reasons for choice of the radial design are given here:

(1) In a machine designed for use in airplanes, the customer may prefer the simplicity and light weight of the radial-bladed impeller to the slightly improved performance of an impeller with backwardly curved vanes, which by necessity requires mixed-flow design.

(2) The radial-bladed machine presenting less mechanical difficulties than the other one will be available for tests at an earlier date.

(3) A vaned diffuser for the radial-bladed impeller, being of the purely radial type, may incorporate more easily variations of the diffuser vanes and within a shorter time.

The impeller size was selected with reference to the requirement of aircraft auxiliary equipment. However, consideration was given to the practical aspects of instrumentation and accuracy of measurement which favor the larger wheel sizes of a given size range. Actually, the best index for sizing a machine is its Reynolds number. In order to remain in the desired Reynolds number range, a impeller diameter of 11 inches was chosen. This diameter is slightly larger than the range of sizes of air conditioning equipment indicated in the exhibit, namely, between 5 and 10 inches.

In order to arrive at the optimum internal shape, the design method laid out in Section III was followed accurately. Some design criteria have to be assumed in this method, and these are discussed below:

As shown in Fig. 6.14, the inlet to the compressor comprises a large bellmouth. Due to the flow curvature, the axial inlet velocity at the design conditions is not constant but varies from hub to shroud. This velocity distribution was determined by the methods of Section III, and is also modified by the impeller itself, whose action has an influence on the axial velocity profile. The flow and blade angles as arrived at in the final design and which take the above-discussed influences into account, as well as the velocity triangles at inlet shroud and at the tip, are presented in Fig. 6.1.

At pressure ratios of a magnitude as required here, a design for high specific speed is a necessary requirement, in order to keep the diffusing passages of the compressor reasonably large and, therefore, the frictional losses down to a minimum. This requirement leads to a large ratio of impeller eye to impeller tip and, consequently, to supersonic relative Mach numbers at the impeller eye. One of the main problems in designing high pressure ratio compressors, therefore, involves the supersonic and transonic flow conditions at the inducer. The design of the inducer section near the shroud was done in accordance with Section III, such that wave propagation upstream of the impeller is reduced to a minimum.

In Section III, certain design criteria for an optimum loading distribution throughout the impeller are presented. At first, these design criteria were somewhat modified. It was originally conceived that in order to postpone possible separation until the radial section of the impeller, the mean relative velocity should not decrease too much within the inlet section of the impeller. Fig. 6.2 shows the computed relative velocity distribution along the shroud. Also indicated is the assumed point of possible separation. The corresponding velocities at the hub are shown in Fig. 6.3.

This design, however, is - as could be seen from tests - extremely sensitive
to the slightest flow separation, and small errors in the assumed boundary
layer thickness could completely upset the flow pattern. These difficulties
were not sufficiently realized at the time the first impeller was designed.
When test results of this impeller were available, the deficiencies of this
design approach were recognized and another impeller was designed which is
based on the design criteria contained in Section III.

The pertinent design data of the compressor are summarized in Table I.
The meridional shape of the impeller is shown in Fig. 6.4. Also indicated in
Fig. 6.4 are the changes made for the second impeller design which is
discussed later. The impeller blade dimensions are compiled in Fig. 6.5.

## TABLE I

| | |
|---|---|
| Tip diameter, inches | 11 |
| Inducer to impeller tip diameter ratio | .682 |
| Inducer hub to inducer tip diameter ratio | .411 |
| Tip Speed corrected to 519 degree R inlet temp ft per sec | 1839 |
| Absolute average Mach number at inlet | .595 |
| Relative Mach number at inducer tip | 1.306 |
| Relative Mach number at inducer hub | .753 |
| Relative flow angle at inducer tip | 63° |
| Relative flow angle at inducer hub | 39° |
| Inlet to outlet relative velocity ratio | 2.04 |
| Outlet absolute Mach number | 1.20 |
| Outlet angle of absolute velocity | 68.2° |
| Tangential velocity to tip speed ratio (slip factor) | .82 |
| Corrected mass rate of flow lb per min | 608.1 |
| Expected pressure ratio | 6:1 |

## 6.2  Fabrication of the Compressor

A cross-sectional drawing of the supersonic compressor is shown in
Fig. 6.6. The compressor has an open-faced radial impeller mounted overhung
on two ball bearings. The impeller consists of two pieces, a steel wheel and

an aluminum inducer. The compressor and the turbine drive have separate
bearing assemblies. A torsion rod transmits the torque from the turbine to
the compressor and takes care of small misalignments of the drive. With
high-pressure ratio compressors, the thrust balancing poses quite a problem.
This balancing is done by connecting a sealed portion of the disc area with
the inlet plenum chamber. By varying the bleed from this sealed off area to
the plenum chamber by means of a valve, the thrust was maintained at reasonable
values at all running conditions. The bleed pipe is indicated in Fig. 6.6 by
a dotted line.

As Fig. 6.6 indicates, the diffusing section is built up of two parallel
stainless steel walls. The distance between the walls can be adjusted, to
accommodate variable impeller tip width which, in turn, allows variation of
the deceleration rate within the impeller.

The radius ratio of the vaneless diffuser was made as large as possible.
so that the flow velocities at the discharge from the diffuser into a collec-
tion chamber are reasonably low. In order to minimize nonaxially symmetric
flow at the diffuser exit, which cannot be avoided when one radial discharge
duct is used, a comparatively large collection chamber has been provided.

The inducer was manufactured by a duplication process from a 10 times
size cavity.

The photographs, Fig. 6.7 to Fig. 6.9, show views of the impeller, including
the shaft assembly, the large collection chamber, and the rear view of the
installation with the turbine drive. Turbine air inlet is from the bottom;
the combustion chamber protruding from the turbine housing is plainly visible.
The hot gases exhaust through an axial exhaust pipe.

## 6.3  Test Equipment and Operation of the Compressor

A drawing of the test installation is presented as Fig. 6.10.

The compressor is driven by a gas turbine capable of producing about 600
horsepower at the compressor design speed of 38,300 rpm. Because of the
considerable power absorption of the test compressor which could not be met
by the available turbine drives, it was necessary to throttle the inlet of
the compressor. This throttling also had the effect of approximating the
Reynolds numbers closer to those found in actual high-altitude flight
conditions.

The compressor air flow is measured with an ASME standard orifice type
flowmeter which is made up of a 10.0-inch duct and a 6.5-inch orifice, and
is located at the compressor inlet upstream of the compressor inlet throttling
valve. The photograph, Fig. 6.11, shows the measuring section. The throttling

valve discharged into an inlet plenum chamber with a volume of about 50 cu ft and from there into the compressor. Fig. 6.11 also shows the plenum chamber and the electrically operated throttle valve ahead of it.

The compressor is instrumented for the measurement of over-all performance, impeller performance, diffuser performance, and compressor pressure rise as a function of linear distance through the machine. The details of the instrument installation are:

A.   Pressure Measurements

1.   Compressor inlet pressure measurements are obtained from two wall taps and two Kiel-type total pressure probes located in the large area (3.0 sq ft) section between the inlet mixing tank and the compressor inlet bellmouth.

2.   Compressor discharge total pressure is measured at the discharge of the vaneless diffuser with four Kiel-type total pressure probes.

3.   A total of 36 static wall taps are located along the compressor inlet bellmouth, the impeller shroud, and on both walls of the vaneless diffuser. Fig. 6.12 shows the position of the static taps along the shroud streamline. At one radial station in the vaneless diffuser, an extra set of wall taps are provided 135 degrees from the original set as a check on the assumption of radial symmetry of the flow.

4.   Other miscellaneous pressures observed during operation of the machine are turbine and compressor oil pressure, turbine fuel pressure, and turbine inlet air pressure.

B.   Temperature Measurements

1.   The compressor inlet temperature is measured with two iron-constantan thermocouples located in the same plane as the inlet pressure measurements.

2.   The compressor discharge temperature is measured with four iron-constantan thermocouples located at the discharge of the vaneless diffuser.

3.   Other temperatures measured were orifice inlet, bearing temperatures, oil inlet temperature, and turbine discharge temperature.

C.   Diffuser Survey Instrumentation

1. Four survey stations are provided in the vaneless diffuser at radius ratios of 1.048, 1.091, 1.180, and 1.360, where the diffuser inside radius is 5.58 in.

2. A remotely controlled probe-positioning device is used which allows the operator to move the survey probe in the yaw and traverse direction while the test machinery is operating.

3. A yaw-total pressure probe was constructed. The probe head is of the cobra type which has proved both reliable and accurate.

4. A total temperature probe was made to the same over-all dimensions as the yaw-total pressure probe. The probe was calibrated and was found to have a recovery factor of approximately 0.90.

5. A system for correct indexing of the survey probes was devised, using a reference surface on the compressor housing and spirit levels attached to the probes.

D. Speed Measurements

1. An EPUT meter (electronic event counting device) is used to obtain the compressor speed in rpm. A monopole speed pickup placed in the vicinity of the driving turbine shaft nut provides the speed signal. The accuracy of the speed measurements is $\pm 0.2$ per cent of the compressor speed.

E. Impeller Rub Warning System

1. Due to the high thrust load on the impeller, a warning device was installed in the impeller shroud to warn the test crew of impending failure. The system consists of a simple d-c circuit with rub taps wired in series. The taps are located in the inducer section and on the radial face of the shroud; the taps are set 0.007 inches in from the surface of the shroud. When one of the rub taps is contacted by the rotating impeller, the circuit is broken and a light on the instrument panel turns on.

The test compressor was operated manually by the manipulation of four valves: the turbine inlet air valve, the turbine fuel control valve, the compressor inlet throttling valve, and the compressor discharge valve. These four valves were successively adjusted until the desired compressor operating conditions were obtained. A time interval of from five to fifteen minutes was required between each data point to allow the temperatures to stabilize. The accuracy of the data to date is within the probable accuracy of instruments being used.

The diffuser survey tests were conducted by first installing the yaw-total pressure probe, setting the test conditions, and obtaining the survey data. Then the compressor was shut down, the yaw-total pressure probe removed, and the total temperature probe installed in its place. Identical test conditions were set up, and the total temperature survey was made.

### 6.4 Test Results

Test results for the original design of the supersonic radial compressor are shown in the following Figs. 6.13 to 6.17. They indicated rather poor performance. When the first static pressure measurements along the shroud were available, it was realized that the small area change within the passage was not sufficient to counterbalance the losses due to friction and flow separation at the comparatively high Mach numbers with the passage. This showed up in the static pressure surveys of Fig. 6.14 where, between station J and L, a considerable dip of the static pressure can be seen. (See Fig. 6.12 for position of the stations.) A continued static pressure rise was not accomplished prior to Station K. This dip, as seen in Fig. 6.14, initiated approximately where the bump in the hub contour starts. Two influences are probably to blame for the pressure drop: (1) insufficient opening of the flow passage in the flow direction and (2) as an aggravating influence on flow separation, inaccurate manufacture of the inducer portion. It was found that the inducer was not made according to print, and the blade angles were a few degrees off.

The over-all performance of the first version of the supersonic radial compressor as shown in Fig. 6.73 indicates insufficient performance over the entire performance range which may be explained to a large extent by the phenomena pointed out above. The flow was approximately 8 per cent short of the design flow. The pressure ratio was 4.6 compared to the design objective of 6.0. The surge behavior was also worse than expected, very probably influenced by flow separation and subsequent velocity redistribution.

In order to trace the cause of the impeller deficiency more accurately, surveys were made at the impeller discharge and are presented in Figs. 6.15 and 6.16. These figures show a very uneven velocity profile and a considerable variation of the flow angle at the impeller discharge, changing from $-15^{\circ}$ at the hub to $+40^{\circ}$ at the shroud. Of interest is a curve of the total temperature between hub and shroud. Temperature differences of almost 100F could be measured between minimum and maximum values.

Based on the knowledge gained from the test data on the first impeller design, a second impeller was designed which intended to eliminate some of the undesirable design features of the first one. In order to utilize the available test setup, only such changes were made which were possible within the shroud contour of the first impeller.

It was, therefore, decided to correct the hub contour in a way as to accommodate our more recent design philosophy for the blade loading of a high compressor impeller. Fig. 6.4 shows the corrected blade design indicated by dotted lines. In addition, the inducer part which was incorrectly manufactured at the first design was redone, and it was made sure that the blade shape conformed with the drawings.

Test results of this compressor are shown in Fig. 6.17 from 50 per cent to 100 per cent speed. The chart indicates that the performance has considerably improved. A maximum pressure ratio of 5.2 could be obtained with 65 per cent efficiency, and the curves for the various speeds were much more uniform and showed a wider volume range than previously. The corrected weight flow was increased to 600 lb, which is equivalent to 99 per cent of the design flow. The surge behavior had also improved, and the surge line followed the conventional pattern more closely.

It must be mentioned that the efficiencies given in Figs. 6.13 and 6.17 are over-all efficiencies from total inlet to total exit at the very large vaneless diffuser. Because of the very large diameter of the diffuser, the diffuser losses are higher than in an optimized machine. With an optimized diffusion section, higher efficiencies have to be expected.
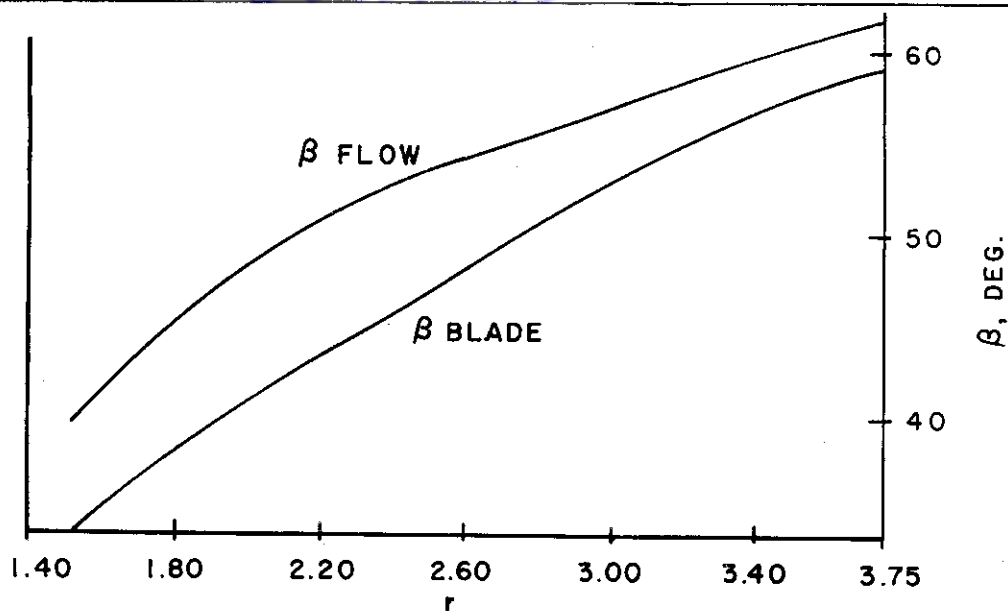
(a) BLADE CAMBER LINE AND FLOW ANGLES AT INLET
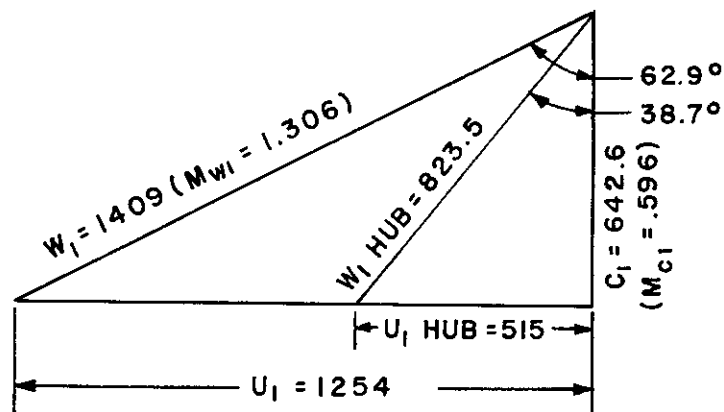
(b) VELOCITY TRIANGLES AT INLET
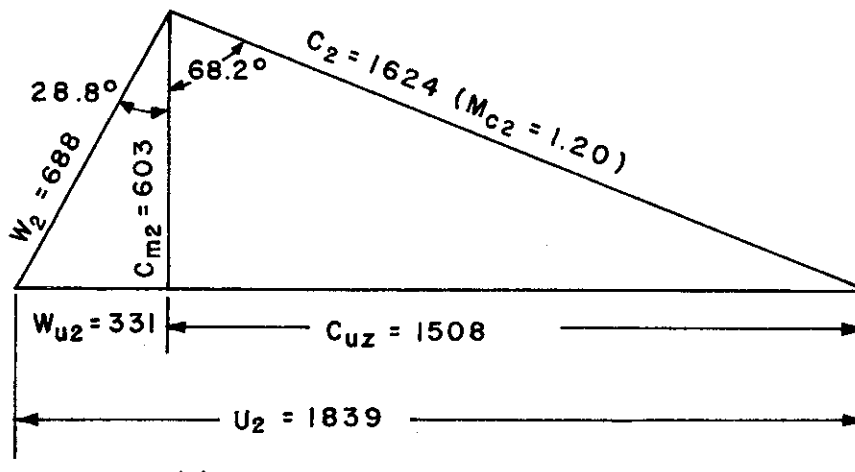
(c) VELOCITY TRIANGLE AT TIP

FIG. 6.1     INLET CONDITIONS OF EXPERIMENTAL COMPRESSOR
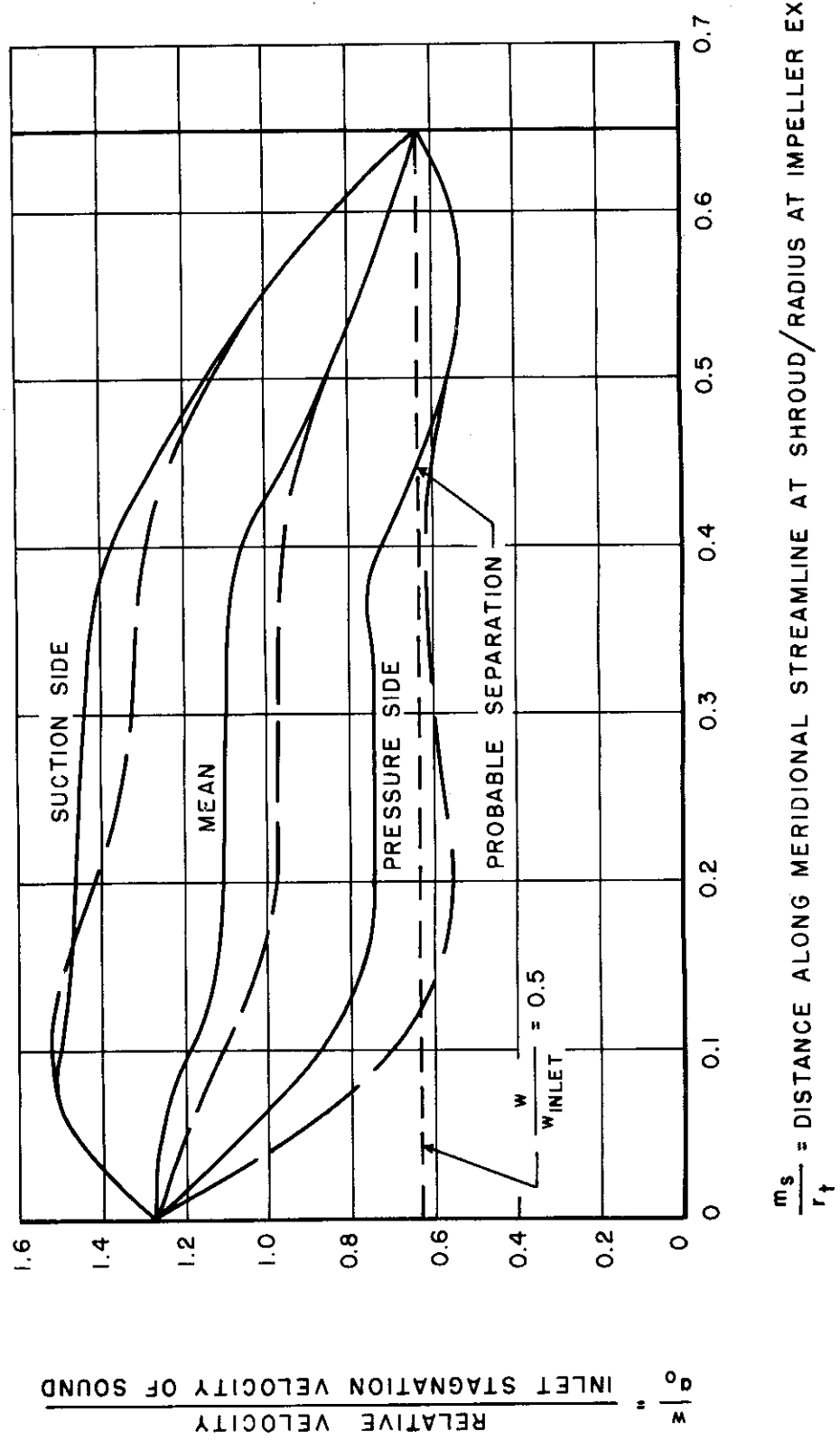
FIG. 6.2    VELOCITIES ALONG BLADE AT SHROUD
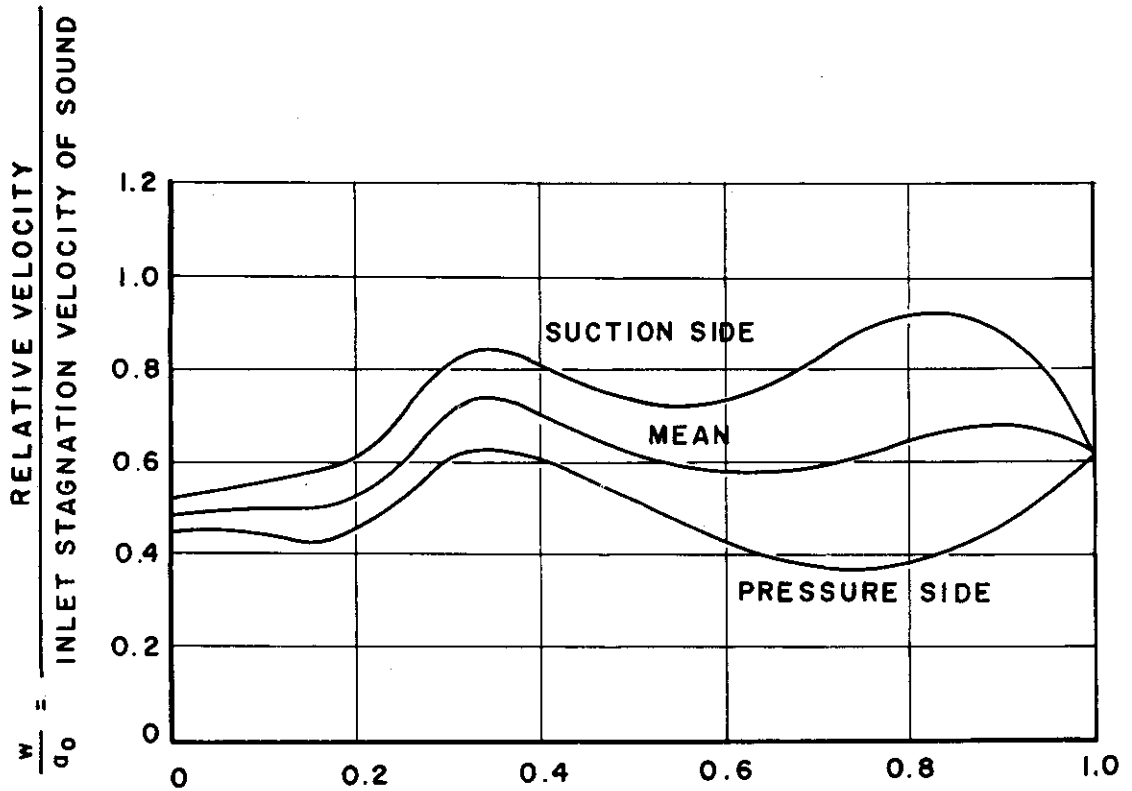
FIG. 6.3     VELOCITIES ALONG BLADE AT HUB
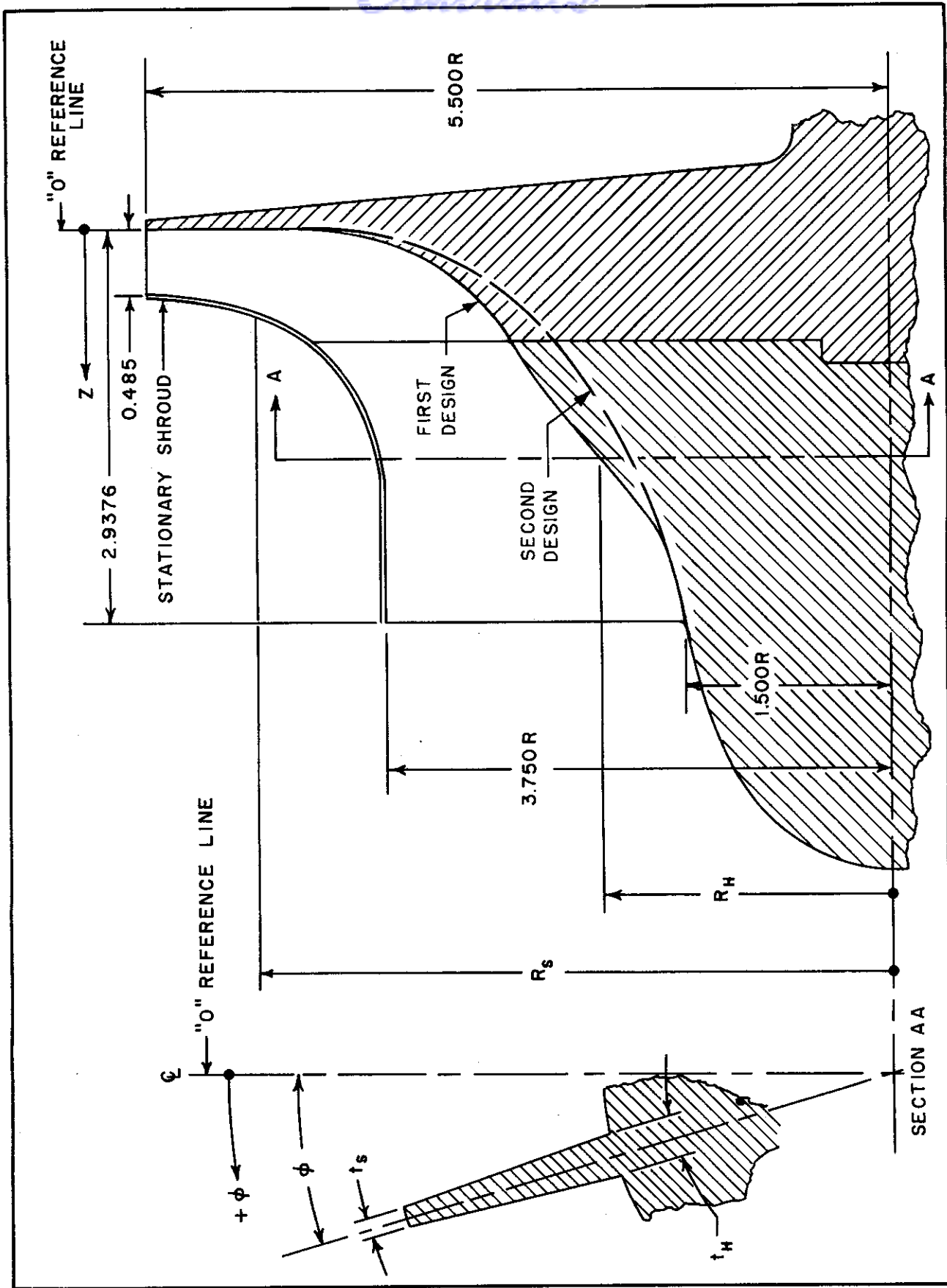
FIG. 6.4    IMPELLER PASSAGE SHAPE

| Z in. | $R_s$ in. | $R_H$ in. | $\phi$ | $t_s$ in. | $t_H$ in. | |
|-------|-----------|-----------|--------|-----------|-----------|---|
| 0 | 5.500 | 4.320 | $0^o$ | 0.150 | 0.331 | EXIT AT HUB LINE (BLADE) |
| 0.220 | 5.500 | 3.460 | $0^o$ | 0.100 | 0.414 | |
| 0.440 | 5.500 | 3.142 | $0^o$ | 0.051 | 0.412 | |
| 0.485 | 5.500 | 3.096 | $0^o$ | 0.040 | 0.410 | EXIT AT SHROUD LINE (BLADE) |
| 0.500 | 5.500 | - | - | - | - | EXIT AT SHROUD LINE (STATIONARY SHROUD) |
| 0.660 | 4.556 | 2.928 | $0^o$ | 0.145 | 0.394 | |
| 0.8376 | 4.252 | 2.802 | $0^o$ | 0.152 | 0.375 | PARTING LINE |
| 1.100 | 4.017 | 2.624 | $0.10^o$ | 0.140 | 0.352 | |
| 1.320 | 3.902 | 2.458 | $0.40^o$ | 0.124 | 0.340 | |
| 1.540 | 3.828 | 2.280 | $1.03^o$ | 0.112 | 0.336 | |
| 1.760 | 3.780 | 2.093 | $2.05^o$ | 0.092 | 0.300 | |
| 1.980 | 3.753 | 1.902 | $3.48^o$ | 0.080 | 0.248 | |
| 2.200 | 3.750 | 1.740 | $5.48^o$ | 0.068 | 0.208 | |
| 2.420 | 3.750 | 1.627 | $8.14^o$ | 0.057 | 0.176 | |
| 2.530 | 3.750 | 1.590 | $9.77^o$ | 0.053 | 0.164 | |
| 2.640 | 3.750 | 1.567 | $11.54^o$ | 0.052 | 0.160 | |
| 2.750 | 3.750 | 1.540 | $13.65^o$ | 0.051 | 0.156 | |
| 2.860 | 3.750 | 1.517 | $16.12^o$ | 0.037 | 0.148 | |
| 2.9376 | 3.750 | 1.500 | $18.00^o$ | 0.020 | 0.144 | ENTRANCE |

NOTES: 1. For  Z = 0  to  0.485  the quantities  $R_s$  and  $t_s$  refer to radii and thicknesses along blade at the tip radius

2. Blade thicknesses  $t_s$  and  $t_H$  are taken in tangential direction. Blades have linear thickness taper between hub and shroud

3. For A = 0.500 to 2.9376 $R_s$ refers to stationary shroud.  Blade clearance is 0.015 in. at Z = 0.500, increasing smoothly to 0.022 at Z = 2.200, and constant to impeller entrance.

4. For symbols, see Fig. 6.4.

FIG. 6.5      COMPILATION OF IMPELLER BLADE DATA
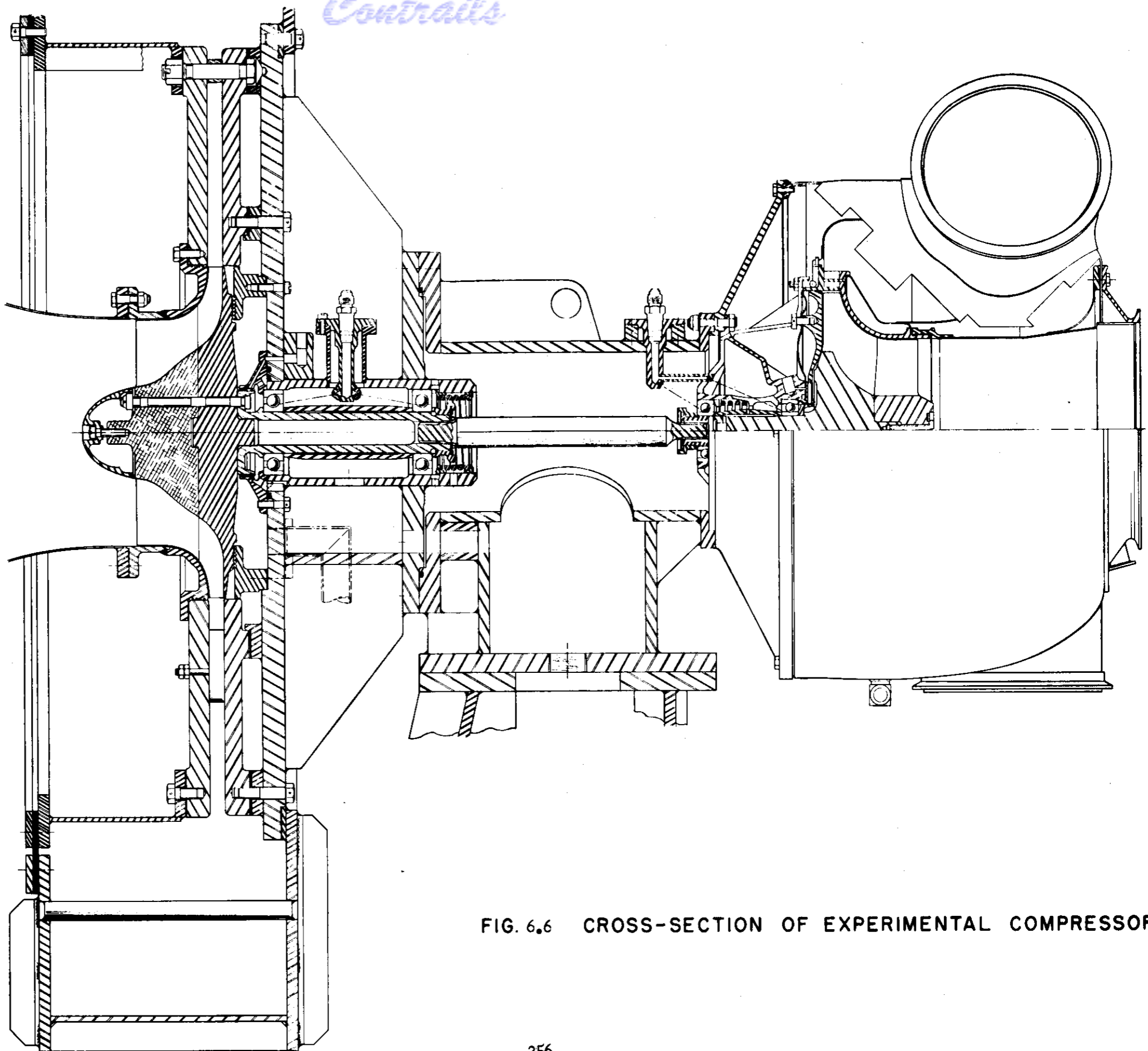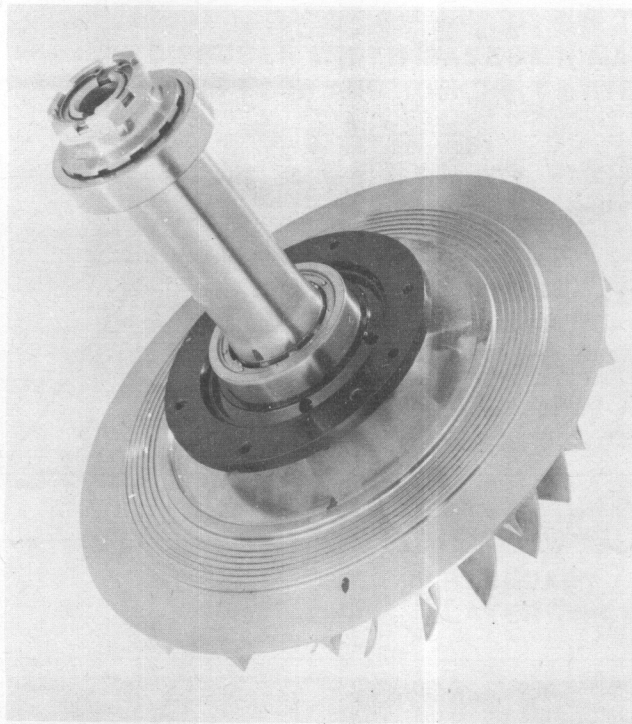
FIG. 6.6   CROSS-SECTION OF EXPERIMENTAL COMPRESSOR
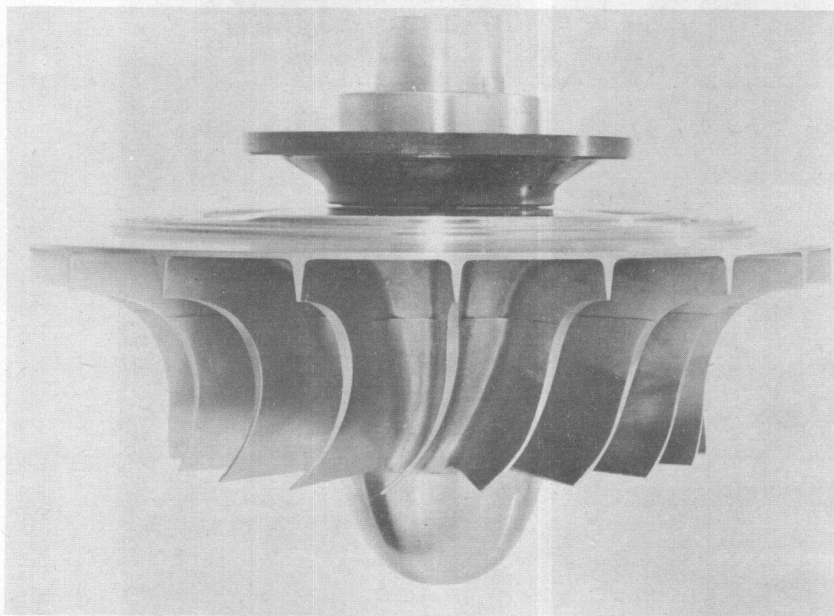
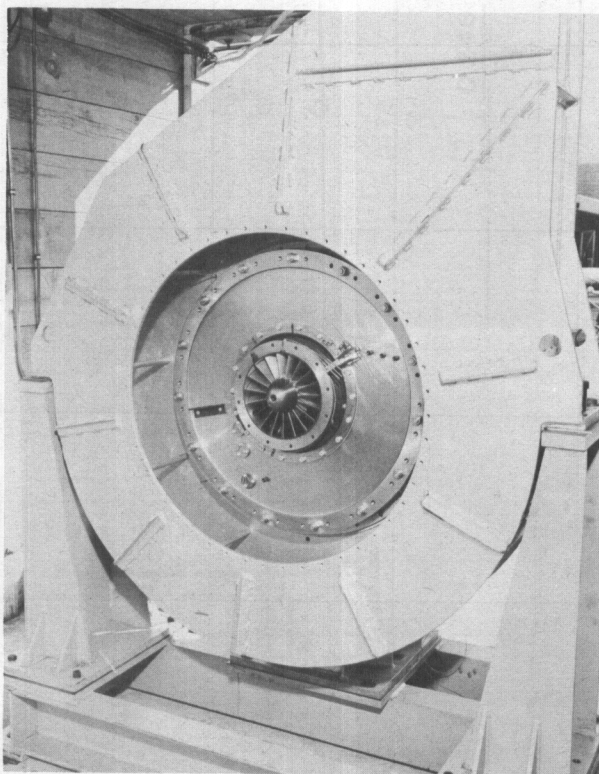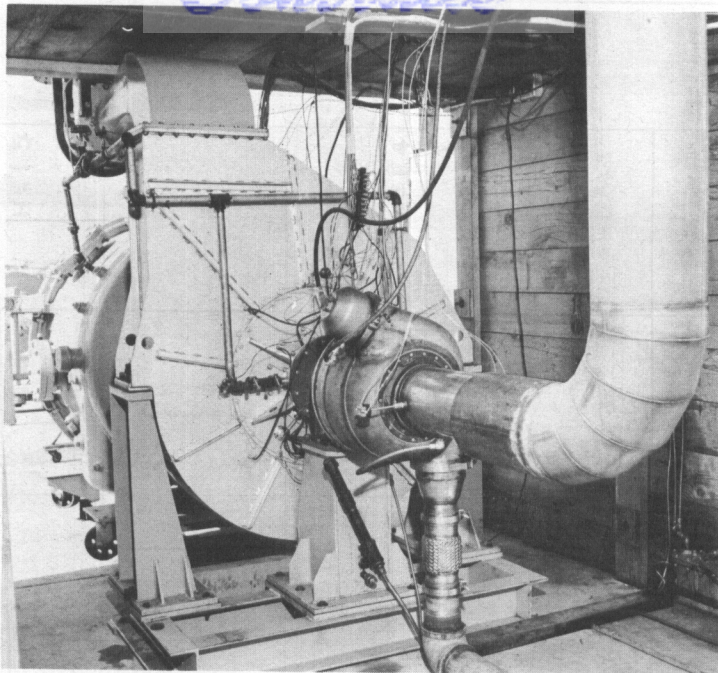| FIG. | 6.7a, 6.7b | VIEWS OF IMPELLER |

| FIG. 6.8a, 6.8b | VIEWS OF IMPELLER BLADING |
|---|---|
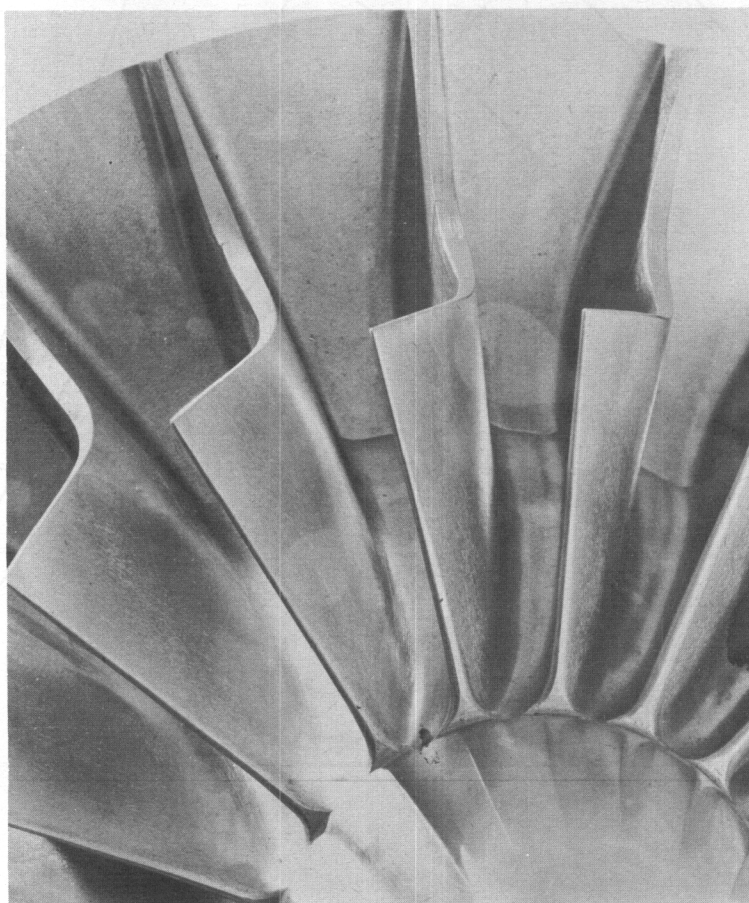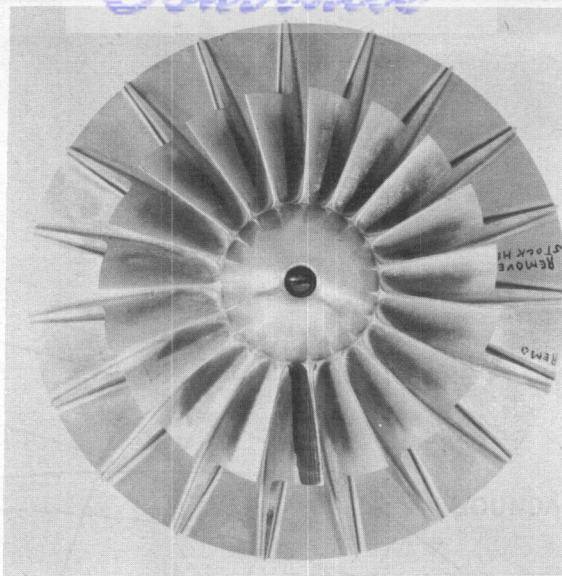
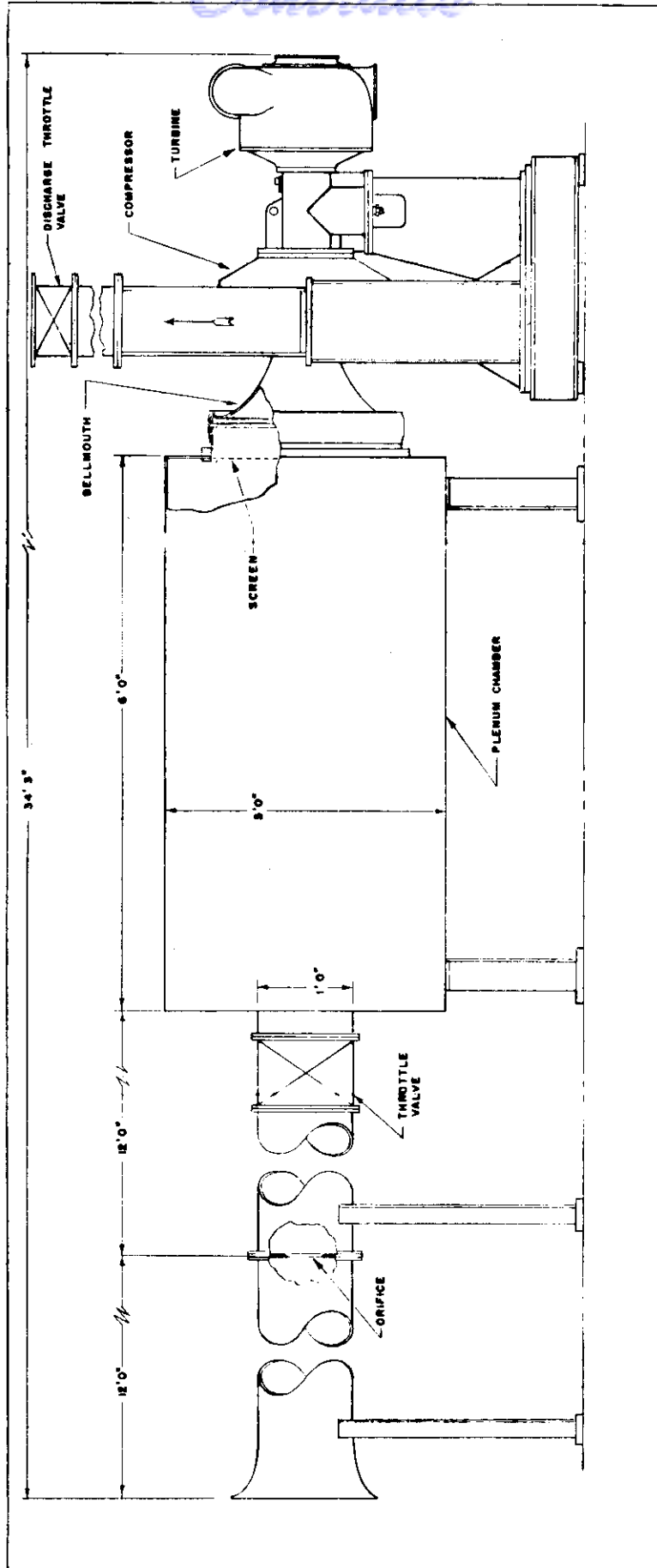FIG. 6.9a, 6.9b   COMPRESSOR ASSEMBLY WITH TURBINE DRIVE

FIG. 6.10 SCHEMATIC OF TEST INSTALLATION
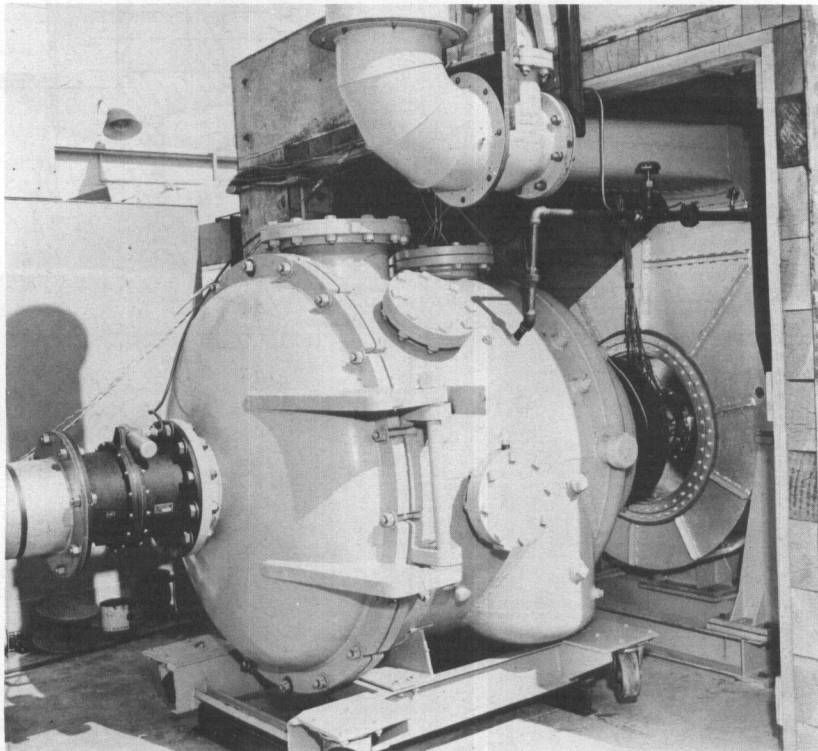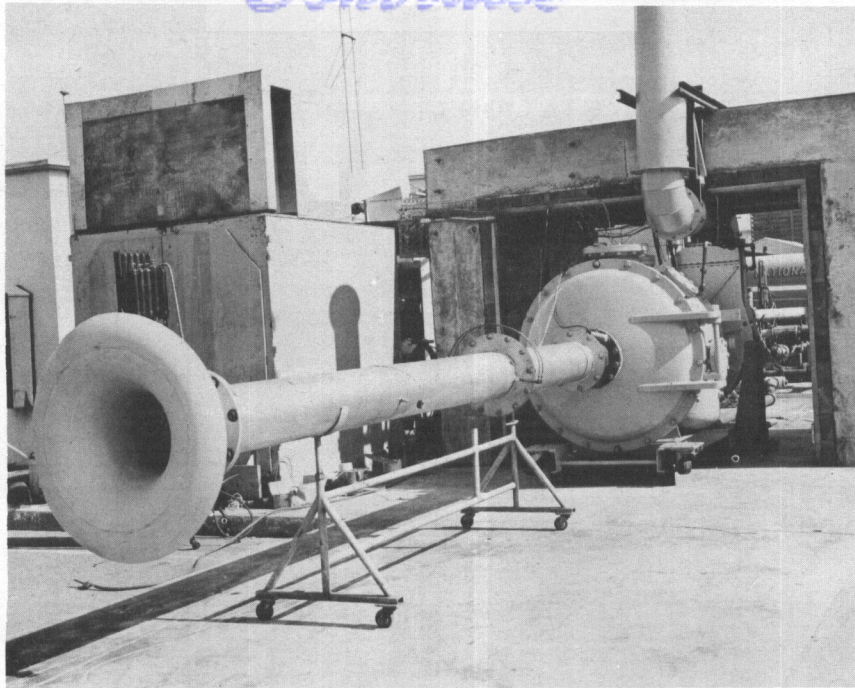
FIG. 6.11a, 6.11b    INLET DUCT AND PLENUM CHAMBER

DISTANCE BETWEEN STATIONS

| | |
|---|---|
| A-B = 2.00 IN. | L-M = 0.50 IN. |
| B-C = 1.00 | M-N = 0.50 |
| C-D = 1.00 | N-O = 0.40 |
| D-E = 0.35 | O-P = 0.25 |
| E-F = 0.25 | P-Q = 0.25 |
| F-G = 0.25 | Q-R = 0.50 |
| G-H = 0.25 | R-S = 0.50 |
| H-I = 0.25 | S-T = 0.50 |
| I-J = 0.25 | T-U = 1.00 |
| J-K = 0.25 | U-V = 1.00 |
| K-L = 0.50 | V-W = 1.00 |

0.15

5.5 IN. RAD.
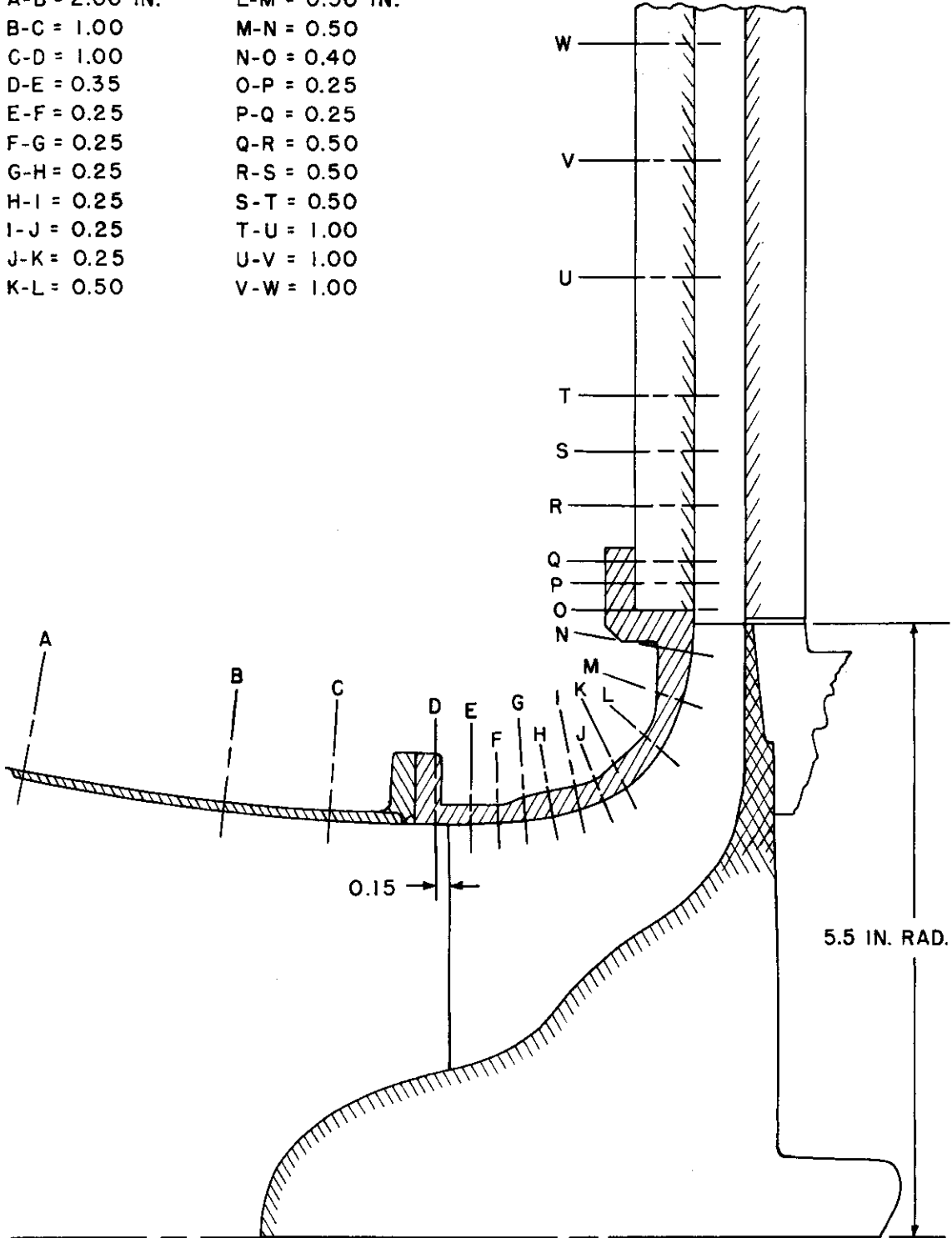
FIG. 6.12     POSITION OF MEASURING STATIONS
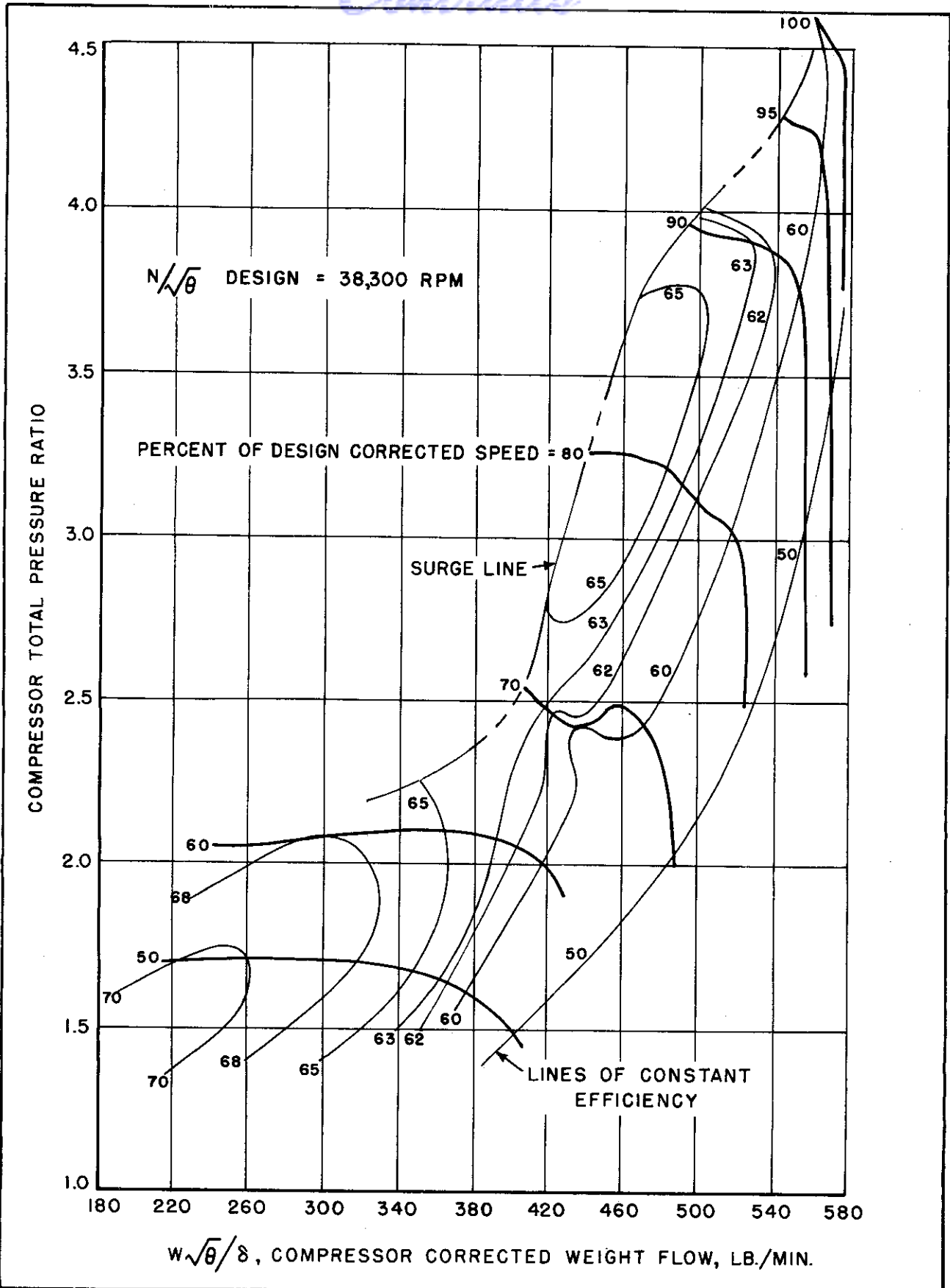
FIG. 6.13   SUPERSONIC RADIAL COMPRESSOR OVERALL
PERFORMANCE, (FIRST DESIGN)

$$\frac{p}{P_{Ti}} = \frac{\text{STATIC PRESSURE AT SHROUD}}{\text{TOTAL PRESSURE AT IMPELLER INLET}}$$
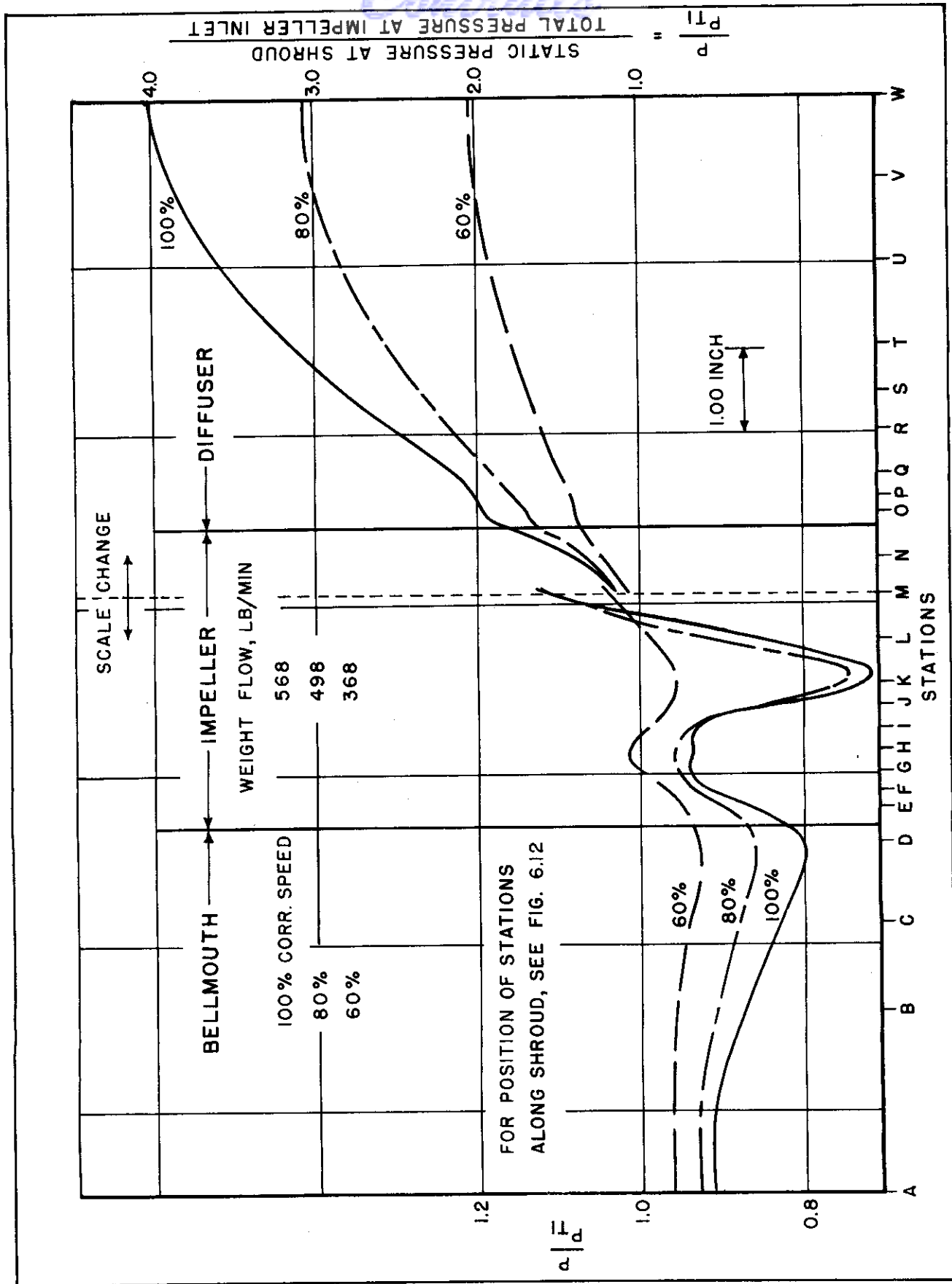
FIG. 6.14    STATIC PRESSURE SURVEYS ALONG SHROUD

**TEST CONDITIONS**

$N/\sqrt{\theta}$ = 38300 RPM

$P_{2T}/P_{1T}$ = 4.55

$T_{2T}$ = 992.5 DEG R

$\eta_{ad}$ = 60.6%
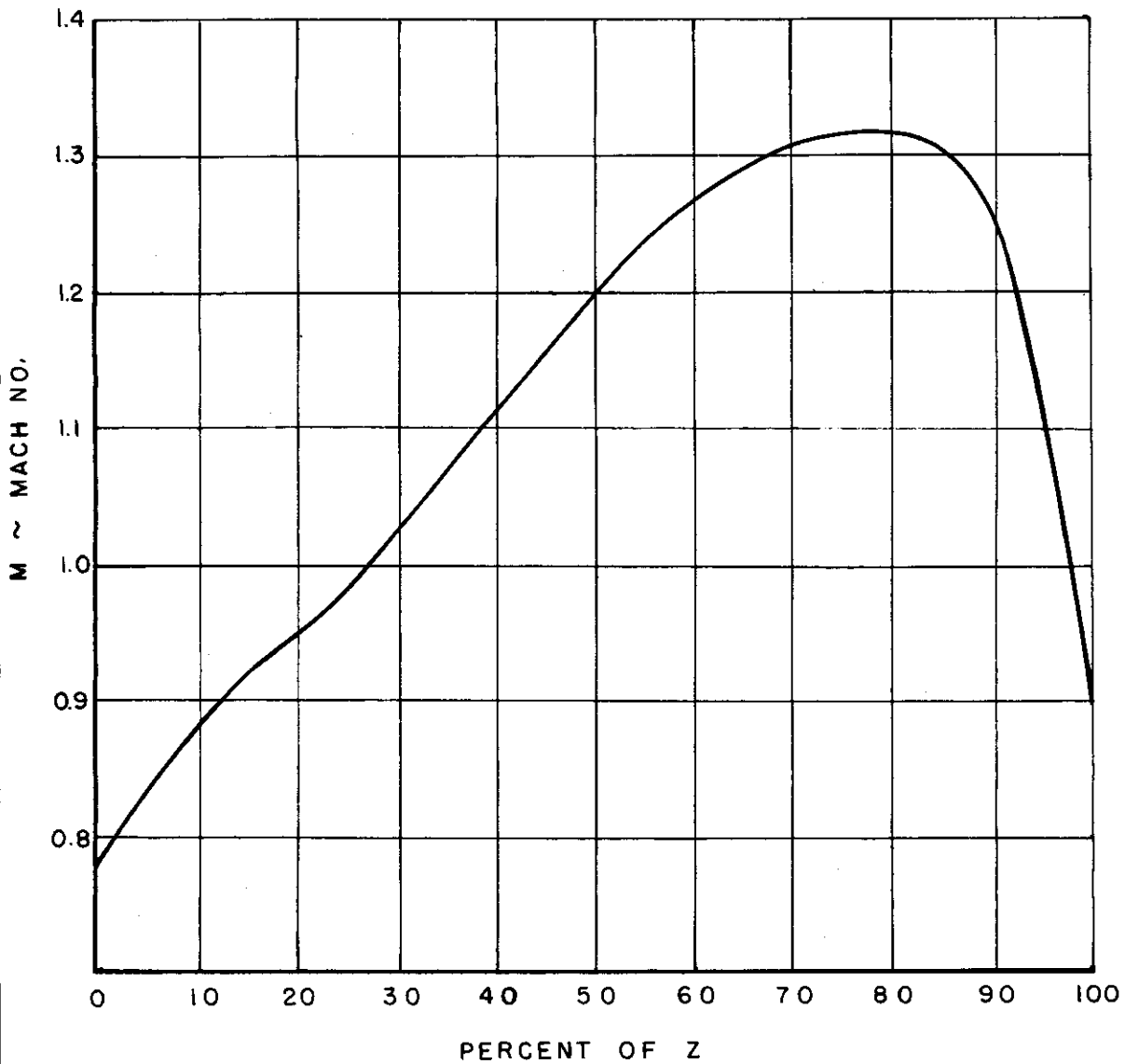
$\dfrac{W\sqrt{\theta}}{\delta}$ = 567 LB PER MINUTE



M ~ MACH NO.

PERCENT OF Z

**FIG. 6.15     IMPELLER DISCHARGE SURVEY RESULTS**
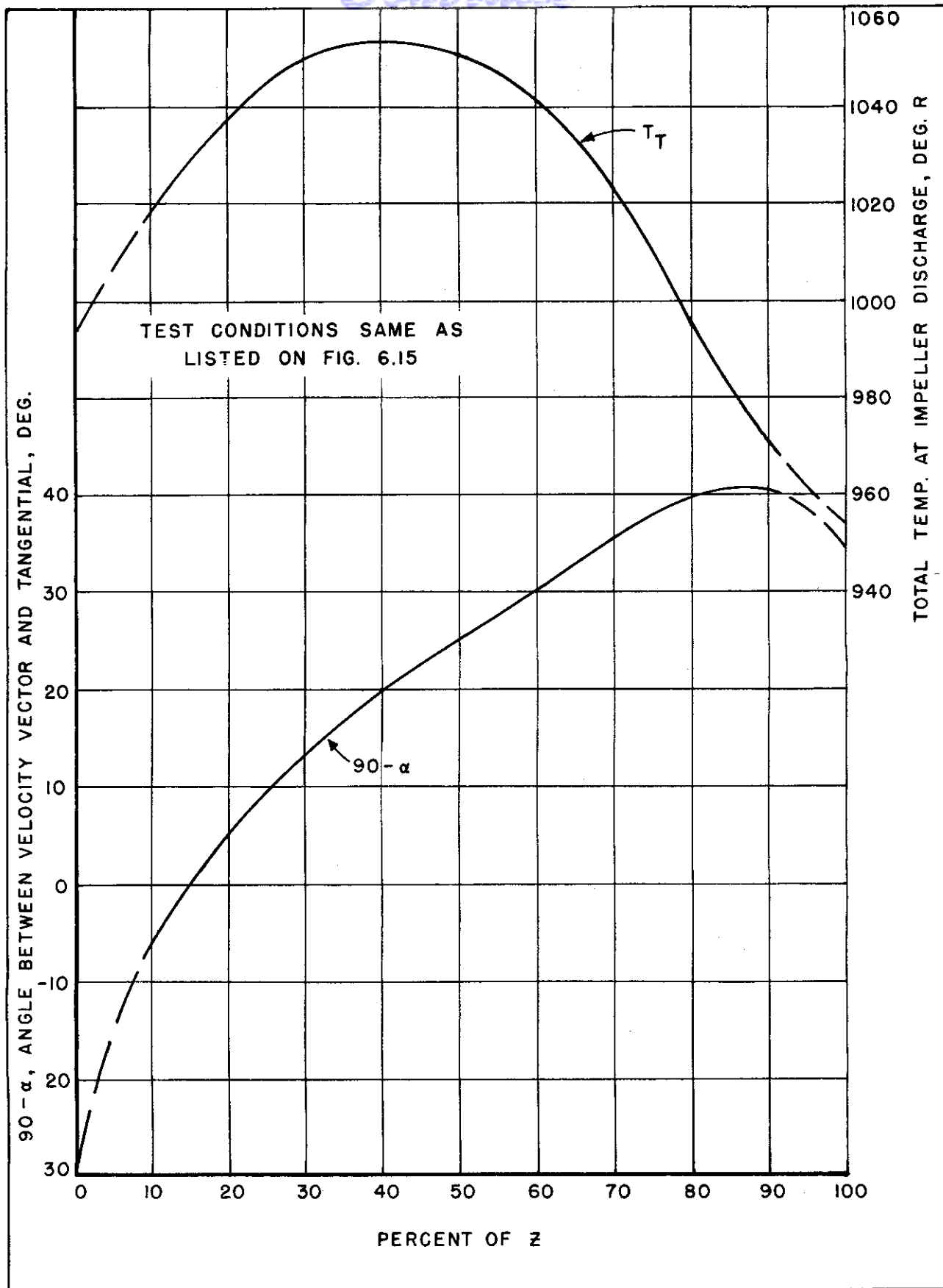
FIG. 6.16    IMPELLER DISCHARGE SURVEY RESULTS

$N/\sqrt{\theta}$ DESIGN = 38,300 RPM

PERCENT OF DESIGN CORRECTED SPEED = 90

SURGE LINE

LINES OF CONSTANT EFFICIENCY

COMPRESSOR TOTAL PRESSURE RATIO

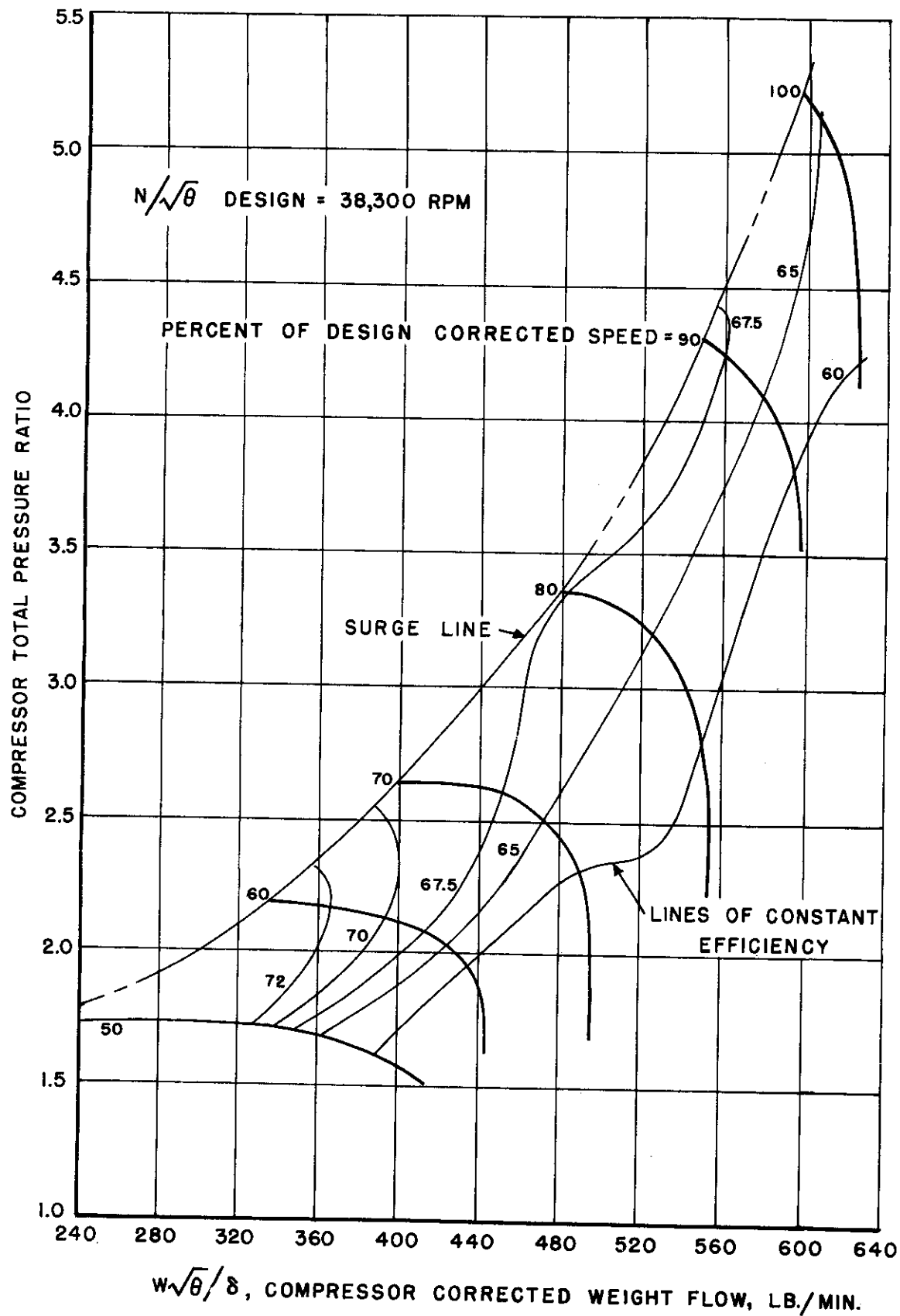$W\sqrt{\theta}/\delta$, COMPRESSOR CORRECTED WEIGHT FLOW, LB./MIN.

FIG. 6.17 SUPERSONIC RADIAL COMPRESSOR OVERALL PERFORMANCE, (SECOND DESIGN)